PREPARATION, CHARACTERIZATION AND MODIFICATION OF POLYANILINE BASED COATING FOR CORROSION PROTECTION OF ACTIVE METALS

A THESIS SUBMITTED TO THE

CENTRAL DEPARTMENT OF CHEMISTRY

INSTITUTE OF SCIENCE AND TECHNOLOGY

TRIBHUVAN UNIVERSITY, NEPAL

FOR THE AWARD OF

DOCTOR OF PHILOSOPHY

IN CHEMISTRY

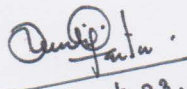BY

DIPAK KUMAR GUPTA

JUNE, 2021

EXTERNAL EXAMINERS

The Title of Ph.D. Thesis : "Preparation, Characterization and Modification of Polyaniline Based Coating for Corrosion Protection of Active Metals"

Name of Candidate: Dipak Kumar Gupta

External Examiners:

(1)   Prof. Dr. Deepak Prasad Subedi
      Department of Natural Sciences
      Kathmandu University
      Dhulikhel, NEPAL

(2)   Prof. Dr. Lakshman Neelakantan
      Metallurgical and Materials Engineering
      Indian Institute of Technology (IIT) Madras
      Chennai, INDIA

(3)   Prof. Dr. Yu Sugawara
      Department of Materials Science
      Graduate School of Engineering
      Tohoku University
      Sendai, JAPAN

March 23, 2022
_____

Dr. Surendra Kumar Gautam
Asst. Dean

DECLARATION

Thesis entitled **" Preparation, Characterization and Modification of Polyaniline Based Coating for Corrosion Protection of Active Metals "** which is being submitted to the Central Department of Chemistry, Institute of Science and Technology (IOST), Tribhuvan university, Nepal for the award of the degree of Doctor of Philosophy (Ph.D.), is a research work carried out by me under supervision of Prof. Dr. Amar Prasad Yadav, Central Department of Chemisty, Tribhuvan University.

This research is original and has not been submitted earlier in part or full in this or any other form to any university or institute, here or elsewhere, for the award of any degree.

———————————

Dipak Kumar Gupta

RECOMMENDATION

This is to recommend that **Mr. Dipak Kumar Gupta** has carried out research entitled **"Preparation, Characterization and Modification of Polyaniline Based Coating for Corrosion Protection of Active Metals"** for the award of Doctor of Philosophy (Ph.D.) in **Chemistry** under my supervision. To my knowledge, this work has not been submitted for any other degree.

He has fulfilled all the requirements laid down by the Institute of Science and Technology (IOST), Tribhuvan University, Kirtipur for the submission of the thesis for the award of Ph.D. degree.

Prof. Dr. Amar Prasad Yadav

Supervisor

Central Department of Chemistry

Tribhuvan University

Kirtipur, Kathmandu, Nepal

JUNE, 2021

LETTER OF APPROVAL

Date:

On the recommendation of **Prof. Dr. Amar Prasad Yadav**, this Ph.D. thesis submitted by **Mr. Dipak Kumar Gupta** entitled **"Preparation, Characterization and Modification of Polyaniline Based Coating for Corrosion Protection of Active Metals"** is forwarded by Central Department Research Committee (CDRC) to the Dean, IOST, T.U.

_____

Prof. Dr. Ram Chandra Basnyat

Head,

Central Department of Chemistry

Tribhuvan University

Kirtipur, Kathamndu

Nepal

ACKNOWLEDGEMENTS

_____

Dipak Kumar Gupta

June, 2021

ABSTRACT

Corrosion is a serious material degradation problem causing huge economic loss. There have been worldwide efforts on mitigating the loss due to corrosion by adopting various prevention strategies. Among them is the use of coating of the conducting polymers which have been found to have excellent environmental stability, ease of synthesis, and high electrical conductivity. Polyaniline (PANI), made from polymerization of aniline monomer, when deposited on metal surface forms a green anti-corrosion coating that has the potential to replace toxic metals-based coating like chromates in corrosion protection. However, an adherent PANI coating on active metal surface is prerequisite for effective corrosion protection. In addition, electrochemical deposition of PANI coating on active metal surface is a challenge as the dissolution potential of the metal is lower than the oxidation potential of the aniline monomer. As a result, the electrochemical synthesis of PANI coating on active metal requires the proper selection of an electrolyte and solvent that intelligently passivates the metal and allows the electropolymerization of aniline.

This study reports on the use of sodium potassium tartrate (Na-K Tartrate) and benzoic acid in the alcohol-water (BAW) as a medium for effective coating of PANI on mild steel (MS) by using electrochemical methods. For the first time, the composition of BAW system was optimized and used for the electropolymerization of aniline. The concentration of both aniline and electrolytes were found to greatly affect the quality of the coating which was optimized for getting best coating. A concentration of 0.3 M aniline in 0.2 M Na-K Tartrate and 0.3 M aniline in 0.04 M BAW was selected as the best composition due to better passivation and polymerization behaviors. In the case of BAW, benzoic acid in 3:1 alcohol-water was the optimized new system as a supporting electrolyte for the electropolymerization of aniline. BAW solution suppressed the dissolution of iron and the contamination-free PANI coating was obtained at a lower potential (less positive) than Na-K Tartrate. PANI coating on MS was accomplished by anodic polarization, cyclic voltammetry (CV), potentiostatic and galvanostatic methods. The results revealed that the electro-conductive passive layer formed before the polymerization started. A compact, pore-free with a fine structured PANI coating in both media was obtained. CV showed a stable PANI coating having no dissolution of iron during the cathodic scan with improved cyclic stabilities. Optimization of PANI coating on MS surface was studied in both electrolytes for better coating conditions. At lower

current density, a compact, uniform, and adherent PANI coating on MS were obtained by the galvanostatic method. A fine, uniform and thick PANI coating was also obtained potentiostatically at 1.4 V.

The prepared PANI coating was characterized by Fourier-transform infrared (FTIR) spectroscopy, Ultraviolet-visible (UV-Vis) spectroscopy, X-ray diffractometer (XRD), Optical microscopy, Scanning electron microscope (SEM) in combination with energy dispersion spectrometer (EDX), Transmission electron microscope (TEM) and Atomic force microscope (AFM).

The corrosion behaviors of PANI coating obtained in Na-K Tartrate and BAW media were investigated in different corrosion media by potentiodynamic polarization and electrochemical impedance spectroscopy (EIS). The corrosion inhibition efficiencies (IE) of PANI coating obtained in BAW were found to be superior to PANI coating obtained in Na-K Tartrate. In 0.1 M NaCl solution, the IE of PANI coating obtained in Na-K Tartrate and BAW were found to be 82.5% and 99.99%, respectively. In the case of 0.1 M H_2SO_4, the IE of PANI coating obtained in Na-K Tartrae and BAW were almost similar i.e. 97.53% and 99.0% respectively. Similarly, in the case of 0.4 M Na_2SO_4, IE of PANI coating obtained in Na-K Tartrate and BAW were 87.17% and 92.0%, respectively. The IE of PANI coating obtained in BAW by the galvanostatic method was higher than PANI obtained in Na-K Tartrate. The corrosion IE estimated from EIS in 0.1 M H_2SO_4, 0.4 M Na_2SO_4, and 0.1 M NaCl media showed PANI coating obtained in BAW electrolyte was superior in all the electrolytes. The corrosion behavior studied from EIS is in good agreement with potentiodynamic polarization. Hence, the BAW reported as the new supporting electrolyte offers excellent PANI coating on MS.

LIST OF ACRONYMS AND ABBREVIATIONS

AFM : Atomic Force Microscopy

cm^{-1} : Per Centimetre

CPE : Constant Phase Element

CR : Corrosion Rate

E_{corr} : Corrosion Potential

EDX : Energy Dispersive X-ray Spectroscopy

EFM : Electrochemical Frequency Modulation

EIS : Electrochemical Impedance Spectroscopy

FTIR : Fourier Transform Infrared Spectroscopy

GDP : Gross Domestic Product

I_{corr} : Corrosion Current

IE : Inhibition Efficiency

IUPAC : International Union of Pure and Applied Chemistry

mA : Milli Ampere

mL : Milliliter

mm : Millimeter

mV : Milivolt

NACE : National Association of Corrosion Engineers

nm : Nanometre

OCP : Open Circuit Potential

OCV : Open Circuit Voltage

PZC : Potential of Zero Charge

R_{ct} : Charge Transfer Resistance

SCE : Saturated Calomel Electrode

TEM : Transmission Electron Microscope

UV : Ultraviolet

LIST OF SYMBOLS

ν	: Frequency
λ	: Wavelength
θ	: Bragg Diffraction Angle
B	: Peak Width of Half Maximun
Z_{real}	: Real Impedance
Z_{imag}	: Imaginary Impedance
V	: Volt
ºC	: Degree Celsius
K	: Scherer Constant
D	: Average Crystalline Size
|Z|	: Impedance Modulus
ϕ	: Phase Shift

LIST OF TABLES

LIST OF FIGURES

TABLE OF CONTENTS

CHAPTER 1

1. INTRODUCTION

1.1 General introduction of corrosion

Corrosion is derived from the Latin word "colossus," which means "eating down" or "consumption by degrees," It is an unpleasant word for an offensive operation (Evans, 1972). Corrosion is a natural phenomenon that follows universal principles. It is the destruction or deterioration of metals or alloys due to oxidation and reduction that occurs when metals or alloys interact with a corrosive atmosphere, failing the structure of metallic surfaces (Ghali *et al.*, 2007; Fontana, Greene, 1986; Sastri, 2011). Rusting is the corrosion of iron and its alloys, and rust is the corrosion product, which is mainly made up of hydrated ferric oxide. Non-ferrous metals only undergo corrosion but not rusting (Uhlig & Revie, 2008).

Uhling and Revie described corrosion as "the destructive attack on the surface of metallic materials (metals or alloys) by chemical or electrochemical reaction with their atmosphere, resulting in their degradation" (Uhlig & Revie, 2008). Until 1960, the term corrosion was only applied to describe metals and their alloys. IUPAC and Fontana were responsible for the broad definition. Corrosion is defined by the International Union of Pure and Applied Chemistry (IUPAC) as "an irreversible interfacial reaction of materials (metallic, ceramic, or polymer) with their environment that results in the materials being consumed or a portion of the environment being dissolved into the material"(Heusler *et al.*, 1989). Corrosion now refers to a wide range of natural and man-made materials, including biomaterials and nanomaterials, and is no longer limited to metals and alloys.

Corrosion's spectrum corresponds to the revolutionary developments in material production that have occurred in recent years. The IUPAC concept of corrosion, on the other hand, has not been universally accepted by the corrosion community.

It is an electrochemical phenomenon that involves two reactions: an anodic (oxidation site) that releases electrons and a cathodic (reduction site) that consumes them. Metal corrosion is caused by the anodic and cathodic reactions mentioned below (Uhlig & Revie, 2008).

The anodic reaction is

$$M \longrightarrow M^{n+} + ne^-$$
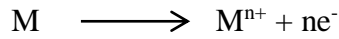
Where 'M' stands for metal, and 'n' stands for the number of electrons that an atom of the metal will easily release.

According to the environment where corrosion is taking place, the possible cathodic reaction can be of the following types.

   a. oxygen reduction in acidic solution

$$O_2 + 4H^+ + 4e^- \longrightarrow 2H_2O$$
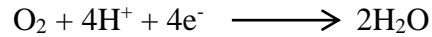
   b. oxygen reduction in neutral or basic solution

$$\tfrac{1}{2} O_2 + H_2O + 2e^- \longrightarrow 2OH^-$$
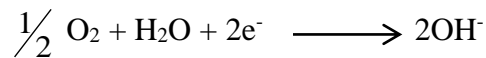
   c. Hydrogen evolution from neutral water

$$2H_2O + 2e^- \longrightarrow H_2 + 2OH^-$$

   d. Metal reduction

$$M^{x+} + ye^- \longrightarrow M^{(x-y)+}$$
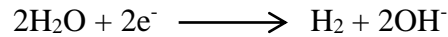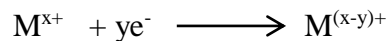
The flow of metal ions into the solution occurs at active areas (anode). As shown in **Fig. 1.1**, corrosion involves the transfer of electrons from the metal to an acceptor at less active regions (cathode), an ionic current in the solution, and an electric current in the metal. The cathodic operation requires an electron acceptor, such as oxygen or oxidizing agents, or hydrogen ions. In the ionic state, metals are more stable than in the atomic state. Metals are converted into their combined state in chemical compounds, much as they are in minerals from which they are derived, according to the thermodynamic principle.

Hence, thermodynamic instability is the cause of corrosion. To calculate the corrosion rate, one must first determine if the metal is stable in the given conditions, i.e., whether or not the anodic and cathodic reactions occur spontaneously. Thermodynamics is concerned with the random occurrence of reactions. Corrosion is therefore a natural occurrence (Mazumder, 2020).
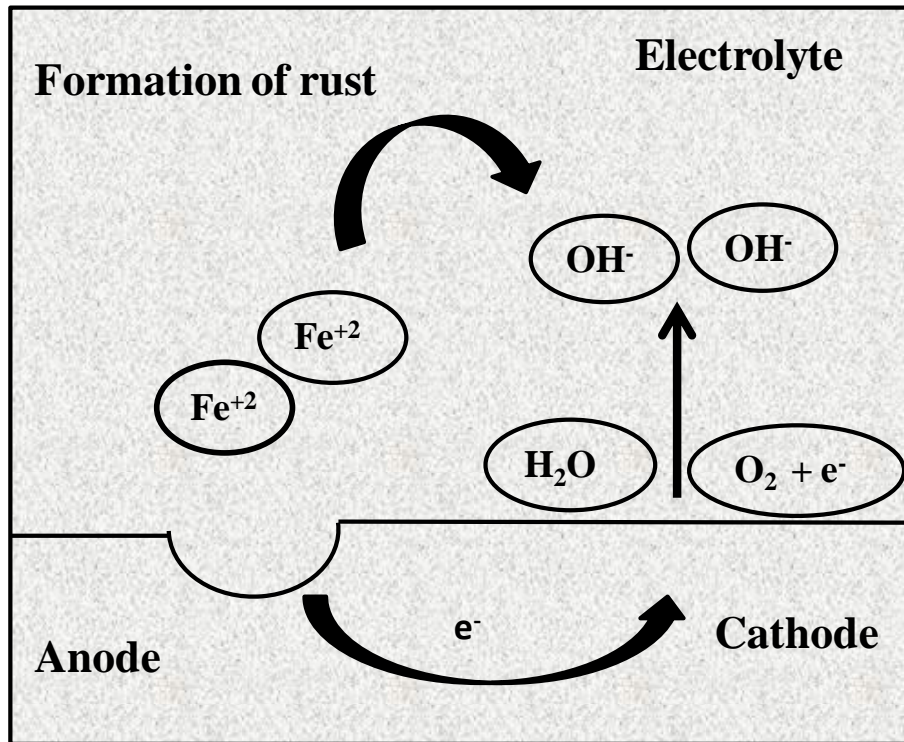
Figure 1.1: A schematic representation of the corrosion on a metal surface in an acidic solution showing both the anodic and cathodic site.

From the following relation

$$\Delta G = -nFE$$

The change in free energy during an oxidation or reduction reaction can be calculated. The symbols n, F, and E stand for the number of electrons involved, Faraday's constant, and equilibrium potential, respectively. Corrosion will occur naturally if the overall free energy change is negative *i. e*. with the decrease in free energy.

1.2 Effects and consequences of corrosion

Corrosion is not the term for deterioration caused by physical forces; instead, degradation, galling, or wear are used. Corrosion has a wide range of implications, and the impact on the effective, stable, and productive operation of equipment or structures is often more severe than simply losing a mass of metal. Even if the amount of metal lost is minimal, failures of various kinds and the need for costly replacements can occur. The following are some of the devastating consequences of corrosion as described by S.A. Umoren (Umoren *et al.*, 2009):

i. People-related hazards or injuries caused by structural failure or breakdown (e.g. bridges, cars, aircraft, etc.).

ii. Owing to the degradation of appearance, the value of the products is reduced.

iii. Fluid contamination in vessels and pipes (for instance beer goes cloudy when small quantities of heavy metals are released by corrosion).

iv. The loss of a metallic component's technically significant surface properties. Friction and bearing properties, ease of fluid movement over a pipe surface, the electrical conductivity of contacts, surface reflectivity, and heat transfer over a surface are just a few examples.

v. Perforation of vessels and valves, causing the contents to escape and possibly harming the environment.

vi. Make industrial machinery with a loss of time availability profile.

vii. Loss of mechanical strength and structural failure or breakdown as a result of metal thickness reduction. As the metal is lost in localized areas, resulting in a crack-like structure, even a small amount of metal loss can cause significant weakening.

viii. Added complexity and cost of equipment that must be constructed to withstand a certain level of corrosion and allow for the easy replacement of corroded components.

ix. Valve, pump, or other mechanical damage or blockage by solid corrosion products.

Table 1.1 lists several catastrophic corrosion injuries that have resulted in fatalities and significant economic losses.

Table1. 1: List of some renowned corrosion accidents (Mazumder, 2020)

Name of accidents	Year	Place	Cause and loss
Silver Bridge Collapse	1967	Ohio, USA	Highway 35 bridge fall in Ohio river, resulted in the deaths of 46 people.
Bhopal Accident	1984	Bhopal,	The holding tank for methylisocyanate (MIC) leaked due to corroded pipelines, pumps,

		India	and other safety features. This incident resulted in the deaths of 3000 people and the injuries of 500,000 others.
Swimming Pool Roof Collapse	1985	Uster, Switzer-Land	The concrete roof backed by stainless steel collapsed after 13 years of use due to stress corrosion cracking. It is said that 12 people were killed in this incident.
The Aloha Incident	1988	Island of Maui, Hawai	Due to multiple corrosion fatigue damage, a 19-year-old Boeing 737 lost a substantial portion of the upper fuselage while in flight. One flight attendant was killed.
Guadalajara Sewer Ex-Plosion	1992	Guadalaja-ra, Mexico	The sewage explosion was caused by galvanic corrosion of a galvanized steel pipeline that had been blocked by a steel fuel pipeline. It claimed the lives of 215 people, wounded 1500 others, and destroyed 1600 structures.
EL AL Boeing 747 Crash	1992	Amster-dam, The Nether-Lands	Since the fuse pins that tie the strut to the wings are weakened by corrosion pits and fatigues, the two right engines detached from the wing, causing the crash. This accident claimed the lives of all four passengers on board as well as more than 50 people on the ground.
The sinking of the	1999	Brittany,	As the result of corrosion in the

Erika		France	main deck coaming, the port side, and starboard inert gas system risers, the tanker cut in half while loading »30000 tons of heavy fuel oil. 19800 tons of oil leaked, wreaking havoc on the region's economy.
Carlsbad Pipeline Explo-Sion	2000	New Mexi-co, USA	A 30-inch natural gas pipeline owned by El Paso Natural Gas collapsed due to extreme internal corrosion.

This incident resulted in the deaths of 12 people and the destruction of three vehicles. |
Prudhoe Bay Oil Spill	2006	Prudhoe Bay, Alaska	The breakdown of BP's field pipeline corrosion control and leak detection systems resulted in a major oil spill. A corroded transit pipeline spilled 267,000 gallons of crude oil.
Rupture of a High-Pres-sure Vessel	2009	Illinois, USA	Corrosion Due to Stress The Nihon Dempa Kogyo (NDK) Company explodes due to cracks in the walls of a pressure vessel. One individual was killed and several people were injured in this blast.
Rupture of a Natural Gas Transmission	2016	Pennsylvania-nia, USA	Corrosion caused a 30-inch diameter natural gas delivery pipeline to burst, along with two other pipelines.

Pipeline			the welds that go along the circumference As a result of this incident, one home was demolished, three homes were partly damaged, and one home was destroyed. Several homes were also evacuated.
Ohio State Fair accident	2017	Ohio, USA	The rust (thickness of the ridge beam's thickness) caused a pendulum-type thrill ride to crash during service. wall has been lowered). One individual was killed and several people were wounded as a result of the malfunction.
Pipelines incidents*	2018	290	6 Fatality and 78 injury
Pipelines incidents*	2019	316	11 Fatality and 35 injury
Pipelines incidents*	2020	281	15 Fatality and 43 injury

*It only represents major pipelines incidents occurred.

1.3 Importance and economic impact of corrosion

Corrosion not only destroys materials, but also causes untimely failure of plants, machinery, and parts, resulting in human and property loss. The following are the primary reasons for corrosion's importance:

a. Safety: Corrosion can cause equipment to malfunction, resulting in reduced efficiency and reliability. It renders the equipment inoperable. Corrosion materials can also be toxic if they come into contact with equipment or water in the pipeline.

b. Conservation: Corrosion research is essential to preserve precious metals, as well as the resources and human effort required to manufacture, fabricate, and repair.

c. Economic: The cost of corrosion research is a major motivator. Individuals or the whole country suffer economic losses as a result of corrosion, either directly or indirectly.

Cost of repairing corroded equipment, buildings, and parts, such as metal roofing, pipelines, condenser tubes, and mufflers, including required labor, are some examples of direct loss due to corrosion.

- The price of repainting the structure
- The cost of constructing and maintaining a cathodic safety system for underground pipelines.
- For the cost of corrosion prevention systems such as adding additives, galvanizing, and dehumidifying machinery storage rooms instead of mild steel for the cost of corrosion protection systems such as adding inhibitors, galvanizing, and dehumidifying storage rooms

The following are some examples of indirect corrosion losses:

- Failure and serious problems were caused by the closure of plants such as nuclear power plants, power plants, process plants, and refineries.
- Leakage in containers, storage tanks, oil transportation lines, and fuel tanks results in the loss of goods such as water and oil. If gas leaks from a corroded pipe and reaches the building's basement, it may cause an explosion.
- Efficiencies are lost as corrosion materials accumulate, reducing heat transfer and piping capability of heat exchanger tubings and pipelines.
- Corrosion products can contaminate chemicals, pharmaceuticals, dyes, packaged goods, and other things, rendering them unsafe to use.
- With adequate knowledge of corrosion, equipment such as reactions vessels, boilers, condenser tubes, oil-well sucker rods, pipelines carrying oil and gas at high pressure, water tanks, and marine structures can be built to be easier, more durable, and light, rather than being overdesigned to withstand high operating pressure and stress.

At the request of the United States Congress, NACE International conducted a report in 1999 to calculate the direct costs of corrosion and corrosion protection in almost every industry field in the world, from transportation to services to food production. Metallic corrosion-related costs accounted for 3.1 percent of annual GDP, or $276 billion a year, according to the two-year report conducted by the USFHWA and NACE in 2002 (Mazumder, 2020). It also discovered that, while corrosion control methods have evolved, there is still more potential for progress in terms of corrosion prevention and public education about its importance.

According to the National Oceanic and Atmospheric Administration, the United States suffered 203 significant weather and climate-related hazards between 1980 and 2016, resulting in $878.3 billion in damages. This amounts to around $24.4 billion a year on average. Corrosion costs about 12 times as much each year. Corrosion, unlike weather and climate-related phenomena, can be regulated.

In 2001, the direct annual per capita cost of corrosion and its control was calculated by NACE International to be about $970 per human. It's also important to think about the indirect costs of corrosion, such as reduced efficiency, increased overhead costs of products and services impacted by corrosion, lawsuits, and delays. According to NACE International, the annual indirect costs of corrosion are estimated to be about $552 billion, or around 6% of GDP.

1.4 Global consequences of corrosion

In 2016, NACE International performed a study in India, Japan, Kuwait, the United Kingdom, and the United States to calculate the cost of worldwide corrosion. The loss was projected to be about $2.5 trillion, or around 3.4 percent of global GDP, according to the organization (*NACE International Institute IMPACT PLUS*, 2020). In 2013, NACE International conducted a global analysis on corrosion costs and preventative strategies, which was used to link the cost of corrosion to the World Bank economic sector and global Gross Domestic Product (GDP) statistics. The **Figs. 1.2** and **1.3** reflect the global and economic region corrosion cost.
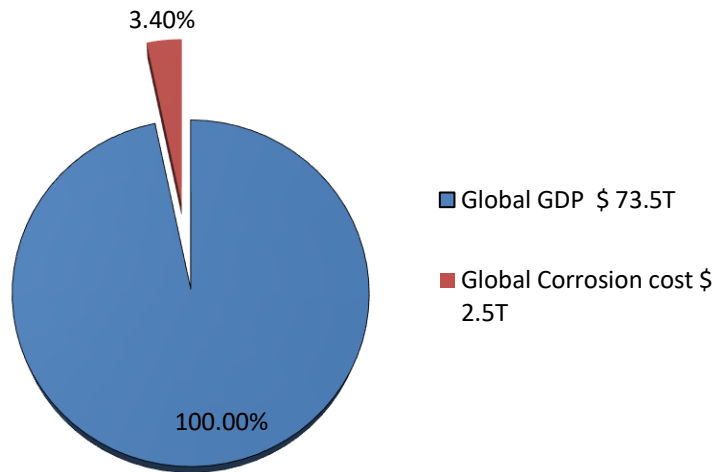
Figure 1. 2: Global corrosion cost (Billion US$)
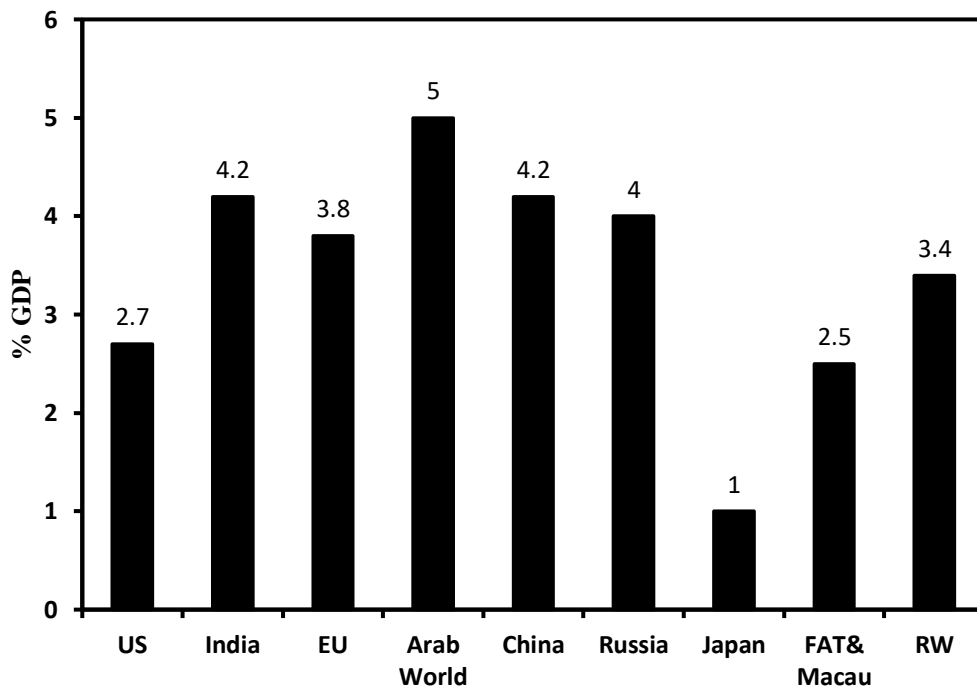
Figure 1. 3: Corrosion cost (Billion US$) of economic regions

The World Bank divided the global economy into economic regions with common economic divisions such as agriculture, industry, and services to address economic segments around the world. Figure 1.4 shows the cost of corrosion (CoC) studied by the economic sector of different economic regions which can be used to estimate the corrosion cost of any country (*NACE International Institute IMPACT PLUS*, 2020).

The CORROSION 2016 conference in Vancouver, British Columbia, examined the corrosion loss economy and recommended corrosion *prevention* techniques as best practices for avoiding 15-35% corrosion loss, or US $375-875 billion. The gas, chemical, and petrochemical sectors, as well as construction, processing, pulp and paper, and transportation (rail, automobile, and aerospace) industries, all contribute significantly to corrosion loss.

According to reports, the US and India each lost more than US $276 billion and Rs 8,000 billion per year due to corrosion damage (The Federal Highway Administration of the United States of America, 2002; C.C. Technologies Laboratories, 2001). Corrosion costs in Japan are expected to be 5258 trillion yen per year.
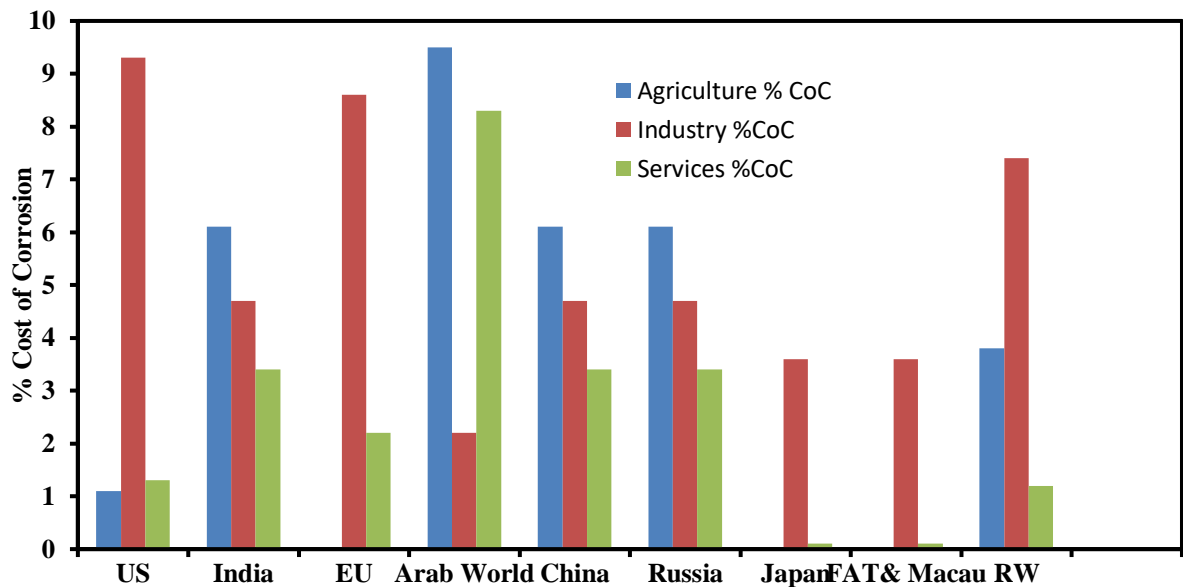
Figure 1. 4: The cost of corrosion (CoC) of the economic sector of different economic regions

Corrosion of reinforcement and subsequent concrete spillage accounts for nearly 95 percent of concrete destruction in the Arab Gulf's coastal area. Per newborn baby in the world is estimated to have a corrosion debt of $40 per year (Ahmad, 2006). Since the practices were embraced in the market and the organizations within it, researchers discovered that new methods used in the automobile industry had the greatest success in corrosion control. More companies would reduce corrosion if they engaged in corrosion prevention and maintenance and integrated the elements into their overall management processes.

Basic research on the corrosion of infrastructure materials such as GI tubing, roofing, and vehicles is limited in Nepal. Furthermore, there is a scarcity of data on ambient conditions and their impact on the deterioration of commonly used materials. In Nepal, data on economic losses caused by corrosion damage is limited. However, the cost of corrosion in Nepal can be approximately calculated based on the cost of corrosion studies conducted by NACE in neighboring countries India and China, as seen in Table 1.2. In 2019, Nepal's GDP was USD 29.813 billion, with agriculture, manufacturing, and the service sector accounting for 27 %, 13.5 %, and 59.5 %, respectively. Estimation of corrosion cost (CoC) on the above basis shows that the corrosion cost of Nepal turns about 1.28 billion USD equivalent to 154 billion NRS (NPR.1.54 kharab) and it is 4.3% of the GDP. The contributions of economic sectors such as agriculture, industry, and services in GDP have been used in the calculation as shown in Table 1.2 (Nabin Karki, 2018).

Table 1. 2: Corrosion cost of Nepal based on corrosion cost study of neighboring countries

S.No.	Sector	% Contribution	Amount (billion $)	% CoC	Amount (billion $)
1	Agriculture	27	8.05	6.1	0.49
2	Industry	13.5	4.05	4.7	0.19
3	Service	59.5	17.74	3.4	0.6
Total					1.28

The tremendous amount of loss due to corrosion in Nepal can be estimated by looking at the budget allocated for education, science, and technology, and the environment which accounts for about 11.64 % of the country's annual budget. Corrosion costs approximately 10.44% of annual expenditure, of which 15% to 35% can be avoided by using appropriate corrosion knowledge, which ranges from NPR 23.1 billion (23 Arab 10 crore) to NPR 53.9 billion (53 Arab 90 crore) (Nabin Karki, 2018).

Thus, corrosion studies are important for different reasons. The following are a few of them:

❖ for constructing engineering systems and materials properly in the early stages of construction

❖ for the prevention of different forms of corrosion-related disasters

❖ for the protection of air, water, and soil contamination and to minimize health hazard

❖ for the conservation of precious natural resources

❖ for the use of corrosion-resistant surgical implants in the human body (Ghali *et al.*, 2007)

1.5 Corrosion prevention

Corrosion is an unavoidable spontaneous phenomenon. However, it can be controlled by employing different methods. Since corrosion is an electrochemical reaction involving two or more half cell reactions, it can be regulated by slowing down either the cathodic or anodic reactions, or both. As the most practical means of mitigating the effects of corrosion, many efforts are made to reduce the susceptibility of the components. The primary goal of corrosion prevention approaches is to ensure the structures' long-term viability and integrity. It reduces the chance of dangerous leaks and explosions. It is a cost-effective way to preserve lives, property, and the environment by reducing the premature loss of products and systems.

The following techniques are applied to protect metals from corrosion:

1. Inspection and monitoring
2. Selection of the appropriate material
3. Environmental change
4. Proper equipment design
5. Use of Inhibitors
6. Electrical protection (cathodic and anodic protection)
7. Coatings

1.5.1 Inspection and monitoring

Structures and equipment should be tested daily to avoid accidental malfunction. It aids in the prevention of serious harm to people, infrastructure, and the environment. It assists the provision of pertinent knowledge and evidence needed to determine the current system in a hostile environment (Davis, 2000). Visual analysis, fiberscope, borescope, caliper instruments, and other devices may be used. In general, inspection entails a one-time, short-term measurement based on the maintenance and inspection schedule.

Monitoring entails taking long-term measurements of corrosion degradation to figure out

how corrosion changes over time and what causes loss. It is carried out to ensure that facilities and systems are in proper working order since it gives early notice of their breakdown (Davis, 2000; Roberge, 2012). Potentiodynamic polarization, AC impedance measurement, weight-loss method, and other electrical and mechanical probes can be used for monitoring.

1.5.2 Selection of the appropriate material

Corrosion activity, physical (electrical conductivity, thermal conductivity), mechanical (tensile strength, density, ductility, fracture durability, etc.), and cost are some of the considerations to consider when choosing materials for a particular reason (Finšgar & Jackson, 2014; Roberge, 2012). Mild steel is applied for a variety of manufacturing and technical materials owing to its inexpensive nature. Since mild steel is easily corroded, austenitic or duplex stainless steels, considering their high cost, are used in some applications due to their corrosion-resistant properties.

The motive for the corrosion resistance of the following respective material candidates can be used as a general guideline for materials selection mainly determined by corrosion aspects. Reducing environments are compliant with comparatively noble metals or steel alloys (for example copper, lead, nickel, and alloys based upon these metals). When metallic materials are used in an oxidizing setting, their corrosion resistance must be dependent on passivity (for example, titanium, and alloys containing appropriate quantities of chromium). Regardless of the law, a metal is normally the most corrosion-resistant when the number of impurities in it is as low as possible. Table 1.3 lists the combination of environmental and materials (Fontana & Greene, 1986). Non-metallic materials have been used in several situations like polymers, rubbers, ceramics, wood, and concrete.

Table 1.3: Some natural combinations of environment and material

Nitric acid	Stainless steels
Caustic solutions	Nickel and nickel alloys
Non-staining atmospheric exposure	Aluminum
Distilled water	Tin
Hot strong oxidizing solutions	Titanium
Concentrated sulfuric acid	Steel

Mild steel, in combination with chemical treatments such as corrosion inhibitors, is still a cost-effective option (Finšgar & Jackson, 2014).

Material procurement normally considered to be of several measures that account environmental factors as well as the total cost of the structure. It involves the following procedures.

- Initial selection: based on previous experience, affordability, and safety considerations
- Laboratory testing: Reevaluation of products that seem to be acceptable under process environments.
- Analysis of laboratory results and other data: Effects of potential impurities, excess temperature, excess pressure, agitation, and air presence in equipment
- Cost-benefit analysis of apparently acceptable materials: material and repair costs, expected life, cost of product deterioration, and hazard exposure
- Final decision

1.5.3 Environmental change

To mitigate corrosion rates, the environment should be altered in the following ways:

a) Lowering (or raising) the ambient temperature.
b) Slowing down (or speeding up) the flow.
c) Reducing (or increasing) the amount of oxygen or aggressive organisms in the environment.
d) Addition of inhibitors

Regarding the first three points, it should be noted that the most common ways to minimize corrosion rates are to lower temperature, flow rates, or the amount of oxygen or aggressive species present on it. The inhibitors, on the other hand, can be classified depending on the reaction (anodic or cathodic) they affect and how they affect polarization properties.

The most commonly used passivating agents are generally inorganic inhibitors, also known as passivation. The oxidizing ones work either by depolarizing the cathodic

reaction (making it more efficient) or by adding a new cathodic reaction. When the inhibitor concentration is high enough (greater than a critical value), the cathodic current density at the primary passivation potential exceeds the critical anodic current density, and the metal is passivated. It is, however, worse than having no inhibitor if the inhibitor concentration is below the critical amount. Chromates and nitrites are examples of oxidizing inhibitors.

Some anodic and cathodic inhibitors are non-passivating. The extract free oxygen from a reaction, such as hydrazine and sodium sulfite, are examples of the latter:

$$N_2H_4 + O_2 \longrightarrow N_2 + 2H_2O$$
$$2Na_2SO_3 + O_2 \longrightarrow 2Na_2SO_4$$
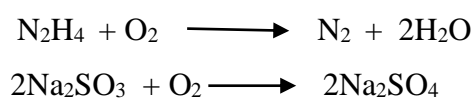
These inhibitors are useful in all conditions where, in the uninhibited state, oxygen removal is the dominant cathodic response, such as in neutral natural waters. Other varieties, on the other hand, must be used in highly acidic solutions. Adsorption inhibitors can also be classified as vapor process inhibitors. These are used to shield wrapped materials from the elements for a short period of time. The inhibitor is combined with the component(s) and works due to its appropriate low saturation strain, resulting in an efficient inhibitor condensate on the metal surface. This prevents the effects of water and oxygen. It should be noted that these inhibitors may increase corrosion on some non-ferrous metals and alloys (Roberge, 2012).

The literature covers a wide range of inhibitors for various metals and habitats, as well as their behavior under various conditions (Shreir & Jarman and Burstein, 1994; Roberge, 2012). In oil and gas processing plants, as well as recirculation facilities, inhibitors are significant for corrosion prevention.

1.5.4 Proper equipment design

The rate of corrosion of the material can also be minimized by the suitable equipment design. The design and material selection processes are interdependent. Here are a few things to consider about designing a piece of equipment. The poor and good designing of materials are shown in **Fig. 1.5**.

1. Where the variation in corrosion strength between two metals joining together is greater in the galvanic sequence, the chance of corrosion is greater. As a result, in the case of electrolytes, certain metal interactions should be avoided. If the use of

certain metals with a greater difference in corrosion potential is desired, insulators such as plastic or rubber should be used to isolate them to prevent corrosion.

2. It should be designed with simple geometry and avoiding heterogeneity in the system.

3. Drainage, testing, and washing should be simple to do.

4. To prevent crevice corrosion, welding is favored over riveting when connecting parts of materials. To remove residual pressures that could contribute to corrosion, the heat-affected zone (HAZ) should be post-weld heat treated (PWHT).

5. The risk of erosion-corrosion may be minimized by thickening fragile sections exposed to high turbulence (high shear stress) or flowing solutions containing suspended solids, such as tube inlets, elbows, curves, agitated vessel impellers, and so on.

6. To monitor oxygen transport from the solvent to the corroding surface, machinery vibration should be minimized as far as possible.

7. To prevent extreme corrosion, equipment should not be left damp for an extended period. By passing nitrogen gas should be dried.

8. Stresses in the system should be minimized.
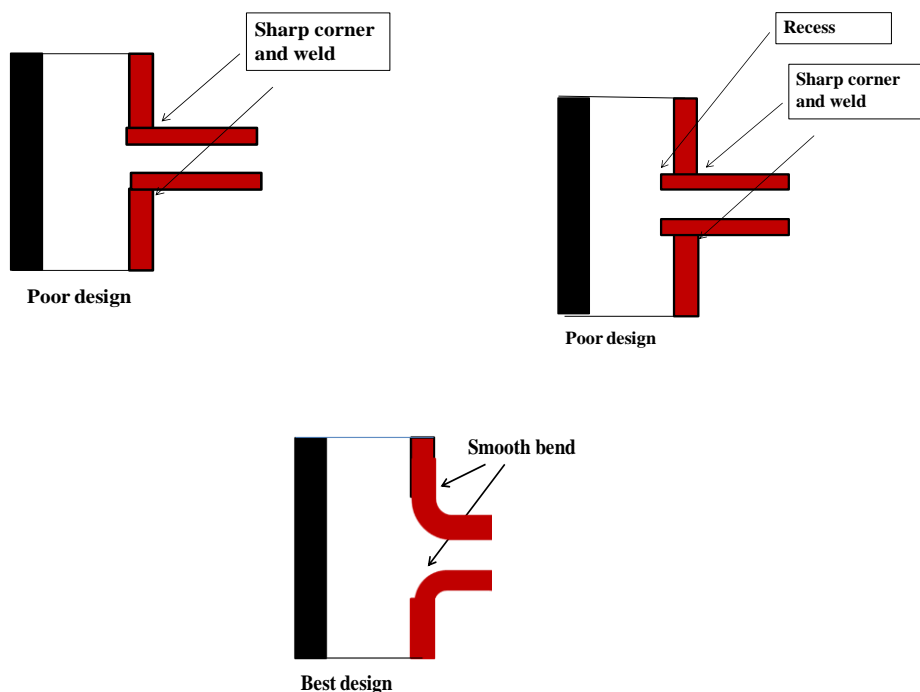
Figure 1. 5: Poor and best designing of materials

1.5.5 Use of Inhibitors

Corrosion inhibitors are one of the most powerful methods for preventing corrosion. Since the nineteenth century, it has been used to prevent corrosion. Baldwin was the first to receive a patent on an inhibitor that used molasses and vegetable oils to discourage acid corrosion from pickling sheet steel (J.B., 1895). Because of cheap and ease of implementation, it is extensively used in the manufacturing field (Dariva & Galio, 2014; Obot *et al*., 2009; Yıldırım & Çetin, 2008). These can be used in a variety of places, including cooling water systems, refinery units, chemical plants, electricity generation, oil and gas processing units, and so on.

Most well-known acid inhibitors are organic compounds with aromatic and heterocyclic rings containing nitrogen, sulphur, and oxygen as their functional groups (El-Etre, 2007; Halambek *et al*., 2010; Ngouné *et al*., 2019) as shown in **Fig.1.6**. These organic compounds absorb on the metal surface, blocking the active sites, forming a protective membrane, and slowing the rate of corrosion (Verma *et al*., 2018). These organic compounds are toxic and hazardous in nature (Mohd & Ishak, 2015; Qiang *et al*., 2018; Saxena *et al*., 2018). Therefore, corrosion scientists are interested in researching sustainable corrosion inhibitors. The most of inhibitors derived from plants are biodegradable, non-toxic, environmentally safe, and less expensive (Halambek *et al*., 2010; Stiadi *et al*., 2020). It has encouraged the search for environmentally-friendly corrosion inhibitors to replace inorganic and organic inhibitors and foster long-term environmental sustainability. In this regard, many attempts have been made to use natural products as inhibitors, called green inhibitors for a better future, a clean environment, and a healthier life. Green inhibitors are now widely regarded as attractive alternative inhibitors. Berberine extracted from *Coptis chinensis* is one of the green inhibitors as shown in **Fig. 1.7** (Li *et al*., 2005; Yıldırım & Çetin, 2008)**.**

Biotin   **benzotriazole**
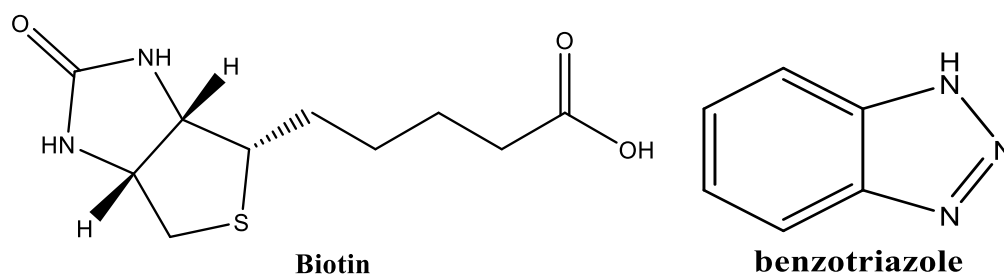
Figure 1. 6: Organic inhibitors (Desai & Indorwala, 2015; Xu *et al*., 2017)
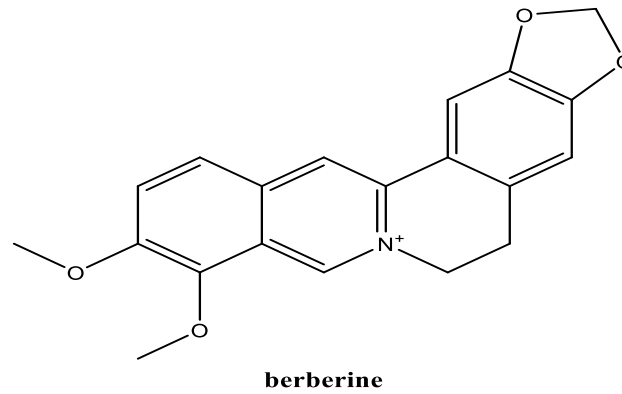
berberine

Figure 1. 7: Berberine extracted from *Coptis chinensis*, used as green inhibitor

1.5.6 Electrochemical protection

It is one of the most significant techniques for corrosion prevention which is of two types:

a. Cathodic protection method

The basic theory of cathodic protection is to apply an external current to a substrate, forcing the electrode potential down to the immune region or, for localized corrosion protection, below a protection potential (E. Bardal, 2004). The cathodic protection system is a corrosion prevention method commonly used to secure underground and undersea metallic systems such as oil and gas pipes, wires, utility poles, concrete supports, heat exchanger condenser tubing, bridges, and other related structures as shown in **Fig. 1.8**. Electrons formed at the anode are absorbed by the cation of the electrolyte solution, and the metal ion at the anode combines with the anion of the solution, resulting in metal dissolution, according to the electrochemical principle of corrosion.
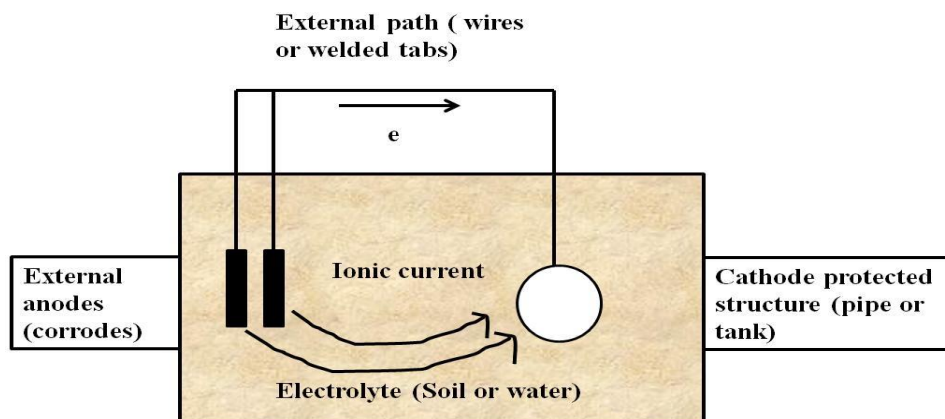
Figure 1. 8: Cathodic protection system showing the protection of underground structure

Cathodic hydrogen evolution is enhanced as additional electrons are supplied to the metal by an external source; anodic metal dissolution is decreased. As a result, the supply of electrons from external sources reduces or removes the potential gap between the cathodic and anodic sites of the metal to be shielded, and corrosion is reduced or eliminated. As the metallic arrangement becomes more negative or cathode, complete cathodic safety is obtained. There are two methods for cathodic defense.

1. **By the application of direct current:** The additional electrons are supplied in this process by direct electric current, which changes the cathode's potential to that of the anodic field. The potential distance between the cathode and the anode is minimized as enough potential is applied to control metal corrosion.

2. **By using sacrificial anode:** It is a simple and inexpensive cathodic safety system that does not require an external power supply. The metal to be covered becomes the cathode, while the more active metal becomes the sacrificial anode and corrodes in this process. Iron, for example, can be shielded by more active metals like copper, magnesium, and aluminum.

b. Anodic protection

Materials with a well-defined and stable passive area and a low passive current density will benefit from anodic safety. The potential is elevated to the passive region by polarizing the substance in the anodic direction (Bardal, 2004). Anodic defense is a strategy for regulating the corrosion of a metal surface by attaching it as an anode to an inert cathode in an electrochemical cell and ensuring that the electrode potential is retained to hold the metal in a passive state. A barrier protecting film is created on the metal surface during the process, which prevents it from corrosion. Only the active-passive metallic material is appropriate for this form. It's preferred in rough conditions like mild steel vessels containing condensed acid or alkali, such as concentrated sulphuric acid. When cathodic security is not cost-effective, this is achieved. For certain metals, such as steel alloys or stainless steel, the use of anodic protection over cathodic protection is favored. Since failure or instability in passivation may accelerate corrosion, it necessitates careful design and control.

1.5.7 Coatings

One of the most common and commonly used methods of corrosion protection is coating. It is a thin film that is deposited on top of a metal surface to enhance its surface

properties. The coating provides a protective layer that eliminates metal interaction with the atmosphere and avoids corrosion. Low cost, low porosity, strong adhesion to the substrate, fire, flame, and abrasion resistance, adequate thickness, and uniform appearance are all considerations to consider when selecting successful corrosion. It can also be environmentally immune to the atmosphere it is exposed to. Coating loss can be related to water accumulation, blistering from gas, and other causes or air inclusion, surface contamination, surface defects, and temperature differentials. In many cases, failure results from inadequate surface preparation and careless application of the coating by relatively unskilled human resources.

Coatings are of three types, viz. metallic, non-metallic, and conversion coatings, which could be further subdivided into many categories.

A. **The metallic coating is carried out by the following methods:**

1) Electroplating
2) Hot dipping of the workpiece in molten metal covered with a flux
3) Spraying of the molten metal on the workpiece

B. The non-metallic coating is of two types.

1) Inorganic coating

 (a) Oxidation (Passivation)

 (b) Phosphating

 (c) Enamels

 (d) Cement coating

2) Organic coating

 (a) Paints

 (b) Lacquers

 (c) Coal tar

 (d) Temporary coating (lubricating oil)

C. Conversion coating

Conversion coating is a coating on the metal surface by electrochemical or chemical processes. Conversion coating provides increased surface stiffness in addition to corrosion resistance. It may also be used as a primer for decorative purposes. Phosphate and chromate coatings, as well as black oxide, are some of the best examples of this

coating form. It is usually applied to aluminum alloys through chromate conversion or anodizing.

1.6 Conducting Polymer

Organic polymers had previously been thought to be insulators before ascertaining that the conductivity of polyacetylene greatly increased when doped with oxidized iodine. The credit for the discovery of conducting polymer goes to Heeger, MacDiarmid, and Shirakawa (MacDiarmid, Alan G, 2001; Shirakawa *et al*., 1977). In 1977, they reported the first conducting polymers in Pennsylvania**.** The Nobel Prize for Chemistry was awarded to Heeger and co-workers in 2000 for the discovery of conducting polymers. Since then, much work has been done into developing new conducting polymers as well as identifying new properties and uses for such materials (Heeger, 2001; MacDiarmid, Alan G, 2001). Conducting polymers are used in a wide range of applications and components, including organic light-emitting diodes (OLEDs), antistatic shielding, electrochromism, organic solar cells, supercapacitors, corrosion protection, electrochemical sensors, and so on.

Thus, conducting polymers have a conjugated system in which electrons can move from one end of the polymer to the other through the extended p-orbital system hence giving them unique optical and electrical properties that allow their use in a large field of applications including corrosion protection (Chiang *et al*., 1978; Rahman *et al*., 2008). Indeed, they constitute a physical barrier towards aggressive chemical reagents and, as they carry polar groups, they may act as polymeric inhibitors and shift the potential of the coated materials to a value where the kinetics of corrosion of the underlying metal is lowered (Roth, 1995). Conducting polymers are in general less toxic and potentially less damaging to the environments than many commonly used metals. The most widely studied organic polymers are polyaniline (PANI), polypyrroles (PPY), and polythiophenes (PTH), which are shown in **Fig. 1.9**.

Polyacetylene
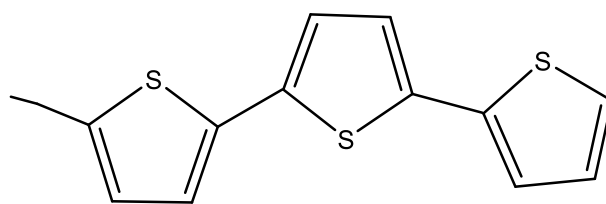
Polythiophene
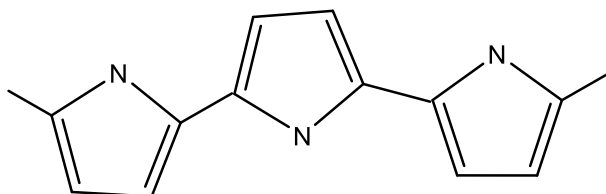
Polypyrrole
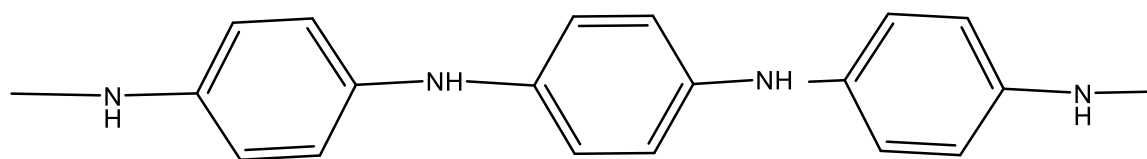
Polyaniline

Figure 1. 9: Some of the well studied conducting polymers

A great deal of research has been done on conducting polymers from the standpoints of chemistry, physics, and material science. Polyaniline, polypyrrole, polyacetylene, and polythiophene are some of the polymers that can be classified as conducting polymers. Because of its stability under normal conditions, polyaniline, also known as PANI was first prepared in 1862 (Letheby, 1862) and produced more than other conducting polymers. There have been several conducting polymers (Hall, 2003; Molapo *et al*., 2012; Pron & Rannou, 2002; Scott, 2010) found so far. Both conducting polymers can be divided into two categories. There are three varieties of conducting polymers based on charge carriers: electron-conducting polymers, proton-conducting polymers, and ion-conducting polymers. Polymers can be divided into different classes based on their chain skeleton (Shah , 2007). The classification of conducting polymers is shown in **Fig.1.10**.

MacDiarmid used conducting polymers for corrosion safety for the first time in 1985, and since then, substantial work has been conducted to research corrosion inhibition on mild carbon steel using various polyaniline and polypyrrole coatings (Ahmad, 2006; Nguyen *et al*., 2004; Nguyen Thi Le *et al*., 2001; Rohwerder & Michalik, 2007). Despite this, the corrosion-prevention function of conducting polymers is little known.

```
                    ┌─────────────────────────┐
                    │  CONDUCTING POLYMERS    │
                    └─────────────────────────┘
                                │
              ┌─────────────────┴──────────────────┐
    ┌──────────────────────────┐      ┌──────────────────────────────┐
    │ Polymers having carbon   │      │ Polymers having no carbon    │
    │ atoms                    │      │ atoms                        │
    └──────────────────────────┘      └──────────────────────────────┘
```
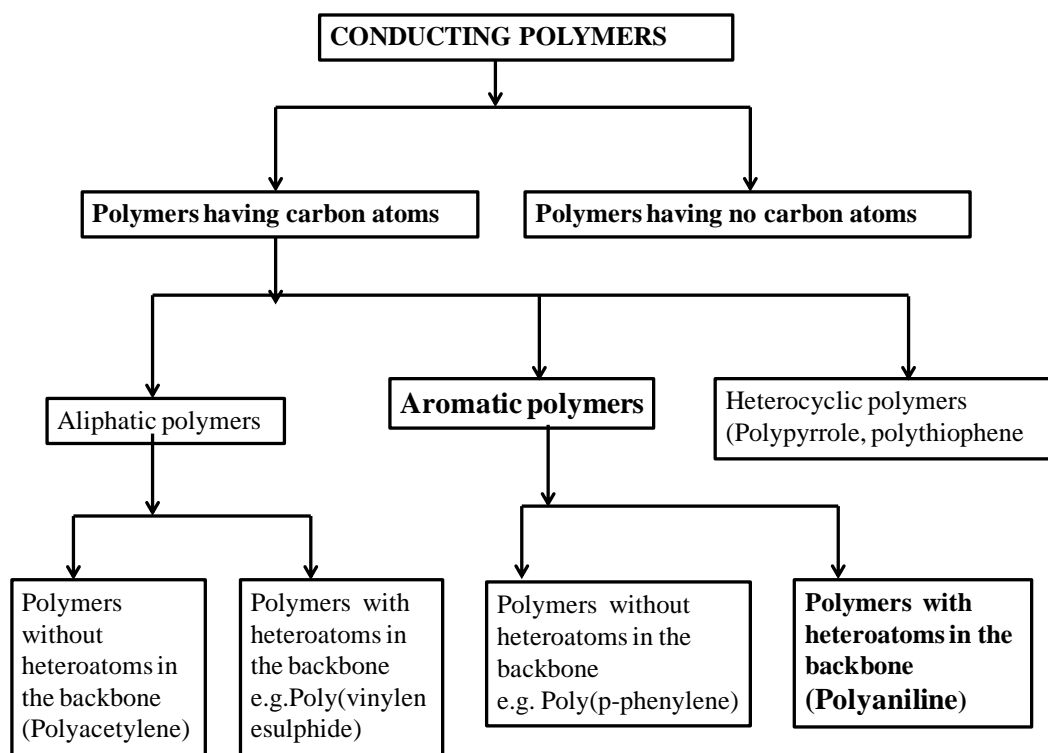
Figure 1. 10: Classification of conducting polymers

One of the most often proposed mechanisms is that conducting polymers have higher oxidation potentials than metals and can react with metals to form a passive layer on the metal surface, which protects the metal by creating a barrier-like passive layer or adjusting the metal's electrochemical potential to a passive range (Ashraf & Shibli, 2007; Hu *et al*., 2006). This process is analogous to how hexavalent chromium-containing coatings shield metal surfaces, making it an appealing alternative to chromate, which is considered to be toxic to humans and the atmosphere.

The most widely used technique for polymerization is based on oxidative coupling. Oxidative coupling involves the oxidation of monomers to form a cation radical followed by coupling to form a di-cation. Repetition leads to the desired polymer. This can be carried out by chemical or electrochemical polymerization. Chemical polymerization is a versatile technique for preparing large amounts of conducting polymers. Unfortunately,

chemical oxidative polymerizations show a number of disadvantages that often result in poor quality polymers.

The aqueous electrochemical method is a cost-effective and environmentally friendly technique to perform conducting polymer coatings. It is extensively used due to its simplicity, and it may be used to form coatings on metal substrates in a single step. It allows for control chemical and physical properties of the coatings efficiently and it can also be easily scaled up for large-scale production. Three different electrochemical techniques can be used to synthesize conducting polymer coatings, including galvanostatic polymerization, potentiostat polarization, and cyclic voltammetry. These conductive polymer coatings can have the same or better properties as the inorganic ones and thus they must allow good adhesion of the subsequent paint layers and make possible some enhancement of corrosion resistance of the painted metal.   The   experimental conditions such as electrode material, electrolyte composition, dopant anion, and pH of the medium have a strong influence on the electro-deposition of conducting polymer.

1.7 Polyaniline (PANI)

Polyaniline (PANI) has been referred to as "aniline black" since the early nineteenth century (Yang & Jenekhe, 1991). It was used to blacken cotton cloth as a dye. Several works (Green and Wdoodhead, 1910; Letheby, 1862) were completed at the turn of the century to resolve the PANI structure. Aniline black was once believed to be an aniline octamer under various oxidation states. It was recently discovered that oxidizing aniline under such conditions creates a polymer. Woodhead and Green were the first to call three simple polyaniline types (described below), and these names are still used today (Green and wdoodhead, 1910).

Polyaniline was discovered as a part of a novel group of macromolecular compounds called conducting polymers in the early 1980s, which was a significant advance in polyaniline science (Diaz & Logan, 1980; Krzysztof Bieńkowski, 2006; MacDiarmid & Epstein, 1989). It has since been the most thoroughly researched polymer in this community. The term "polyaniline" refers to a group of polymers that can be represented using the formula shown in **Fig. 1.11** (MacDiarmid & Epstein, 1989).
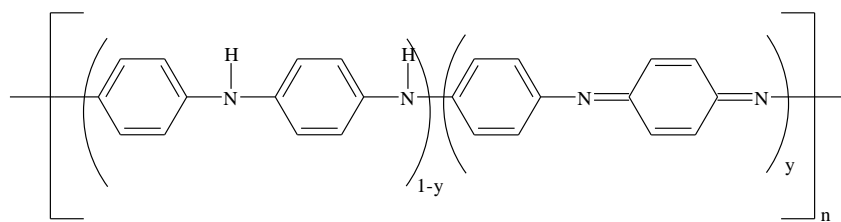
Figure 1. 11: General structural formula of PANI

Polyaniline is one of the most widely studied conducting polymers, since the work of DeBerry (Camalet *et al*., 2000). He found that polyaniline passivated the surface of stainless steel in sulphuric acid when deposited electrochemically. Some other conductive polymers that have been tested are Polypyrrole (PPy), Polythiophene (PTH), and their derivatives. The application of the conducting material takes place directly by electrodeposition in the active material or by the coating of formulated solutions of these polymers. The efficiency and mechanism of corrosion protection is still under study (Ahmad & MacDiarmid, 1996; Inzelt, 2000).

Aqueous electrodeposition of conductive polymers on metals like stainless steel, titanium, nickel, or aluminium have been reported (De Berry, 1985), however, the use of iron, mild steel or zinc as substrates have been less well investigated (Beck *et al*., 1994) despite their technological importance and widespread use in infrastructure. The electrodeposition of conducting polymers on oxidizable metals is not easy, since thermodynamic data predict that the metal will dissolve before the electropolymerization potential of the monomer is reached. Thus, to achieve the deposition of a conducting polymer on steel it is necessary to find electrochemical conditions which lead to partial passivation of the metal and decrease its dissolution rate without preventing electropolymerization.

1.8 Oxidation states of polyaniline

Polyaniline can exist in three oxidation states which are

- Leucoemeraldine, fully reduced form
- Emeraldine, half oxidized form
- Pernigraniline fully oxidized form

These all forms can be represented by a single structural formula as given below
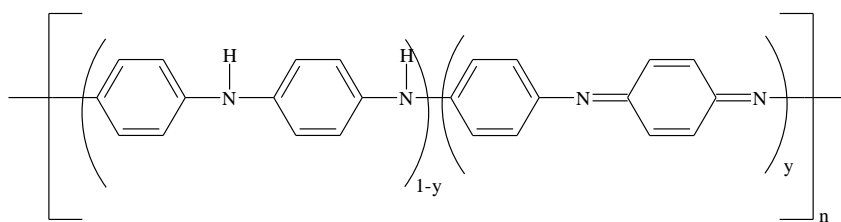
Figure 1. 12: Different forms of PANI (adapted from Bhadra *et al*., 2019; Molapo *et al*., 2012). When, y=0, Leucoemeraldine;y=0.5, Emeraldine; and y=1, Pernigraniline

Polyaniline is unusual in that it can be converted into another state chemically or electrochemically, as seen in **Fig. 1.12**. The oxidation state of the PANI is so vulnerable that even metallic interaction will change its pernigraniline to emeraldine and leucoemereldine (Dhawan & Trivedi, 1991). As seen in **Fig. 1.13**, the color of PANI can also be used to determine its oxidation state. Changes in color and conductivity can also indicate a change of state (Zor & Yakar, 2007). The states of PANI can also be altered by doping with different cations and anions.
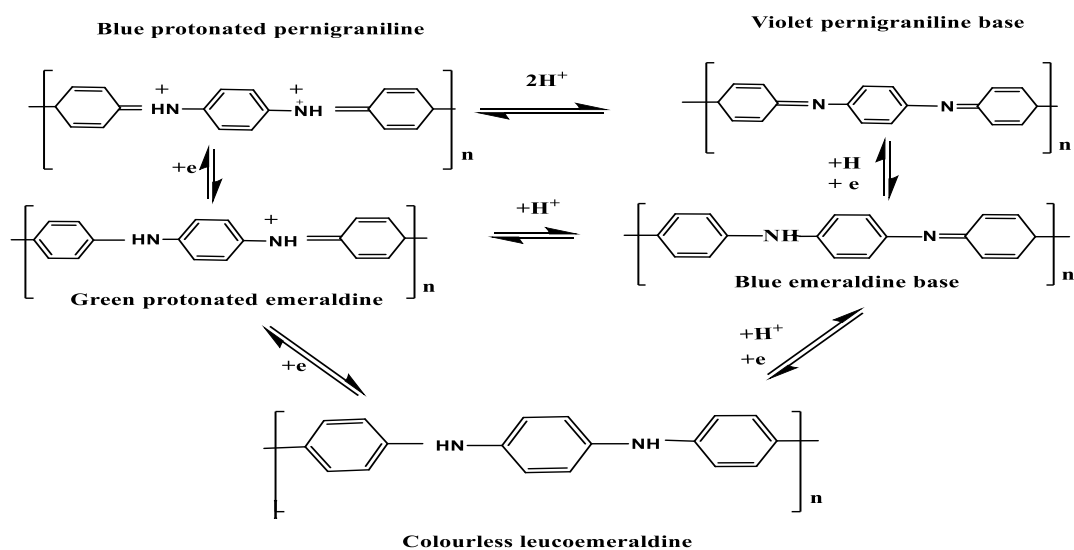
Figure 1. 13: Different form of PANI and its mutual conversion (adapted from Stejskal *et al*., 2010)

The semi-oxidized form of PANI, emeraldine base (dark blue powder with metallic gloss), is stable in air and can be preserved for a long time without chemical changes. The emeraldine form of PANI is extensively studied.

In comparison to other conjugated structures, PANI contributes to conjugation not only by π electrons of aromatic rings (π – π interaction) but also by interactions between lone electron pairs of nitrogen atoms and electrons (π - interactions). Furthermore, in

emeraldine base, there are comparatively close hydrogen bond interactions between amine and imine groups in neighboring chains. The very challenging processibility of polyanilines in their base state is due to these phenomena.

PANI base becomes partial dissolute when solvent–polymer hydrogen bond interactions replace interchain interactions. NMP (N-methyl pyrrolidinone), TMU (tetramethylurea), and DMA (N, N-dimethylacetamide) are some of the solvents that dissolve emeraldine base. The gelation process is observed in concentrated PANI solutions. A mixture of solvents can be used to prevent this process to occur (a combination of electron donors and acceptors that interact with amine and imine groups, respectively).

Conjugation, along with the presence of hydrogen bonds, is the cause of insolubility in the majority of common solvents, as well as the infusibility of PANI. The polymer decomposes slowly without melting at high temperatures (above 400 °C) (Krzysztof Bieńkowski, 2006).

1.9 Conductivity of PANI and its mechanism

The electronic structure of a material determines its electrical properties. The valence band is represented by the Highest Occupied Molecular Orbital (HOMO), and the conduction band is represented by the Lowest Unoccupied Molecular Orbital (LUMO), according to band theory. The difference between these two bands is referred to as the band gap. The width of the band gap determines the electrical properties of a substance. Electronic conduction occurs as electrons from the valence band are excited into the conduction band.

The material remains an insulator when the energy difference between the valence band and the conduction band is on the order of many-electron volts. If the difference is less than 1 eV, the material is called a semiconductor, and if the two bands overlap, the martial is conductor.

Metals conduct electricity due to presence of free electrons and they are also known as electronic conductor. Traditional polymers, on the other hand, have dispersed electrons due to the wide distance between the valence and conduction bands. As a result, their conductivity ranges from 10^{-18} to 10^{-8} S/cm. **Fig 1.14** shows the conductivity of conducting polymers in comparison to other components ranging from quartz to copper. In each aniline of the polymer skeleton, PANI consists of delocalized electrons in the aromatic ring and a lone pair of non-bonded electrons in the N-atom. Between PANI's

valance and conduction bands, there is an energy difference. This allows non-doped PANI to have electrical conductivity. The electrical conductivity of un-doped PANI is comparable to that of semiconductors and/ or insulators.
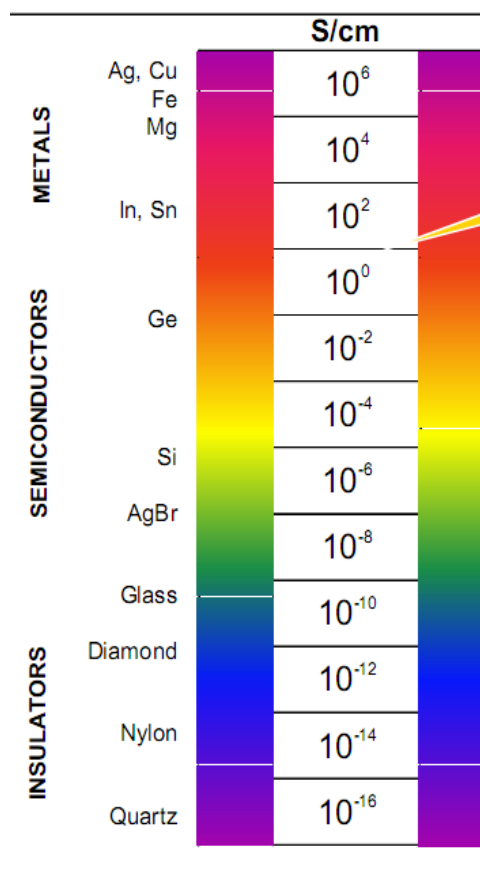
Figure 1. 14: Conductivity of conducting polymers compared to other materials from quartz (insulator) to copper (conductor)

When UV-visible data are used to measure the band gap of different oxidation states, the electronic band structures are connected to one of PANI's oxidation states as shown in **Fig. 1.15**. The PANI in the ES form has three distinct bands: one at 330 nm ascribed to the π- π* band, and two bands in the visible range at 430 and 800 nm related to the π - polaron band and polaron-π* band transitions. PANI emeraldine base form has a low wavelength π - π* band and a strong absorption band at 600 nm, which is attributed to a local charge transfer between a quinoid ring and the surrounding imine-phenyl-amine units (intramolecular charge transfer excitation) (Molapo *et al.*, 2012).
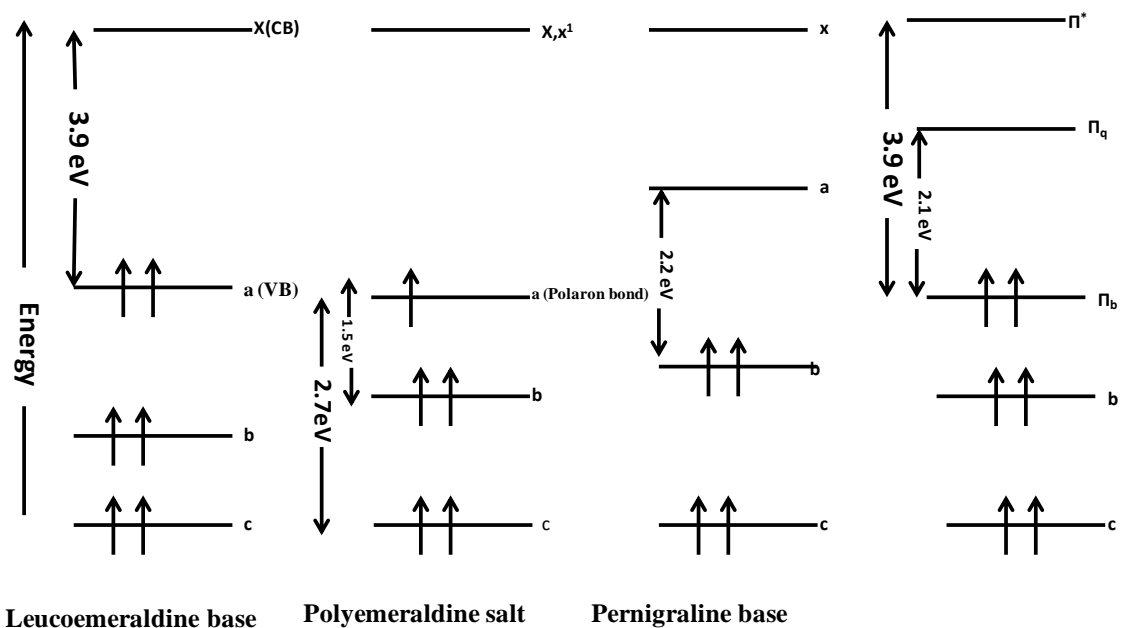
Figure 1. 15: The different band gaps present in PANI redox states (Molapo *et al.*, 2012)

The electrical properties of PANI are altered by chemical doping. Chemical doping of conducting polymers differs from semiconductor doping in that in semiconductors, electrons are inserted (n-type) or withdrawn (p-type) from the valence band keeping the entire structure stays rigid but in conducting polymers, electronic excitations are followed by disturbance or relaxation of the lattice surrounding the excitation, resulting in defect states along the polymer chain. This is redox doping (Pron & Rannou, 2002). The other doping method is non-redox doping, which uses protic acid to increase the number of electrons shared with the polymer chain following doping. Several important factors influence the electrical activity of protic-doped polyaniline. Individual chain properties, inter-chain interactions, chain-dopant interactions, structural disorder, sample morphology, sample preparation conditions, handling, and grafting (Huang & MacDiarmid, 1993; Stejskal *et al.*, 2010) are just a few examples. Polyaniline doped with camphor sulphonic acid has yielded extremely high conductivity (200-400 S/cm) while remaining stable. Doping with metal cations (Dimitriev *et al.*, 2005; Smertenko *et al.*, 2004) compositing, and copolymerization all affect PANI conductivity. This is attributed to morphological changes in the samples.

The mechanism of conductivity of emeraldine base is better explained by molecular orbital theory as described earlier. The conductivity of PANI differs from that of most electroconducting polymers because the radical cation is formed at the nitrogen atom, whereas in electroconducting polymers the radical cation is formed at carbon. Nitrogen,

on the other hand, is also used in the conjugated double bond system. As a result, the electrical conductivity of polyaniline is affected by both the degree of oxidation and the degree of protonation (Genies & Tsintavis, 1985; Pron & Rannou, 2002).

In PANI, defects such as solitons, polarons, and bipolarons serve as charge carriers and support electrical conductivity. Solitons are solitary wave defects with zero spin that can be charged or neutral. A radical cation or polaron is formed when an electron is separated from a polymer chain. The hole formed in the valance band does not delocalize in this case. The charge is borne through the chain by the polaron, which has high mobility. Bipolaron is generated when another electron is separated from the polaron. Bipolaron has higher stability than polaron because of the +2e charge and zero spin. Unpaired electrons at nitrogen atoms are referred to as cation radicals, but they are simply polarons. The polaron lattice, which is responsible for the high conductivity of polyaniline in the form of emeraldine salt, is generated by redistribution of polarons along the polymer chain (Gordon G. Wallace, *et al*., 2008). Even though both bipolaron and polaron theoretical models of emeraldine salt conductivity have been proposed (Gordon G. Wallace, *et al*., 2008; Tanaka *et al*., 1990), it was recently confirmed that, aside from the lack of spineless bipolarons in polyaniline, formation of polarons as charge carriers explained high conductivity of PANI (Mu & Kan, 1998). Conductivity of PANI is dependent on the doping (proton) stage, as previously stated (Chiang *et al*., 1978; Gordon G. Wallace, *et al*., 2008). When compared to polyaniline in the form of emeraldine salt, polyaniline reaches its maximum conductivity at a doping degree of 50% (Tanaka *et al*., 1990).

The amine and imine content of the emeraldine base is equal. It forms emeraldine salt when doped with acid, in which the imine sites are protonated to form bipolar one or dication. This demonstrates that the conductivity of PANI is highest in the emeraldine salt type. Some amine sites are protonated for higher doping levels, and some imine sites are left unprotonated for lower doping levels. Thus, the polaron conductivity model describes the drop in conductivity when emerald salt is oxidized to pernigraniline and then reduced to leucoemeraldine. The conductivity order of magnitude ranges from 10^{-2} S cm^{-1} for undoped emeraldine to 10^{3} S cm^{-1} for doped emeraldine salt (Gordon G. Wallace, *et al*., 2008; Inzelt, György, 2008).

The conjugated bindings in PANI shift about due to defect movement, forming quinoid units rather than benzene units. As seen in **Fig. 1.6b**, quinoid units have a smaller

bandgap and higher energy in the valance band than benzene units. As a result of the doping of PANI, the sum of quinoid units and hence the conductivity increases.

Mathai *et al*., (2003) have identified a Schottky form conduction system in plasma polymerized PANI as an ionic conductivity.

1.10 Polymerization of aniline

Conducting polymers can be synthesized by chemical or electrochemical polymerization method. Chemical polymerization is a versatile technique for preparing large amounts of conducting polymers but it has several disadvantages that often result in poor quality polymers.

The aqueous electrochemical method is an environmentally friendly and cost effective technique to achieve conducting polymer coating. It is widely applied owing to its simplicity and it can be used as a single step method to form coatings on metal surfaces. It allows efficient control of chemical and physical properties of the coatings and it can also be easily scaled up for large-scale production. These conducting polymer coatings can have the same or better properties as the inorganic ones and thus they must allow good adhesion of the subsequent paint layers and cause some betterment in corrosion resistance of the painted metal. Electrochemical polymerization of aniline results in the deposition of polyaniline (PANI) directly onto the metal surface which acts as a corrosion protection coating. The electrodeposition of conducting polymers on oxidizable metals appears to be a cheap alternative treatment since it utilizes the environmentally safe electrodeposition bath.

The oxidative coupling method is the most commonly used. The oxidation of monomers to form a cation radical is followed by coupling to form a di-cation in oxidative coupling. The ideal polymer is obtained by repetition. Chemical or electrochemical polymerization processes may be used to do this.

1.10.1 Chemical Polymerization

Chemical polymerization (Rimbu *et al*., 2006) is a simple and versatile method for producing huge quantities of conducting polymers. Chemical synthesis can be done in an acidic medium with a solution containing the monomer and an oxidant. Formic acid, oxalic acid (CH_3COOH), hydrochloric acid (HCl), sulfuric acid (H_2SO_4), phosphoric acid (H_3PO_4), nitric acid (HNO_3)' is the most commonly used acids(Sathiyanarayanan *et al*., 2008). Oxidants include ammonium persulfate (($NH_4)_2S_2O_4$), potassium dichromate

($K_2Cr_2O_7$), cerium sulfate ($Ce(SO_4)_2$), sodium vanadate ($NaVO_3$), potassium ferricyanide ($K_3(Fe(CN)_6)$), potassium iodate (KIO_3), ferric chloride ($FeCl_3$), auric chloride ($AuCl_3$), copper nitrate ($Cu(NO_3)_2$), copper chlorate ($Cu(ClO_4)_2$) hydrogen peroxide (H_2O_2), and several lewis acids (Devkota, 2016; Prasutiyo *et al.*, 2020; Vivekanandan *et al.*, 2011). PANI film is oxidized to pernigraniline in the presence of ammonium persulfate (APS), while PANI film is not fully oxidized to pernigraniline in the presence of an organic oxidant. Polymers in their doped and conducting state are formed as a result of oxidative chemical polymerizations. By exposing the substance to a strong reducing agent such as ammonia or hydrazine, the neutral polymer may be isolated. Chemical oxidative polymerizations have the advantage of forming soluble polymers as heterocyclic and other aromatic monomers are correctly substituted. Orthodox analytical methods can be used to determine the primary structure of these polymers. The design of the polymerization conditions also facilitates scale-up and large-scale polymer processing.

Unfortunately, chemical oxidative polymerizations have several drawbacks (Shah, 2007) that lead to low-quality polymers. For example, Lewis's acid-catalyzed polymerizations result in the oxidized polymer, which is believed to be more stable, precipitating from the polymerization medium and restricting the degree of polymerization. Furthermore, the use of strong oxidizing agents will cause the polymer to over-oxidize and eventually decompose. Another problem of this approach is that the polymer is generated by a solvent with an excess of oxidant and a medium with a higher ionic strength. As a result, there are impurities in the products that are difficult to remove.

1.10.2 Electrochemical Polymerization

For the preparation of electrically conducting conjugated polymers, electro-polymerization is a popular oxidative process. Smooth, polymeric films can be electrochemically synthesized onto conducting substrates and their electrical and optical properties can be conveniently measured using a variety of electrochemical and coupled in situ techniques. A three-electrode cell with a working electrode (WE), a reference electrode (RE), and a counter electrode (CE) or auxiliary electrode (AE) is a standard electrochemical technique. Wes may be made out of a variety of materials. Iron, mild steel, chrome, nickel, copper, palladium, titanium, silver, indium-tin-oxide coated glass plates, and stainless steel is the most widely used as Wes (El-Shazly & Al-Turaif, 2012). Polymer films can also be grown using semiconducting materials such as n-doped silicon, gallium arsenide, cadmium sulphide, and semi-metal graphite (Zor & Yakar, 2007). A

saturated calomel electrode (SCE) or an Ag/AgCl electrode is often used as the reference electrode (RE). A gold or platinum wire or graphite electrode is usually used for the CE or AE. Aqueous or organic solutions can be employed for electrochemical synthesis. Electrochemical monomer polymerization on an electrode surface has several benefits over chemical methods.

- Purity of the product
- low processing costs and technological simple
- clear regulation of the thickness of the polymer films deposited on WEs
- the doping level can be controlled by varying the current and potential overtime
- polymer synthesis and deposition can be done simultaneously;
- the deposited films are easily characterized using UV-visible, infrared, and Raman spectroscopy
- the doping anion incorporated with polyaniline acts as a passive layer stabilizer when the method is used

A single coat of polyaniline often offers the same level of protection as three layers of conventional coating. This results in a significant saving of materials and expense. As a result, this method of preparing electrically conducting polymers becomes the preferred method.

1.11 Modes of electro-polymerization of aniline

Aniline can be electrochemically polymerized in a variety of ways. The approach chosen is determined by the aim of the study and available techniques. The following are some of the methods used for this purpose (El-Shazly & Al-Turaif, 2012; N. Huang *et al*., 2008; Subathira & Meyyappan, 2011):

- **Anodic Polarization**: The deposition mechanism of the PANI formation is studied by anodic polarization.

- **Cyclic Voltammetry:** In this method, the potential is swept between two potentials. Oxidation and reduction reactions in forward and backward scans are studied, as well as the coating of metallic surfaces to prevent corrosion can be achieved.

- **Potentiostatic:** A constant potential is selected where polymerization occurs or completes, and the metal surface in the electrolyte is exposed for polymerization. This method produces a uniform layer.

- **Galvanostatic:** This method is similar to potentiostatic but a constant current is chosen. This method is preferred because a uniform and fine coating can be achieved.

- **Potential Pulse:** Four potential pulses are used to electropolymerized aniline. Equlibriumization of the cell takes place at zero potential. At 0.6V formation of Emeraldine salt takes place. Then the next polymerization takes place at 0.8-0.9V for the proper deposition of polyaniline. Again at 0.3V polyaniline transforms to Emeraldine salt form. The time of each potential selection depends upon the experimental condition.

1.12 Factors affecting the electropolymerization of aniline

Electrochemical polymerization of aniline onto metal surface requires low pH (1-2) as the oxide layer of metal is not stable in this pH range and allows direct deposition of PANI onto a metal surface. The experimental conditions such as electrode material, electrolyte composition, dopant anion, and pH of the medium have a strong influence on electropolymerization.

1.12.1 Doping Anion

Aniline polymerization is carried out electrochemically in strongly acidic aqueous electrolytes. The conjugate base of the acid is described by the doping anions introduced in polyaniline. Doping of anion plays a direct role in the formation of PANI salts *i. e.* emeraldine salt or prenigraniline salt. In imine nitrogen, it resides as anion and maintains electroneutrality. The presence of a type of anion has a direct influence on PANI morphology, conductivity, electrochemical activity, and the polymerization itself. The degree of doping depends upon the type of acid used.

The presence of oxalate ion for the electrodeposition of PANI helps to form a passive layer on oxidizable metal surfaces like mild steel, aluminum. Also, the anion of PANI affects the ion-exchange selectivity.

1.12.2 Electrolyte Composition

Electrochemical Polymerization of aniline is also achieved in non-aqueous solutions such as acetonitrile, but aqueous solutions are more preferable because of their environmental and economic benefits. Acid solutions such as sulphuric acid, phosphoric acid, and oxalic acid are commonly used. Solvent plays an important role in the development of PANI various forms. Polymerization is influenced by aniline and electrolyte concentrations, as well as deposition time. Surfactants, such as CTAB, and emulsifiers, affect the film morphology. Metal cation involvement has a strong influence on film morphology. This is due to the interaction of metal cation with imine nitrogen of PANI skeleton.

1.12.3 Electrode Material

Aniline can be easily polymerized electrochemically using inert electrodes such as platinum, copper, various graphite, carbons, or indium-tin-oxide glasses. But it is very difficult to polymerize aniline onto active metals such as iron, mild steel because metal dissolution occurs before polymerization. However, the primary reason for using active metal for polymerization is to prevent corrosion. Therefore an appropriate electrolyte must be found that allows for strong passivation of the metal without inhibiting further electrochemical polymerization. As a result, there are many ways to polymerize aniline on active metal surfaces. Oxalic acid is the most common electrolyte used in the electrochemical deposition of polyaniline on steel and aluminum (Camalet *et al*., 1996; Camalet *et al*., 2000; Martyak *et al*., 2002). Oxalic acid forms iron-oxalate as a primary coating on the metal surface on which polymerization occur. Any of the solutions include aniline polymerization on mild steel with polypyrrole pretreatment and using a PANI and polypyrrole composites. PANI has also been coated with p-sulphonic acid, sodium benzoate, and other chemicals. Recently, it was discovered that phenyl phosphinic acid can form extremely adherent PANI on mild steel surfaces.

The nature counter electrode has also been discovered to play an important role in electrodeposition.

1.13 Mechanism and Kinetics of Electropolymerization of Aniline

Both the mechanism and the kinetics of aniline electrochemical polymerization have been thoroughly studied (Inzelt, 2000). It is believed that the polymerization is initiated by the oxidation of the aniline to a radical cation (stabilized by resonance) which involves

following four steps. The mechanism suggested by Molapo *et al.*, (2012) is summed up as follows:

Step I: Oxidation of Monomer

Oxidation of aniline to a radical cation is stabilized by resonance forms. This step is the slowest in the reaction which is the rate-determining step
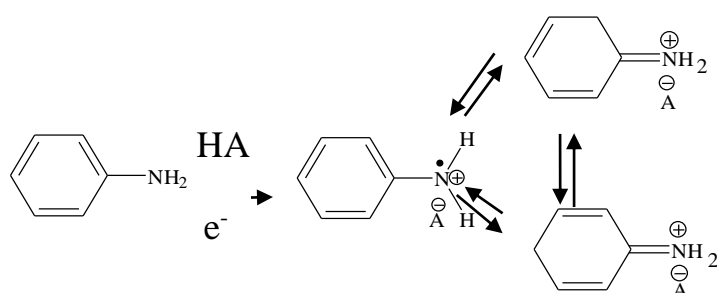
Figure 1. 16: Oxidation of monomer during electrochemical polymerization of aniline

The oxidation of aniline is an irreversible phenomenon that occurs at higher positive potentials than the redox potential of polyaniline (Inzelt & György, 2008)

Step II: Radical coupling and re-aromatization

The head-to-tail coupling of the N- and para-radical cations help this step, which results in the formation of a dicationic dimer. This dimer is then proceeds to re-aromatization, which allows it to return to its neutral state, yielding p-aminodiphenylamine as an intermediate (PASPA). As a result of this process, two protons are also ejected.
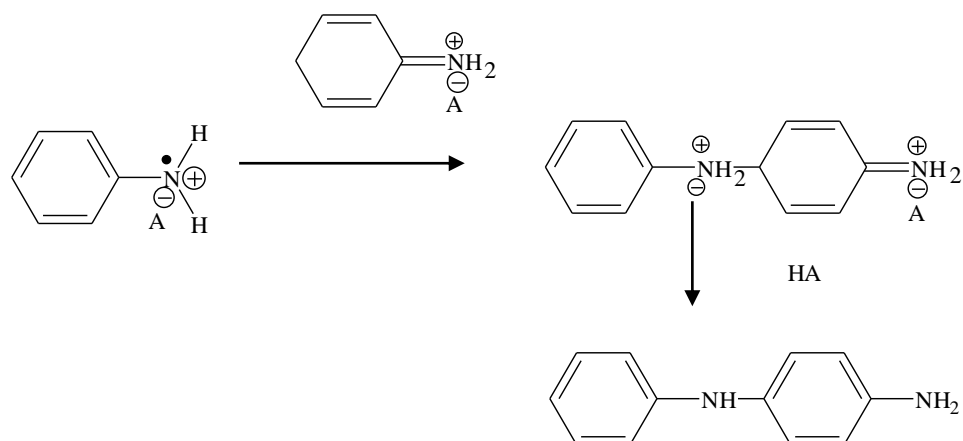
Figure 1. 17: Radical coupling and re-aromatization during electrochemical polymerization of aniline

Step III: Chain propagation

The dimer is oxidized to a radical cation in the propagation process, and it can then couple with the radical cation produced by the oxidation of the monomer or another dimer-type radical cation.
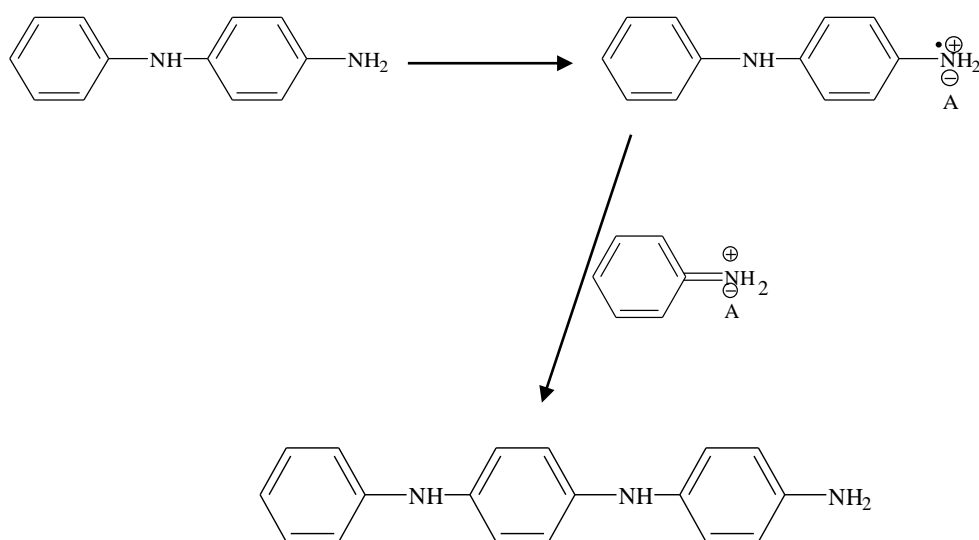
Figure 1. 18: Chain propagation during electrochemical polymerization of aniline.

Step IV: Oxidation and doping of the polymer

The following reaction shows the oxidation and doping of the polymer during an electrochemical polymerization reaction in an acid solution which dopes the polymer to yield PANI/HA.
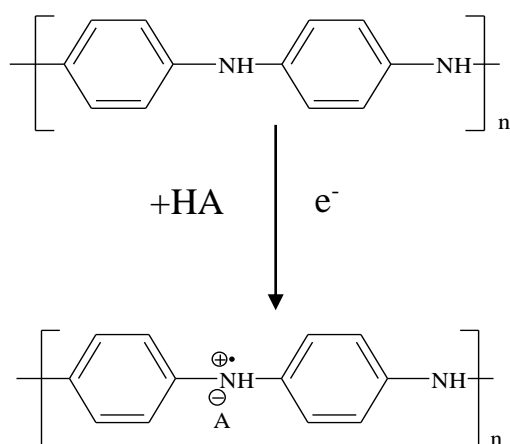
Figure 1. 19: Oxidation and doping of the polymer during electrochemical polymerization of aniline.

1.14 PANI as Corrosion Inhibitor

Corrosion inhibitor is a compound used to prevent the oxidation of metals; it may be a surface coating, a paint undercoat, an additive, or a part alloyed with the metal. According to ISO 8044, a corrosion inhibitor is a chemical compound that can decrease the rate of corrosion in a corrosion system with the presence of a limited amount of the corroding agent without changing the concentration of the corroding agent. Polyaniline, a conducting polymer, serves as a corrosion inhibitor The inhibition action of PANI and substituted aniline is due to interaction of π -electron cloud of the aromatic ring and unshared electrons on N-atom of aniline and steel surface by vacant d-orbital leads to the formation of co-ordinate bond between Fe-N. This PANI layer prevents direct interaction between the metal and the corrosive atmosphere, allowing corrosion prevention. PANI can be applied to the steel surface in two ways to protect it from corrosion.

- Oxidative polymerization and subsequent coating using different agents like NMP, ECO acrylic paint, epoxy-coal tar etc.

- Electrochemical deposition onto metal surface

Since the oxidation potential of mild steel is much lower than that of aniline, electropolymerization of aniline on oxidizable metal is difficult. As a result, melting of the metal occurs before electropolymerization begins. As a result, it is crucial to find an electrolyte that will result in less metal dissolution and more electropolymerization.

1.15 Corrosion protection by PANI

De Berry (1985) reported that electrodeposited PANI film was able to reduce the corrosion rate of stainless steel by forming an oxide layer between the metal and PANI. Due to several possible oxidation states of PANI and different experimental parameters in the study of corrosion protection, it is difficult to predict the universal corrosion protection mechanism. Every special condition should be analyzed separately. Among the several possible mechanisms of corrosion protection of PANI on steel are essentially three types.

- Barrier properties (involving a physical action)

- Corrosion inhibition (involving a chemical action)

- Anodic protection (involving an electrochemical action)

1.15.1 Barrier protection mechanism

Metal oxidation occurs as anodic reaction

$$Fe \longrightarrow Fe^{++} + 2e^-$$

The presence of PANI on metal surfaces makes proper availability of water and oxygen than needed for corrosion. So, the cathodic reaction occurs as

$$H_2O + \tfrac{1}{2} O_2 + 2\,e^- \longrightarrow 2\,OH^-$$

The electrons generated at the anodic site go through the metal to the cathodic site. On the other hand, the flow of hydroxyl ions across the PANI layer, *i. e.* from inside to outside or lateral diffusion, hinders mobility. As a result, the cathodic reaction is reduced. Thus net corrosion rate of the metal is lowered.
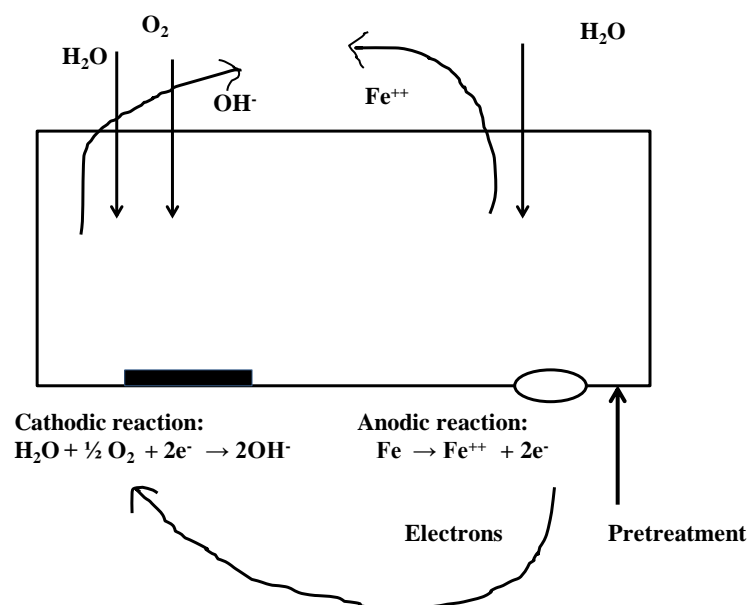
Figure 1. 20: Cartoon of the barrier corrosion protection mechanism (Deflorian, 2012)

1.15.2 Corrosion Inhibition Mechanism

The presence of organic compounds in contact with the metal surface could affect both anodic and cathodic reactions. In this case, the organic compound is called an inhibitor. The organic coating forms hydrophobic film attached to the metallic surface which provides a barrier layer against the attack of corrosive ion and results decrease in the dissolution of the metallic surface (Hinton *et al.*1991).
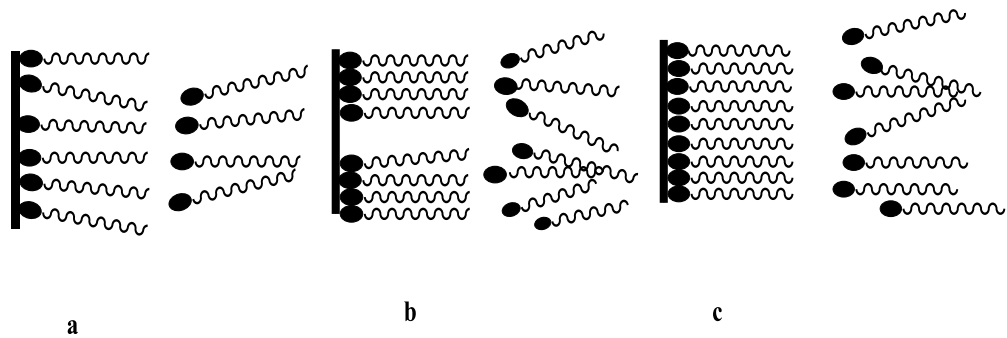
Figure 1. 21: Steps of adsorption of inhibitor (Deflorian, 2012)

1.15.3 Anodic Protection Mechanism

Anodic protection is a corrosion protection strategy based on an anodic polarization by controlling the potential in a zone where the metal tends to be passive. Anodic protection indicates that the OCP of the metal surface is shifted to a more positive direction. Different researchers have explained the anodic protection mechanism differently. Some of them are:-

a. Formation of metal/PANI complex

According to this mechanism, the metal oxidizes to form a metallic oxide at the interface which is an anodic reaction and the cathodic reaction is the reduction of PANI. PANI is lately re-oxidized either by atmospheric or oxygen from the solution. This theory invokes that organic coating shifts the potential of metal to the Nobel direction where metal tends to be passive. The general anodic protection mechanism of ICP is as described by Kinlen *et al.*, (1999) shown in the following equation

$$1/n \text{ M} + 1/m \text{ PANI}^{m+} + y/n \text{ H}_2\text{O} \longrightarrow 1/n \text{ M(OH)}_y^{(n-y)+} + 1/m \text{ PANI}^0 + y/n\text{H}^+$$

$$m/4\text{O}_2 + m/2 \text{ H}_2\text{O} + \text{PANI}^0 \longrightarrow \text{PANI}^{m+} + m \text{ OH}^-$$
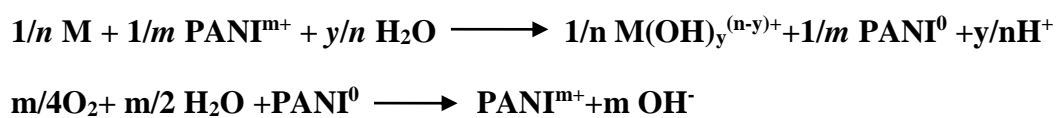
Where, M is metal, and PANI is polyaniline polymer.

b. Wesseling scheme of anodic protection of PANI (Deflorian, 2012)
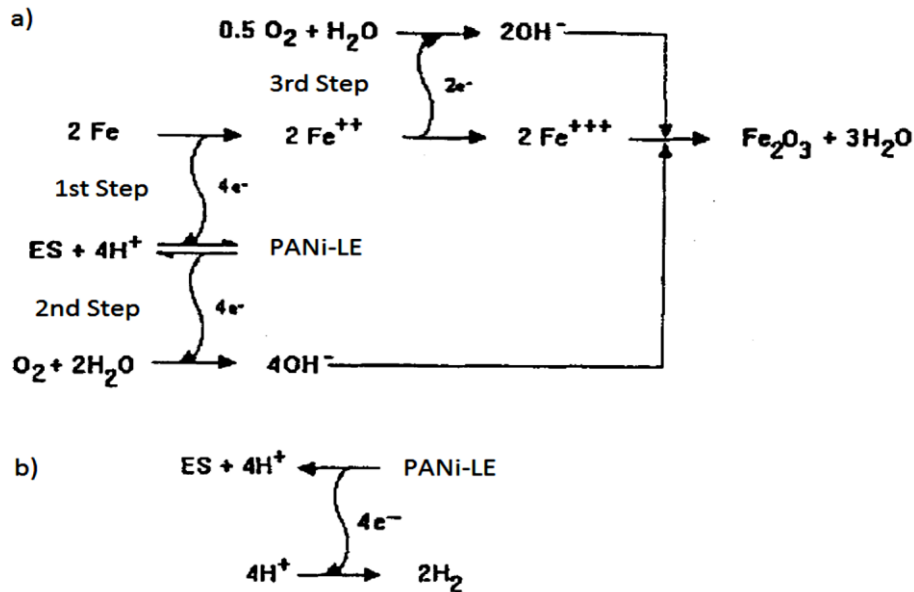
Figure 1. 22: Wesseling model for the corrosion inhibition of PANI (Deflorian, 2012)

c. Ormecon model
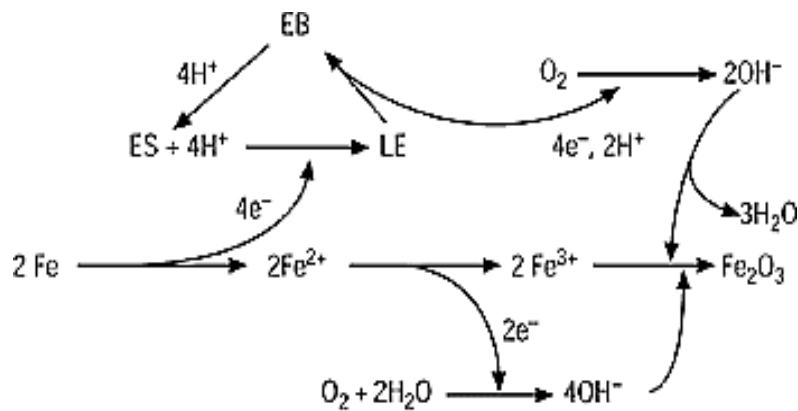
Figure 1. 23: Ormecon model for the corrosion inhibition of PANI adapted from Ananda Kumar *et al.*, (2008)

d. Schauer model

An anodic corrosion protection mechanism has been proposed by Schauer (adapted from the source Deflorian, 2012). According to him, the cathodic reaction interface moves from the metal surface to the PANI surface since PANI is conductive and electroactive. Metal oxidation occurs in this anodic reaction, while PANI reduction and oxygen reduction occur in the cathodic reaction. This PANI can be oxidized again. The metal ion

and PANI form a complex, which reduces the reduction reaction. The cathodic reaction slows down, lowering pH and stabilizing metallic oxide on the metal surface.

The figure shows layers labeled: Mild Steel with $Fe \rightarrow Fe^{++} + 2e$, PANI Primer, Top Coat with $H_2O + \frac{1}{2}O_2 + 2e^- \rightarrow 2OH^-$, and Medium. Labels: Interface I, Interface II, Interface III.
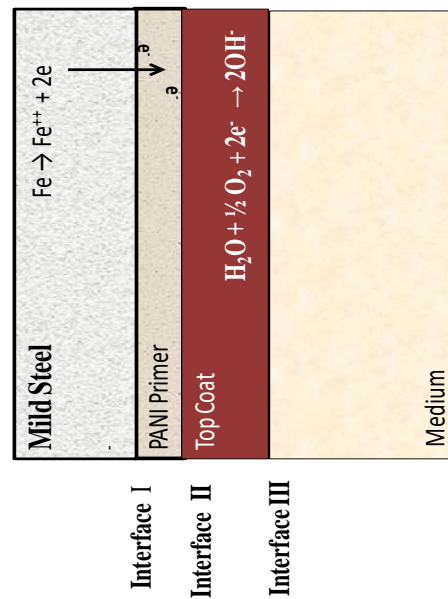
Figure 1. 24: Schauer PANI protection mechanism (Deflorian, 2012)

e. Souza Model (de Souza, 2007)

A blend formed by camphor sulphonate-doped polyaniline powder in m-cresol was used by Souza for iron. It has been observed that the formation of a passive film between the polymeric coating and the metallic substrate is the essential condition for protection. Metallic cations form a passivating complex with the dopant anion, which improves the barrier property of different metals modified polyaniline coating system.

$E \rightarrow L + $ CSA$^-$

Oxidation (M^{n+})
Reduction (CSA$^-$)

M^{n+} CSA$^-$ → [MOCSA]complex

$M \rightarrow M^{n+} + ne^-$

E = emeraldine
L = leucoemeraldine
CSA$^-$ = camphorsulphonate anion

Polyaniline acrylic blend coating
Coating/interface
Metal
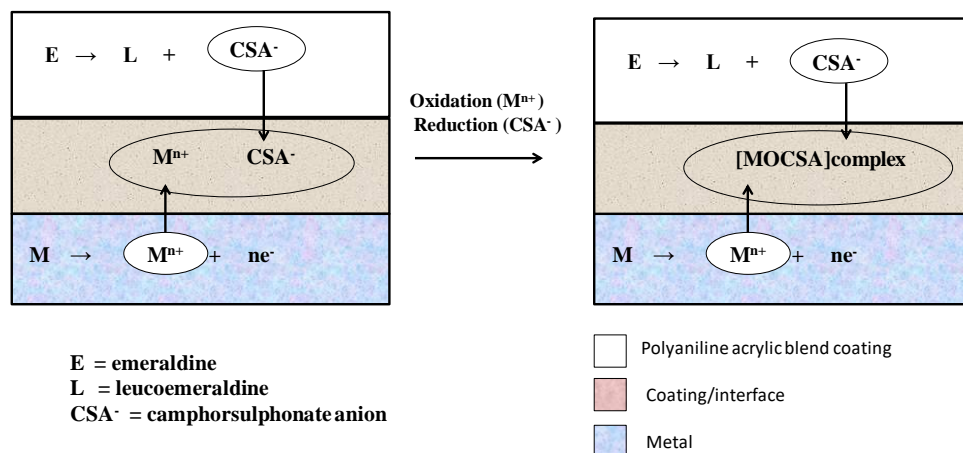
Figure 1. 25: Schematic diagram of the mechanism of metal passivation by polyaniline acrylic bend coating

1.16 Rationale

Corrosion causes massive loss of materials, resulting in human and property loss. As a result of corrosion, the economic loss is estimated to about $2.5 trillion, or around 3.4 percent of world GDP (*NACE International Institute IMPACT PLUS*, 2020). Many attempts are made to minimize the vulnerability of the components as the most feasible way of minimizing the impacts of corrosion. The fundamental strategy of corrosion prevention is to ensure the long-term viability and integrity of the structures and to reduce huge economic loss incurred by it. Hence, corrosion inhibitors are an efficient and cost-effective way to prevent corrosion in a variety of aqueous conditions for numerous alloy systems, including aluminum, zinc, and steel. However, due to increasing environmental concerns and regulations restriction, the use of traditional inhibitors is being discouraged due to their harmful effects on humans and nature during their manufacturing and usage. Therefore, there is a need to find alternative corrosion-resistant coatings that are both ecologically benign and less hazardous. Therefore, a lot of research has been done in recent years to try to meet this need. It has been about two decades since conducting polymers have been researched as an alternative to chromium and phosphate based coating. There has been good progress in achieving good coating on some metals. However, the results are not satisfactory for active metals and steel due to poor mechanical and bad anticorrosion properties. Therefore, more research is needed to achieve desirable corrosion protection coatings on steel. Thus, the reason behind this study is;

    (i)   Corrosion is a real problem in terms of economy loss.

    (ii)   Conducting polymer is a green coating.

    (iii)   Little known about the role of passivating agent on the effect of anti-corrosion process of conducting polymer.

    (iv)   No such study has been done in Nepal so far. Therefore such study is significant for academic and industrial applications.

1.17 Research Objective

General Objective of the study is:

This study is undertaken to find a good anticorrosion coating for mild steel (MS) based on polyaniline as conducting polymer. The polymerization parameter such as supporting electrolytes, concentration, and the dopant concentration and the dependence of the

morphology and conductivity of the passive film and its effect on the polymerization will be investigated.

Specifically objectives of the study are:

1. To study the effect of electrolyte on passivation of mild steel surface
2. To optimize the electrolyte composition, dopant type and additives for better polymerization of aniline
3. To characterize the interface layer between metal and polyaniline layer
4. To observe the effect of parameters such as electrolyte compositions on polymerization, morphology and conductivity of film
5. To propose the polymerization mechanism
6. To study the performance of polyaniline against corrosion in various media

CHAPTER 2

2. LITERATURE REVIEW

Alchemists have tried and failed throughout history to transform base metals into noble metals. Early efforts to prevent metal degradation were mainly scientific and focused on the application of organic and metallic coatings. Metal corrosion inhibitors have been identified since the middle ages. There were obvious safeguards in place to protect metallic structures built by early artisans, often at the cost of a great deal of time and effort. There are various practical techniques for protecting metals from corrosion. Changing the environment is the most common method for corrosion protection. Corrosion inhibitors are the means by which this is achieved. The use of polymeric compounds as corrosion inhibitors has increased dramatically over the last three decades. Polythiopene (Pth), polypyrrole (Ppy), and polyaniline (PANI) are examples of conducting polymers that have opened up new possibilities in the field of anti-corrosive organic coatings. Among the many conducting polymers available, the most promising conducting polymers are polyaniline and polypyrrole for corrosion protection (Zor & Yakar, 2007). Polypyrrole (PPy) has been the most studied coating (Beck *et al*., 1994; Hulser & Beck, 1990) since it requires a relatively neutral pH, for which it is easier to find a passivation state of zinc and iron.

The most investigated conducting polymer (CP) is polyaniline (PANI)), a promising polymer due to its excellent environmental stability, simplicity of synthesis, and high electrical conductivity (Abdel-Gaber *et al*., 2020; Masdarolomoor *et al*., 2019; Popović & Grgur, 2004; D. Sazou *et al*., 2007). In corrosion protection, the PANI film involves coatings, which work as a primer layer in a coating system. The PANI has an excellent potential to replace toxic metal, such as chromates, in corrosion protection and is considered a green anti-corrosion candidate (Boshkova *et al*., 2019; Wang *et al*., 2020; Zhu *et al*., 2018).

Polyaniline (PANI), a recognized conducting polymer, has been electrochemically prepared in aqueous acidic and neutral media onto active metals (Fe, Zn, Cu, Al, Ni) (Ananda Kumar *et al*., 2008; Kartsonakis *et al*., 2012; Lacroix *et al*., 2000; Özyılmaz *et al*., 2005; Rayati & Arefinia, 2020; Sazou & Georgolios, 1997; Zor & Yakar, 2007). Generally, a good PANI coating is obtained in acidic media with low pH (Camalet *et al*., 1996). However, if the substrates are active metals, the electropolymerization of aniline

becomes a challenge as the dissolution of metal leads oxidation of aniline (Camalet *et al*., 1996; Deberry, Viehbeck, 1984). These problems can be solved by developing electrochemical conditions that reduce metal dissolution rate by forming a partial passivation layer at a potential lower than the potential of aniline monomer. Under such conditions, the function of electrolytes in electropolymerization is significant. It should only passivate the metal surface partially and allows the passage of charge so that oxidation and subsequent polymerization of aniline can be achieved on the passivated metal surface.

Despite such difficulties, electrodeposition of conductive PANI films on mild steel from an aqueous nitric medium has been achieved but the coating was found to be not good (Roth, 1995). A better result was obtained by Wessling and coworkers (Roth, 1995; Wessling, 1994) who reported that mild steel sheets dip-coated with PANI showed a real improvement in their behavior in a corrosive medium.

DeBerry (1985) was the first to realize electrochemically depositing PANI as corrosion inhibitor on stainless steel which reduced the rate of corrosion in acidic media. Camalet *et al* (Camalet *et al*., 1996) discovered that the development of passive Fe(II)-oxalate PANI films with a layer of oxalic acid resulted in highly adherent PANI films with a layer of oxalic acid. Steel was well-protected in acidic chloride solutions. The next year, Ahmad and MacDiarmid (Ahmad & MacDiarmid, 1996) discovered that chemically deposited PANI had the ability to bind to other molecules

The primary ambiguity is the PANI coating's poor adherence to active metal surfaces. A PANI coating by using mineral acid electrolytes has been reported to produce a weak adhesion onto MS surface, hence low corrosion inhibition (Abdiryim *et al*., 2005). However, PANI formation using oxalic acid as an electrolyte produced an adhesive and functional anti-corrosion coating (Camalet *et al*., 1996; Fusalba & Bélanger, 1999). It is reported that the electropolymerization of aniline on MS surface can be achieved by various electrochemical methods employing different electrolytic solutions such as oxalic acid ($C_2H_2O_4.2H_2O$) (Camalet *et al*., 1996), sodium benzoate (C_6H_5COONa) (Popović & Grgur, 2004), sodium salicylate ($C_7H_5NaO_3$) (Pawar *et al*., 2006), perchloric acid ($HClO_4$) (Fomo *et al*., 2016), phosphoric acid (H_3PO_4) (Ganash *et al*., 2011), sodium oxalate ($Na_2C_2O_4$) (Özyılmaz *et al*., 2005), benzene sulphonic acid ($C_6H_6O_3S$) (Dhawan & Trivedi, 1991), p-toluene sulfonic acid ($C_7H_8O_3S$) (Dhawan & Trivedi, 1991),

acetonitrile (C_2H_3N)–lithium perchlorate ($LiClO_4$) (Tüken *et al.*, 2004), etc. with suitable mechanical and anti-corrosion properties.

Tüken *et al.*, (2004) synthesized polyaniline on mild steel (MS) in acetonitrile–$LiClO_4$ for corrosion protection. Polyaniline film could not be obtained on mild steel by direct electro-oxidation of aniline in $LiClO_4$ containing acetonitrile medium, because sufficient passivity of the surface could not be achieved; therefore, a primer coating was used. The optimum conditions for the electro-preparation of polyaniline and polythiophene films in acetonitrile solutions containing anhydrous acid have been reported (Bazzaoui *et al.*, 2004; Can *et al.*, 2000)

Bernard *et al.*, (1999) demonstrated that PANI deposited from metanilic acid produced a better copolymer coating. This is because metanilate is incorporated into the polymeric backbone. Later, in their analysis, Moraes *et al.*, (2003) discovered that after the electrodeposition of polyaniline on stainless steel, it acts as a corrosion inhibitor in a 3% NaCl solution, as shown by a significant change in the corrosion potential to noble values. A variety of the same relevant patents have emerged over time (Herrasti, 2003). The application of PANI directly to the metal surface, on the other hand, is not recommended through electrodeposition is the main issue face by most researchers. This is because the electrodeposition of PANI on metals requires a very low pH, necessitating an acidic medium, and achieving adherent PANI on the metal surface is also a problem in the electrodeposition of polyaniline.

Wessling & Posdorfer (1999) investigated the durability of polyaniline as a primer and then sealed with various topcoats using EIS in 1998 and discovered that the steel was extremely corrosion resistant. Many other studies have shown that using polyaniline as a primer, in combination with an epoxy or other topcoat provides effective corrosion resistance. Multiple layer coatings should be avoided, according to Talo *et al.*, (1997), since mixing polyaniline with topcoat is a more realistic solution. They found that various forms of polyaniline mixed into epoxy coatings effectively protected mild steel from corrosion in a saline solution.

Huh *et al.*, (2003) concluded with Talo *et al.*, (1997) that several layer coatings cannot be used in coating formulations. They discovered that polyaniline blend coatings are excellent coating materials for protecting iron from corrosion. PANI adhesion to mild and galvanized steels is weak, according to Araujo *et al.*, (2001), and this lack of adhesion

contributes to poor results even though PANI is applied with a top coat. This demonstrates that when PANI is applied directly to a metal surface, it has low adhesion, which can impair its ability to inhibit corrosion.

By blending PANI with epoxy, better adhesion can be obtained because epoxy increases the adhesion of the coating to the substrates due to the presence of —OH bonds. Including the fact that all of the studies focused on mixing polyaniline with epoxy. These studies used a high concentration of polyaniline in their coatings. Laco *et al*., (2005) investigated the use of polyaniline to protect carbon steel from corrosion. The amount of polyaniline applied to the alkyd resins was varied up to 6% by weight. An analysis of polyaniline-containing paint for corrosion protection was conducted by Samui & Phadnis (2005).

PANI can be used in paint formulations up to 20% by weight. It was reported that one of the reasons for the long delay in putting polyaniline into practice was its toxicity where adequate doping and development of stabilized polyaniline are needed insolubility. In order to make room for the use of nanoparticles, dispersion of coatings must be considered.

According to Armelin *et al*., (2007), conducting polymer (CP) is added at a very low concentration (less than 1% by weight) already adequate in terms of providing adequate corrosion resistance to the substrates They demonstrated in their study that a modified PANI provided the best results. The corrosion safety was used even when the PANI concentration was very low (0.3 wt%). However, they did not differ the volume of PANI in the coatings and the epoxy used often comprises a solvent mixture and anticorrosive additives (Zn dust) of which the introduction of these compounds into the atmosphere is undesirable because they are not biodegradable.

Akbarinezhad (2014) also stated that only 1 wt.% of PANI was added in the PANI epoxy blend coating and this coating formulation was proven to be effective in inhibiting corrosion of steel in sodium chloride solution.

Kamaraj *et al*., (2009) used the same volume of benzoate doped polyaniline. In their research on the corrosion safety of iron, paint formulations discovered that in neutral media, the coating protects steel better than in acid media. Previous studies, obviously, did not differ the amount of PANI in their coatings. As a result, the precise selection of PANI that can provide adequate protection is unknown.

Özyılmaz *et al*., (2005) used oxalic acid solution to electrochemically synthesize polyaniline (PANI) on Ni (Nickel) plated mild steel (MS) and unplated mild steel (MS) under cyclic voltammetric conditions. Ac impedance spectroscopy and anodic polarization curves were used to test the corrosion efficiency of PANI coated and uncoated electrodes in 3.5 % NaCl. The PANI top coat gave significant resistance to the MS/Ni electrode, while the polymer layer reduced the porosity of the Ni coating. The corrosion resistance of Ni plating with PANI top coat (MS/Ni/PANI) was higher and provided protection for much longer periods, according to the findings.

Ananda Kumar *et al*., (2008) investigated the formation of polyaniline (PANI) and PANI–metal bilayer coatings as a method of mild steel corrosion safety. Electropolymerization of aniline in an oxalic acid medium formed the PANI sheet. The PANI + Ni and PANI + Zn hybrid layer coatings were prepared by sequential deposition of the PANI layer followed by electrodeposition of the metal layer. The PANI layer was porous by itself, but the porosity of the PANI + Ni and PANI + Zn bilayer coatings was greatly reduced due to the metal clusters' ability to fill the PANI layer's pores.

Electrochemical impedance spectroscopy with Nuquist and Bode plots, as well as potentiodynamic polarization experiments, is used to assess the coatings' efficacy in preventing corrosion. Scanning electron microscopy was used to investigate the morphology of the polymer and polymer–metal bilayer deposits. The corrosion protection provided by the PANI layer was provided by a barrier layer mechanism, and the level of corrosion protection provided by it was reduced due to its porous nature. The deposition of metal nanoparticles or clusters filled the pores of the PANI layer in PANI + Ni and PANI + Zn bilayer coatings, increasing their corrosion resistance. Between the two types of PANI–metal bilayer coatings studied, PANI + Zn coating offered better corrosion resistance compared to that of PANI + Ni.

Polyaniline (PANI) and poly (N-methyl aniline) (PNMA) had been electrodeposited on mild steel from an oxalic acid bath using cyclic the voltammetric technique. The development of electroactive polymer compounds on mild steel was verified using Fourier transform infrared spectroscopy. (Narayanasamy & Rajendran, 2010) had studied the corrosion resistance behavior of mild steel in 3.5 percent NaCl solution by PANI and PNMA using potentiodynamic polarization and electrochemical impedance spectroscopy. The results show that copolymer coatings and composite-bilayer coatings have better

corrosion resistance than homopolymer coatings. Better corrosion protection was exhibited by metal–PANI–PNMA than the metal–PNMA–PANI layer.

Sakhri *et al*., (2010) examined the anticorrosion properties of mild steel sheets coated with plasticized chlorinated rubber and active pigments such as polyaniline emeraldine salt or zinc phosphate. Salt spray and immersion tests in a 3.5% NaCl solution were used to compare them. Electrochemical impedance analysis was used to evaluate corrosion inhibitory activity, and the results showed that polyaniline outperformed zinc phosphate in terms of corrosion safety. Fourier transform infrared - attenuated absolute reflectance spectroscopy was used to characterize polyaniline pigments.

A simple composite of PANI and Polypyrrole was electrodeposited on stainless steel by Subathira & Meyyappan, (2011) for corrosion protection. Results showed that the deposition time and monomer concentration has a direct impact. Also, corrosion potential was shifted to a more positive direction on compositing. Ding *et al*., (2002) used PANi-thiokol rubber composite for the corrosion inhibition of mild steel and found that the corrosion potential of the composite was about 100mV more positive than that with PANI alone.

Sathiyanarayanan *et al*., (2006) used PANI blended with coal tar for corrosion protection of steel. PANI-PO$_4$ was found with efficiency. This might be due to redox property. Nanocomposite of PANI with clinoptilolite was prepared Olad & Naseri, (2010). The anticorrosive properties of a 20µm thickness coating of the composite with various weight ratios of clinoptilolite content on iron coupons showed enhanced anticorrosive properties. H. Huang *et al* prepared PANI/CeO$_2$ composite and found that PANI/ CeO$_2$ is not a blended mixture but there exists a strong interaction at the interface of CeO$_2$ and PANi. This fact was evidenced by the increase of conductivity of the composite. The maximum conductivity obtained was 11.68 S/cm at 17.5 wt% of CeO$_2$ compared to 3.78 S/cm for PANI

The type of solvent and the concentration of metal cation as a dopant is found to influence the PANI layer. Izumi *et al*., (2010) noticed that the solvent has a great effect on the doping Fe (III) on EB-PANI to its different oxidation state. The formation of ES-PANI is favored in DMF while PB- PANI is formed in a greater extension in NMP and DMA. In acidic m-cresol, only ES-PANI is produced in Fe(III) /EB-PANI. Izumi *et al*., (2010) also noticed the effect of Eu(III) on the PANI skeleton is both concentration dependent and

molar ratio dependent. With concentrated solution, there is no coordination between the metal cation and PANI skeleton. But at low concentration EB-PANI oxidizes to PB-PANI.

Thus from these studies, it is seen that metal cations can be used to improve PANI layer and thus be used as an anticorrosive membrane. Jeyaprabha *et al*., (2006) studied the effect of Ce^{4+} on PANI formation in oxidative polymerization. The Ce^{4+} ion on PANI was found to form complexes with transition metal ions and thereby change the morphology and structure and enhance the corrosion inhibition. The enhanced performance of PANI in presence of Ce (IV) may be due to the formation of metal amine complex with more quinoid moiety which facilitates strong adsorption and higher coverage of the metal surface. Sathiyanarayanan *et al*., (2008) studied the influence of metal cations Zn^{2+} and Mn^{2+} on the inhibitive effect of PANI. They found that metal cations interact directly with PANI via protonation of imine nitrogen atom of quinoid group on PANI and induce chemical and conformational change. The presence of metal cation was found to have enhanced corrosion inhibition. The higher inhibition efficiency of PANI in presence of metal cation is due to the electron rich benzoid group.

Shabani-Nooshabadi, (2015) electrochemically synthesized a homogeneous and adherent polyaniline/zeolite nanocomposite (PZN) coating on a copper (Cu) in a sodium oxalate solution. Three stages (electro-adsorption of monomer and electrolyte and initiation of passive film formation, growth and impingement of the passive film and decomposition of the latter, and formation of composite coatings) were observed during the formation of PZN coatings, and three periods relevant to these stages were recorded. The PZN coating offered effective protection (99.2% in a 3.5 wt% NaCl solution). The PZN-coated copper had a much lower corrosion risk than bare copper (about 130 times).

Nautiyal & Parida, (2016) compared the electrodeposition of PANI coatings on carbon steel from oxalic acid and sodium salicylate electrolyte mediums. The film formation was found to be medium-dependent. The nature of the PANI film formed was influenced by the degree of passivation in oxalic acid. The passivation curve was not observed in the salicylate medium. The films in this medium were clear and adhered well. By comparing the CV in the oxalic acid and salicylate mediums, the deposition rate in the former medium was observed to be faster, as the current value in the oxalic acid medium is one order higher.

Mahato & Cho, (2016) reported the synthesis of highly crystalline graphene integrated polyaniline nanostructured composites as corrosion protection coatings. In 0.1 M HCl, the corrosion current on the coated surface decreased by 3–4 orders of magnitude. The composite coating with the highest graphene loading (1.92 wt%) had the best protection. The coatings formed a physical barrier to the corrosive atmosphere as well as non-wetting properties. The pit-like outgrowths on the coated surfaces (recovered after the experiment) showed a network-like structure in high magnification photographs. These net-like structures are thought to have formed as a result of weaker cross-linking of polymer chains at random locations, allowing solvent molecules to pass through Owing to the optimum and uniform dispersion of the graphene nanoflakes in the composite structure, which enables improved surface coverage, better protection of the steel was achieved.

W. Li, (2018) studied the corrosion behavior of electrochemically synthesized the PANI/c-MWCNTs on the surface of MS. Despite the comparatively high corrosiveness of the medium (acidic solution) concentration, these nanocomposite coatings were found to provide effective corrosion resistance for mild steel. The nanocomposite coatings effectively shielded against corrosion by forming a robust interface between the MS configuration and the polymer during electrodeposition, effectively blocking corrosive ions.

Al-Owais & El-Hallag, (2019) deposited PANI on stainless steel (SS) by cyclic voltammetric technique. In 0.5 M, 1 M, and 2 M H_2SO_4 aqueous acid solutions, the voltammetric findings showed that the PANI serves as a better protective layer on the stainless steel surface against corrosion. The polymerization process required passivation of the substrate and monomer oxidation prior to PANI film formation

Khodaei *et al.*, (2019) investigated the protection performance of epoxy-based nanocomposite coating reinforced by a zeolite complex on mild steel in 3.5 wt% NaCl media. Immersion testing revealed that the epoxy-based nanocomposite coating provides effective and long-lasting protection. Improved-barrier characteristic and ohmic-resistance of used nanocomposite coatings result in improved anticorrosion efficiency of explored epoxy-based nanocomposite coatings. Nanocomposite coating showed 99.72% protection efficiency.

Wang *et al*., (2020) studied the one-step electrochemical synthesis of poly(vinyl pyrrolidone) modified polyaniline coating with controlled microstructure on stainless steel for high corrosion protection performance. The morphology of PVP-PANI coatings was significantly affected by hydrogen bonding interactions between PVP and PANI. The composite coating prepared in a solution containing 1.0 wt% of PVP showed lower roughness and more uniform size of PANI particles, compared with pure PANI coating. Electrochemical measurements revealed that obvious noble shifts in the corrosion potential were observed with composite PVP- PANI coatings.

Rajyalakshmi *et al*., (2020) reported the synthesis and characterization of carbon nanotube (CNT) doped polyaniline (PANI) composites for improved corrosion resistance and electrical properties in steel. PANI–CNT nanocomposites were made by polymerizing aniline in the presence of carbon nanotubes in situ. The thick multilayered chains of CNTs in the 25 wt. % PANI–CNTs sample provided high corrosion resistance. The 25 wt. % PANI–CNT coating on mild steel was found to be good for corrosion resistance, indicating that the steel is protected due to the improved oxygen barrier.

Abdel-Gaber *et al*., (2020) investigated electrochemical polymerization of aniline on stainless steel substrate from different electrolytes. In acetic acid, the maximum rate of deposition was achieved. PANI coating protected stainless steel from corrosion in alkaline solutions, and it may be used as a coating material to shield stainless steel from corrosion in corrosive aqueous solutions. On polymer films, the anions acetate and oxalate have a stabilizing effect.

Xue *et al*., (2020) prepared the copolymers of polyaniline/polythiophene (PANI/PTH) by an electrochemical method on a stainless steel surface containing both aniline and thiophene in a 0.3 mol/L oxalic acid solution. Using polarization curve analysis and electrochemical impedance spectroscopy (EIS), the anti-corrosion efficiency of the PANI/PTH on stainless steel surfaces was investigated in acidic media. Scanning electron microscopy (SEM) was also used to examine the surface morphology of PANI/PTH composite conductive copolymers. The PANI/PTH copolymers firmly adhered to the stainless steel surface, according to the findings. In comparison to bare stainless steel, composite conductive copolymers of PANI/PTH on the stainless steel surface produced strong anti-corrosion behavior; additionally, the corrosion potential was improved by around 400 mV, while the current density in the corrosion media was reduced by two orders of magnitude. The above findings matched the effects of the SEM characterization.

The PANI/PTH had a uniform, dense, and glossy structure, indicating that it had better anti-corrosion action, according to the SEM spectrum.

Polyaniline (PANI)-coated basalt rockwool wastes (BRWs) prepared as fillers to serve in coatings for the anticorrosion analysis were reported by Fang *et al*., (2021). The PANI-coated BRW (PANI@BRW) had improved dispersion stability in many traditional solvents and improved the epoxy resin coating's anticorrosion efficiency. After 30 days of immersion, the coating with 5% fillers was found to have a high protection efficiency of 97.7%. This research not only offers a potential solution to the problems posed by BRW, but it also transforms these wastes into useful materials. Rangel-Olivares *et al*., (2021) synthesized PANI based nanocomposites with metal oxides by in situ chemical oxidative polymerization process and achieved coating on commercial steel. The anticorrosion performance was examined in 3.5% NaCl by electrochemical methods. The electrochemical study showed that the anti-corrosion properties of coatings made with TiO_2ANPs was superior to those synthesized with SiO_2 and CeO_2 NPs

CHAPTER 3

3. MATERIALS AND METHODS

3.1 Materials

Commercial grade mild steel (MS) was purchased from the local market of Kathmandu. Different chemicals used for the experiment were purchased from the local market.

Aniline ($C_6H_5NH_2$), Sodium chloride (NaCl), Sodium sulphate (Na_2SO_4), Sodium sulphite (Na_2SO_3), Sulphuric acid (H_2SO_4), Nitric acid (HNO_3), Oxalic acid ($H_2C_2O_4.2H_2O$), and ethanol (C_2H_5OH) were purchased from Fisher Scientific, India. Sodium orthophosphate ($Na_3PO_4.12H_2O$), succinic acid ($C_4H_6O_4$), sulphanilic acid ($C_6H_7NO_3S$), sodium potassium tartrate ($KNaC_4H_4O_6.4H_2O$), Acetone (C_3H_6O), Dimethyl sulphoxide (DMSO) and benzoic acid (C_6H_5COOH) were procured from Merck, India. Cerrous sulphate $Ce(SO_4). 4H_2O$ was obtained from Loba Chemie Pvt. Ltd and Lathanium nitrate $La(NO_3)_3$ was recieved from Fluka, Switzerland. Aniline was double distilled in the presence of nitrogen gas before use as shown in **Fig. 3.1**. Other chemicals mentioned in this study were used without further purification. Milli water water was prepared at the Central Department of Chemistry, Tribhuvan University, Kirtipur. Different solutions of the required concentrations were prepared in milli water.

Figure 3. 1: Apparatus set up for distillation of aniline

3.2 Preparation of solution

0.5 M NaCl solution: 7.305 g of NaCl was dissolved in distilled water in 250 mL volumetric flask and diluted up to the mark.

0.5 M Oxalic acid: 15.758 g of oxalic acid was dissolved in distilled water in 250 mL volumetric flask and diluted up to the mark.

1 M H_2SO_4: 27.80 mL of concentrated H_2SO_4 was taken in a 500 mL volumetric flask and it was diluted up to mark. 0.5 M H_2SO_4 was then prepared by series dilution.

0.5 M HNO_3: 27.80 mL of concentrated H_2SO_4 was taken in a 500 mL volumetric flask and it was diluted up to mark. 0.5 M H_2SO_4 was then prepared by series dilution.

0.5 M Sodium orthophosphate ($Na_3PO_4.12H_2O$) solution: 23.75 g of sodium orthophosphate was dissolved in distilled water in 250 mL volumetric flask and diluted up to the mark.

0.5 M Succinic acid: 5.904 g of succinic acid was dissolved in distilled water in 100 mL volumetric flask and diluted up to the mark.

0.05 M Sulphanilic acid: 2.165 g of sulphanilic acid was dissolved in distilled water in a 250 mL volumetric flask and it was diluted up to mark.

0.5 M Sodium benzoate: 18.01 g of sodium benzoate was dissolved in distilled water in 250 mL volumetric flask and it was diluted up to mark.

0.5 M Sodium potassium tartrate: 70.555 g of sodium potassium tartrate was dissolved in distilled water in a 500 mL volumetric flask and it was diluted up to mark.

0.1 M Benzoic acid in alcohol: 6.1 g of benzoic acid was dissolved in 3:1 alcohol- water in 100 mL volumetric flask and it was diluted up to mark.

0.5 M Aniline: Aniline was double distilled in the presence of nitrogen gas before use and then 23.04 mL of aniline was taken in a 500 mL volumetric flask and it was diluted up to mark.

Aniline in oxalic acid: 100 mL of 0.1M, 0.2M, 0.3M, and 0.4M aniline in oxalic acid were prepared by taking the required volume of 0.5 M aniline in 100 mL volumetric flask and made up to the mark with 0.5 M oxalic acid solution.

Aniline in sodium benzoate: 100 mL of 0.1M, 0.2M, 0.3M and 0.4M aniline in sodium benzoate were prepared by taking the required volume of 0.5 M aniline in 100 mL volumetric flask and made up to the mark with 0.5M sodium benzoate.

Aniline in sodium potassium tartrate: 100 mL of 0.1M, 0.2M, 0.3M and 0.4M aniline in sod. pot. tartrate was prepared by taking the required volume of 0.5 M aniline in 100 mL volumetric flask and made up to the mark with 0.5 M sodium potassium tartrate solution.

Aniline in benzoic acid: 100 mL of 0.1M, 0.2M, 0.3M, and 0.4M aniline in benzoic acid in 75% alcohol, were prepared by taking the required volume of 0.5 M aniline in 100 mL volumetric flask and made up to the mark with 0.5 M benzoic acid in alcohol as shown in table 3.1.

Table 3.1: Different concentration of aniline solution in BAW

Volume of 0.5M aniline	Volume of 0.1M benzoic acid in 3:1 alcohol	Concentrations of aniline in benzoic acid in alcohol- water	Concentrations of benzoic acid in resulting mixture solution
80.0 mL	20.0 mL	0.4M	0.08M
60.0 mL	40.0 mL	0.3M	0.06M
40.0 mL	60.0 mL	0.2M	0.04M
20.0 mL	80.0 mL	0.1M	0.02M

3.3 Preparation of MS Sample

Commercial grade MS, purchased from Kathmandu, Nepal's local market, was cut into pieces of 3 cm × 3 cm x 0.15 cm, and samples having dimensions 1cm×1cm×0.15cm were cut for surface investigation such as SEM –EDX, AFM. The samples were then polished by a series of silicon carbide (SiC) papers of different grades (#100 to #2000) until the working surface turned smooth as shown in **Fig. 3.2**.After polishing, the abraded samples were cleaned with hexane and ultrasonicated in ethanol for 10 minutes and dried with compressed air before each measurement.
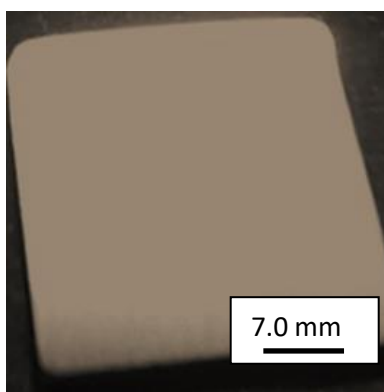
Figure 3. 2: Digital image of polished MS sample

3.4 Electrochemical measurements

3.4.1 Open Circuit Potential (OCP) measurement

OCP also known as the open-circuit voltage (OCV) is one of the electrochemical methods to evaluate the corrosion performance of the organic coatings. It is also the electrode potential at which no net current flows through the external circuit of the electrochemical cell. Using a high impedance voltmeter, the OCP of a corroding metal/alloy is measured as the voltage between the metal/alloy (working electrode) and a reference electrode. It generally occurs between two device terminals when separated from the circuit involving no external load. The voltage difference between a metal introduced in media solution with a suitable reference electrode (generally, standard calomel electrode) can be used to determine the change of OCP over time. The measurement of OCP can give the information about;

- Data for corrosion monitoring in the electrolytic solution.
- Information about the free corrosion potential as the starting point for the application of electrochemical protection methods.
- Information about the passive film formed on the metal surface.
- Data for control of the protection potential during electrochemical protection.
- A method for determining whether the corrosion system is in the active or the passive state.

OCP was recorded for each electrochemical experiment using a Hokuto Denko HA-151 potentiostat controlled by a self-made LabVIEW software interfaced with an IBM computer (S. Neupane, 2013). In a 3-electrode system, MS sample was used as a working electrode, a saturated calomel electrode (SCE) as a reference electrode, and a graphite rod

as a counter electrode as shown in **Fig. 3.3**. Then OCP was recorded for 30 minutes at an interval of 2 minutes before each experiment to get a steady-state condition.
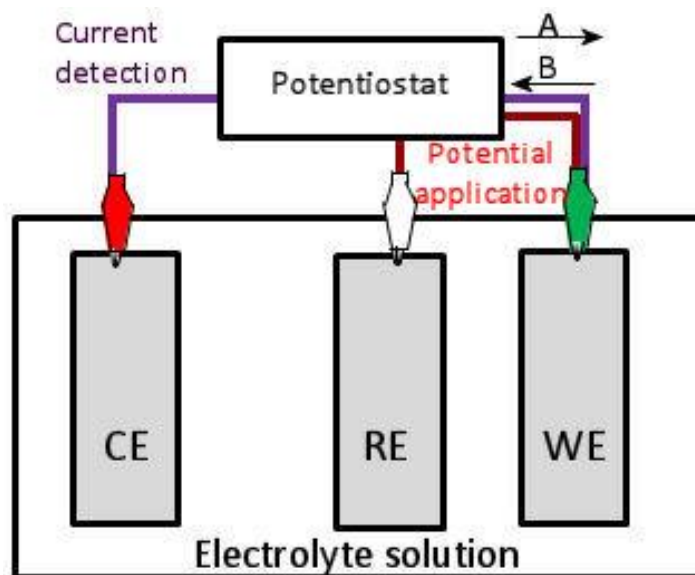
Figure 3.3: Three electrode cell set up

3.4.2 Anodic polarization

Abraded MS samples were applied to electrochemical polarization using a Hokuto Denko HA-151 potentiostat controlled by a self-made LabVIEW software interfaced with an IBM computer as shown in **Fig. 3.4** (Neupane, 2013). A 3-electrode system using MS sample as a working electrode, a saturated calomel electrode (SCE) as a reference electrode, and a graphite rod as a counter electrode were used for the polarization. Open circuit potential (OCP) was recorded for 30 minutes before each anodic polarization to get a steady-state condition. Then, anodic polarization was done in sodium orthophosphate, succinic acid, sulphanilic acid, Na-K Tartrate, BAW, and oxalic acid solutions. The concentration of aniline as a monomer was varied from 0.1 M to 0.4 M. Similarly, the influence of La (III) and Ce (IV) on PANI coating was also studied.

Figure 3.4: Apparatus set up for anodic polarization using Hokuto Denko HA-151 potentiostat

3.4.3 Cyclic voltammetry

Cyclic voltammetry (CV) was also carried out for the optimized concentration composition of polymerization of aniline on MS sample and to check the cathodic stability of the coating. The influence of La (III) and Ce (IV) on PANI coating was also studied. It was carried out with potential ranges from -0.1 to 1.4 V at a scan rate of 20mV/s

3.4.4 Galvanostatic polarization

Deposition of the PANI was carried out galvanostatically, applying an anodic current pulse to a MS immersed in a solution of 0.3M aniline containing 0.2M sodium potassium tartrate (Na-K Tartrate) and 0.3 M aniline containing 0.04 M benzoic acid in 3:1 alcohol-water (BAW) separately. The influence of current densities in the deposition of PANI onto MS was studied

3.4.5 Potentiostatic polarization

Deposition of the PANI was also carried out potentiostatically, applying 1.4 V potential to a MS immersed in a solution of 0.3M aniline containing 0.2M sodium potassium tartrate (Na-K tartrate) and 0.3 M aniline containing 0.04 M benzoic acid in 3:1 alcohol-water (BAW) separately. The influence of La (III) in the deposition of PANI onto MS was also studied.

3.5 Characterization of PANI coating

3.5.1 Attenuated Total Reflectance- Fourier Transform Infra-Red (ATR-FTIR) Spectroscopy

Fourier transform infrared spectroscopy is a method for determining and measuring light emission in the infrared spectrum at different wavelengths. It may also be used as a quantitative tool to determine the sum of ingredients in a mixture and to classify uncertain products. The continuum produces absorption peaks, which frequency are resulting from atom bond vibrations. The sum of each substance present in the substrate is determined by the scale of the peaks.

In ATR-FTIR spectroscopy, an infrared (IR) beam is transmitted through an optically thick ATR crystal. ATR crystal is made up of a high-refractive-index material (usually diamond or germanium) that can provide a high total internal reflection at a particular incidence angle. Internal absorption of the IR beam at the ATR crystal surface produces a momentary wave that reaches through the sample at a depth of penetration (Dp) of 0.5-5 m. The wavelength of IR light, the angle of incidence, and the refractive index of the ATR crystal all influence the magnitude of Dp. Since exiting the crystal, the internally reflected beam is captured by a detector, where it is analyzed and viewed as an ATR-FTIR continuum. ATR-FTIR spectroscopy does not require any further sample preparation. It has several advantages like minimum sample *i. e*. a drop of sample on the crystal, fast and easy to clean the surface of the crystal, and investigation of sample in its natural states. As a result, it is thought to be a good method for testing materials. ATR-fundamental FTIR's theory is depicted schematically in **Fig. 3.5.**

a   b
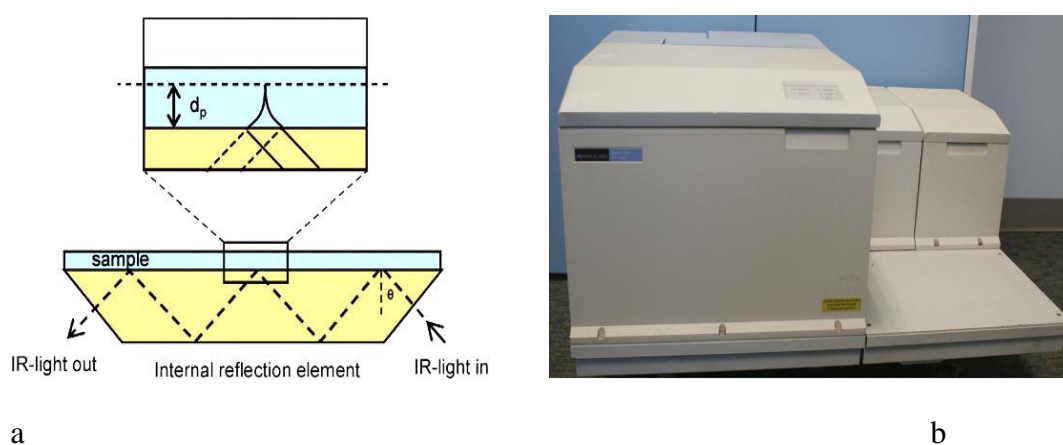
Figure 3.5: a. A schematic illustration of ATR-FTIR principle b.Perkin Elmer Spectrum GX FTIR spectrophotometer

Using a Perkin Elmer Spectrum GX FTIR spectrophotometer, functional groups in polyaniline (PANI) were confirmed by obtaining infrared emission spectra with wavenumber ranges from 500 to 4000 cm-1 in attenuated total reflectance (ATR) mode. A few drops of pure acetone were used to dissolve the PANI coating on the MS sample. The dissolved PANI coating was ultrasonically dispersed in pure acetone for 10 minutes and FTIR characterization was performed.

3.5.2 UV-Visible spectroscopy

UV spectroscopy is the measurement of a beam of light's absorption as it travels through a layer, or of reflectance as the beam of light is reflected at the sample's surface. It is used to investigate a variety of characterization methods, including material absorption, transmission, and reflectivity, as well as optical and electronic properties.

The ultraviolet region varies from 10 to 400 nanometers. It consists of two parts: the near-ultraviolet (quartz) region (200-400 nm) and the far-ultraviolet (vacuum) region (10-200 nm). The visible region ranges from 400 to 800 nm. The excitation of an electron from a lower to a higher molecular orbital is caused by the absorption of electromagnetic radiation in the UV and visible regions (electronic energy level). So, it is also known as electronic spectroscopy because it includes electronic transitions. It is used to detect the existence of conjugated multiple bonds or aromatic rings. The following electronic transitions may occur in UV-visible region:
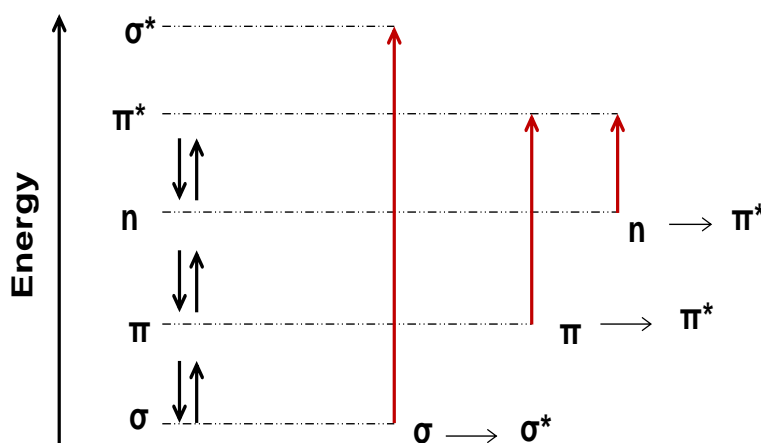
a

Figure 3.6: a. A schematic illustration of electron transition b. Shimazdu UV/Vis spectrophotometer

Each absorption band refers to the energy difference between the ground and excited states. The Planck equation describes the relationship between energy difference and wavelength.

$$\Delta E = h\nu = hc/\lambda \qquad [3\text{-}1]$$

Where E is the energy required to promote an electron from the ground state to the excited state, h is Planck's constant, ν is the frequency, c is the speed of light, and λ is the wavelength. The longer the wavelength of the absorption band, the less energy is needed to excite the electrons, according to Planck's equation. The absorption bands reveal the sample's molecular composition and can vary in wavelength and strength as molecular interactions and environmental factors change.

UV-visible spectrometry follows Lambert-Beer's law. A UV/Vis spectrophotometer records a UV or visible spectrum (**Fig. 3.6**) as a plot of absorbed radiation wavelengths versus absorption rate in terms of absorbance (optical density) A or molar absorptivity (molar extinction coefficient) ε. According to Lambert-Beer's law

$$\log\frac{I_0}{I} = A = \varepsilon c l \qquad [3\text{-}2]$$

Where I_0 is the incident radiation intensity, I is the radiation intensity distributed by the sample solution, and absorbance, also known as optical density, is a measurement of how much something absorbs light. E stands for molar absorptivity or molar extinction coefficient, c for solute concentration (mol/L), and l for sample-path volume (cm). The number of absorption molecules determines the medium. The molar absorptivity at maximal absorption, Ernax or log 10 Emax, is typically used to express the amplitude of

an absorption band in the UV or visible range. λmax is the wavelength at which the highest absorption occurs.

The UV-Vis spectra of the PANI coatings were recorded using a Shimazdu UV/VIS 2600 Spectrophotometer. Shimazdu UV/VIS 2600 Spectrophotometer was used to record UV-Vis spectra of the PANI coatings. The scanning range for the measurement was 200-800 nm at a medium scanning rate and resolution of 1.0 nm. Using pure acetone as a blank, the baseline correction of the spectrophotometer was carried out. A 2.0 mL quartz cuvette with a 1.0 cm path length was used for sampling and all the samples were loaded into it . The PANI coating was taken out in pure acetone by following the procedure applied for FTIR measurement. Here, the dispersed PANI was diluted 10 times with pure acetone to obey Lambert-Beer's law.

3.6 Surface Characterization of PANI coating

3.6.1 Scanning electron microscopy and energy-dispersive X-ray spectroscopy

By scanning a directed beam of high-energy electrons, scanning electron microscopy (SEM) produces an image of a sample. As electrons communicate with a sample, they provide a range of signals that provide information about the sample's surface morphology and chemical composition.

The interaction of a focused, energetic beam of electrons with a sample produces a variety of signals, including secondary electrons (SE), backscattered electrons (BSE), characteristics X-rays, continuous X-rays, and fluorescence X-rays. As incident electrons interact with a sample's atomic nucleus, the electrons deflect elastically across an angle of around 180°, resulting in BSE. The kinetic energy loss in this form of interaction is negligible. Secondary electrons create topographic information about the sample, while backscattered electrons produce images of comparison that hold information about atomic number variations. The higher the atomic number of a sample, the more elastically dispersed BSE it contains, resulting in a brighter picture. In other words, the brighter the region of the BSE picture, the heavier the elements present. The elemental composition of a sample is determined by BSE. When an incident beam of electrons collides elastically with an atom, a poorly bound valence electron of the atom's K-orbital is ejected, resulting in secondary electrons (SE). SEs is the ejected electrons with a kinetic energy of less than 50 eV. The two impulses that are widely used to create pictures are secondary and backscattered electrons.

A scanning electron microscope in ccmbination with an energy dispersion spectrometer (SEM-EDS) was used to characterize a polyaniline (PANI) coating on an MS sample in order to get its functionality, phase, and surface morphology, as well as elemental compositions. A JEM-1200EX electron microscope (JEOL, Tokyo, Japan) was used to record SEM images of PANI at a voltage of 200 kV.

Figure 3.7: JEM-1200EX Scanning electron microscope in combination with an energy dispersion spectrometer (SEM-EDS)

3.6.2 Transmission electron microscopy (TEM)

Transmission electron microscopy (TEM) is a powerful material science technique that involves sending a high-energy beam of electrons into an ultra-thin sample. The interactions between the electrons and the sample are used to analyze characteristics including crystal structure, nanoparticle dispersion in nanocomposites, and microstructures inside biological tissues. TEM may be used to investigate layer development, composition, and flaws. Quantum wells, wires, and dots may be analyzed using high resolution to determine their quality, shape, size, and density.

The TEM works on the same principles as a light microscope, except instead of light, it utilizes electrons. Because electrons have a considerably shorter wavelength than light, the resolution of TEM images is several orders of magnitude greater than that of light microscope images. As a result, TEM may reveal the tiniest details of interior structure, down to individual atoms in some circumstances.

The basic working principle of TEM is that the image is produced on the fluorescent screen or charged coupled device (CCD) by causing electrons to flow through the material, either using the transmitted beam or the diffracted beam as shown in **Fig. 3.8**.

When stream of electrons produced by the electron gun is allowed to fall on the specimen using the magnetic condensing lens, the beam is partially transmitted and partially diffracted depending on the angle of incidence. To produce the image, both of these beams are recombined at the E-wald sphere. The phase contrast image is the result of combining the two images.

An amplitude contrast must be obtained in order to increase the intensity of image and contrast. This can only be accomplished by utilizing the transmitting beam, which eliminates the diffracted beam.

The resulting beam is then transmitted through the magnetic objective lens and the aperture to remove the diffracted beam. The aperture is set so that the diffracted image is no longer visible. As a result, the final image produced only from the transmitted beam is magnified by passing it through the projector lens. A fluorescent screen or CCD is used to record the magnified image. Bright Field image is the image with high contrast. It is also worth noting that the brilliant field image obtained is only due to elastic scattering (no energy change), *i. e.*, transmitted beam alone.

The thicker the material, the more electrons are dispersed, resulting in a darker image, because fewer electrons reach the screen for visualization.

The transmission electron microscopy (TEM) technique was used to illustrate the PANI structure and particle size. TEM images of PANI were recorded on a JEM-1200EX electron microscope (JEOL, Tokyo, Japan) operated at 200 kV. PANI was dispersed in acetone and sonicated. The copper grid was dipped in the PANI dispersed in acetone, dried, and loaded for the characterization.
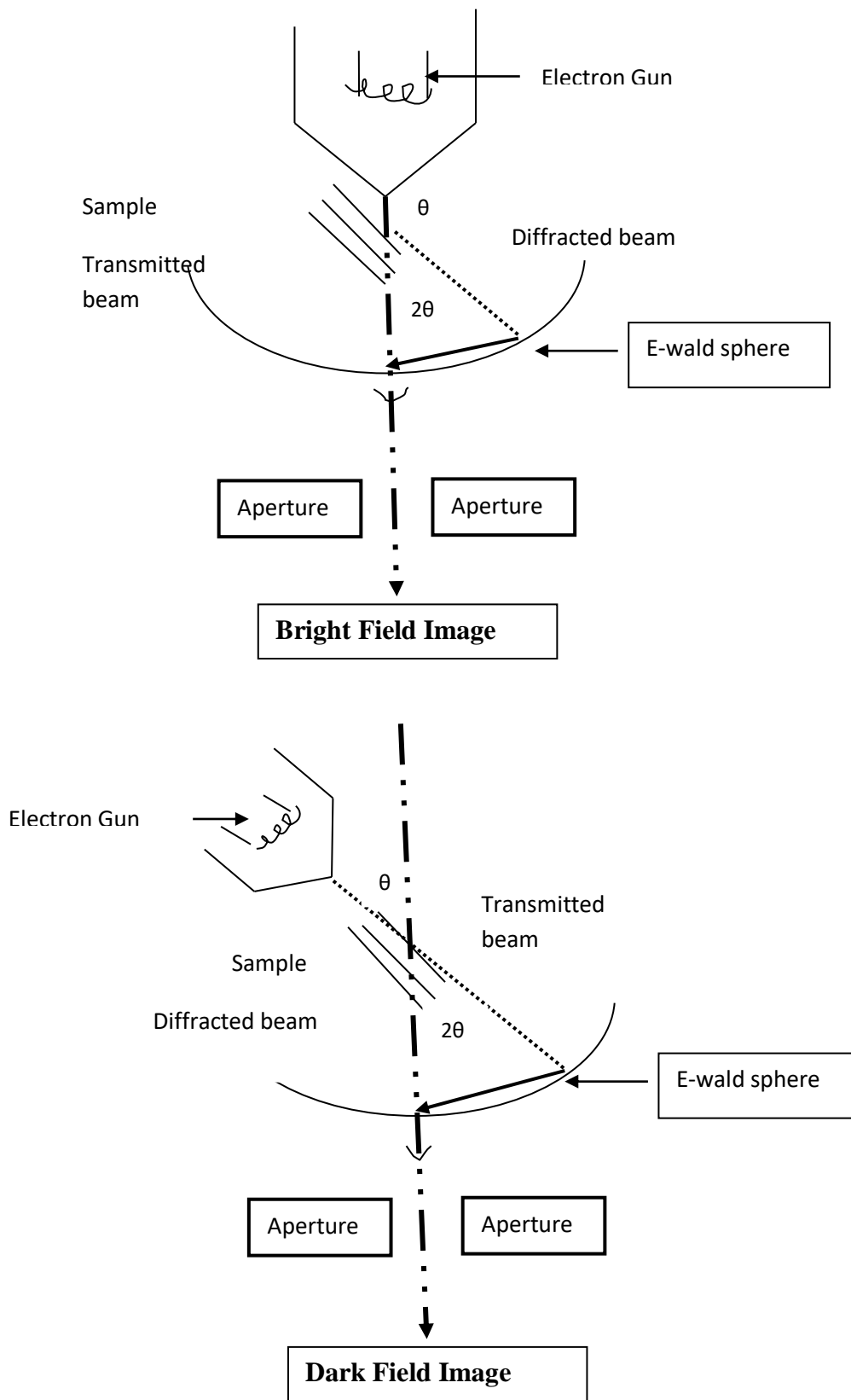
Figure 3. 8: A schematic illustration of TEM principle

3.6.3 X-ray diffraction (XRD)

The analytical technique of X-ray diffraction (XRD) is widely used for the study and characterization of molecular and crystal structure. XRD may also be used to evaluate the qualitative and quantitative detection of different chemical compounds, as well as to measure the intensity/degree of crystallinity of compounds and to detect stacking faults, a type of defect. The diffraction pattern is also useful in the Powder XRD technique for identifying the purity of the sample and determining the occurrence of impurities.

A monochromatic light/beam is directed or moved on a specimen/sample in X-ray Diffraction to determine/resolve structural details of the material in the crystal web. XRD is a common technique for analyzing crystal structure and atomic spacing (the distance between atom nuclei in a material).

The monochromatic light/x-ray and crystal samples are used in XRD. These x-rays are produced by a cathode ray tube and are then filtered to create monochromatic radiation that is collimated and directed towards the sample. The interaction of the incident ray with the sample results in a diffracted ray (constructive interference). This ensures Bragg's Law condition, as given below.

$$n\lambda = 2dSin\theta \qquad [3\text{-}3]$$

Where, λ is the wave length of the rays, θ is the angle between the incident ray and the surface of the crystal, d- Spacing between layer of atoms and n is a whole number integer.

This law is related to the diffraction angle of the crystal sample, lattice spacing (physical size of the unit cell in the crystal lattice), and electromagnetic radiation. Average crystalline size can be estimated using following Debye-Scherer equation [3-4]:

$$\mathbf{D = k\lambda/\beta cos\theta} \qquad [3\text{-}4]$$

Where D is the average crystalline size, k is the Scherer constant, λ is the wavelength of X-ray, β is the peak width of half maximum, and θ is Bragg diffraction angle.

An EMPYREAN diffractometer was used to investigate the crystalline structure of PANI as shown in **Fig. 3.9**. A few drops of DMSO were added to the PANI coating to detach it from the MS surface. The PANI solution in DMSO was spread over a glass plate grid, and then dried at room temperature (RT), and XRD was performed on it. The XRD data was obtained by employing a monochromatic Cu Kα of wavelength 1.5406 Å at an

accelerating voltage of 40 kV and a current of 30 mA. The operating conditionwas 2θ scanning between 5° to 60° at a step size of 0.013º.

Figure 3.9: EMPYREAN powder XRD diffractometer

3.6.4 Atomic force microscopy (AFM)

AFM (atomic force microscopy) is a mechanico-optical instrument capable of detecting forces in the piconewtons (10–12 N) range. AFM, like, many other Scanning Probe Microscopes (SPM), scans the sample with a tip (or, more broadly, a probe) in contact or non-contact with the sample surface, depending on the scanning mode. In constant height or constant force mode, it measures attractive or repulsive forces between the tip and the sample. The probe is a micro-sized cantilever with a tip at one end; a piezodriven unit moves the probe over the sample (or vice versa) in three dimensions with nanometric precision; a way to track the tip location as it moves; and a feedback mechanism controls how quickly the tip slides or taps over the sample surface. As a result, AFM has become an important tool for studying the morphology of the nanoworld. Furthermore, as a force transducer, the cantilever has been extensively used to analyze surface and molecular interactions."

The scanning modes, also known as image acquisition modes, refer to the distance maintained between the probe (tip) and the sample while scanning, as well as the directions the tip travels on the sample's surface and the pressures between the sample and tip. There are three different modes available: non-contact, contact, and tapping.

The tip deflection changes the path of the reflected laser beam for surface imaging, changing the intensity difference between the top and bottom sets of photodetectors (AFM signal).

The morphology and the roughness of the coatings were determined by using NT-MDT atomic force microscopy (AFM) at a scan size of 5μm as shown in **Fig. 3.10**. The roughness and rms values were noted for each coating that was tested.

Figure 3. 10: NT-DMT Atomic force microscope

3.6.5 Optical microscopy

A polarizing microscope is a type of microscope that investigates the optical properties of specimens using polarized light. Polarized light is transverse wave light with a directional vibration. A polarizing plate (polarizing filter) or polarizing prism is a device that polarizes light. The method is often used to convert natural light to linearly polarized light. There are two kinds of polarizing microscopes: those that use reflected light and those that use incident light. The optical microscope is shown in **Fig. 3.11**.

Figure 3.11: Optical microscope, Radical Scientific, India, reflection mode with an attached USB ProCam

The surface morphology of the PANI coated MS surface was observed using a light polarizing microscope, Radical Scientific, India, running in a reflection mode with an attached USB ProCam . The images were recorded for the PANI coatings before and after polarization tests.

3.7 Corrosion study

3.7.1 Corrosion study by potentiodynamic polarization

The most commonly used electrochemical technique for the corrosion testing is the potentiodynamic polarization measurement. It is a simple and rapid deciding technique for assessment of corrosion current, corrosion potential, corrosion rate, and efficiency of corrosion protection. This methodology can provide important details regarding corrosion mechanisms and the susceptibility of certain corrosion materials in specific settings. The potentiodynamic polarization approach entails adjusting the potential of the working electrode across a large range at a required rate while monitoring the current generated as a function of time or potential (Pierre, 2008). Depending on the direction of polarization, the change in potential causes an oxidation or reduction process on the electrode surface to create current. In other words, potentiodynamic polarization is the process of determining the current-potential relation of the sample. As the potential is changed away from the corrosion potential, the current response is monitored. To polarize the electrode of interest, a three-electrode corrosion system is applied.

The working electrode becomes the anode when the potential in the polarization is shifted in a more positive direction than the corrosion potential, and the polarization is known as anodic polarization. The working electrode loses electrons in anodic polarization. In cathodic polarization, the potential is shifted in a more negative direction than corrosion

potential. In cathodic polarization, the working electrode becomes a cathode and acquires electrons, which is occasionally followed with electrodeposition. Cyclic polarization occurs when both cathodic and anodic polarization are done in a cyclic pattern.

Tafel extrapolation is the most widely used method in the electrochemistry to study corrosion behavior. Tafel's law states that the logarithm of the current density in an electrochemical reaction changes linearly with the electrode potential, (at potentials removed from the open-circuit rest potential) (McCafferty, 2005).

In a corrosion system, oxidation of metal (corrosion) and reduction of some species in solution takes place. That is it involves two or more half cells.

For a single electrode reaction, relation of the net current density, I, to the electrode potential, E is expressed by Butler-Volmer equation [3-5]

$$I = I_0[e^{\alpha nF(E- E_0)/RT} - e^{-(1-\alpha)nF(E- E_0)/RT}] \qquad [3-5]$$

Where, I_0 = exchange current density (rate of half-cell reaction) at the equilibrium potential E_0, a = transfer coefficient (usually 0.5), n = number of electrons transferred

In 1938 Wagner and Traud put forward the electrochemical theory of corrosion. According to them, the net measured current (I_m) for a corrosion system at equilibrium is zero due to equal rate of athodic and anodic reaction.

$$I_m = I_{red} - I_{ox} = 0 \qquad [3-6]$$

When a metal comes in contact with a solution, it assumes a potential that is independent of the metal and the nature of the solution. Ecorr refers to this potential as open circuit potential or corrosion potential. The corrosion rate is determined electrochemically by determining Icorr, which is the net rate of metal dissolution or hydrogen evolution at Ecorr at the freely corroding state. For such state, Butler-Volmer equation is modified as,

$$I = I_{corr}[e^{\alpha nF(E- E_{corr})/RT} - e^{-(1-\alpha)nF(E- E_{corr})/RT}] \qquad [3-7]$$

When the rate of back reaction is negligible, Equation [3-7] gives:

$$E = a + b \log I \qquad [3-8]$$

Where a and b are constants.

Equation [3-8] is Tafel's law. Furthermore, in Equation [3-7], when E = Ecorr then I = Icorr. This is the basis for the Tafel extrapolation.

When potential is applied in both the anodic and cathodic directions to polarize the specimen, the experimental polarization curve begins at Ecorr and becomes linear on a semi-logarithmic plot at high current densities. The polarization curve, which generally consists of two diverging logarithmic plot lines representing anodic and cathodic currents, is obtained by plotting the potential as the function of current density (I) or (logI) at each measured point. The linear sections of the anodic and cathodic plots are extended back to their junction to carry out extrapolation. At the point where these two lines intersect is the Ecorr and the corresponding current is the corrosion current (I_corr) as shown in the **Fig. 3.12.**
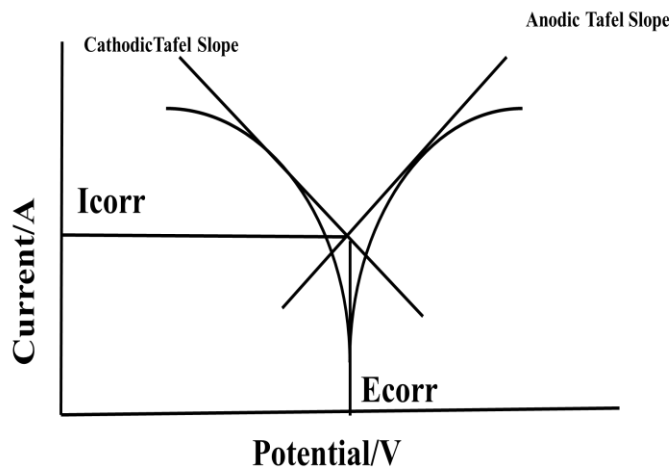
Figure 3. 12: Tafel plot for potentiodynamic polarization

By finding the I_corr, the corrosion inhibition efficiency (*IE*) can be calculated by the following relation(Shabani-Nooshabadi*et al*., 2018):

$$\text{Inhibition efficiency (}IE\text{) in \%} = \frac{Icorr - I'corr}{icorr}\ x\ 100 \qquad [3\text{-}9]$$

Where I_{corr} is the corrosion current of MS and I'_{corr} is the corrosion current of PANI coated MS.

Tafel extrapolation also aids in the determination of Ecorr, cathodic, and anodic slope. The kind of inhibitor, whether cathodic, anodic, or mixed, is indicated by the Ecorr value. The effect of the inhibitor on the corrosion process is shown by a change in cathodic anodic slope.

Corrosion tests were performed in 0.1M NaCl, 0.4 M Na_2SO_4, the mixture of 0.1 M NaCl and 0.4 M Na_2SO_4, 0.1 M H_2SO_4 and 0.4 M Na_2SO_3 solution at room temperature by potentiodynamic polarization using a Hokuto Denko HA-151 potentiostat controlled by a self-made LabVIEW software interfaced with an IBM computer. Open circuit potential (OCP) was allowed to stabilize for 30 minutes before each potentiodynamic polarization. The polarization curves were obtained by scanning potential ±300 mV from the OCP at 1 mV/sec scan rate. From the polarization curves, the corrosion current (I_{corr}), corrosion potential (E_{corr}) and Tafel slopes were determined from the Tafel extrapolation method, and corrosion inhibition efficiency (*IE*) was calculated.

3.7.2 Corrosion study by electrochemical impedance spectroscopy (EIS) technique

Electrochemical impedance microscopy (EIS) is an electrochemical method that has been commonly used to investigate the corrosion resistance and coating performance of underlying materials in real time. It is the most promising electrochemical technique for the analysis of the corrosion mechanism which requires AC impedance measurements. Electrical resistive and capacitive properties of the metal/solution interface over a large frequency range can be determined by this type of multifrequency AC electrochemical measurement technique. From the curve fitting software, the solution resistance (R_s), charge transfer resistance (R_{ct}), and double-layer capacitance (C_{dl}) can be determined by applying the EIS results.

As AC impedance is applied to an electrochemical system, EIS provides kinetic and mechanistic understanding about corrosion. It can be used to determine rate, inhibitor efficiency, coating performance, and passive layer characteristics in the field of corrosion. The strength of EIS lies in the fact that it is simply a steady-state method capable of accessing the relaxing phenomenon with several orders of magnitude different relaxation times. The impedance approach was first applied to the calculation of corrosion intensity by Epelboin *et al*. (Zhang & Lyon, 1994) and Haruyama (Muto *et al*., 1994) developed the statistical study of the impedance of mixed potential electrodes.

In contrast to other electrochemical techniques such as potentiodynamic polarization, EIS does not cause sample disruption, so it can be used in situ for long-term evaluations. Because of the following cause, EIS has several advantages over potentiodynamic polarization:

a. The electrochemical test system is perturbed to a minimum by the very limited excitation amplitude (in the range of 5-10 mV) used in EIS. As a result, errors produced by the technique are reduced in EIS.

b. Since it provides data on both electrode capacitance and charges transfer kinetics, EIS provides useful mechanistic information.

c. In EIS, a potential scan is not performed such that it can be extended to a solution of low conductivity (Sastri, 2011).

EIS usually operates by applying an AC potential to the sample through a reference electrode and then measuring the current passing between the sample and a counter electrode, as seen in **Fig. 3.13**. The potential is applied and the current is collected using a potentionstat, the impedance is calculated using a Frequency Response Analyzer (FRA), and the operation is operated by computer software.

Figure 3. 13: Apparatus set up for electrochemical impedance spectroscopy using CH electrochemical workstation

Sweeping the AC potential frequency and calculating impedance over a large frequency transition produces a continuum. In addition, the amplitude of the perturbation AC potential is kept small to keep the device in the linear regime, which ensures that the applied potential does not induce a permanent change in the sample state. The current reaction to a sinusoidal potential in the linear regime is a sinusoid with the same

frequency but changed in phase. The excitation signal can be expressed as a function of time as given below

$$E(t) = E_0 \cos(\omega t) \qquad\qquad [3\text{-}10]$$

Where, E(t) is the potential at time t, E_0 is the amplitude of the signal, and ω is the radial frequency ($\omega = 2\pi f$). In a linear system, the response signal, I_t, is shifted in different phase (θ) and has a amplitude, I_0:

$$I(t) = I_0 \cos(\omega t - \theta) \qquad\qquad [3\text{-}11]$$

An equation similar to Ohm's Law allows one to calculate the impedance of the system as:

$$Z = \frac{E(t)}{I(t)} = \frac{E_0 \cos(\omega t)}{I_0 \cos(\omega t - \theta)} = Z_0 \frac{\cos(\omega t)}{\cos(\omega t - \theta)} \qquad\qquad [3\text{-}12]$$

Therefore, the impedance is expressed in terms of magnitude, Z_0, and a phase shift, θ.

The impedance of an electrochemical interface is a complex number, which can be represented either in polar coordinates or in Cartesian coordinates:

$$Z(\omega) = |Z|e^{j\theta} \qquad\qquad [3\text{-}13]$$

$$Z(\omega) = Z' + j\,Z'' \qquad\qquad [3\text{-}14]$$

where IZI is the impedance modulus, $j = \sqrt{-1}$, Z' and Z'' are the real and imaginary part of the impedance related to the magnitude of the impedance and phase by

$$|Z(\omega)| = \sqrt{(Z')^2 + (Z'')^2} \qquad\qquad [3\text{-}15]$$

$$\tan\theta = \frac{Z''}{Z'} \qquad\qquad [3\text{-}16]$$

$$|Z|\cos\theta = Z' \qquad\qquad [3\text{-}17]$$

$$|Z|\sin\theta = Z'' \qquad\qquad [3\text{-}18]$$

The EIS spectra can be shown in a variety of ways. The imaginary part of the impedance, Z, is plotted against the real part of the impedance, Z, in a Nyquist plot. The magnitude Z of the impedance and the phase angle θ of the impedance are plotted against frequency in

a Bode and Phase plot. Fitting EIS spectra with equivalent electrical circuits whose components can describe a physical or electrochemical property of the system

Metal corrosion is primarily an electrochemical process. However, there are no electrochemical techniques for specifically measuring the rate of corrosion. They are based on a variety of theories. In most cases, polarization resistance is determined using the impedance equation, which, according to Stern and Geary, is related to corrosion rate by an inverse proportionality relationship (1957)

$$i_{corr} = k \, R_p^{-1} \qquad \text{[3-19]}$$

Here k is a proportional constant whose value depends on the Tafel slopes.

The EIS results for the metal in the given environment are used to generate an equivalent circuit that represents the electrochemical system under investigation. A basic equivalent circuit representing an electrode-solution interface is shown in **Fig. 3.14**. Curve fitting software is used to fit the impedance spectra using this comparable circuit model. In the circuit model, the constant phase element (CPE) is applied to account for electrode surface non-homogeneity caused by surface roughness, inhibitor adsorption, dislocations, grain boundaries, and the development of a porous layer in metal corrosion in hostile acidic environments.
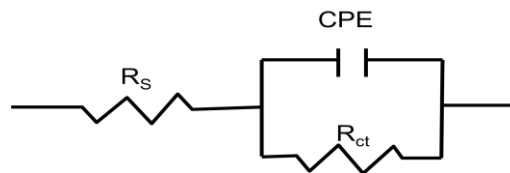
Figure 3. 14: The equivalent circuit model used to fit the impedance spectra.

The impedance of CPE is described by equation [3-20]

$$Z_{CPE} = Y_0^{-1}(j\omega)^{-n} \qquad \text{[3-20]}$$

Where Y_0 represents the magnitude of the CPE, j, the imaginary number ($j^2 = -1$), ω, being angular frequency ($\omega = 2\pi f$), and n, the CPE exponent ($-1 \leq n \leq +1$), whose value is used to gauge the non-homogeneity or roughness of the surface. For n=0, the CPE represents a pure resistor, when n= -1, an inductor and for n= +1, a pure capacitor

The properties of the electrode interface, mechanisms involved in corrosion, effect, and inhibition efficiency of inhibitor are revealed by analyzing changes in electrochemical parameters such as solution resistance (Rs), charge transfer resistance (Rct), and double-layer capacitance (Cdl) obtained from software. For example, using inhibitor, the increase in phase angle in the Bode-phase plot, the value of impedance at low frequencies in the Bode-modulus plot, and the capacitive loop diameter in the Nyquist plot reveal inhibitor adsorption on the metal surface, and the extent of increment implies inhibitor effectiveness. Once the value of Charge transfer resistance is obtained from curve fitting software, inhibition efficiency of corrosion inhibitor can be calculated by the equation [3-20].

$$IE\% = \frac{R_{ct} - R_{ct}^0}{R_{ct}} \times 100\% \qquad [3\text{-}21]$$

Where R_{ct}^0 and R_{ct} are charge transfer resistances in the presence and absence of inhibitor.

Similarly, double layer capacitance can be calculated by the equation [3-22].

$$C_{dl} = \frac{1}{2\pi R_{ct} f_{max}} \qquad [3\text{-}22]$$

The frequency at which the greatest imaginary component of the impedance is achieved is denoted by fmax. The rise in the thickness of the electric double layer or the decrease in the local dielectric constant owing to the adsorption of inhibitor molecules on the metal surface can be attributed to a drop in the value of Cdl. Equation expresses the relationship between thickness and dielectric constant with Cdl.

$$\delta_{org} = \frac{\varepsilon_0 \varepsilon_r A}{C_{dl}} \qquad [3\text{-}23]$$

Where δ_{org} is the thickness of the protective layer, ε_0 is the dielectric constant, ε_r is the relative dielectric constant, and A is surface area.

Relaxation time (τ) is the amount of time it takes for the charge distribution to return to equilibrium following an electrical disruption. If no disturbance is introduced to replace the Cdl, relaxation time is the product of double-layer capacitance and charge transfer resistance.

$$\tau = C_{dl} R_{ct} = \frac{1}{2\pi f_{max}} \qquad [3\text{-}24]$$

Electrochemical impedance spectroscopy (EIS) was performed in the CH 660 electrochemical work station at the OCP. The AC response of MS and PANI coated MS in 0.1M NaCl, 0.4 M Na_2SO_4, and 0.1 M H_2SO_4 was measured using EIS. At OCP, a superimposing sine wave signal of 10 mV peak to peak at frequencies ranging from 100 kHz to 0.01 Hz was used to evaluate the AC response. By fitting the response with an equivalent circuit, the AC signal's response in terms of charge transfer resistance (Rct) and double layer capacitance was examined. Using Z-view 2 software, these parameters were obtained from the equivalent circuit.

CHAPTER 4

4. RESULTS AND DISCUSSION

4.1 Selection of electrolytes for the polymerization of aniline onto MS sample

Polymerization of aniline onto mild steel (MS) surface is difficult as oxidation potential of mild steel is more negative than oxidation potential of aniline. When acids are used as an electrolyte, the mild steel surface actively dissolves at that potential. When polarization was performed using sulphuric acid, nitric acid, phosphoric acid, hydrochloric acid, sodium chloride, and sodium acetate, there was no passivation and polymerization of aniline. Therefore it is necessary to find the suitable electrolyte that inhibits the dissolution of steel and provide more electropolymerization.

Concentrated nitric acid passivated mild steel. When aniline was tried to polymerize onto MS surface using dilute nitric acid, the attempt was failed which shows that electrically inactive surface formed does not allow polymerization. Aniline requires some cation and anion for polymerization.

As passivation of MS surface with active electrical composition is essential for polymerization of aniline, the selection of electrolytes is an indispensable and inevitable process. For this purpose, the anodic polarization of MS was performed using electrolytes such as succinic acid, sulphanilic acid, sodium orthophosphate, sodium potassium tartrate (Na-K Tartrate), and benzoic acid in 3:1 alcohol-water (BAW) solutions. Open circuit potential (OCP) of MS was measured in each cases for 30 minutes before carrying out anodic polarization. The **Fig. 4.1.1** depicts the variation of OCP of MS in different electrolytes. The OCP of MS in all electrolytes remained constant after 5 minutes, indicating the formation of the stable passive film. The OCP shifts to a noble direction in the presence of sodium ortho phosphate and 0.1 M benzoic acid in 3:1 alcohol-water (BAW) compared to succinic acid, sulphanilic acid and sodium potassium tartrate (Na-K tartrate), indicating the inhibition of the dissolution of the MS due to the instantaneous surface coverage of the MS. The OCP of MS shifts to positive by more than 85 mV in sodium ortho phosphate and BAW indicating the anodic type of inhibitor.
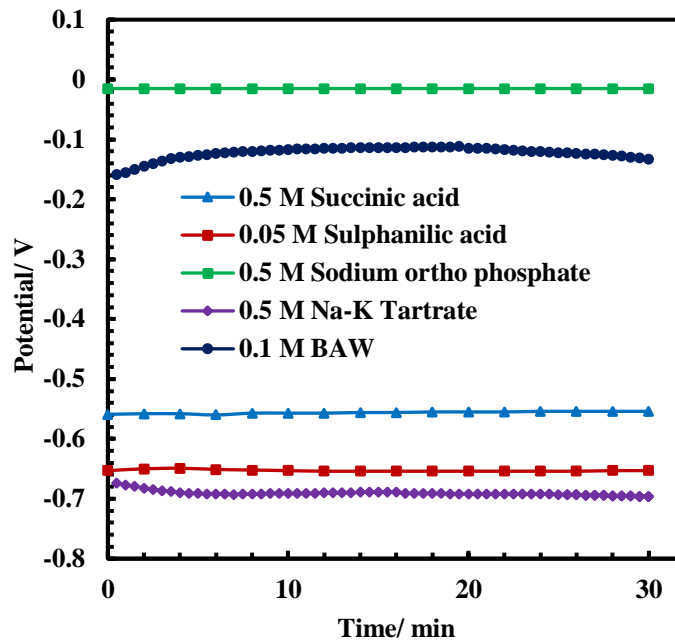
Figure 4.1.1: OCP of MS surface in succinic acid, sulphanilic acid, sodium orthophosphate, 0.5 M Na-K Tartrate and 0.1 M BAW solutions

The **Fig. 4.1.2** shows the polarization of MS in succinic acid, sulphanilic acid, and sodium orthophosphate solutions. The polarization curves showed active dissolution of iron and no electroactive passive filmed formed til 2.0 V because there was no polymerization of aniline. The passivation of MS is essential but not adequate condition for the polymerization of aniline. Thus, succinic acid, sulphanilic acid, and sodium orthophosphate solutions only act as corrosion inhibitor but not help in aniline oxidation. Sodium orthophosphate acts as anodic inhibitor as it limits the dissolution of MS surface due to formation of Fe-phosphate.

The passivation of the MS surface is essential but not adequate condition for polymerization. The effects of Na-K tartrate and BAW on passivation, together with the curve obtained in oxalic acid on the MS sample are depicted in **Fig. 4.1.3**. The polarization curve in Na-K Tartrate demonstrates a resembling polarization behavior to oxalic acid medium. In a 0.5 M Na-K Tartrate solution, the OCP is -0.640 V, and active dissolution of MS takes place up to a potential of -0.52 V, as represented by the increase in current.

The formation of the Fe-tartrate passive layer causes passivation of the MS surface at potentials positive than -0.52 V. The thickening of the passive layer is responsible for the increase in current between -0.36 V and +0.013 V.
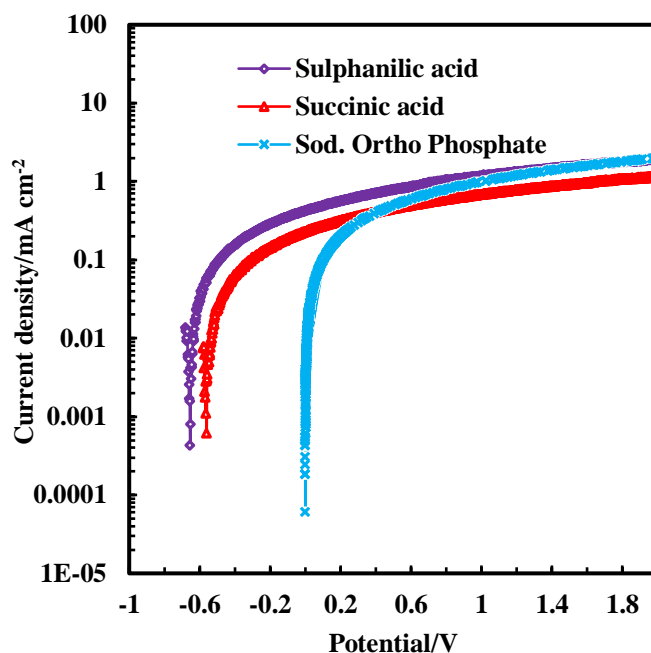
Figure 4.1.2: Anodic Polarization of MS surface in succinic acid, sulphanilic acid, and sodium orthophosphate solutions (Gupta *et al.*, 2021)

The electrical activation of the Fe-tartrate layer is due to the charge leakage. As a result, electropolymerization of aniline could take place under such conditions. At the potential more positive than +0.013 V, the dissolution of the passive layer took place. The visual observation of the surface showed the formation of a white layer on the MS surface. Finally, a breakdown potential appears at +0.7 V. However, this potential is lower as compared to +1.2 V in oxalic acid (Ganash *et al.*, 2011).

In the case of polarization using benzoic acid, it is to be mentioned that benzoic acid is insoluble in water but soluble in alcohol. However, benzoic acid-alcohol solution is not conducting. After studying various combinations, the alcohol-water in a 3:1 ratio was chosen for the appropriate conductivity. In a 3:1 alcohol-water solution, 0.1 M benzoic acid solution was prepared after deliberation so that on further dilution, no precipitation of benzoic acid took place.

An increase in the quantity of water or benzoic acid, or a reduction in the amount of alcohol, caused the precipitation of benzoic acid. The polarization curve of the MS in 0.1 M benzoic acid in the 3:1 alcohol-water (BAW) system is presented in **Fig. 4.1.3**. Unlike Na-K Tartrate and oxalic acid solutions, it does not have a clear active-passive zone, but the current increases gradually with potential.
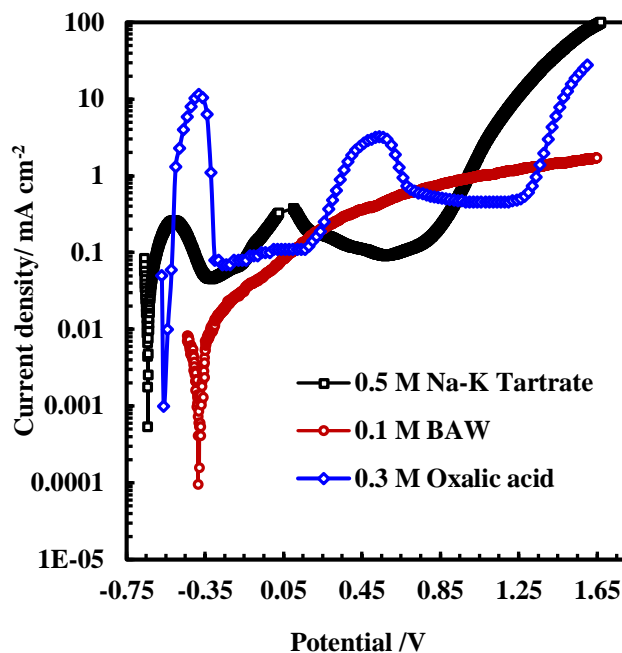
Figure 4.1.3: Anodic Polarization of MS surface in 0.5 M Na-K Tartrate, 0.1 M BAW, and 0.3 M oxalic acid solution (Gupta *et al*., 2021)

The OCP is notably shifted to the noble value at -0.38 V as compared to Na-K tartrate and oxalic acid solutions. The formation of the Fe-benzoate layer causes the noble shift of OCP. This layer was most likely formed during 30 min immersion at OCP. The dissolution of MS is certainly limited by the Fe-benzoate layer due to its barrier effect (Popović & Grgur, 2004). The current increased gradually with shift of potential in a positive direction. The rise of the current between -0.3 V and -0.15 V represents the thickening of the passive layer. It indicates that the passive layer is electrically active, and there is leakage of charge from the Fe-benzoate layer, which can be used in the aniline oxidation. The dissolution of the passive layer resulted the shoulder between the potential of -0.15 V and +0.09 V. Oxygen evolution is observed after +1.1 V.

SEM image of the MS surface anodically polarized in 0.5 M aqueous Na-K tartrate solution is shown in **Fig. 4.1.4a** together with a corresponding EDX spectrum. The presence of C, N, O, Na, K, and Fe are distinct in EDX, which confirmed the formation of the Fe-tartrate layer on the MS surface. The passive layer was composed of a thick and polygons shape granular particles of Fe-tartrate covering the MS surface.
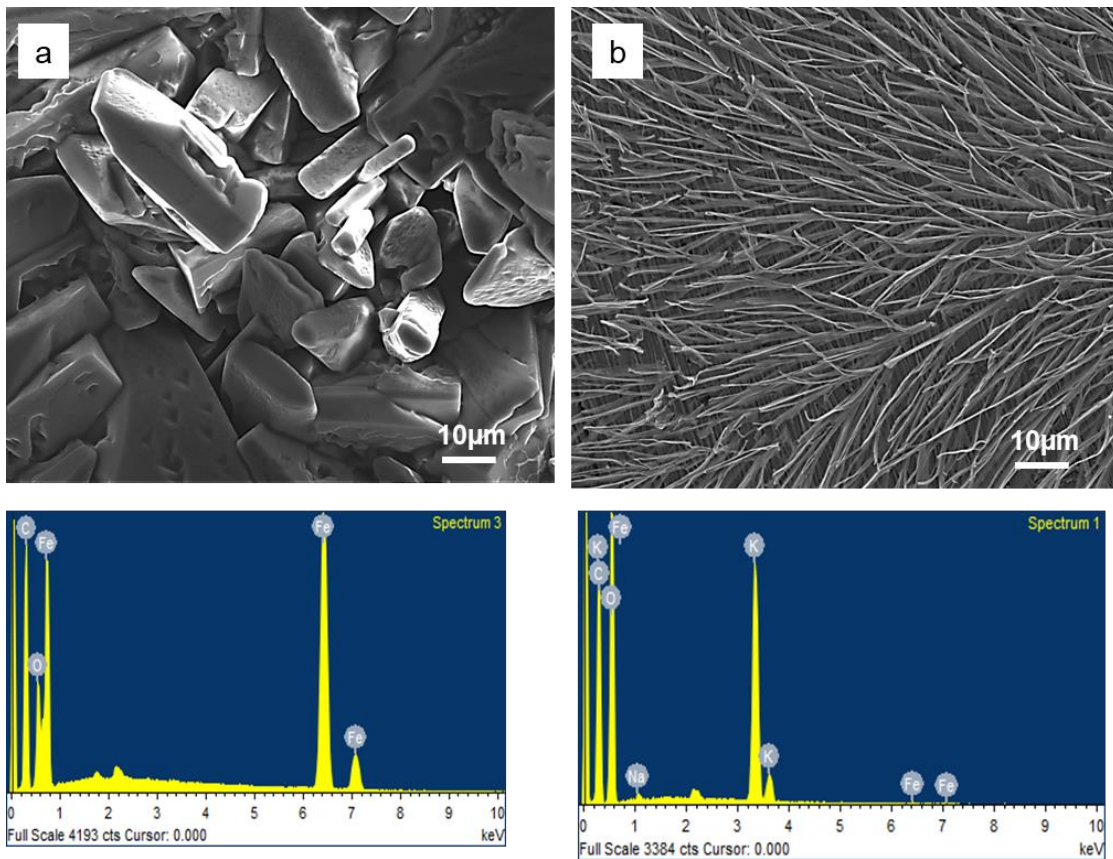
Figure 4.1. 4: SEM images of MS sample anodically polarized in (a) 0.5 M Na-K Tartrate (b) 0.1 M BAW with their corresponding EDX elemental analysis (Gupta *et al*., 2021)
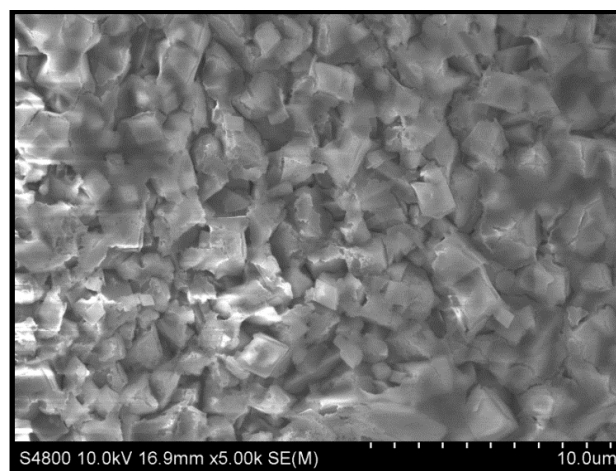
Figure 4.1.5: The SEM image of MS sample polarized in 0.3 M oxalic acid solution

Similarly, SEM image of the MS sample anodically polarized in 0.1 M BAW is shown in **Fig. 4.1.4b**. A thin dendritic layer due to the formation of Fe-benzoate is obvious, indicating the presence of C, O, and Fe elements as supported by the EDX result. The SEM image of MS sample polarized in 0.3 M oxalic acid solution is shown in **Fig. 4.1.5**

for comparison. Next, at the optimized composition of monomer and electrolytes, the effect of a passive layer on the oxidation and polymerization of aniline is studied.

4.2 Electrochemical synthesis of PANI in Na-K Tartrate

4.2.1 Optimization of the concentration of Na-K Tartrate

The nature of surface passivation is also affected by the concentration of the electrolyte. Therefore, the concentration of electrolyte has to be optimized. Also, the optimization of concentration is important with an economic point of view as it saves excess use of chemicals. **Fig. 4.2.1** shows the anodic polarization of MS in 0.1 M to 0.5 M Na-K-Tartrate solutions. The general characteristics of the polarization curves are similar to **Fig. 4.1.3**. There is a marginal shift of OCP towards positive values with the increase in concentration. The peak current for dissolution of Fe diminishes, and passivation achieves rapidly with an increase in concentration.
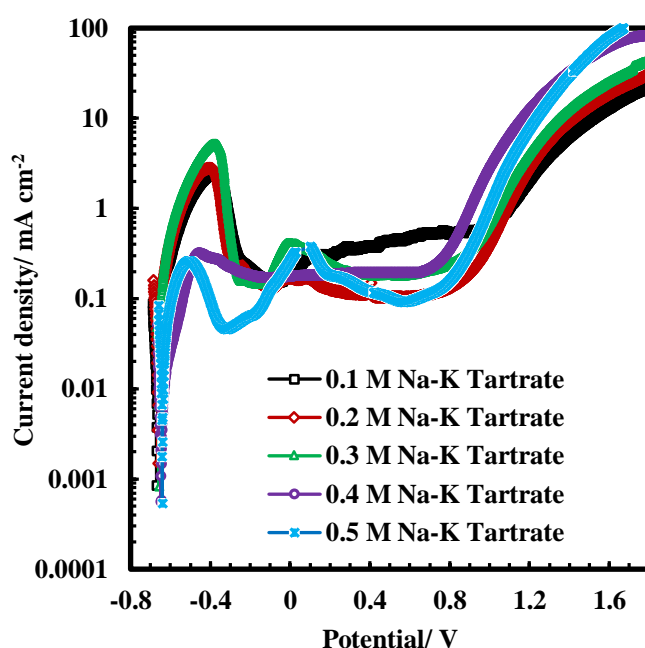
Figure 4.2.1: Anodic polarization of MS in various concentrations of Na-K Tartrate solutions at a scan rate of 1 mV/s (Gupta *et al*., 2021)

From the polarization curves, 0.4 M Na-K Tartrate was chosen as the optimum concentrations for polymerization of aniline.

4.2.2 Electropolymerization of aniline in Na-K Tartrate

After optimizing the concentration of Na-K Tartrate, electropolymerization of aniline onto MS sample was carried out using a 0.1 M aqueous solution of aniline in 0.4 M Na-K Tartrate. **Fig. 4.2.2** shows the polymerization curves of aniline in 0.4 M Na-K Tartrate, and 0.3 M oxalic acid. Na-K Tartrate and oxalic acid show like polarization behaviors. The dissolution of Fe occurs near the OCP, followed by passivation at -0.47 V, as represented by decreasing current in Na-K Tartrate. The current suddenly fell off, causing passivation due to the formation of Fe-tartrate. On further increasing the potential, oxidation and subsequent polymerization of aniline occurs in a wide potential range of +0.40 V to +1.4 V. The current hump, shoulder, and plateau regions in between above potential range are indicative of the formation of various forms of PANI. The oxidation of aniline begins at +0.40 V represented by a sharp increase in the current. At potential +0.66 V, the current starts to decrease. This peak corresponds to the transformation of leucoemeraldine to emeraldine (Diaz & Logan, 1980; Genies & Tsintavis, 1985).
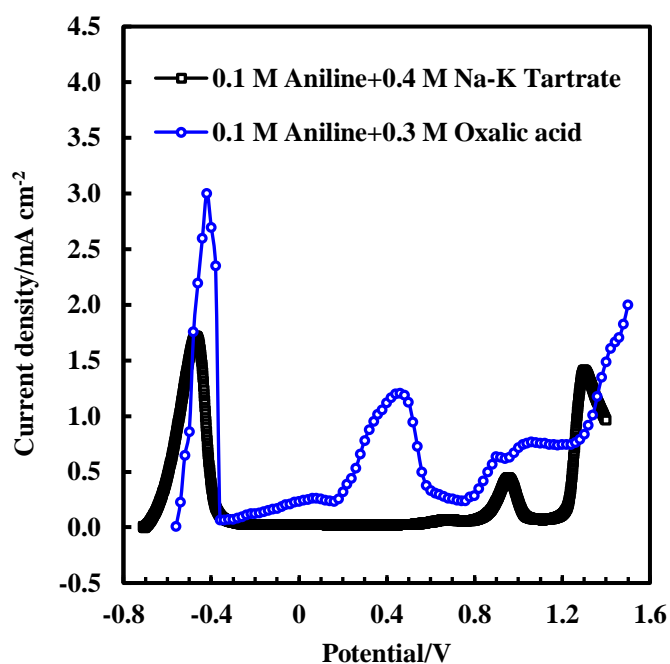
Figure 4.2.2: Anodic Polarization of MS in 0.4 M Na-K Tartrate and 0.3 M oxalic acid solutions containing 0.1 M aniline in each at a scan rate of 1.0 mV/s (Gupta *et al*., 2021)

The current again rises at +0.8 V due to the conversion of emeraldine to pernigraniline with a pronounced peak at +0.97 V and, oxygen evolution is observed after +1.1 V. At +0.43 V, +0.506 V, +1.4 V, and +1.6V, the conversion of leucoemeraldine to emeraldine, emeraldine to pernigraniline, green-colored PANI, and blue-green emeraldine salt are

observed, respectively (Camalet *et al.*, 1998; Genies & Tsintavis, 1985; Martyak *et al.*, 2002; Stejskal *et al.*, 2010; Zor & Yakar, 2007).

4.2.3 Optimizing the concentration for polymerization of aniline in Na-K Tartrate

Anodic polarization was carried out in various concentrations of Na-K Tartrate solutions containing different amounts of aniline to optimize the concentrations of electrolyte and aniline. **Fig. 4.2.3** shows the polarization curves of MS in with concentrations of Na-K Tartrate and aniline. The concentrations of both varied from 0.1 M to 0.4 M. Polarization behavior is similar to that in **Fig. 4.2.2** where dissolution, passivation, and polymerization occurs with potential. As the concentration of aniline increases, the OCP shifts gratually to a positive direction, and passivation occurs swiftly. From the results, a concentration of 0.3 M aniline in 0.2 M Na-K Tartrate is chosen as the best composition due to better passivation and polymerization behaviors. The visual observation showed a non-adhesive PANI layer formation at 0.4 M aniline concentration, also confirmed by scotch-tape method.
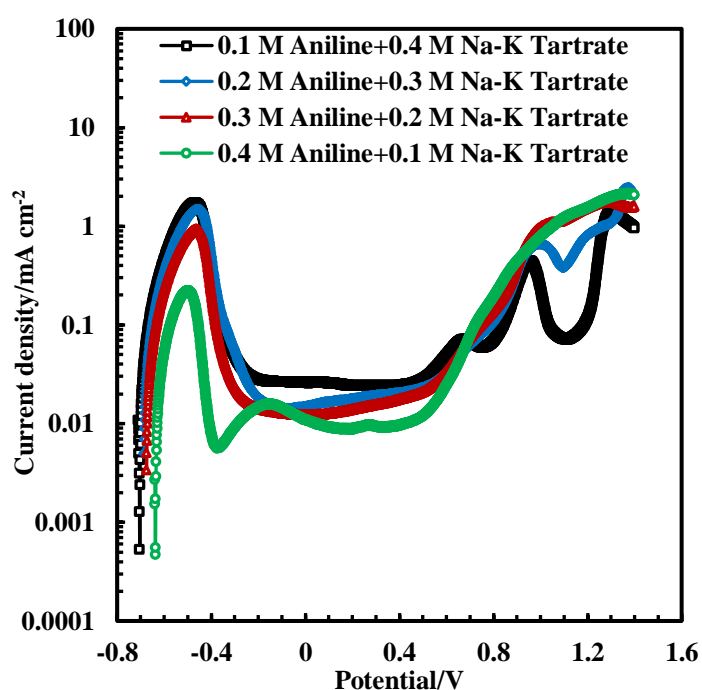
Figure 4.2.3: Anodic polarization of MS in different concentration of aniline in varying concentrations of Na-K Tartrate, The scan rate was 1mV/s and polarization was started after remained at OCP for 30 min. (Gupta *et al.*, 2021)

The concentration of 0.3 M aniline in a 0.2 M Na-K tartrate was selected as the best composition for aniline polymerization due to better passivation and polymerization behaviors. **Fig. 4.2.4** shows the polarization curves of MS in 0.3M aniline in 0.2M Na-K

Tartrate representing dissolution, passivation, and polymerization with potential. The dissolution of iron took place near the OCP, followed by passivation at -0.452 V, as indicated by the declining current. The current density suddenly decreased, resulting passivation due to the formation of Fe-tartrate. On further increasing the potential, oxidation and subsequent polymerization of aniline took place in a wide potential range of 0.40 V to 1.4 V. The current hump, shoulder, and plateau regions in between above potential range were indicative of the formation of various forms of PANI. The oxidation of aniline began at 0.42 V, shown by a current raised. At potential 0.74 V, the current started to decline. This peak corresponded to the conversion of leucoemeraldine to emeraldine (Diaz & Logan, 1980; Genies & Tsintavis, n.d.). The current again began to rise at potential of 0.87 V, which indicated the conversion of emeraldine to pernigraniline with a pronounced peak at 0.97 V. The oxygen evolution reaction at the potential more positive than 1.1V was observed. It has been reported that conversion of leucoemeraldine to emeraldine took place at 0.43V, from emeraldine to pernigraniline took place at 0.506V, green coloured PANI was obtained at 1.4V, and blue-green emeraldine salt was formed at 1.6V (Martyak *et al*., 2002; Stejskal *et al*., 2010; Zor & Yakar, 2007).
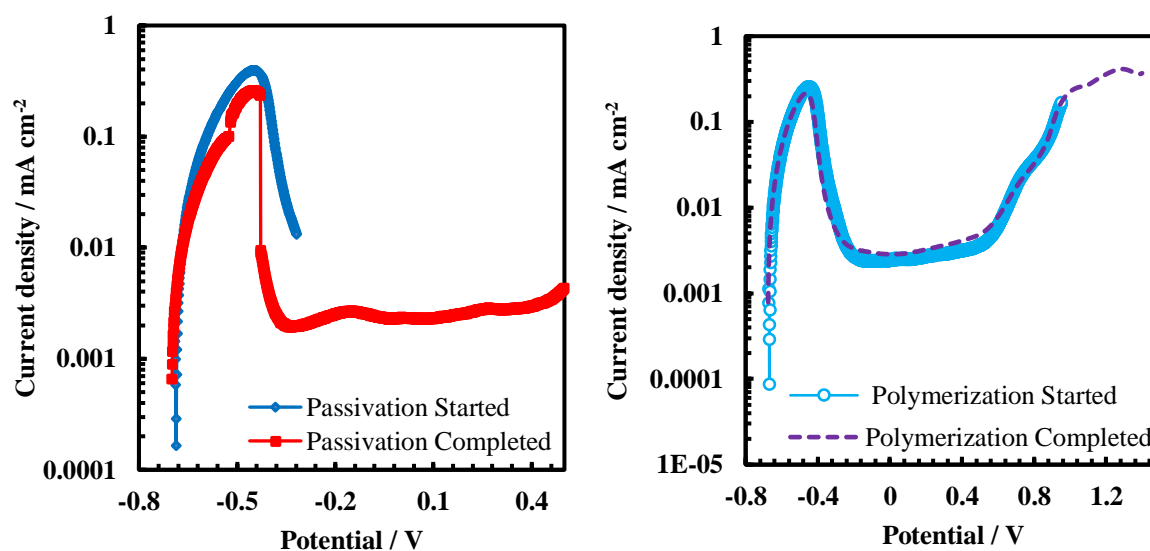
Figure 4.2.4: Anodic polarization of MS in 0.3M aniline in 0.2M Na-K Tartrate at different stages

4.2.4 Effect of CV on polymerization

Cyclic voltammetry (CV) was carried out in various concentrations of Na-K tartrate solutions containing different amounts of aniline to optimize the concentrations of electrolyte and aniline. **Fig. 4.2.5** shows the CV curves of MS in with concentrations of Na-K Tartrate and aniline. The concentrations of both varied from 0.1 M to 0.4 M. A stable voltammogram with no anodic peak during cathodic scan is obtained. From the results, a concentration of 0.3 M aniline in 0.2 M Na-K Tartrate is chosen as the best composition due to better coating and its adhesion.
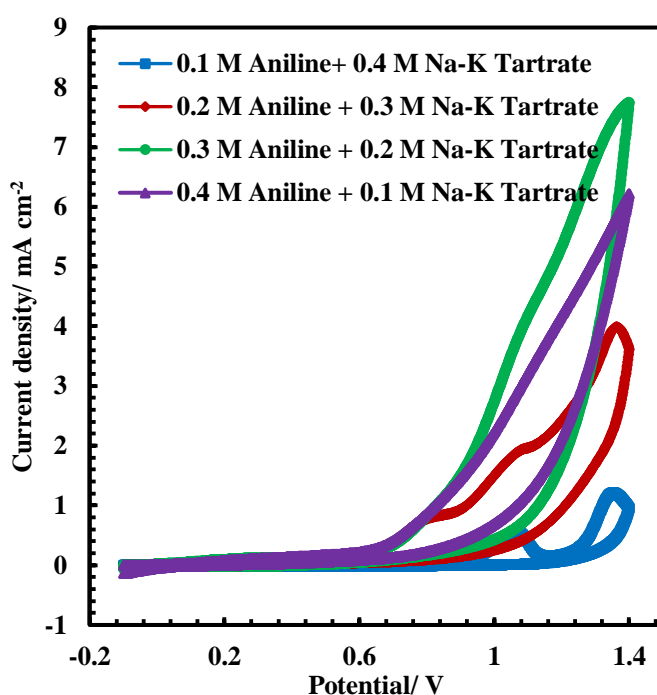
Figure 4.2.5: Cyclic voltammetry of MS in different concentration of aniline in varying concentrations of Na-K Tartrate at 20mV/s scan rate

PANI formation and its stability in the acidic medium have been the subject of many researches (Fomo, 2016; Ganash *et al*., 2011; Mohd *et al*., 2012; Zor & Yakar, 2007). The PANI coating formed during CV indicated an anodic dissolution peak at +0.3 V vs SCE in the cathodic scan, **Fig. 4.2.6**. Anodic dissolution peak in cathodic scan resulted from the breakdown of the PANI coating and iron-oxalate layer formed in the previous anodic scan. Therefore, the dissolution of Fe occurred from the MS surface during the cathodic scan. Such behavior has been found to disappear after several cycles of CV. However, such behavior shows to stability issues of PANI coating in oxalic acid medium (Camalet

et al., 1996). **Fig. 4.2.6** shows the cyclic volatmmograms of MS in solutions containing 0.3 M aniline in 0.2 M Na-K Tartrate solutions. Unlike in oxalic acid solution, a stable voltammogram with no anodic peak during cathodic scan is observed. The polymerization occurs in various steps, as discussed in section 4.2.2, **Fig. 4.2.2** and lower current values in Na-K Tartrate solutions reflects the better coating as compared to oxalic acid. The results reveal that Na-K Tartrate offer better alternatives for polymerization of aniline onto MS surface with cyclic stabilities.
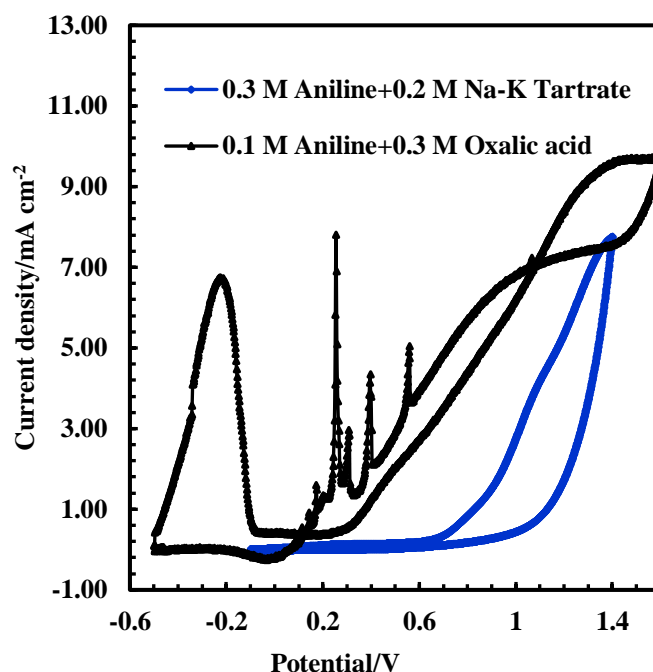
Figure 4.2.6: PANI coating on MS obtained by cyclic voltammetry in 0.3 M aniline+0.2 M Na-K Tartrate, and 0.1 M aniline+0.3 M Oxalic acid solutions (Gupta *et al.*, 2021)

The anodic peaks disappeared after the first scan, and peak current density decreases when the number of cycles increases (Kellenberger *et al.*, 2014; Machnikova *et al.*, 2008). Current values decreased with the number of scans, as shown in **Fig. 4.2.7**. Moreover, the thickness of homogenous and sticky PANI films increased with a number of scans. The result reveals that the thickening of PANI occurs with an increase in the number of cycles and its stability.
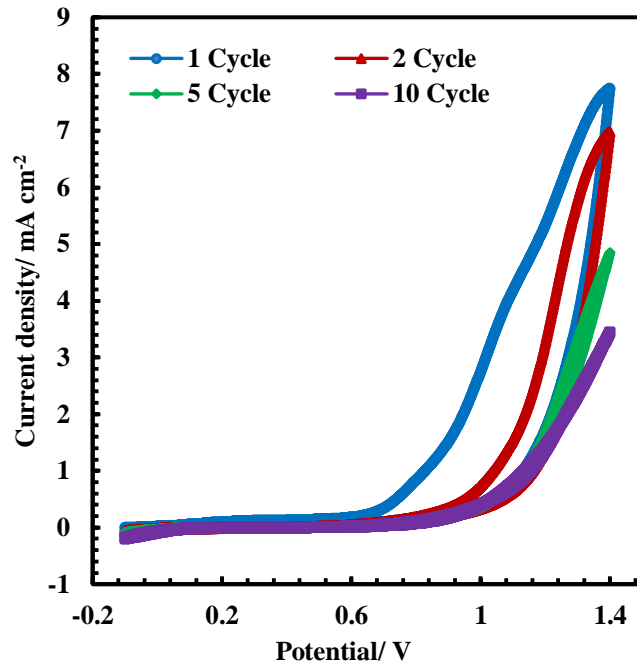
Figure 4.2.7: Voltammogram for polymerization of 0.3M aniline in 0.2M Na-K Tartrate with different cycles

4.2.5 Effect of scan rate on formation of PANI in Na-K Tartrate

At low sweep rates, 5–10 mV/s, a well-defined anodic peak is seen as shown in **Fig. 4.2.8**. Above 20mV/s, no well-defined anodic wave was seen in the CV.
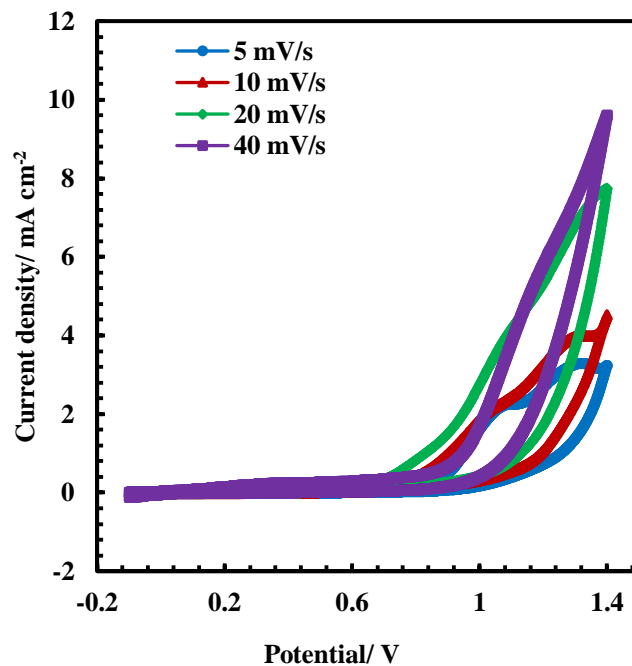
Figure 4.2.8: Effect of scan rate in cyclic voltammetry of electropolymerization of 0.3M aniline in 0.2M Na-K Tartrate

Therefore, to deposit a layer of iron tartrate before PANI's deposition requires a scan rate of ≤ 20 mV/s. With continued polarization, a small increase in current density is observed between + 0.1 and + 1.3 V. Three small waves are seen at + 0.60, + 0.94 and + 1.3 V (Martyak *et al.*, 2002).

4.2.6 Potentiostatic polymerization of PANI in Na-K Tartrate

Fig. 4.2.9 shows the chronoamperogram. It is observed that aniline polymerization begins at the very beginning. Passivation of mild steel surface begins at the beginning, as shown in **Fig. 4.2.9** due to the formation of iron tartrate which drops the current abruptly. The applied voltage 1.4 V is also sufficient for aniline polymerization. As a result, aniline polymerization began at the very beginning. After 72 seconds, there is a limiting current in the electrolyte containing just aniline. But after 50 seconds there is limiting current in the electrolyte containing 5 m mol La (III) solution.

The chronoamperogram of PANI also shows a sudden drop in current, but the reduction of current in PANI prepared from electrolyte containing La(III) is abruptly. These two observations show that the presence of rare earth metal salt tailors the PANI film.
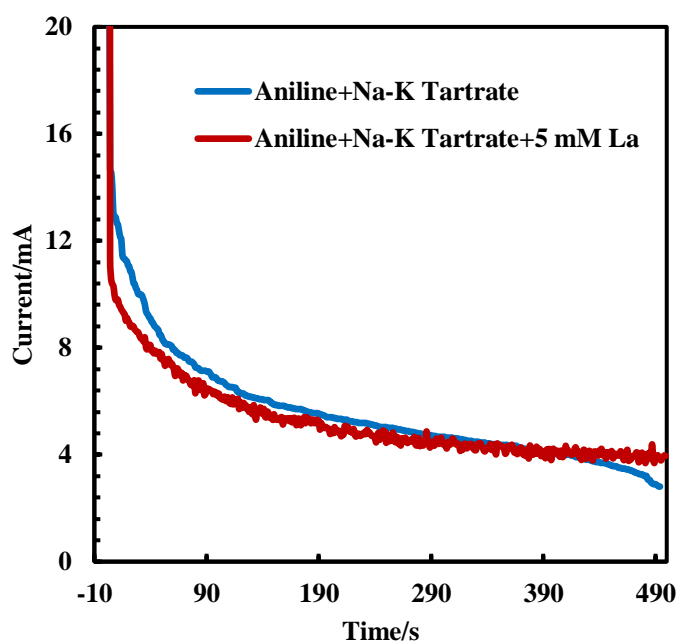
Figure 4.2.9: Chronoamperogram for electropolymerization of 0.3M aniline in 0.2M Na-K Tartrate

4.2.7 Galvanostatic deposition of PANI in Na-K Tartrate

The electrochemical deposition of PANI onto MS was achieved at various current densities. **Fig. 4.2.10** shows the chronopotentiometric behavior of MS immersed in the polymerizing solution of 0.3 M aniline + 0.2 M Na-K tartrate at a current density of 0.50 mAcm^{-2}, 0.75 mAcm^{-2}, 1 mAcm^{-2} and 2 mAcm $^{-2}$, respectively. From the evolution of potential with time, it is clear that no induction period associated with MS dissolution is seen at the beginning. This behavior reflects that very little dissolution of the MS occurs as soon as current is applied unlike in the case of oxalic acid where a clear induction period is observed (inset in **Fig. 4.2.10**).

During the early stages of polarization, the potential remains at about -0.3 V (**Fig. 4.2.10**), and the MS dissolves anodically over a time that is dependent on the applied current density.
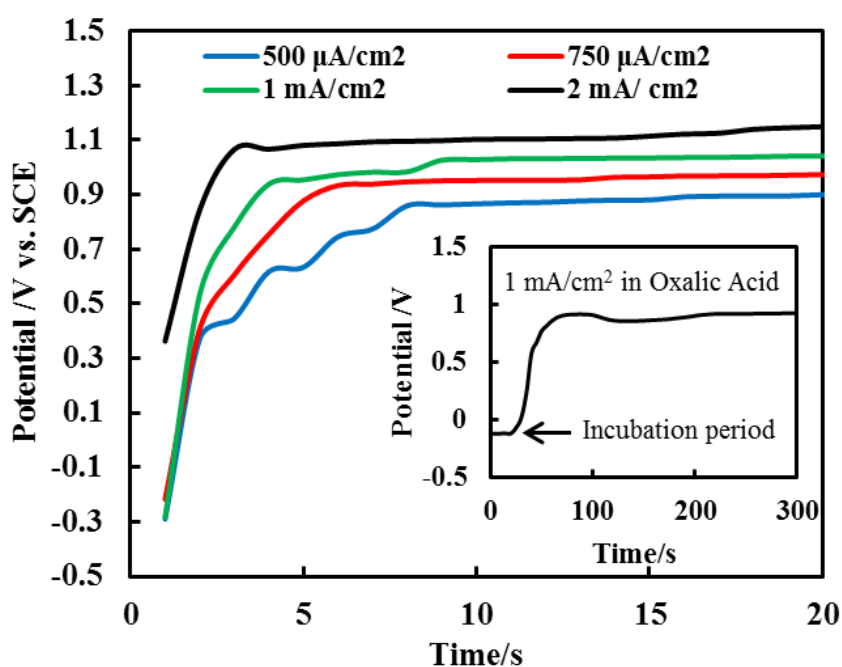
Figure 4.2.10: Electrochemical deposition of a PANI on MS in 0.3M aniline in 0.2M Na-K Tartrate at different current densities

The charge (Q) passing through the electrode before increase of potential is determined by the relation (Camalet *et al*., 1996; Eftekhari, 2004).

$$Q = It \qquad\qquad\qquad \textbf{[4-1]}$$

Where I is the current density in mA/cm^2 and t is the time in second.

In the case of oxalic acid solution, a charge of 275 mC cm^{-2} is required for oxidation of aniline (Camalet *et al*., 1996), whereas in the case of Na-K tartrate, merely a charge of 0.5 mC cm^{-2} is needed for the oxidation of aniline. Therefore, Na-K tartrate results in minimization of energy used for polymerization and deposition of PANI on MS in addition to preventing the loss of iron.

The potential of the MS increases with increase in current density during the polarization process, which indicates for the decrease of metal dissolution with the increase of applied current (Lacroix *et al*., 2000). At a lower current density (0.5 mA cm^{-2}), the potential increased sharply from -0.289 V to 0.407 V and then increased to 0.859 V with waves which represent the passivation and dissolution of MS till 8 sec. The passivation is due to the formation of Fe-tartrate. The potential then increases gradually with the commencement of the oxidation of aniline and formation of PANI take place. The charge needed for the oxidation of substrate electrode depends on current density as well as experimental conditions like medium, and substrate electrode (Eftekhari, 2002). For the current density 0.75 mA cm^{-2} and 1 mA cm^{-2}, the potential increased from -0.281V to 0.933 V in 6 sec and -0.282 V to 0.938 V in 4 sec, respectively. In the case of current density 2 mA cm^{-2}, the potential abruptly increased from 0.362 V to 1.06 V in 2 sec. This is attributed to the MS surface passivation with the increase in current density. A slightly decrease in potential thereafter is attributed to passivation followed by a constant potential due to continuous growth and surface coverage by PANI.

When a nearly constant value of potential is obtained, polymerization on the outer surface is not visually observed. As the polarization proceeds, the potential slightly increases and traces of external polymerization start to be detected. Finally, potential stabilizes for a longer time with the formation of PANI on the outer surface which is obvious and thickening also occurs. These results are similar to those reported for the electrodeposition of aniline onto MS (Camalet *et al*., 1996; Kazum & Kannan, 2016; Lacroix *et al*., 2000) and polypyrrole into porous silicon (Moreno *et al*., 1999).

The mechanism for the electrochemical deposition of PANI is understood to proceed through a radical cation which reacts with a second radical cation to give a dimer which further reacts with cation of aniline to form polyaniline (Dhawan & Trivedi, 1991). The possible reaction mechanism is summarized as;

Firstly, dissolution of iron occurs as indicated by initial potential value

$$Fe \rightarrow Fe^{2+} + 2e \qquad\qquad\qquad \textbf{[4-2]}$$

With the presence of tartrate ion in the solution, the dissolved Fe^{2+} forms an insoluble Fe-tartrate and precipitate at MS surface forming a passivation layer

$$Fe^{2+} + C_4H_4O_6^{--} \rightarrow FeC_4H_4O_6 \downarrow \qquad\qquad \textbf{[4-3]}$$

With the blockade of active dissolution of metal, the available charge is used for the oxidation of aniline which undergoes polymerization with the formation of radical cation. This leads to gradual increase of the potential. The mechanism of dissolution, passivation, oxidation and polymerization is given below.

Aniline

Aniline
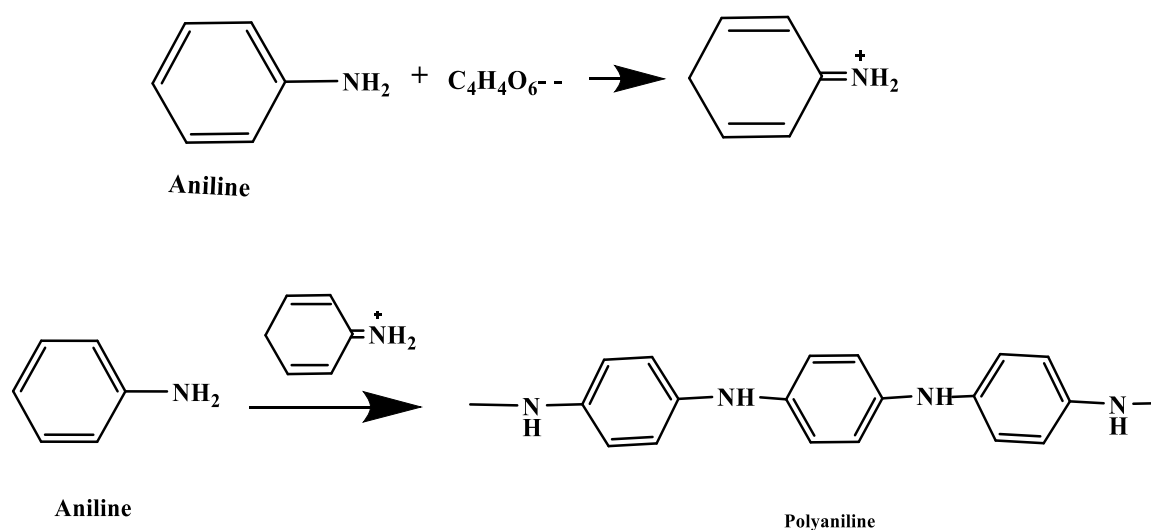
Polyaniline

4.2.8 Effect of La(III) and Ce(IV) on polymerization of aniline in Na-K Tartrate

The presence of La (III) and Ce (IV) affects the current potential curve of aniline polymerization on mild steel. In the presence of La(III), the current-potential behavior of aniline polymerization is similar to Na-K Tartrate. Ce(IV) shifted OCP slightly positive and hence the passivation region decreased. The current value begins to increase with the polymerization of aniline due to increase in conductivity and the pronounced oxygen evolution reaction at the potential more positive than 1.1V is observed.
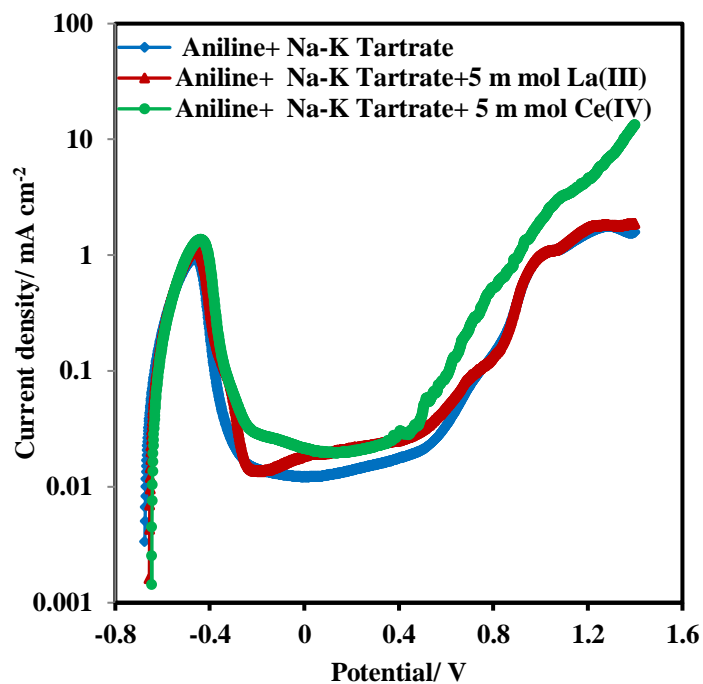
Figure 4.2. 11: Effect of La(III) and Ce(IV) on polymerization of aniline in Na-K Tartrate

4.2.9 Effect of La(III) and Ce(IV) on polymerization of aniline in Na-K Tartrate by CV

A potential window of -0.1V and 1.4V was chosen for CV polymerization of aniline onto mild steel surfaces. Doping aniline with La (III) and Ce(IV), there is decrease in peak current, but there is no distinct reversible response as shown in **Fig. 4.2.12**. Same nature of leucoemeraldine to emeraldine conversion and emeraldine to pernigraline conversion appears in La (III) and Ce(IV) doped aniline too. Peak current fell steadily on consecutive scans.
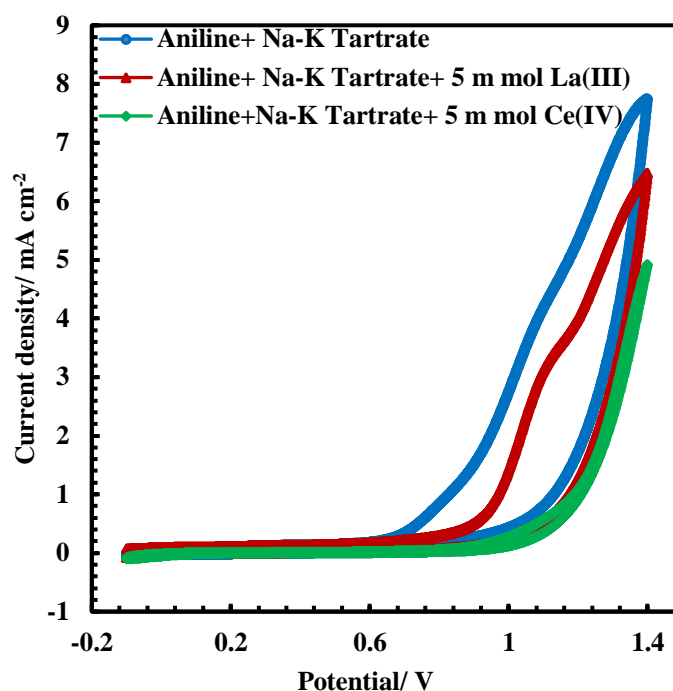
Figure 4.2.12: Effect of La(III) and Ce(IV) on polymerization of aniline in Na-K Tartrate

4.2.10 Characterization of PANI coating formed in Na-K Tartrate

4.2.10.1 FTIR- spectra

ATR-FTIR measurements were performed on both the PANI coatings after taking out the coating with acetone. **Fig. 4.2.13** shows the FTIR spectra of PANI obtained from Na-K tartrate. The band at 3415 cm^{-1} is assigned to the N-H stretching vibrations of amine groups. The band near 3005 cm^{-1} is attributed to the N−H bond between amine and imine sites, and 2924 cm^{-1} is due to aliphatic C-H stretching of acetone. The obtained signals are distinguished between benzenoid rings and quinoid rings from the bands in the range of 1350-1960 cm^{-1} region of the spectrum. Intensive bands close to 1716 cm^{-1} corresponds to C=O of acetone, and the one near 1423 cm^{-1} and 1364 cm^{-1} corresponds to the semi quinoid - N -ring mode of oxidized polyaniline. The 1223 cm^{-1} band corresponds to C-N vibration(Fusalba & Bélanger, 1999; Kawashima & Goto, 2011; Medhat Ibrahima and Eckhard Koglin, 2005; Rao *et al*., 2012). The band intensity at 1423 cm^{-1} is stronger (benzenoid form) than that at 1560 cm-1(quinoid form) since PANI contains semiquinoid –N- ring and more potent benzenoid form, makes emeraldine salt. The band at 1093 cm^{-1} was related to N=Q=N and 531 cm^{-1} is related to the C-N-C bonding mode of the aromatic ring (Kawashima & Goto, 2011; Mostafaei & Zolriasatein, 2012).

Figure 4.2.13: FTIR spectra of PANI prepared from aniline in Na-K Tartrate (Gupta *et al.*, 2021)

4.2.10.2 UV-Vis spectrum

A sharp peak and a shoulder of PANI are observed in a UV-Vis spectrum presented in **Fig. 4.2.14.** PANI synthesized in Na-K tartrate indicates an energetic, broadband at 354 nm which corresponds to the $\pi \rightarrow \pi^*$ transition in the benzoid ring and a weak band
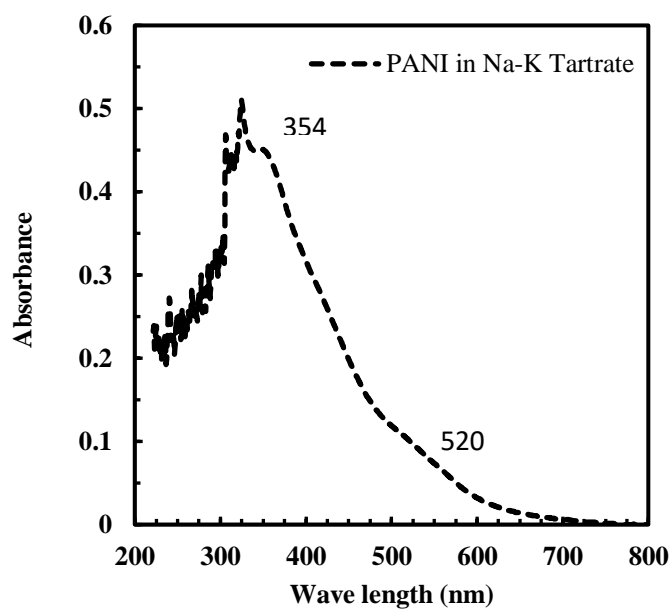
Figure 4.2.14: UV-Vis spectra of PANI prepared from aniline in Na-K Tartrate (Gupta *et al.*, 2021)

(shoulder) at 520 nm is due to the transition of benzenoid rings into quinoid rings (π–polaron transition) (Canales *et al.*, 2014; Huang & MacDiarmid, 1993).

4.2.10.3 X-ray diffraction

X-ray diffraction was used to study the effect of electrolytes on the crystallinity of the PANI coating. XRD patterns of PANI in Na-K Tartrate are shown in **Fig. 4.2.15.** A broad diffraction peak in the range of 10 to 30, 2θ values reveals diffraction from the parallel and perpendicular periodicity of the PANI chain (Mostafaei & Zolriasatein, 2012). The diffraction at $2\theta= 22.82°$ (PANI from Na-K Tartrate) shows the Bragg's reflection occurring from (020) Millar planes (Amaechi *et al.*, 2015; Bera *et al.*, 2017; Sydulu Singu *et al.*, 2011). Bare MS shows an iron peak at $44°\,2\theta$. A similar observation is obtained from SEM images (**Fig. 4.2.18e**). Moreover, the peak diffracted at an angle of 22.82 with d-spacing 3.89 Å, shows low crystallinity of the PANI due to the repetition of benzoid and quinoid rings in the PANI chains(Abdiryim *et al.*, 2005; Bandgar *et al.*, 2014; Mostafaei & Zolriasatein, 2012; Sathiyanarayanan *et al.*, 2005; Wan *et al.*, 1994; Wan & Li, 1998).
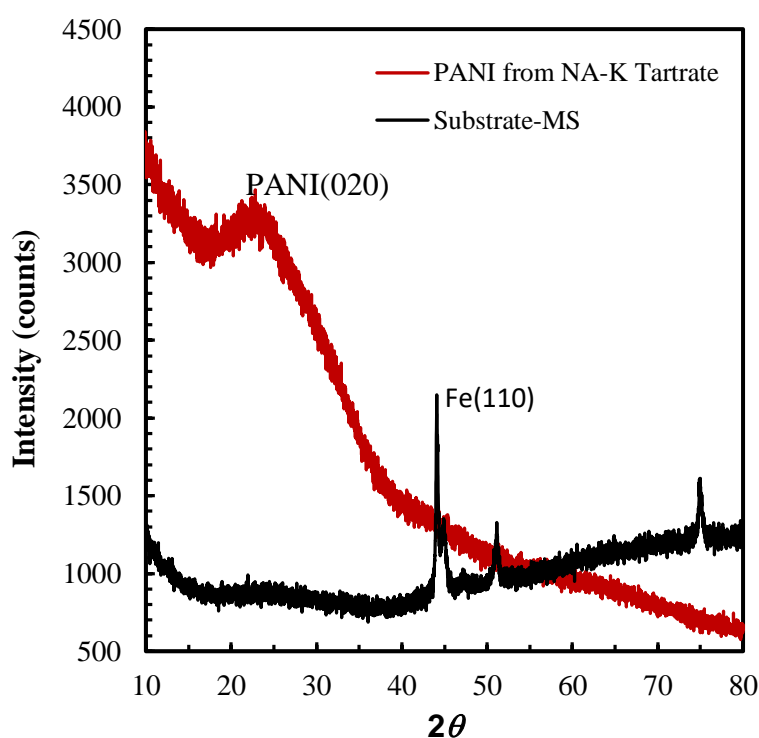
Figure 4.2.15: XRD spectra of PANI prepared from aniline in Na-K Tartrate, and bare mild steel(Gupta *et al.*, 2021)

4.2.11 Optical image

Fig. 4.2.16 shows optical micrographs of the Bare MS and different stages during PANI coatings. The images at OCP and passivation of the Sample show a rough surface. Moreover, roughness of surface seems reduced in PANI coatings by potentiostatic than CV or anodic polarization. The optical image shows a uniform and compact PANI coating but on doping with La(III), PANI becomes smaller and spherical in size.
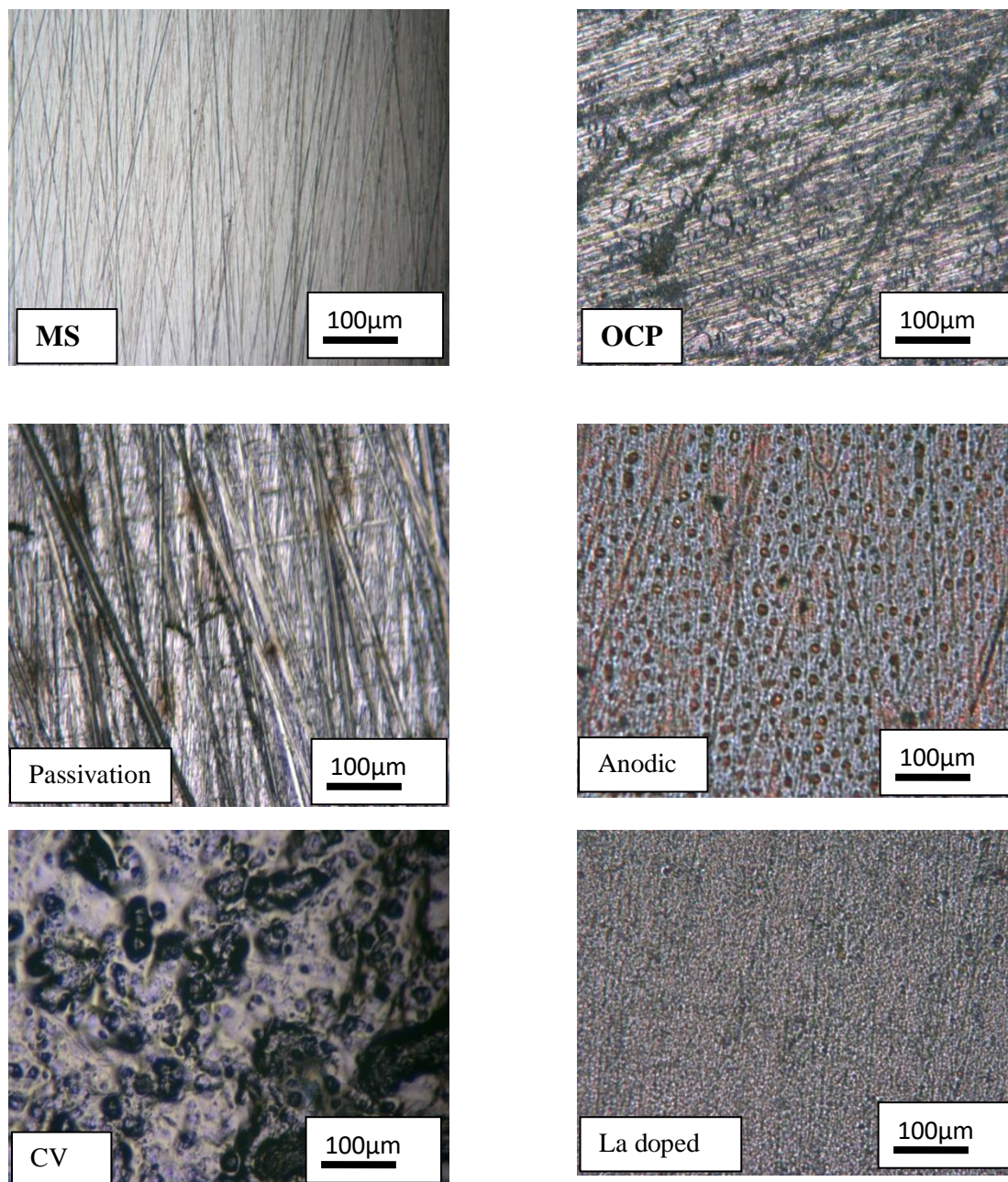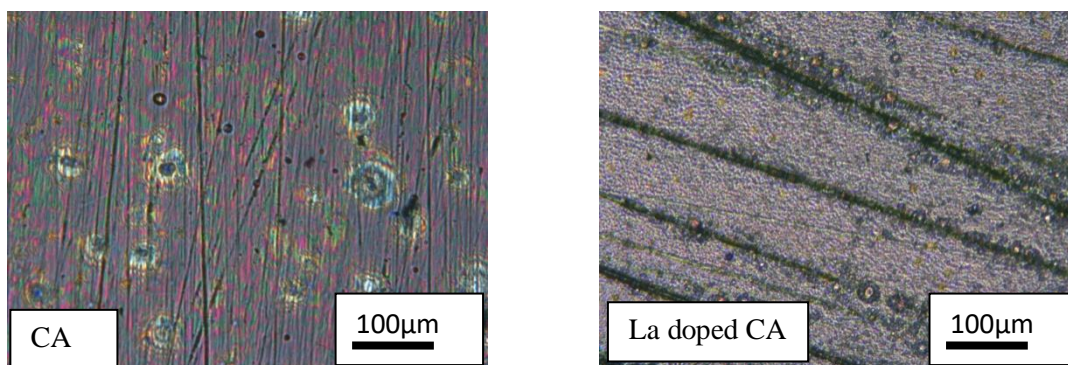
Figure 4.2.16: Optical images of MS at different stages of PANI coating in Na-K Tartrate, and PANI prepared by CV and chronoamperometrically.

The morphology of the PANI film is strongly influenced by current density. **Fig. 4.2.17** shows the optical image of the PANI coated MS surface at different current densities. The optical image shows a uniform and compact PANI coating at current density of 0.5 mA cm^{-2}. The PANI coating becomes thinner with the increase in current density (1 and 2 mA cm^{-2}).

0.5 mAcm^{-2}

0.75 mAcm^{-2}

1 mAcm^{-2}

2 mA/cm^{-2}
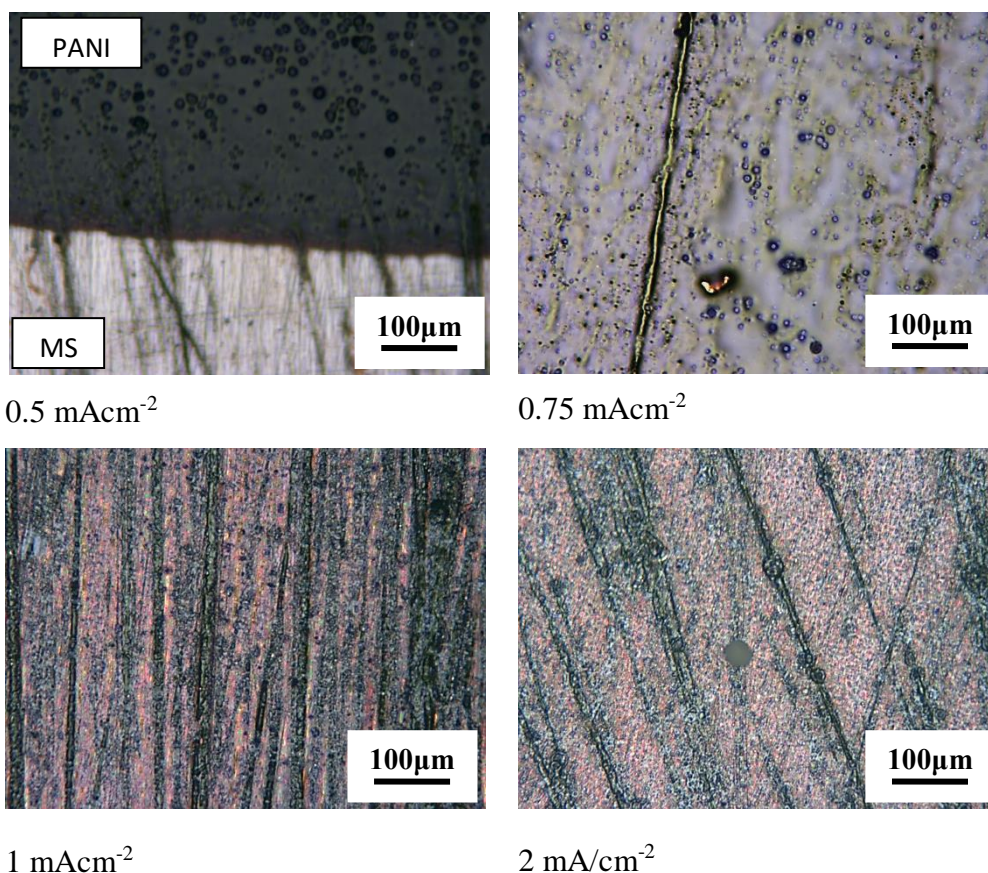
Figure 4.2.17: Optical images of PANI deposited on MS by galvanostatically at various current densities

This is because the higher current density leads to both passivation and oxidation of MS surface. Therefore, only some amount of charge is used for oxidation of aniline. In addition, at higher current density, oxidation of PANI can also take place. The electrolyte solution was visibly contaminated with brown precipitates dissolved out from outer layer of PANI. At low current density spherical shape PANI coating is formed.

4.2.12 Scanning electron microscopy (SEM)

Fig. 4.2.18 shows the SEM micrograph of PANI deposition on MS during anodic polarization at various states and PANI deposited by CV methods. The microgram 4.2.18 (a), (b) and (c) shows morphology at OCP, passivation started and passivation completed respectively. The **Fig. 4.2.18(c)** shows smoot surface due to formation of Fe-tartrate at completion of passivation. **Fig. 4.2.18(d)** shows rough surface when polymerization of aniline just started due to the leakage of charge from the surface. There is no much difference in morphology of PANI prepared by anodic polarization and CV methods. **Fig. 4.2.18(e) and (f)** indicates a worm-like compact, pore-free and fine grain coating in the nanometer dimension, which was visible only at very high magnification. The EDX result showed the presence of N and C supported the formation of PANI. The mapping showed the distribution of particles.

OCP
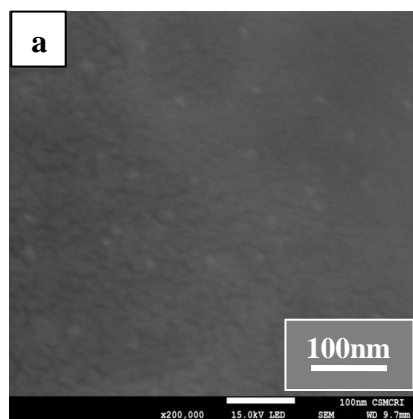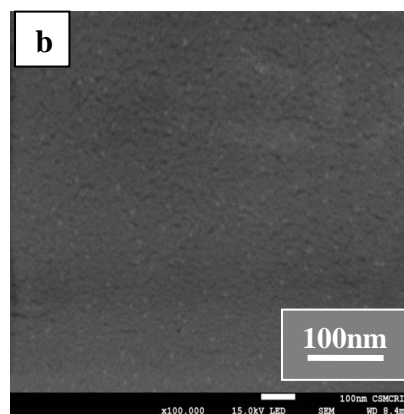
Passivation started
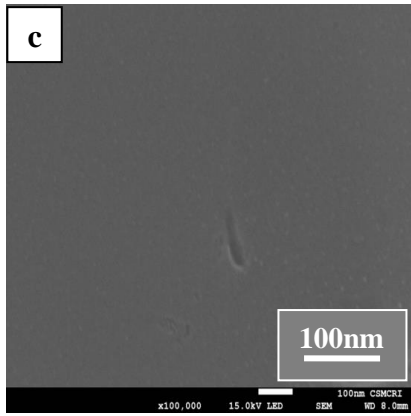
Passivation completed
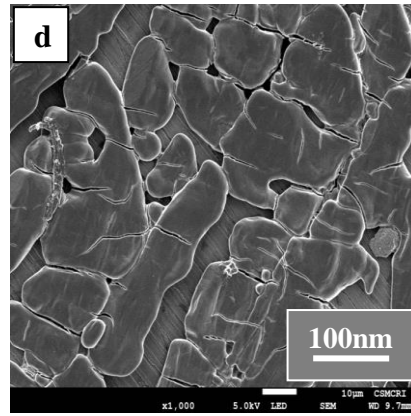
Polymerization started
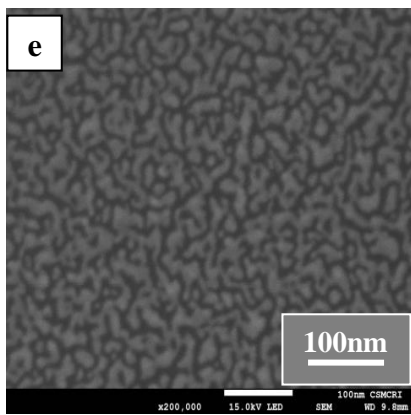
PANI prepared by anodic polarization
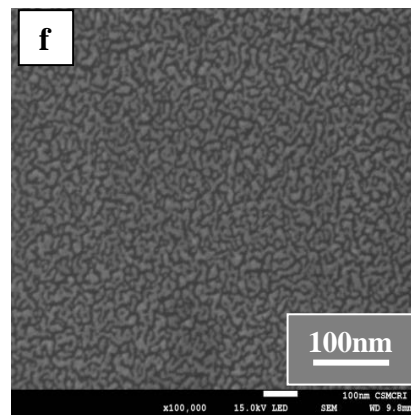
PANI prepared by CV

Figure 4.2.18: SEM micrograph of PANI deposition on MS during anodic polarization at various states and PANI deposited by CV methods from 0.3M aniline in 0.2 M Na-K Tartrate

	wt%
C	64.50
N	6.64
O	1.67
Fe	27.19
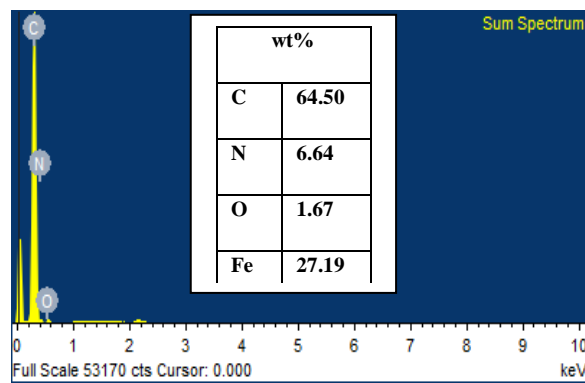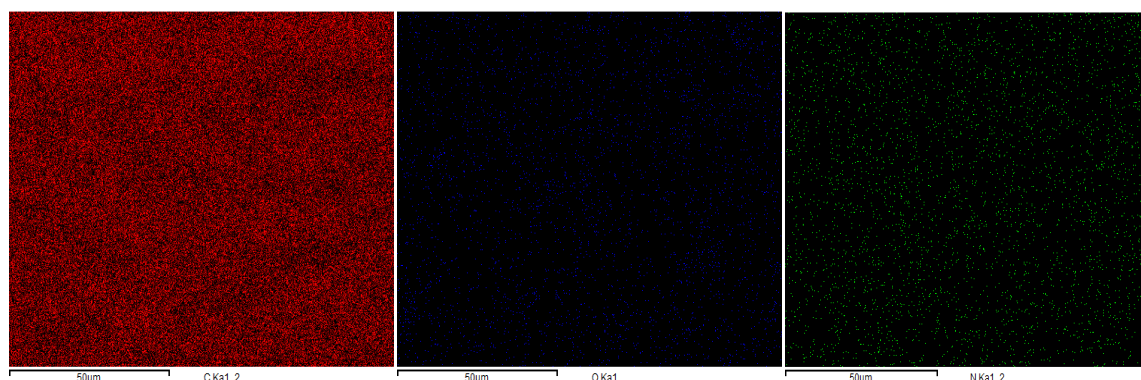
Figure 4.2.19: EDX and Mapping of PANI prepared from 0.3M aniline in 0.2M Tartrate

Fig. 4.2.20 shows the SEM micrograph with EDX of PANI deposited on MS from 0.3 M aniline in 0.2 M Na-K tartrate containing La (III). The micrograph shows spherical and compact PANI with blister. The EDX result shows the presence of N, C, O and La supports the tailoring of PANI.

	% Wt
C	67.32
N	7.78
O	24.71
La	0.19
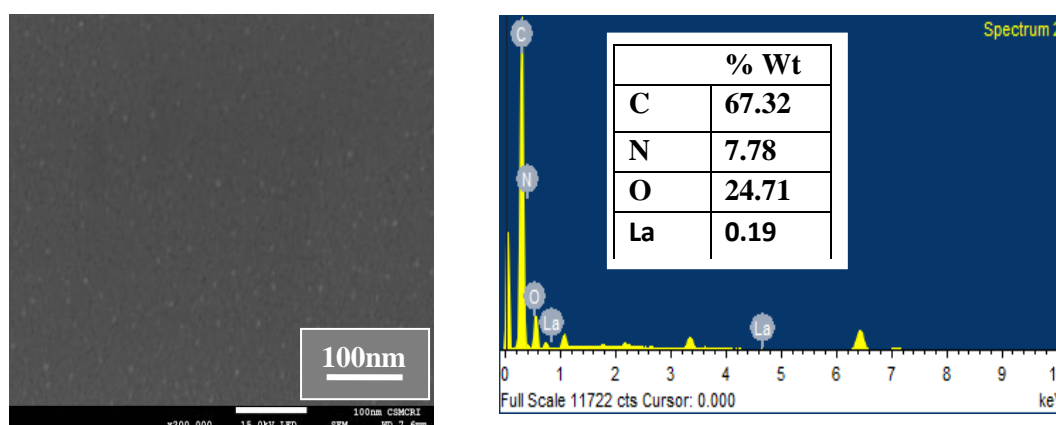
Figure 4.2.20: SEM micrograph of PANI deposited on MS from 0.3M aniline + 0.2 M Na-K Tartrate + La (III)

4.2.13 Transmission electron microscopy (TEM):

TEM micrographs indicated nanostructures of the PANI. **Fig. 4.2.21** shows nano-particles have a spherical shape, with very small size (240 to 1900 nm), and there was aggregation due to their large surface area and the interaction between the particles.

Fig. 4.2.22 shows TEM images of PANI doped with La (III). PANI doping with La has smaller size than PANI and its average size ranges from 180 nm to 280 nm which is in agreement with SEM micrographs.
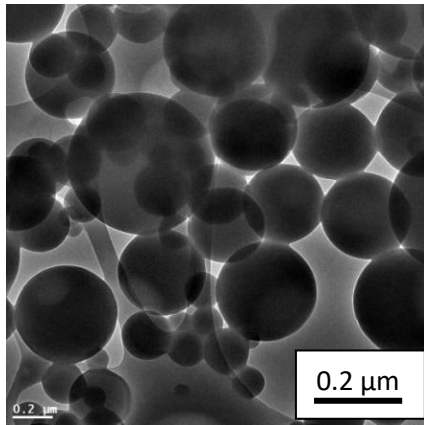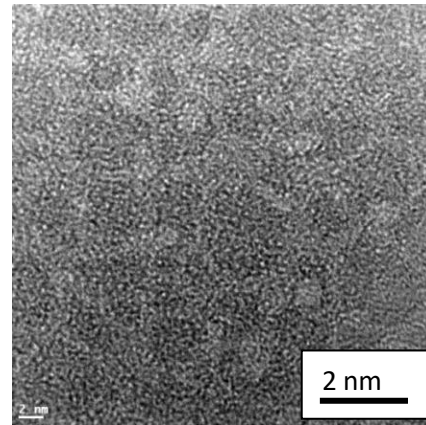
a) 0.2 μm   b) 2 nm

Figure 4.2.21: TEM images of PANI prepared from 0.3M aniline in 0.2M Na-K tartrate
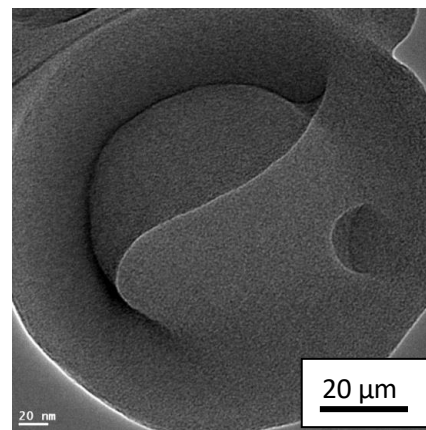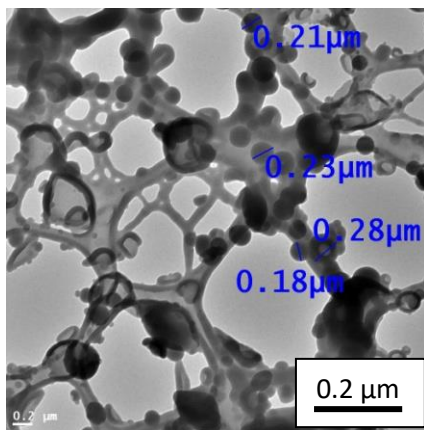
Figure 4.2.22: TEM images of PANI prepared from 0.3M aniline in 0.2M Na-K tartrate containing La (III)

4.2.14 Atomic Force Microscopy (AFM)

In addition to SEM and TEM images, Atomic Force Microscopy (AFM) images of PANI coating have been taken. **Fig. 4.2.24** shows 2D and 3D images of PANI coated MS obtained by AFM. The images showed the regular and homogeneous PANI coating from both anodic and cyclic voltammetry. 3-D images showed some islands on the surface corresponding to the nucleation sites (Buron *et al*., 2011). The change in mean roughness and the rms roughness of coating showed that PANI coating by CV on MS is smooth and uniform coating.

(a) MS
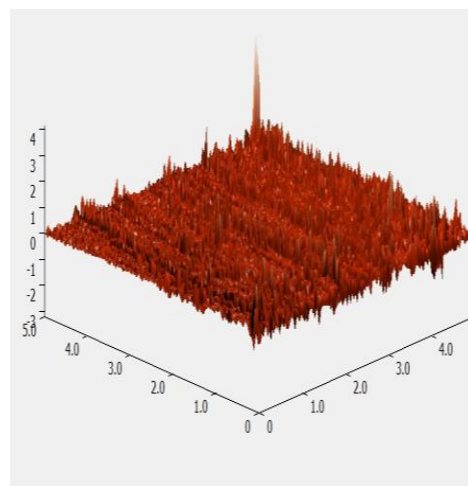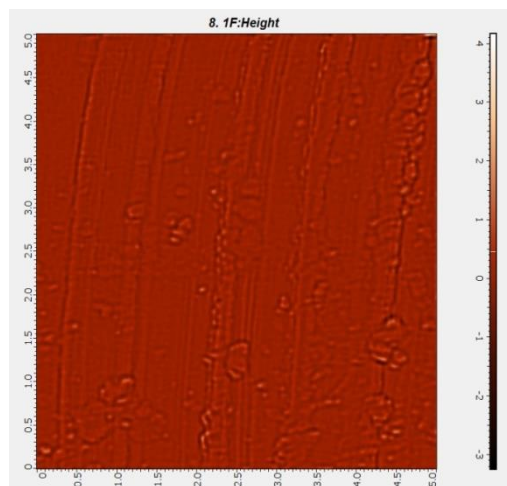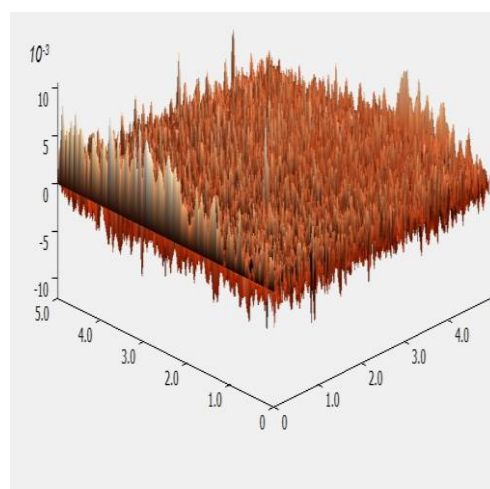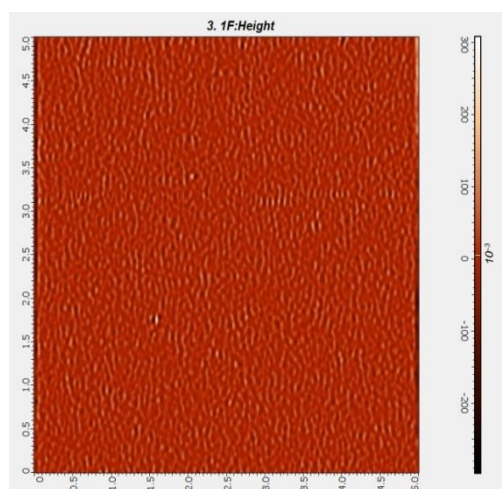
(b) PANI by anodic polarization
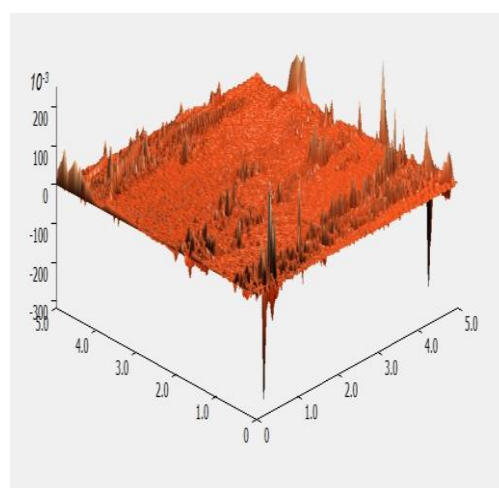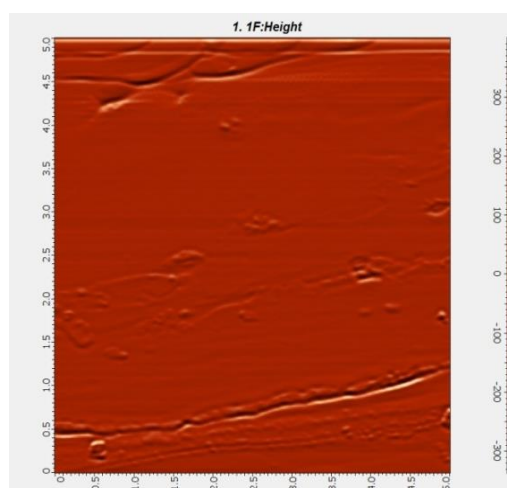
(c) PANI prepared by CV

Figure 4.2.23: AFM images (a) MS (b) PANI prepared by anodic polarization and (c) PANI
prepared by CV

Table 4. 1: Roughness of PANI coatings from Na-K Tartrate on MS

	Mean Roughness (μm)	RMS Roughness (μm)
Bare Mild Steel (MS)	0.159	0.234
PANI Coating by Anodic	0.0308	0.04
PANI Coating by CV	0.0168	0.0366

4.3 Electrochemical synthesis of PANI in BAW

4.3.1 Optimization of the concentration of BAW

Fig. 4.3.1 shows the anodic polarization of MS in 0.1 M to 0.02 M BAW solutions. The general characteristics of the polarization curves in electrolytes are similar to **Fig. 4.1.1**. There is a marginal shift of OCP towards positive values with the increase in concentration in the solutions. In BAW in **Fig. 4.3.1**, a positive shift of OCP and lowering of passivation current with the concentration is observed.
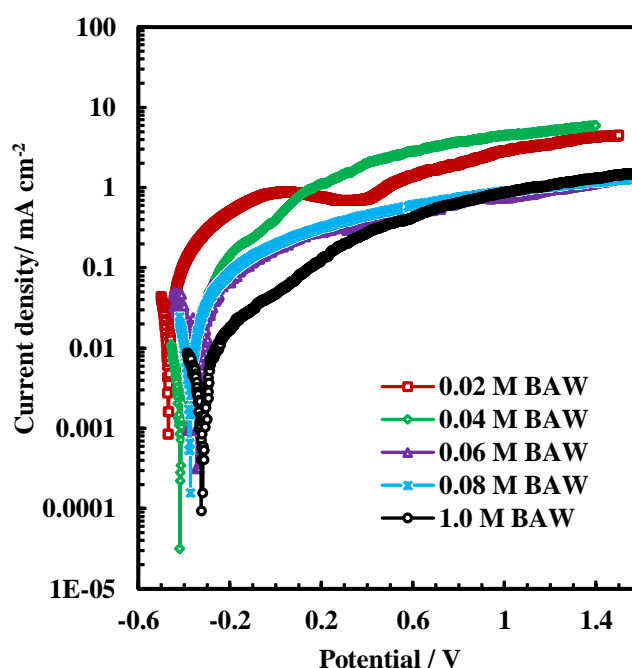
Figure 4.3.1: Anodic polarization of MS in various concentrations of BAW at a scan rate of 1 mV/s (Gupta *et al.*, 2021)

From the polarization curves, 0.08 M BAW was chosen as the optimum concentrations for polymerization of aniline.

4.3.2 Electropolymerization of aniline in BAW

After optimizing the concentration of BAW, electropolymerization of aniline onto MS sample was carried out using a 0.1 M aqueous solution of aniline in 0.08 M BAW solutions. **Fig. 4.3.2** shows the polymerization curves of aniline in 0.08 M BAW, and 0.3 M oxalic acid.

In BAW, the Fe-dissolution current is small, most likely due to the formation of Fe-benzoate layer at OCP. After the initial decrease in current from -0.14 V till +0.37 V, the current increases progressively with humps and shoulder formation till +1.37 V. As mentioned above, the formation of different forms of PANI also occurs in this potential range. The visual observations showed the formation of a brown colored coating on the MS surface. The features of polarization curves displaying oxidation and polymerization of aniline are not present in **Fig. 4.1.2** and **Fig. 4. 3.1** due to the absence of aniline.
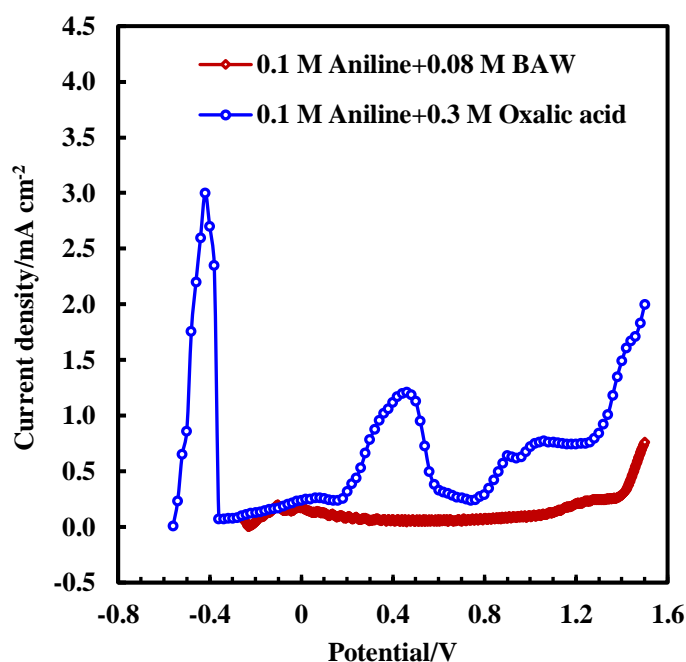
Figure 4.3.2: Anodic Polarization of MS in 0.08 M BAW, and 0.3 M oxalic acid solutions containing 0.1 M aniline in each at a scan rate of 1.0 mV/s (Gupta *et al.*, 2021)

4.3.3 Optimizing the concentration for polymerization of aniline in BAW

The effect of aniline concentration and BAW on polymerization is presented in **Fig. 4.3.3**. The concentration of aniline is varied from 0.1 M to 0.4 M while the concentration of benzoic acid varied from 0.08 M to 0.02 M in 3:1 ethanol-water system. In 0.1 M aniline and 0.08 M BAW, slight dissolution of iron is observed, and a rise in the concentration of

aniline decreases the dissolution of Fe. This phenomenon is also observed in the Na-K Tartrate solution (**Fig. 4.2.3**). This indicates the effect of monomer concentration on dissolution and passivation of MS at OCP, which needs to be investigated further. The OCP shifts to positive value with an increase in the concentration of aniline, and a better PANI coating was obtained at a lower potential (less positive) as compared to Na-K tartrate solution. This is possibly due to the formation of Fe-benzoate layer(Popović & Grgur, 2004), which limits the Fe-dissolution, and the available charge is used for aniline oxidation. From **Fig. 4.3.3**, 0.3 M aniline in 0.04 M BAW is chosen as the best composition because the higher concentration of both resulted in the non-adhesive coating as confirmed by visual observation and scotch-tape adhesion test.
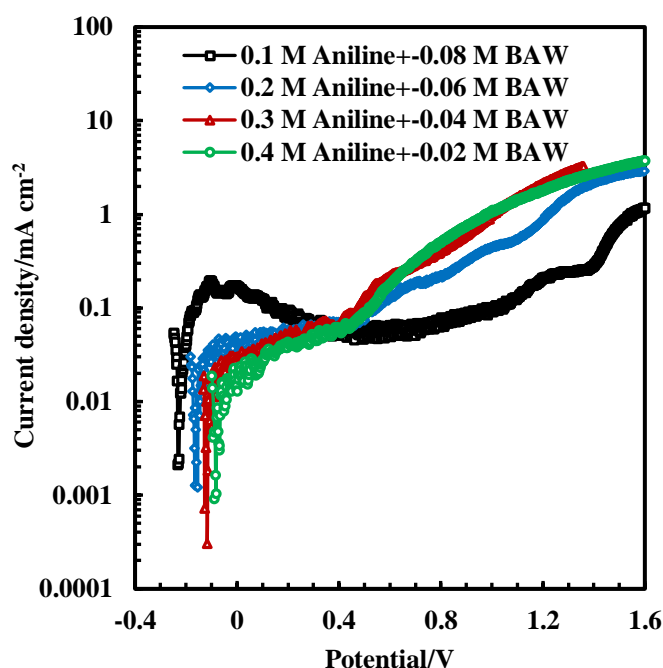
Figure 4.3.3: Anodic polarization of MS in different concentration of aniline in varying concentrations of BAW solutions. The scan rate was 1mV/s and polarization was started after remained at OCP for 30 min. (Gupta *et al*., 2021)

4.3.4 Deposition of PANI in BAW by CV

Cyclic voltammetry (CV) was carried out in various concentrations of BAW solutions containing different amounts of aniline to optimize the concentrations of electrolyte and aniline. **Fig. 4.3.4** shows the CV curves of MS in various concentrations of BAW and aniline. The concentrations of aniline varied from 0.1 M to 0.4 M while concentration of benzoic acid varied from 0.08 M to 0.02 M in 3:1 ethanol-water system. A stable voltammogram with no anodic peak during cathodic scan is obtained. From the results, a

concentration of 0.3 M aniline in 0.04 M BAW is chosen as the best composition due to better coating and its adhesion.
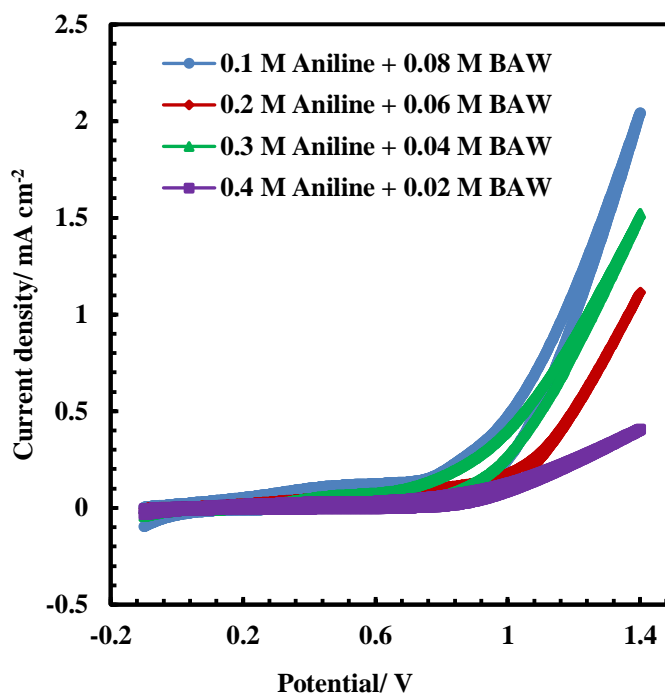
Figure 4.3.4: Cyclic voltammetry of MS in different concentration of aniline in varying concentrations of BAW at 20mV/s scan rate

Fig. 4.3.5 shows the cyclic volatmmograms of MS in solutions containing 0.3 M aniline in 0.04 M BAW solutions along with 0.1 M aniline in 0.3 M oxalic acid. A stable voltammogram with no anodic peak during cathodic scan is observed unlike in oxalic acid solution. The polymerization occurs in various steps, as discussed in section 4.2.5, **Fig. 4.2.5** and lower current values in BAW solutions reflects the better coating as compared to oxalic acid. The results reveal BAW offer better alternatives for polymerization of aniline onto MS surface with improved surface morphologies and cyclic stabilities.

The anodic peaks disappeared after the first scan, and peak current density decreases when the number of cycles increases (Kellenberger *et al*., 2014; Machnikova *et al*., 2008). Current values decreased with the number of scans, as shown in **Fig. 4.3.6**. Moreover, the thickness of homogenous and sticky PANI films increased with a number of scans. The result reveals that the thickening of PANI occurs with an increase in the number of cycles and its stability.
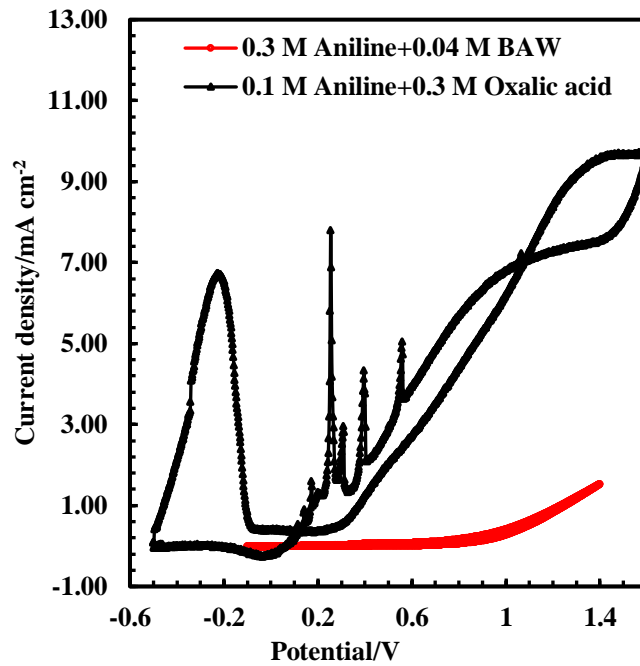
Figure 4.3.5: PANI coating on MS obtained by cyclic voltammetry in 0.3 M aniline+0.04 M W BA, and 0.1 M aniline+0.3 M Oxalic acid solution (Gupta *et al.*, 2021)

At low sweep rates, 5–10 mV/s, a well-defined anodic peak is seen as shown in **Fig. 4.3.7**. Above 20 mV/s, no well-defined anodic wave was seen in the CV.
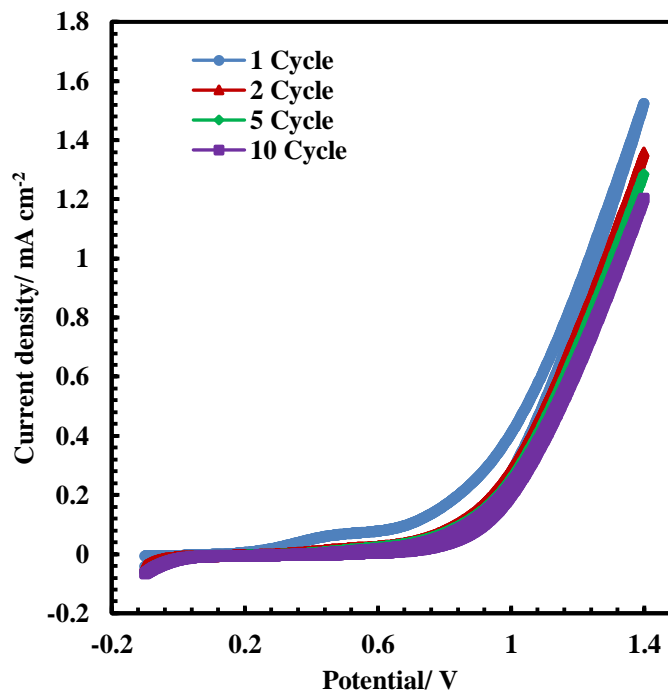
Figure 4.3.6: PANI coating on MS obtained by cyclic voltammetry in 0.3 M aniline+0.04 M BAW with different cycles at the scan rate of 20mV/s

Therefore, to deposit a layer of iron benzoate before deposition of PANI, requires a scan rate of ≤ 20 mV/s. With continued polarization, a small increase in current density is observed between $+ 0.167$ and $+ 0.6$ V.
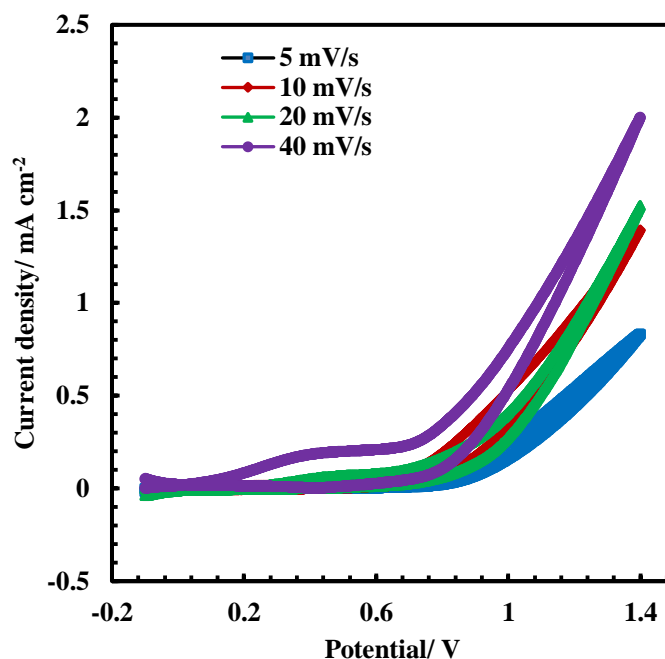
Figure 4.3.7: PANI coating on MS obtained by cyclic voltammetry in 0.3 M aniline+0.04 M W BA with the different scan rate

4.3.5 Potentiostatic polymerization of aniline in BAW

Fig. 4.3.8 shows the chronoamperogram of aniline in BAW and aniline in BAW containing 5 m mol La(III). It can be observed that aniline polymerization begins at the very beginning. Passivation of mild steel surfaces begins at the very beginning. As a result of the formation of iron benzoate, the current drops abruptly. The applied voltage 1.4 V is also sufficient for aniline polymerization. After 48 seconds, there is a limiting current in the electrolyte containing just aniline. But after 120 seconds there is limiting current in the electrolyte containing La(III) solution.

The drop in current is significantly slower in the presence of La(III). These observations show that the presence of rare earth metal salt tailors the PANI film.
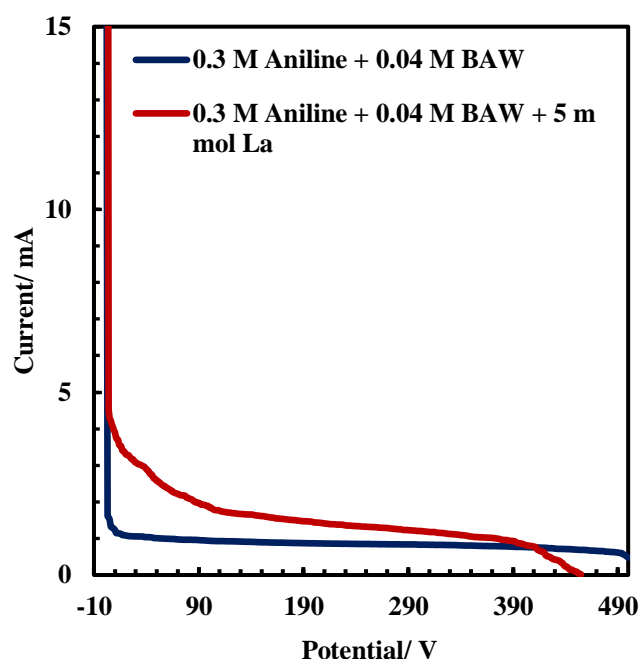
Figure 4.3.8: PANI coating on MS obtained by cyclic voltammetry in 0.3 M aniline+0.04 M W BA with the different scan rate

4.3.6 Galvanostatic polymerization of aniline in BAW

The electrochemical deposition of PANI onto MS was achieved at various current densities. **Fig. 4.3.9** shows the chronopotentiometric behavior of MS immersed in the polymerizing solution of 0.3 M aniline + 0.04 M BAW at a current density of 100 μAcm^{-2}, 200 μAcm^{-2}, and 300 μAcm^{-2}, respectively. From the evolution of potential with time, it is clear that no induction period associated with MS dissolution is seen at the beginning. This behavior reflects that very little dissolution of the MS occurs as soon as current is applied unlike in the case of oxalic acid where a clear induction period is observed (inset in **Fig. 4.3.9**).

During the early stages of polarization, the potential remains at about -0.270 V (**Fig. 4.3.9**), and the MS dissolves anodically over a time that is dependent on the applied current density. The charge (Q) passing through the electrode before increase of potential is determined by the relation (Camalet*et al*., 1996; Eftekhari, 2004).

$$Q = It \qquad\qquad\qquad \textbf{[4-8]}$$

Where I is the current density in mA/cm^2 and t is the time in second.

In the case of oxalic acid solution, a charge of 275 mC cm^{-2} is required for oxidation of aniline (Camalet *et al*., 1996), whereas in the case of BAW, merely a charge of 0.1 mC

cm^{-2} is needed for the oxidation of aniline. Therefore, BAW results in minimization of energy used for polymerization and deposition of PANI on MS in addition to preventing the loss of iron.

The potential of the MS increases with increase in current density during the polarization process, which indicates for the decrease of metal dissolution with the increase of applied current (Lacroix *et al*., 2000). At a lower current density (0.1 mA cm^{-2}), the potential increased sharply from -0.270 V to 0.270 V and then increased to 0.912 V with waves which represent the passivation and dissolution of MS till 8.5 sec. The passivation is due to the formation of Fe-benzoate. The potential then increases gradually with the commencement of the oxidation of aniline and formation of PANI take place. The charge needed for the oxidation of substrate electrode depends on current density as well as experimental conditions like medium, and substrate electrode (Eftekhari, 2002). For the current density 0.2 mA cm^{-2} and 0.3 mA cm^{-2}, the potential increased from -0.200 V to 0.634 V in 4 sec and 0.612 V to 0.739 V in 3 sec, respectively. This is attributed to the MS surface passivation with the increase in current density. A slightly decrease in potential thereafter is attributed to passivation followed by a constant potential due to continuous growth and surface coverage by PANI.

When a nearly constant value of potential is obtained, polymerization on the outer surface is not visually observed. As the polarization proceeds, the potential slightly increases and traces of external polymerization start to be detected. Finally, potential stabilizes for a longer time with the formation of PANI on the outer surface which is obvious and thickening also occurs. These results are similar to those reported for the electrodeposition of aniline onto MS (Camalet *et al*., 1996; Kazum & Kannan, 2016; Lacroix *et al*., 2000) and polypyrrole into porous silicon (Moreno *et al*., 1999).

The mechanism for the electrochemical deposition of PANI is understood to proceed through a radical cation which reacts with a second radical cation to give a dimer which further reacts with cation of aniline to form polyaniline (Dhawan & Trivedi, 1991). The possible reaction mechanism is summarized as;

Firstly, dissolution of iron occurs as indicated by initial potential value

$$Fe \rightarrow Fe^{2+} + 2e \qquad\qquad \textbf{[4-9]}$$

With the presence of tartrate ion in the solution, the dissolved Fe^{2+} forms an insoluble Fe-benzoate and precipitate at MS surface forming a passivation layer
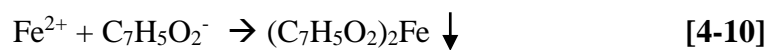
$$\text{Fe}^{2+} + \text{C}_7\text{H}_5\text{O}_2^- \rightarrow (\text{C}_7\text{H}_5\text{O}_2)_2\text{Fe} \downarrow \qquad\qquad \textbf{[4-10]}$$

With the blockade of active dissolution of metal, the available charge is used for the oxidation of aniline which undergoes polymerization with the formation of radical cation. This leads to gradual increase of the potential. The mechanism of dissolution, passivation, oxidation and polymerization is given below.
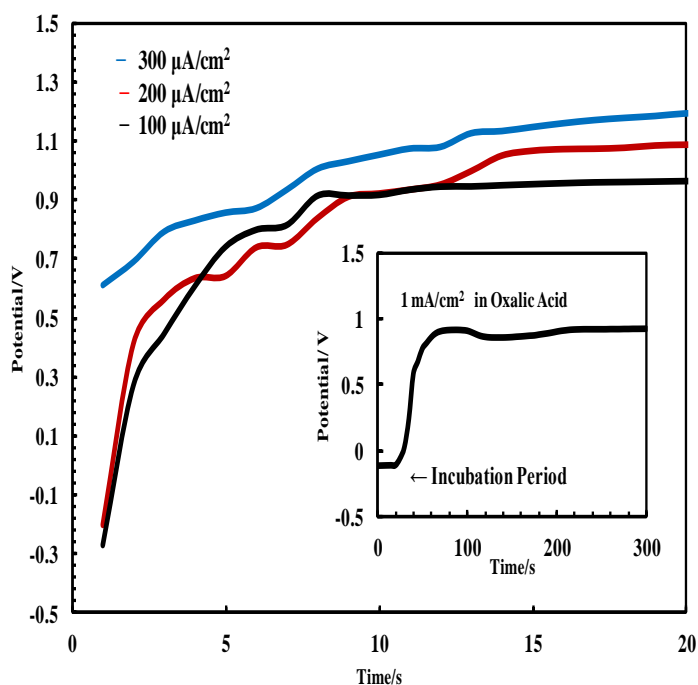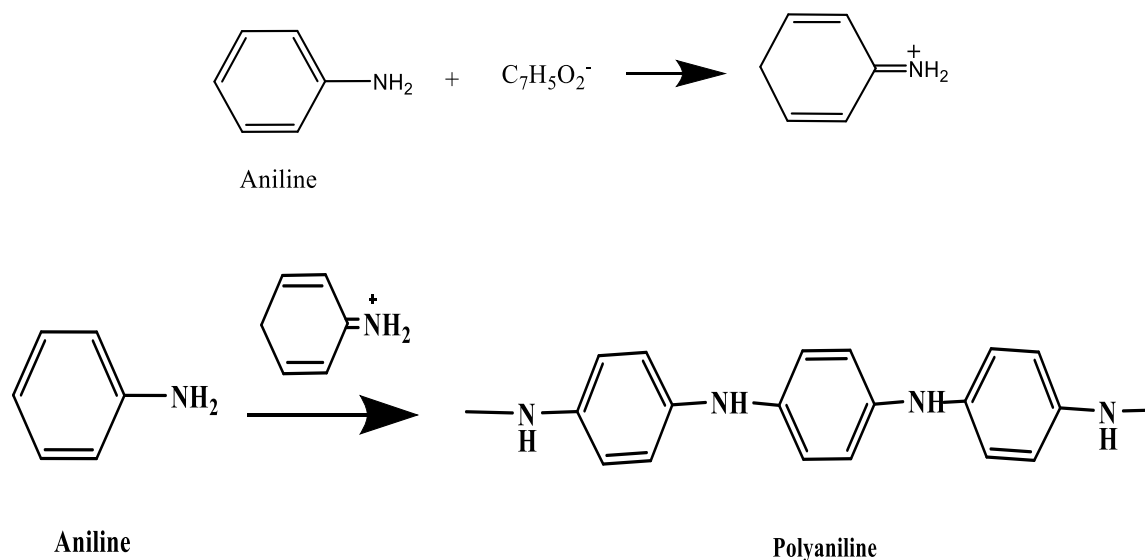
Figure 4.3.9: Electrochemical deposition of a PANI on MS in 0.3M aniline in 0.04 M BAW at different current densities

4.3.7 Effect of La(III) and Ce(IV) on polymerization of aniline in BAW

The presence of La (III) and Ce (IV) affects the current potential curve of aniline polymerization on mild steel. In the presence of La(III) and Ce(IV), the current-potential behavior of aniline polymerization is similar to BAW. The current value begins to increase with the polymerization of aniline due to increase in conductivity and the pronounced oxygen evolution reaction at the potential more positive than 1.1V was observed.
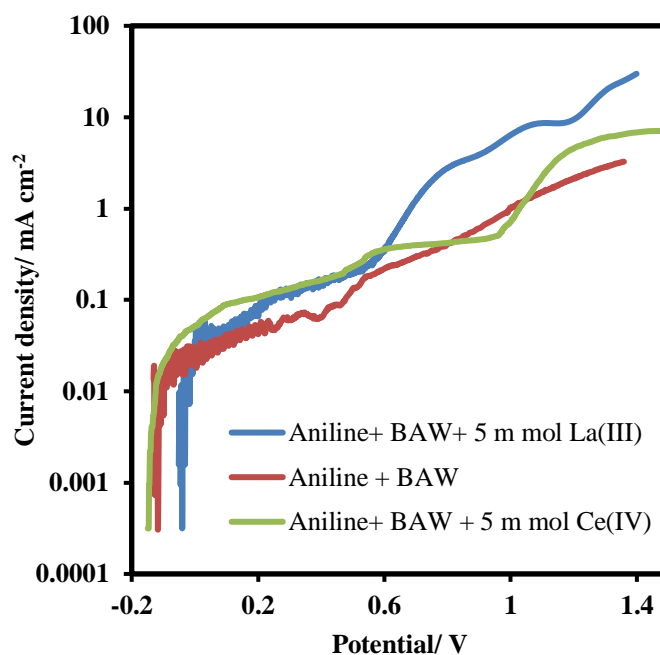
Figure 4.3.10: Effect of La(III) and Ce(IV) on polymerization of aniline in BAW

4.3.8 Effect of La(III) and Ce(IV) on polymerization of aniline in BAW by CV

A potential window of -0.1V and 1.4V was chosen for CV polymerization of aniline onto mild steel surfaces. Doping aniline with La (III) and Ce(IV), there is decrease in peak current, but there is no distinct reversible response as shown in **Fig. 4.3.11**. Same nature of leucoemeraldine to emeraldine conversion and emeraldine to pernigraline conversion appears in La (III) and Ce(IV) doped aniline too. Peak current fell steadily on consecutive scans.
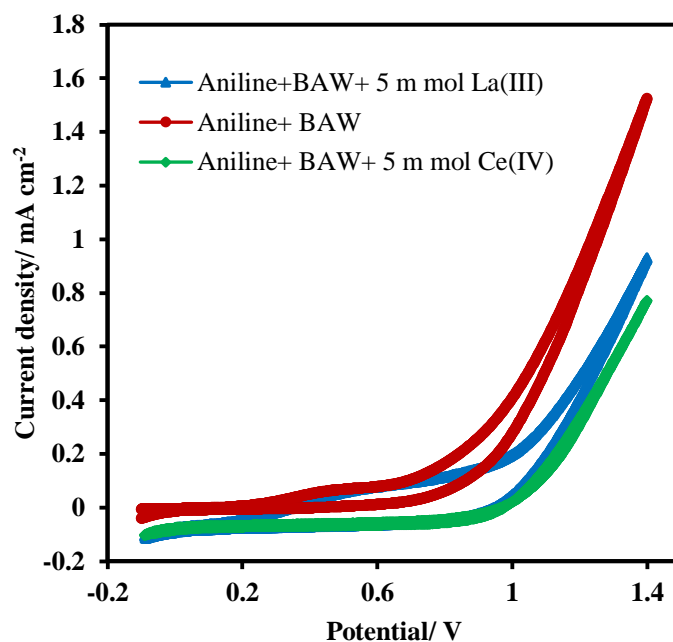
Figure 4.3.11: Effect of La(III) and Ce(IV) on polymerization of aniline in BAW by CV

4.3.9 Characterization of PANI coating obtained in BAW

4.3.9.1 FTIR- spectra

ATR-FTIR measurements were performed on the PANI coating after taking out the coating with acetone. **Fig. 4.3.12** shows the FTIR spectra of PANI obtained from BAW solutions. The band at 3415 cm^{-1} is assigned to the N-H stretching vibrations of amine groups. The band near 3005 cm^{-1} is attributed to the N−H bond between amine and imine sites, and 2924 cm^{-1} is due to aliphatic C-H stretching of acetone. The obtained signals are distinguished between benzenoid rings and quinoid rings from the bands in the range of 1350-1960 cm^{-1} region of the spectrum. Intensive bands close to 1716 cm^{-1} corresponds to C=O of acetone, and the one near 1423 cm^{-1} and 1364 cm^{-1} corresponds to the semi quinoid - N -ring mode of oxidized polyaniline. The 1223 cm^{-1} band corresponds to C-N vibration (Fusalba & Bélanger, 1999; Kawashima & Goto, 2011; Medhat Ibrahima and Eckhard Koglin, 2005; Rao *et al.*, 2012). The band intensity at 1423 cm^{-1} is stronger (benzenoid form) than that at 1560 cm^{-1}(quinoid form) since PANI contains semiquinoid –N- ring and more potent benzenoid form, makes emeraldine salt. The band at 1093 cm^{-1} was related to N=Q=N and 531 cm^{-1} is related to the C-N-C bonding mode of the aromatic ring(Kawashima & Goto, 2011; Mostafaei & Zolriasatein, 2012).

Figure 4.3.12: FTIR spectra of PANI prepared from aniline in BAW solutions (Gupta *et al*., 2021)

4.3.9.2 UV-Vis spectra

A sharp peak and a shoulder of PANI are observed in a UV-Vis spectrum presented in **Fig. 4.3.13.** The PANI prepared in BAW shows a sharp peak at 325 nm due to the $\pi \rightarrow \pi^*$ transition in the aromatic (benzoid) ring (Shabani-Nooshabadi, Ghoreishi *et al*., 2014). A shoulder at 430 nm is features of polyaniline oxidized to an oxidation state slightly lower than emeraldine, and another shoulder at 560 nm is due to the transition of benzenoid rings into quinoid rings (π–polaron transition) (Huang & MacDiarmid, 1993).
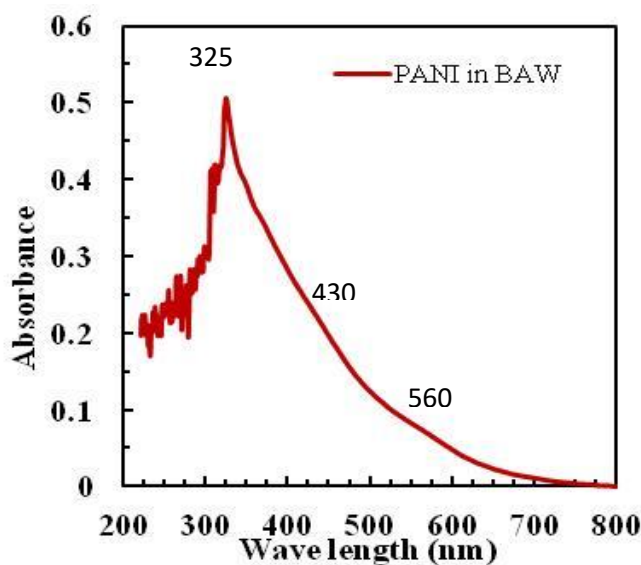
Figure 4.3.13: UV-Vis spectra of PANI prepared from aniline in BAW (Gupta *et al*., 2021)

4.3.9.3 X-ray diffraction

The effect of electrolytes on the crystallinity of the PANI coating was studied by X-ray diffraction. XRD patterns of PANI in BAW solution is shown in **Fig. 4.3.14.** A broad diffraction peak in the range of 10 to 30, 2θ values reveals diffraction from the parallel and perpendicular periodicity of the PANI chain (Mostafaei & Zolriasatein, 2012). The diffractions at $2\theta= 29.7^o$ show the Bragg's reflection occurring from (200) Millar planes (Amaechi *et al*., 2015; Bera *et al*., 2017; Sydulu Singu *et al*., 2011). Bare MS indicates an iron peak at 44° 2θ. As compared to peak at 22.82^o (Na-K Tartrate), the peak at 29.7^o (BAW) is broader. The crystallite size of PANI prepared in BAW is smaller than of Na-K tartrate. A similar study is made from SEM images (**Fig. 4.3.17d**). Moreover, the peak diffracted at an angle of 29.7 with d-spacing 2.89 Å, show low crystallinity of the PANI due to the repetition of benzoid and quinoid rings in the PANI chains (Abdiryim *et al*., 2005; Bandga r*et al*., 2014; Mostafaei & Zolriasatein, 2012; Sathiyanarayanan *et al*., 2005; Wan *et al*., 1994; Wan & Li, 1998).
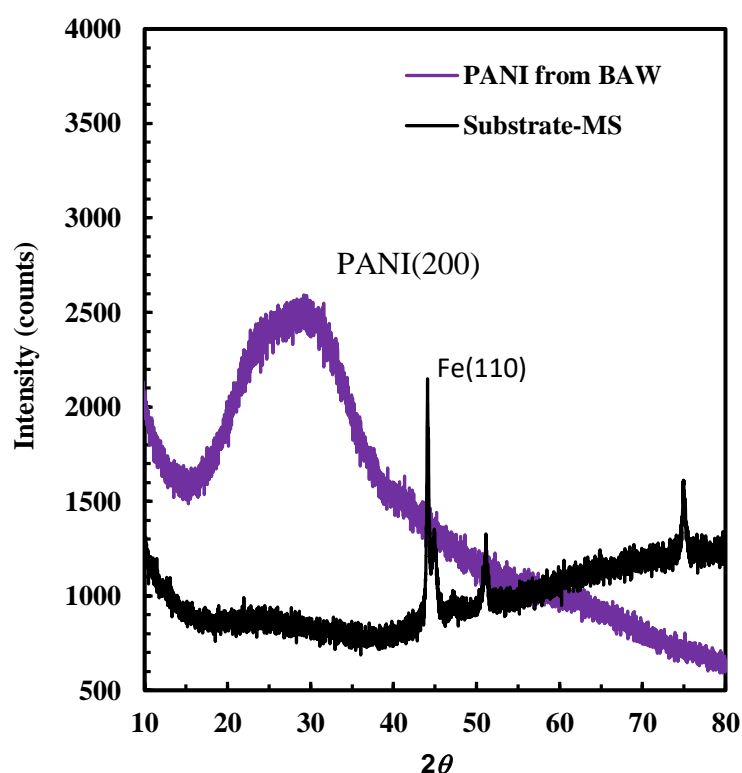
Figure 4.3.14: XRD spectra of PANI prepared from aniline in BAW, and bare mild steel(*Gupta et al.*, 2021)

4.3.10 Optical microscopy

Fig. 4.3.15 shows optical micrographs of the Bare MS and different stages during PANI coatings. The images at OCP and passivation of the Sample show a rough surface. Moreover, roughness of surface seems reduced in PANI coatings by potentiostatic than CV or anodic polarization. The optical image shows a uniform and compact PANI coating but on doping with La (III), PANI becomes fine and spherical in size.

MS

OCP

Anodic

CV

CA

La doped CA
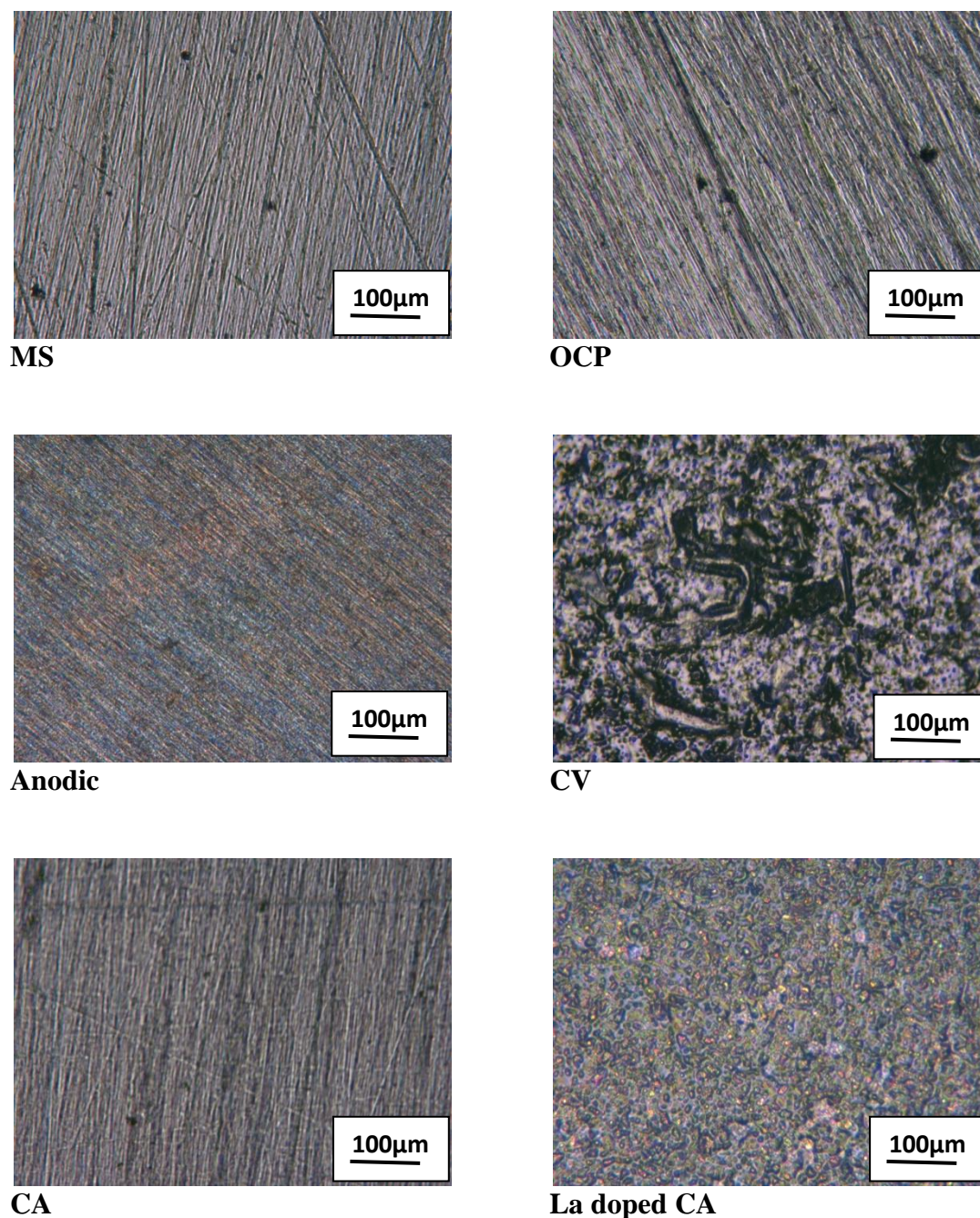
Figure 4.3.15: Optical images of MS at different stages of PANI coating in BAW, and PANI prepared by CV and chronoamperometrically

The morphology of the PANI film is strongly influenced by current density. **Fig. 4.3.16** shows the optical image of the PANI obtained in BAW coated MS surface at different current densities. The optical image shows a uniform and compact PANI coating at current density of 100 **µA** cm^{-2}. The PANI coating becomes thinner with the increase in current density.

100 µA/cm^2   **200 µA/cm^2**   **300 µA/cm^2**
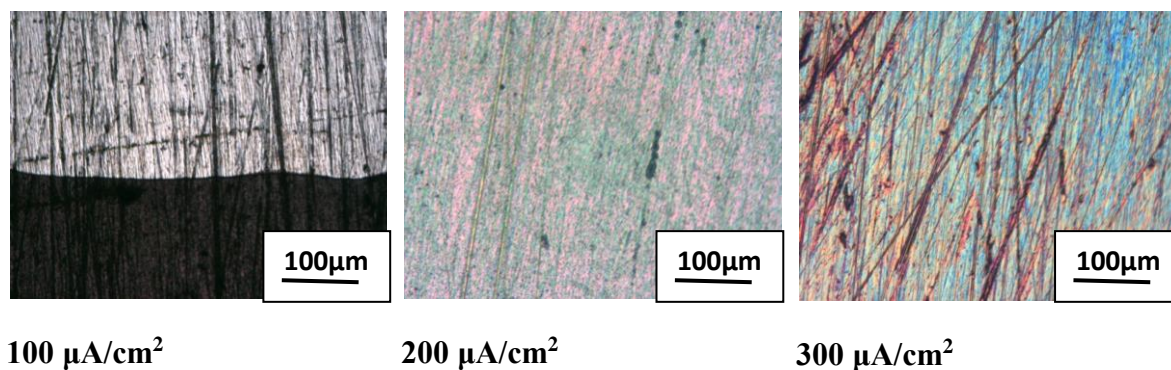
Figure 4.3.16: Optical images of PANI deposited on MS by galvanostatically at various current densities

This is because the higher current density leads to both passivation and oxidation of MS surface. Therefore, only some amount of charge is used for oxidation of aniline. In addition, at higher current density, oxidation of PANI can also take place. At low current density spherical shape PANI coating is formed.

4.3.11 Scanning electron microscopy (SEM)

Fig. 4.3.17 shows the SEM micrograph of PANI deposition on MS during anodic polarization at various states and PANI deposited by CV methods. The micrographs in Fig.4.3.17 (a), (b) and (c) show morphology at OCP, before polymerization and just polymerization started. **Fig. 4.3.17(b)** shows spherical shape due to formation of Fe-benzoate before polymerization of aniline. **Fig. 4.3.17 (c)** shows rough and flattened when polymerization of aniline just started due to the leakage of charge from the surface. **Fig. 4.3.17 (d)** shows a high magnification SEM image of PANI coating obtained in 0.3 M aniline and 0.04 M benzoic acid**.** The formation of compact and fine grains in the range of 10 nm is observed on the surface, which is further confirmed by the EDX mapping. There is much difference in morphology of PANI prepared by anodic polarization and CV methods. **Fig. 4.3.17(e)** indicates PANI prepared by CV which is a smooth, compact, pore-free and fine grain coating in the nanometer dimension, which was visible only at

very high magnification. The EDX result showed the presence of N and C supported the formation of PANI. The mapping showed the distribution of particles.

OCP

Before polymerization

Just polymerization started

Polymerization completed

CV

PANI obtained in oxalic acid
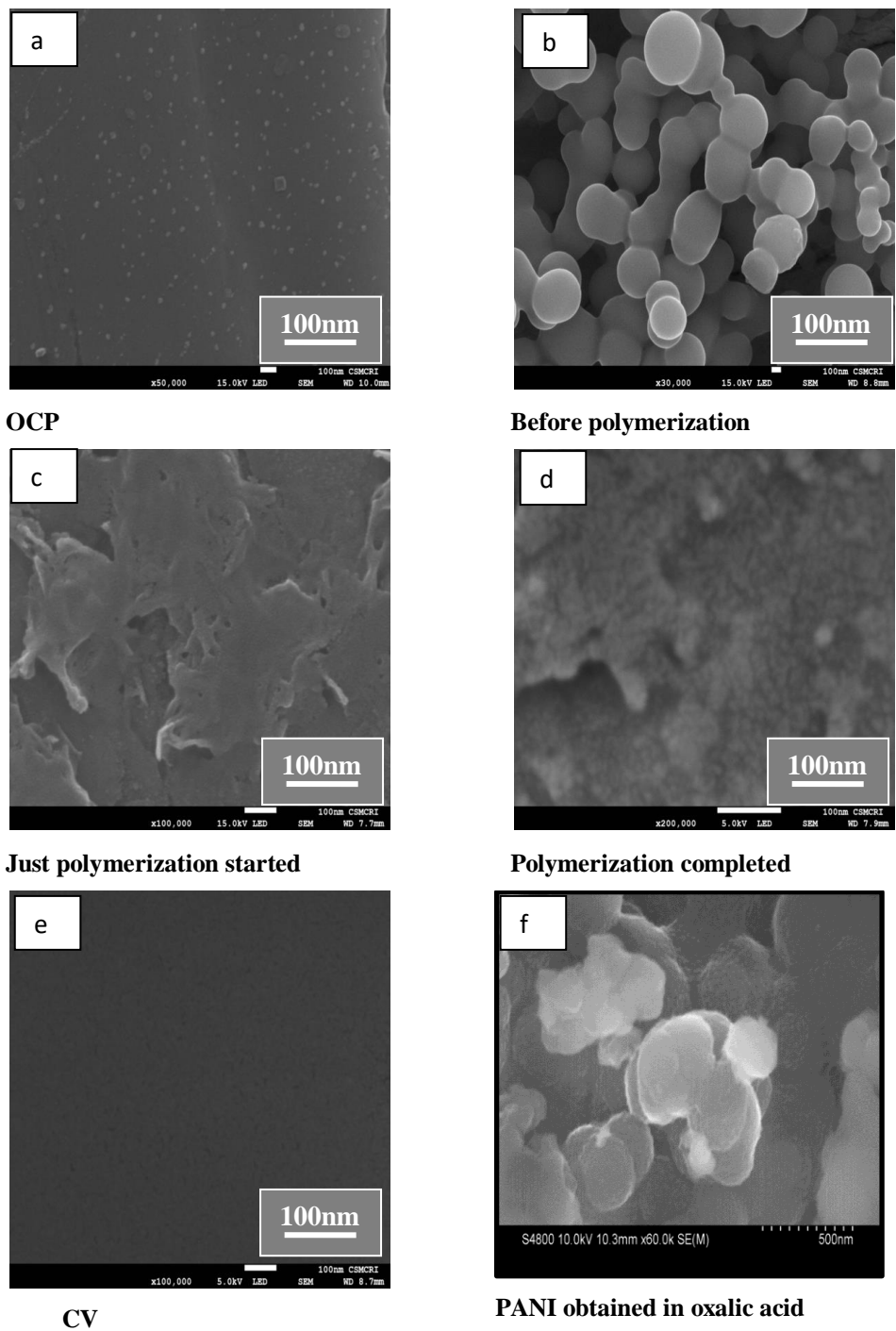
Figure 4.3.17: SEM micrograph of PANI deposition on MS during anodic polarization at various states and PANI deposited by CV methods from 0.3M aniline in 0.04 M BAW and PANI deposited from oxalic acid

SEM micrograph of PANI deposited on MS sample from aqueous oxalic acid solution shows a more massive grain structure having a diameter of 100-200 nm shown in **Fig**. 4.3.17(f).

Wt%	
C	50.92
N	5.27
O	4.79
Fe	39.03
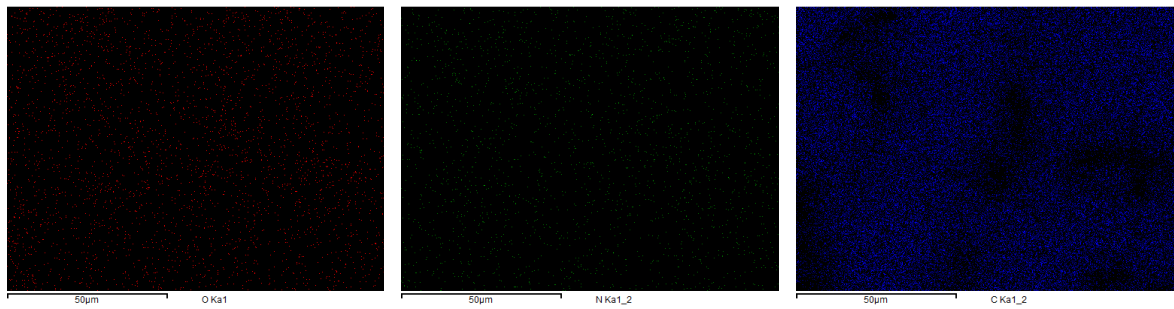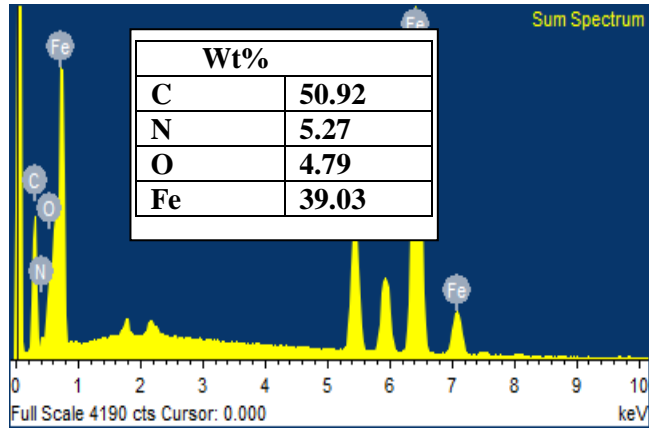
Figure 4.3.18: EDX and Mapping of PANI prepared from 0.3M aniline in 0.04 M BAW

Fig. 4.3.19 shows the SEM micrograph with EDX of PANI deposited on MS from 0.3 M aniline in 0.04 M BAW containing La (III).

Wt%	
C	84.09
O	15.67
La	0.31
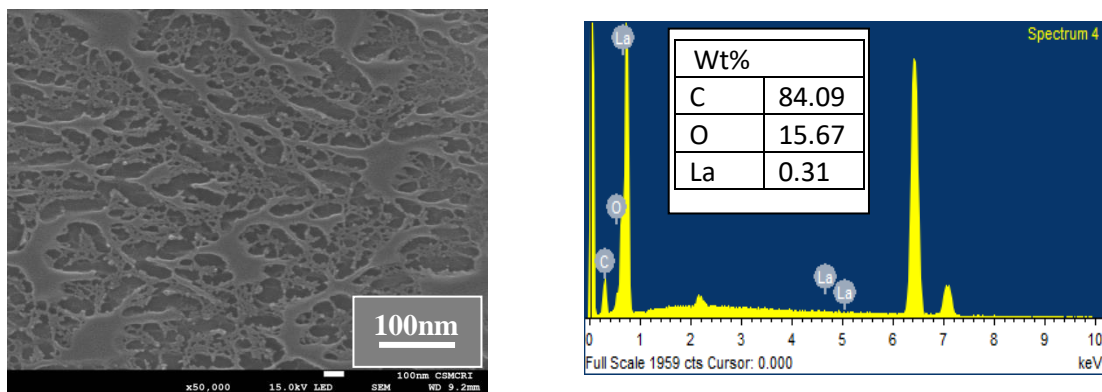
Figure 4.3. 19: SEM micrograph of PANI deposited on MS from 0.3M aniline + 0.04 M BAW + La (III)

The micrograph shows denditric nanofiborous PANI. The EDX result shows the presence of N, C, O and La supports the tailoring of PANI**.**

4.3.12 Transmission electron microscopy (TEM)

TEM micrographs indicated nanostructures of the PANI. **Fig. 4.3.20** shows nano-particles have a spherical shape, with very small size (140 to 400 nm), and there was aggregation due to their large surface area and the interaction between the particles.
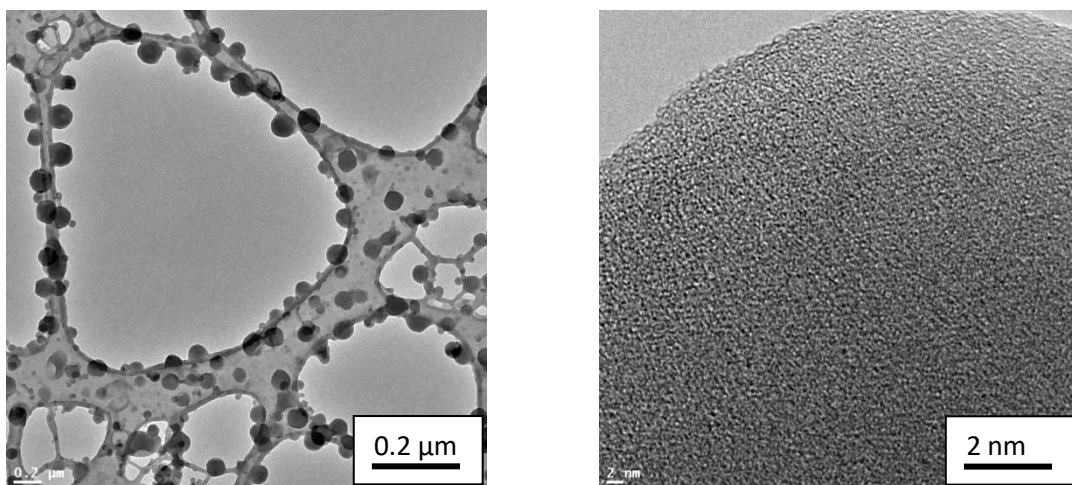
Figure 4.3.20: TEM images of PANI prepared from 0.3M aniline in 0.04 M BAW

Fig. 4.3.21 shows TEM images of PANI prepared from 0.3 M aniline in 0.04 M BAW with La (III). PANI doping with La has smaller size than PANI and its average size ranges from 90 nm to 300 nm which is in agreement with SEM micrographs.
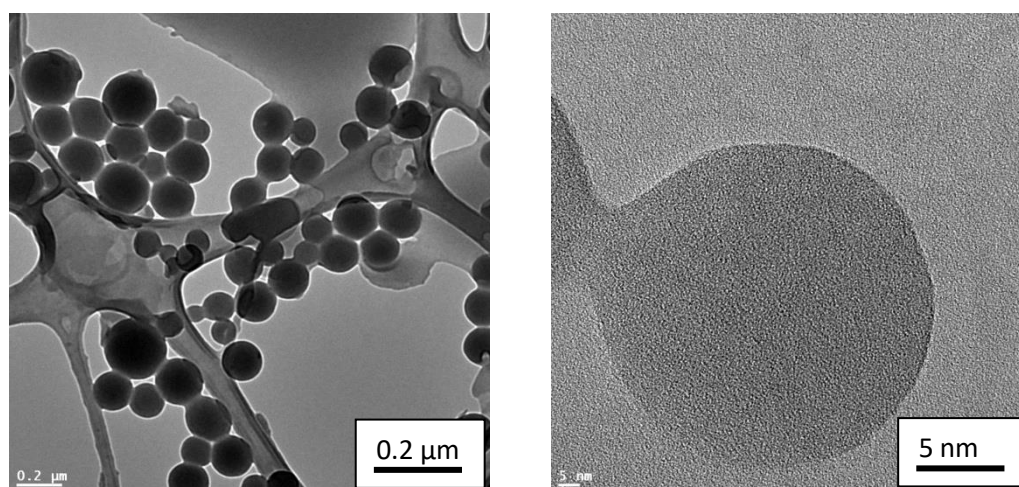
Figure 4.3.21: TEM images of PANI prepared from 0.3M aniline in 0.04 M BAW containing La (III)

4.3.13 Atomic Force Microscopy (AFM)

In addition to SEM and TEM images, Atomic Force Microscopy (AFM) images of PANI coating have been taken. **Fig. 4.3.22** shows 2D and 3D images of PANI coated MS obtained by AFM. The images showed the regular and homogeneous PANI coating from both anodic and cyclic voltammetry. 3-D images showed some islands on the surface corresponding to the nucleation sites (Buron *et al*., 2011). The change in mean roughness and the rms roughness of coating showed that PANI coating by CV on MS is smooth and uniform coating.

(a) MS
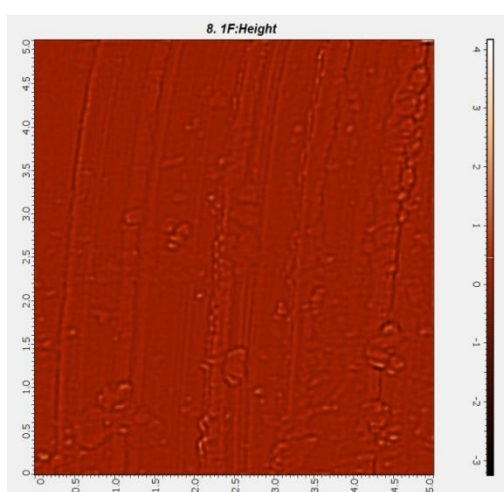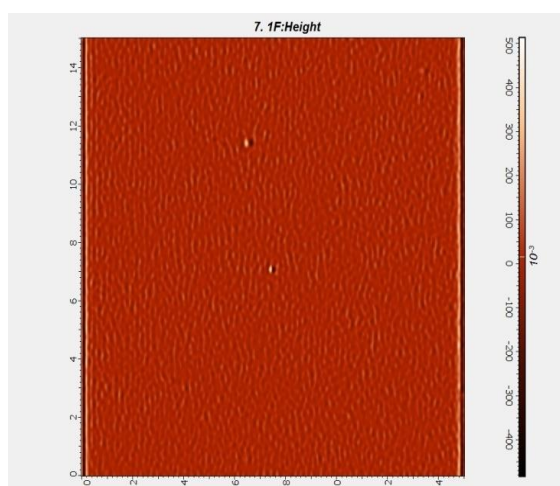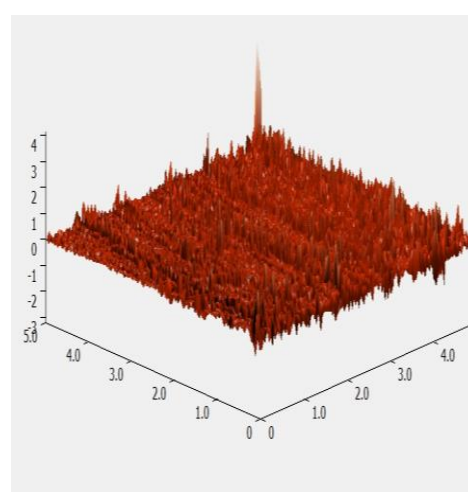
(b) PANI by anodic polarization
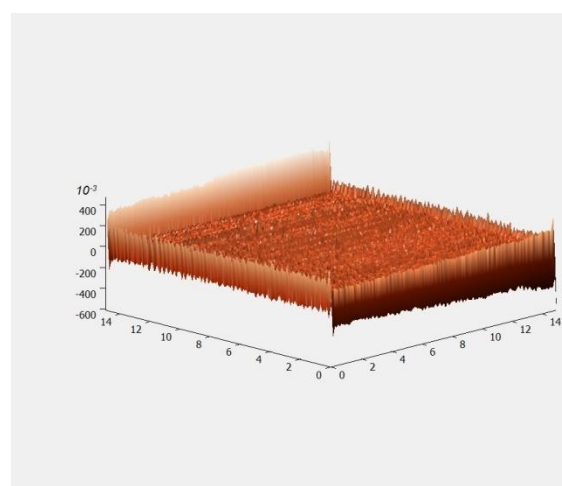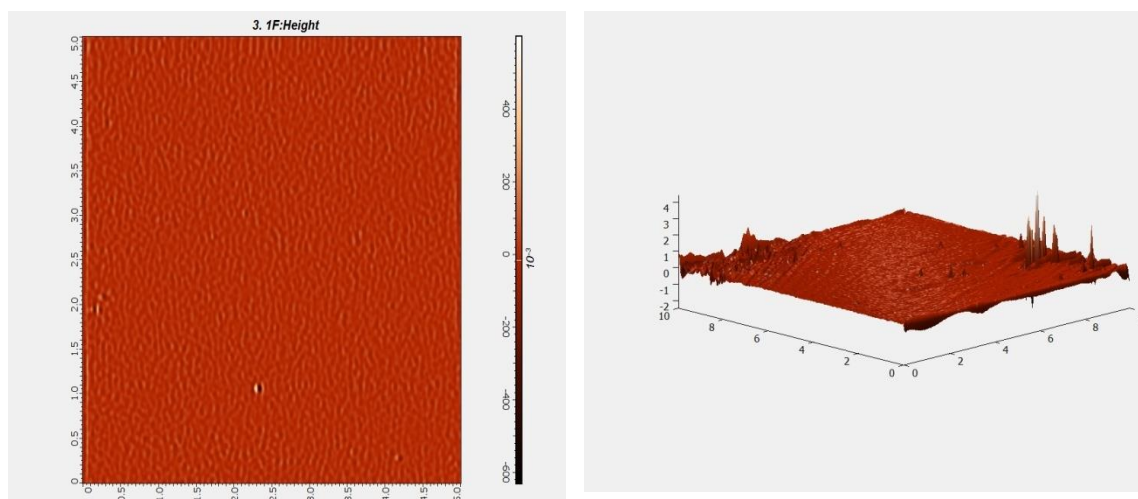
(c) PANI by CV

Figure 4.3.22: AFM images (a) MS (b) PANI prepared by anodic polarization and (c) PANI prepared by CV

Table 4. 2: Roughness of PANI prepared 0.3 M aniline in 0.04 M BAW on MS

	Mean Roughness (μm)	RMS Roughness (μm)
Bare Mild Steel (MS)	0.159	0.234
PANI Coating by Anodic	0.0130	0.0235
PANI Coating by CV	0.00315	0.00542

To sum up, an optimized condition for effective passivation and polymerization of aniline onto mild steel surface has been obtained in Na-K Tartrate and BAW as noble electrolytes.

4.4 Corrosion study

4.4.1 Corrosion protection of PANI from Na-K Tartrate in 0.1M NaCl

Fig. 4.4.1 shows the potentiodynamic polarization curves of both the coating in 0.1 M NaCl solution. For comparison, polarization curves of bare MS and PANI coating in the presence of oxalic acid as electrolyte are also shown together. Corrosion current density (i_{corr}), corrosion potential (E_{corr}), anodic slopes, cathodic slopes, and corrosion inhibition efficiency were obtained from the polarization curves and presented in Table 4.2.

The coating of MS by PANI has resulted in lowering i_{corr} by one to two orders of magnitude which reflects better corrosion protection. i_{corr} is much lowered in PANI coating obtained in BAW, while PANI coating obtained in Na-K Tartrate shows almost

similar i_{corr} to that obtained in oxalic acid. The polarization curves show a significant reduction in cathodic current density. However the corrosion inhibition efficiency is estimated to 82.50% showed by PANI coating obtained in Na-K Tartrate.
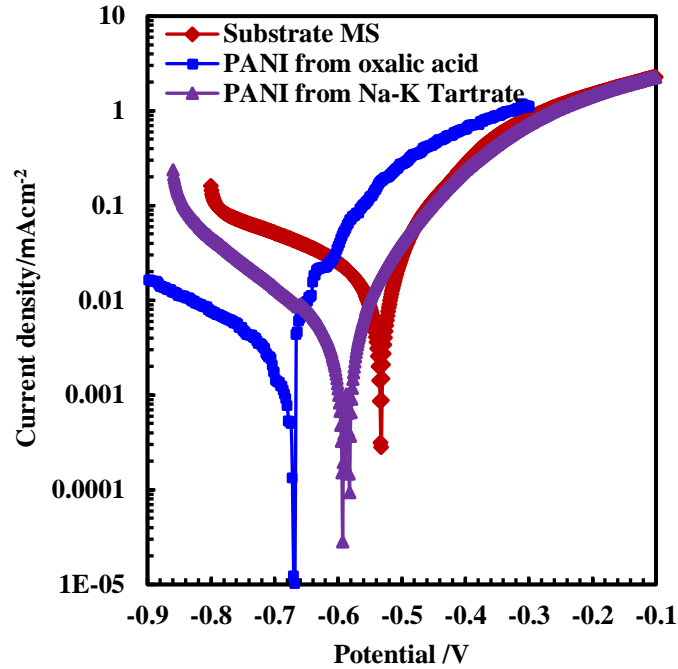
Figure 4.4.1: Potentiodynamic polarization curve showing corrosion protection in 0.1M NaCl (Gupta *et al.*, 2021)

The OCP of PANI shifted to 57 mV negative compared to MS. PANI coating obtained in Na-K Tartrate acts as a mixed type corrosion inhibitor because the change in OCP value is less than 85 mV(Gvozdenovi *et al.*, 2012). The anodic Tafel slope (βa) and cathodic Tafel slope (β$_c$) are characteristic of such coatings on MS in aqueous saline media and in acidic media (Mahato & Cho, 2016; Pawar *et al.*, 2006; Shabani-Nooshabadi & Karimian-Taheri, 2015). The corrosion prevention by PANI coating has been reported to be due to inhibitory action of the functional group C = N which can be adsorbed on the metal surface (Jafari *et al.*, 2016). Soluble PANI can absorb on the metal surface and decrease the anodic and cathodic reaction (Jafari *et al.*, 2016). The anodic reaction is the dissolution of iron while cathodic reaction is the diffusion controlled reduction of oxygen on PANI coating in the above medium (Rajyalakshmi *et al.*, 2020):

$$\text{Anodic:} \quad Fe \rightarrow Fe^{2+} + 2e \qquad\qquad [4\text{-}4]$$

$$\text{Cathodic:} \quad H_2O + \tfrac{1}{2}\, O_2 + 2e \rightarrow 2OH^- \qquad\qquad [4\text{-}5]$$
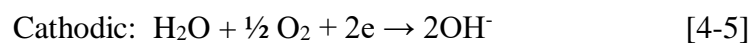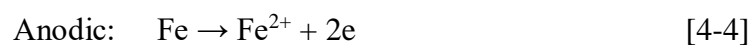
Table 4.3: Electrochemical polarization parameters for PANI from Na-K Tartrate in 0.1 M NaCl

Sample	β_a (V/decade)	β_c (V/decade)	i_{corr} (mA/cm^2)	E_{corr} (V vs SCE)	Corrosion Rate (mm/year)	Inhibition Efficiency (%)
Bare MS	0.108	-0.254	0.02004	-0.537	0.0294	
PANI/oxalic acid	0.086	-0.196	0.00266	-0.674	0.0057	86.72
PANI/Na-K Tartrate	0.083	-0.164	0.0035	-0.594	0.0017	82.50

4.4.2 Corrosion behavior of PANI from Na-K Tartrate in 0.4 M Na$_2$SO$_4$, mixture of 0.1M NaCl and 0.4M Na$_2$SO$_4$ and 0.1 M H$_2$SO$_4$

Corrosion behavior of PANI coated MS in various media (0.4 M Na$_2$SO$_4$, 1:1 Mixture of 0.1M NaCl and 0.4M Na$_2$SO$_4$ and 0.1 M H$_2$SO$_4$) have been investigated. **Fig. 4.4.2 and 4.4.3** show potentiodynamic polarization curves. Corrosion current density (i_{corr}), corrosion potential (E_{corr}), anodic and cathodic slopes, and corrosion protection efficiency values are the electrochemical parameters which were obtained and shown in Table 4.3.

The corrosion current density on the bare MS surface was much greater (approx. 87 – 97 orders of magnitude) than the PANI coated surfaces. In general, a lower I_{corr} value (indicating a decline in the corrosion current) reflects better corrosion protection. PANI coated MS showed a lower corrosion current density. The shift of OCP of PANI coated MS to a positive direction compared to bare MS surface suggests a forming a barrier for the aggressive medium. However, the change in the OCP value of PANI coating compared to the MS is less than 85 mV, reflecting that PANI coating acts as a mixed type inhibitor. Lowering the corrosion current and corrosion rate was observed only for coatings thicker than 1 μm, and these results were attributed to barrier effect [5].

The figure reveals only a marginal shift of OCP, confirming a mixed type behavior of the inhibitor molecules in 0.1M H$_2$SO$_4$ acid solution. It was noted that the corrosion rate (CR) of the PANI coating was 0.00082 mm/year, much lower than that of the MS. The corrosion inhibition efficiency was 97.53%. The PANI coating shows excellent corrosion

protection in acidic solution. The cathodic Tafel constant (β_c) shows values near120 mV/decade corresponds to two-electron transfer during oxygen reduction.

In 0.4 M Na_2SO_4 solution, OCP of PANI coated MS shifted slightly negative than MS. It was noted that the corrosion rate (CR) of the PANI coating was lower than that of the MS. The corrosion current of PANI coating decreased by approximately 87 times, and corrosion inhibition efficiency was 87.17%. The PANI coating shows good corrosion protection in 0.4 M Na_2SO_4 solution. The cathodic Tafel constant (β_c) shows values near120 mV/decade correspond to two-electron transfer during oxygen reduction.

Similarly, in the 1:1 Mixture of 0.1M NaCl and 0.4M Na_2SO_4, OCP of PANI coated MS shifted to positive by 33mV, representing a mixed type of inhibitor. The corrosion inhibition efficiency was 89.58%. The cathodic Tafel constant (β_c) shows values 188 mV/decade correspond to some complex reactions occurring at the surface. On the other hand, the anodic Tafel constant (βa) values are almost the same in the nature of the oxidation reaction. Literatures also report a decline in corrosion currents in aqueous saline media and in acidic media with PANI as corrosion protection coating (Ananda Kumar *et al.*, 2008; Mahato & Cho, 2016; Pawar *et al.*, 2006).
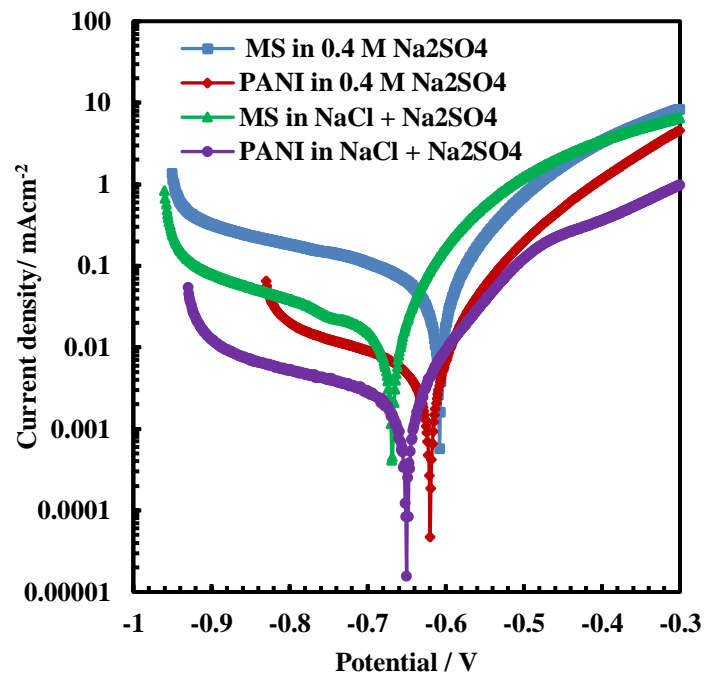
Figure 4.4. 2: Tafel plot showing corrosion protection in various media
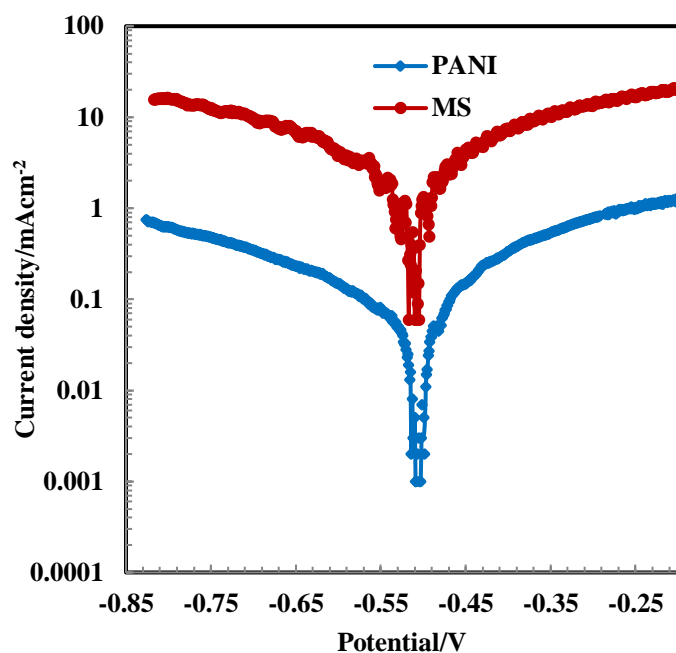
Figure 4.4.3 : Tafel plot showing corrosion protection in 0.1M H_2SO_4

Table 4. 4: Electrochemical polarization parameters for PANI coated MS in different media

Media	Sample	β_a (V/decade)	β_c (V/decade)	i_{corr} (mA/cm²)	E_{corr} (V vs SCE)	Corrosion Rate (mm/year) CR=(I$_C$xM/dxn)x3270	Inhibition Efficiency (%)
0.1M H_2SO_4	MS	0.127	-0.159	0.00159	-0.524	0.0185	
	PANI Coated MS	0.106	-0.165	0.000071	-0.520	0.00082	97.53
0.4M Na_2SO_4	MS	0.076	-0.217	0.0478	-0.621	0.554	
	PANI Coated MS	0.064	-0.208	0.006	-0.634	0.0696	87.17
Mixture	MS	0.087	-0.282	0.0191	-0.669	0.221	
	PANI Coated MS	0.087	-0.188	0.00199	-0.65	0.023	89.58

To explain the above results, the following has to be considered, for MS in the above medium the following reactions take place (Rajyalakshmi *et al*., 2020):

131

Anodic: $Fe \rightarrow Fe^{2+} + 2e$ **[4-6]**

Cathodic: $H_2O + \frac{1}{2} O_2 + 2e \rightarrow 2OH^-$ **[4-7]**
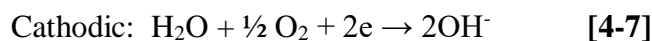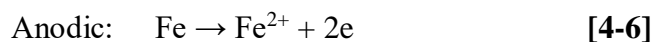
4.4.3 Corrosion protection of galvanostatically prepared PANI from Na-K Tartrate in 0.4 M Na_2SO_3

The potentiodynamic polarization of PANI coated MS in 0.4 M Na_2SO_3 solution was carried out to study its corrosion behavior. **Fig. 4.4.4** shows the corresponding potentiodynamic polarization curves of PANI coating obtained at various current densities. From the polarization curves, corrosion current density (i_{corr}), corrosion potential (E_{corr}), Tafel slopes and corrosion inhibition efficiency (IE) values are obtained and compared in **Table 4.4**.
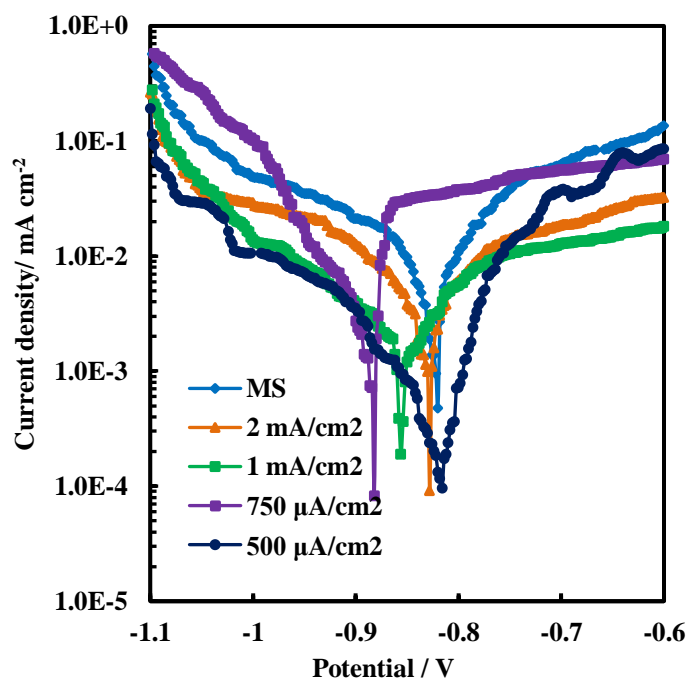
Figure 4.4.4: Potentiodynamic polarization behaviour of MS and PANI coated MS in 0.4 M Na_2SO_3

i_{corr} of the bare MS is much higher than the PANI coated MS. A lower i_{corr} value reflects better corrosion protection. The i_{corr} of PANI coated MS decreased by approximately 90 times, and a corrosion IE of 89.43% is obtained for the PANI deposited at the current density of 0.5 mA cm^{-2}. Similarly, the corrosion IE is found to be 87.8%, 82.11% and 74.79% for PANI deposited at current density of 0.75 mAcm^{-2}, 1 mAcm^{-2} and 2 mAcm^{-2}, respectively.

The anodic and cathodic polarization curves do not show a typical Tafel slope for iron dissolution (60 mV/decade) and hydrogen evolution (120 mV/ecade) (Mahato & Cho, 2016). This is due to participation of PANI in the reaction due it its redox properties. It can be seen that the anodic Tafel slope of PANI coated MS obtained at 1 and 2 mA cm^{-2} is similar to bare MS. This is in agreement with the finding that at these current densities the PANI coating thickness was decreased. On the other hand, the cathodic curve is influenced by the presence of PANI and it differs from MS.

A clear shift in the OCP of PANI coated MS is not seen though it shifted slightly in negative direction. The shift of OCP value of PANI coating compared to the MS is less than 85 mV, reflecting that PANI coating acts as a mixed type inhibitor (Gupta et al., 2021b).

Table 4.5: Corrosion behaviour of PANI coated MS at different current densities in 0.4 M Na$_2$SO$_3$ by potentiodynamic polarization

Current density (mA/cm^2)	β$_a$ (V/decade)	β$_c$ (V/decade)	i$_{corr}$ (mA/cm^2)	E$_{corr}$/V	Inhibition Efficiency (%)
MS	0.09	-0.116	0.037	-0.820	
2	0.096	-0.076	0.0031	-0.816	74.79
1	0.088	-0.064	0.0022	-0.848	82.11
0.75	0.044	-0.06	0.0015	-0.882	87.80
0.50	0.048	-0.07	0.0013	-0.818	89.43

The change in surface morphology after polarization in 0.4 M Na$_2$SO$_3$ solution is shown in **Fig. 4.4.5.** It shows not much change in the morphology of the PANI coating obtained at 0.5 and 0.75 mA cm^{-2}. On the other hand, at higher current density (1 and 2 mAcm^{-2}), the surface developed a much different morphology due to dissolution of the PANI coating and hence enhanced dissolution of substrate MS. The results clearly show that both the morphology of the PANI coating and its corrosion protection ability greatly depends on the current density employed for electropolymerization of aniline onto MS

surface which can be helpful in obtaining an optimized condition for electrodeposition of PANI on MS in Na-K Tartrate electrolyte.

0.5 mAcm^{-2} in Na$_2$SO$_3$ 0.75 mAcm^{-2} in Na$_2$SO$_3$

1 mAcm^{-2} in Na$_2$SO$_3$ 2 mA/cm^{-2} in Na$_2$SO$_3$
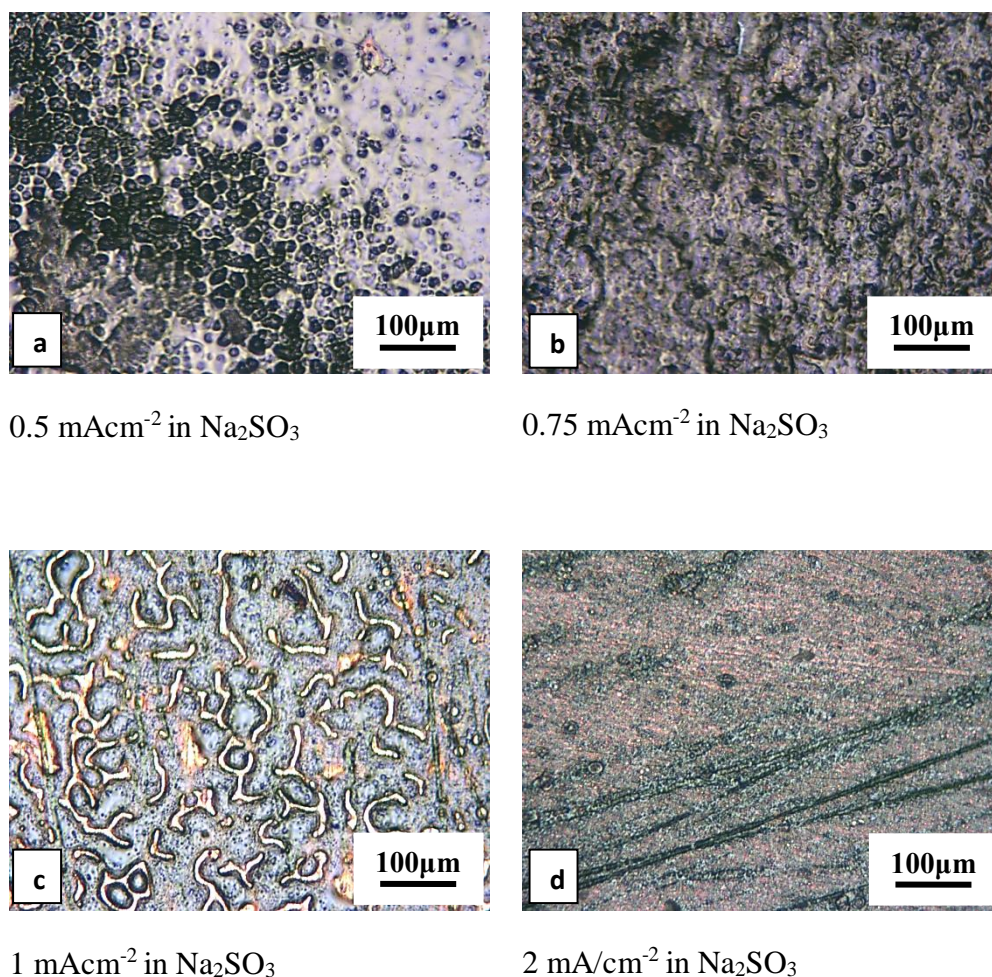
Figure 4.4.5 : Optical images of PANI deposited on MS by galvanostatically at various current densities after polarization in 0.4 M Na$_2$SO$_3$ solution

In order to further check the stability of the PANI coating at higher oxidation potential, the polarization was carried out at the anodic limit of -0.3 V. **Fig. 4.4.6** shows such potentiodynamic polarization curve till the anodic potential limit of -0.3 V. It shows a current peak at -0.6 V and then a decrease of current followed by steady increase after -0.45 V. This behaviour is attributed to breakdown of the PANI film at higher positive potential. The visual observation confirmed the contamination of the electrolyte due to breakdown of the PANI coating. This is further confirmed by optical image of the surface as shown in **Fig. 4.4.7** which shows the development of worm like pore structure due to breakdown of PANI.
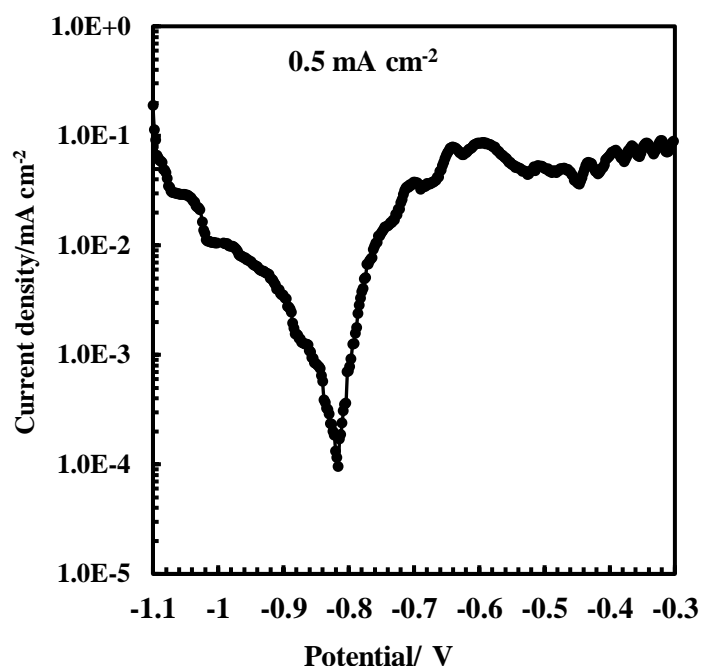
Figure 4.4.6: Potentiodynamic polarisation behaviour of PANI prepared at 500 μA/ cm^{-2} in 0.4 M Na$_2$SO$_3$ showing breakdown of PANI film and passive layer
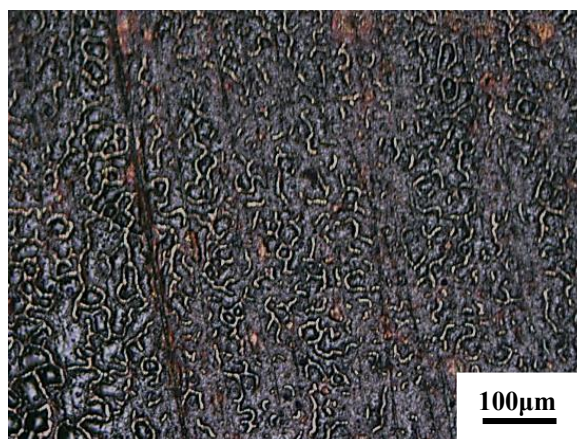
Figure 4.4.7 : Optical images of a PANI on MS potentiodynamically polarized in 0.4 M Na$_2$SO$_3$ solution up to -0.2V

4.4.4 Corrosion inhibition efficiency of PANI from BAW in 0.1 M NaCl

Fig. 4.4.8 shows the potentiodynamic polarization curves of PANI from BAW coating in 0.1 M NaCl solution. Polarization curves of bare MS and PANI coating in oxalic acid as electrolyte are also shown together for the comparison. The electrochemical parameters such as corrosion current density (i_{corr}), corrosion potential (E_{corr}), anodic slopes, cathodic slopes, and corrosion inhibition efficiency were obtained from the polarization curves and presented in Table 4.6.

The coating of MS by PANI has resulted in lowering i_{corr} by one to two orders of magnitude which indicates better corrosion protection. i_{corr} is much lowered in PANI coating obtained in BAW. The polarization curves show a significant reduction in cathodic current density. However, in PANI coating obtained in BAW, the anodic current density is also suppressed appreciably and the corrosion inhibition efficiency is estimated at 99.99% compared to 82.50% inhibition efficiency showed by PANI coating obtained in Na-K Tartrate. Such a high inhibition efficiency has been reported in epoxy based multi-layer coatings (Shabani-Nooshabadi, Mollahoseiny, *et al.*, 2014).
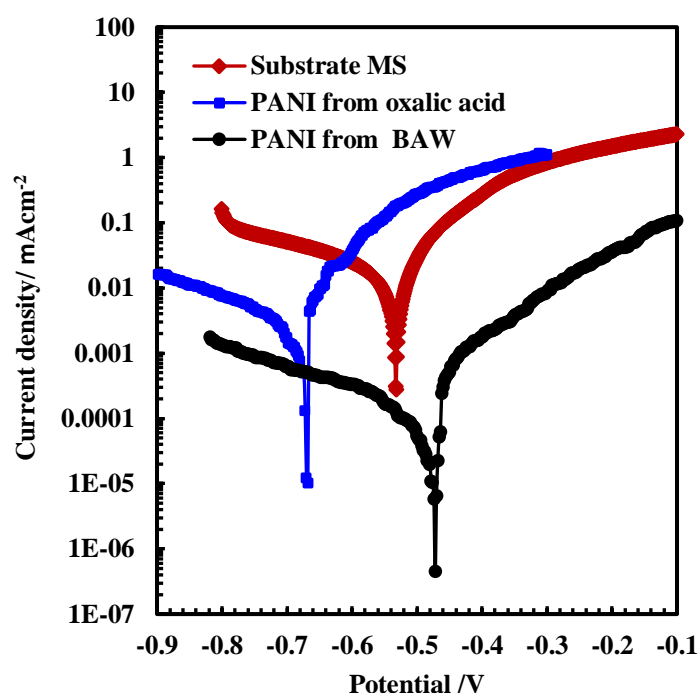
Figure 4.4.8: Potentiodynamic polarization showing corrosion protection in 0.1M NaCl (Gupta *et al.*, 2021)

The OCP of PANI coating obtained in BAW shifted significantly to positive (anodic) direction suggesting the formation of an efficient barrier for the aggressive medium (Shabani-Nooshabadi *et al.*, 2018) and thus revealing the improved corrosion protection of the coated MS (Jafari *et al.*, 2016). PANI coating obtained in BAW acts as a mixed type of corrosion inhibitor of corrosion because the change in OCP value is less than 85 mV, (Gvozdenovi *et al.*, 2012).

The anodic Tafel slope (β_a) and cathodic Tafel slope (β_c) are characteristics of such coatings on MS in aqueous saline media and in acidic media (Mahato & Cho, 2016; Pawar *et al.*, 2006; Shabani-Nooshabadi & Karimian-Taheri, 2015). The corrosion

prevention by PANI coating has been reported to be due to inhibitory action of the functional group $C = N$ which can be adsorbed on the metal surface (Jafari *et al.*, 2016). Soluble PANI can absorb on the metal surface and decrease the anodic and cathodic reaction (Jafari *et al.*, 2016). The anodic reaction is the oxidation of iron while cathodic reaction is the diffusion controlled reduction of oxygen on PANI coating in the above medium (Rajyalakshmi *et al.*, 2020):

$$\text{Anodic:} \quad Fe \rightarrow Fe^{2+} + 2e \qquad\qquad [4\text{-}10]$$

$$\text{Cathodic:} \quad H_2O + \frac{1}{2}O_2 + 2e \rightarrow 2OH^- \qquad\qquad [4\text{-}11]$$
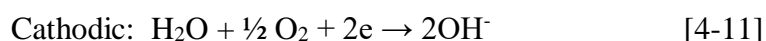
Table 4. 6: Electrochemical polarization parameters for PANI coated MS in 0.1 M NaCl

Sample	β_a (V/decade)	β_c (V/decade)	i_{corr} (mA/cm^2)	E_{corr} (V vs SCE)	Corrosion Rate (mm/year)	Inhibition Efficiency (%)
Bare MS	0.108	-0.254	0.02004	-0.537	0.0294	
PANI/oxalic acid	0.086	-0.196	0.00266	-0.674	0.0057	86.72
PANI/ BAW	0.078	-0.246	0.00002	-0.492	0.00043	99.99

4.4.5 Corrosion inhibition efficiency of PANI from BAW in 0.4 M Na$_2$SO$_4$, mixture of 0.1M NaCl and 0.4M Na$_2$SO$_4$ and 0.1 M H$_2$SO$_4$

Corrosion behavior of PANI coated MS in various media (0.4 M Na$_2$SO$_4$, 1:1 Mixture of 0.1M NaCl and 0.4M Na$_2$SO$_4$ and 0.1 M H$_2$SO$_4$) have been investigated. **Fig. 4.4.9 and 4.4.10** show potentiodynamic polarization curves. Corrosion current density (i_{corr}), corrosion potential (E_{corr}), anodic and cathodic slopes, and corrosion protection efficiency values are the electrochemical parameters which were obtained and shown in Table 4.7.

The corrosion current density on the bare MS surface was much greater (approx. 92 – 99 orders of magnitude) than the PANI coated surfaces. In general, a lower i_{corr} value (indicating a decline in the corrosion current) reflects better corrosion protection. PANI

coated MS showed a lower corrosion current density. The shift of OCP of PANI coated MS to a positive direction compared to bare MS surface suggests a forming a barrier for the aggressive medium. However, the change in the OCP value of PANI coating compared to the MS is less than 85 mV, reflecting that PANI coating acts as a mixed type inhibitor. Lowering the corrosion current and corrosion rate was observed only for coatings thicker than 1 μm, and these results were attributed to barrier effect (Gvozdenovi *et al*., 2012).

The figure reveals only a marginal shift of OCP, confirming a mixed type behavior of the inhibitor molecules in 0.1M H_2SO_4 acid solution. It was noted that the corrosion rate (CR) of the PANI coating was 0.997 mm/year, much lower than that of the MS. The corrosion inhibition efficiency was 99.0%. The PANI coating shows excellent corrosion protection in acidic solution. The cathodic Tafel constant (β_c) shows values near120 mV/decade corresponds to two-electron transfer during oxygen reduction.

In 0.4 M Na_2SO_4 solution, OCP of PANI coated MS shifted slightly negative than MS. It was noted that the corrosion rate (CR) of the PANI coating was lower than that of the MS. The corrosion current of PANI coating decreased by approximately 91 times, and corrosion inhibition efficiency was 91.37%. The PANI coating shows good corrosion protection in 0.4 M Na_2SO_4 solution. The cathodic Tafel constant (β_c) shows values near120 mV/decade correspond to two-electron transfer during oxygen reduction

Similarly, in the 1:1 Mixture of 0.1M NaCl and 0.4M Na_2SO_4, OCP of PANI coated MS shifted to positive by 33mV, representing a mixed type of inhibitor. The corrosion inhibition efficiency was 94.48%. The cathodic Tafel constant (β_c) shows values 274 mV/decade correspond to some complex reactions occurring at the surface. On the other hand, the anodic Tafel constant (β_a) values are almost the same in the nature of the oxidation reaction. Literatures also report a decline in corrosion currents in aqueous saline media and in acidic media with PANI as corrosion protection coating (Kumar *et al*., 2008; Mahato & Cho, 2016; Pawar *et al*., 2006).

To explain the above results, the following has to be considered, for MS in the above medium the following reactions take place (Rajyalakshmi et al., 2020b):

$$\text{Anodic:} \quad Fe \rightarrow Fe^{2+} + 2e \qquad\qquad [4\text{-}12]$$

$$\text{Cathodic:} \quad H_2O + \tfrac{1}{2} O_2 + 2e \rightarrow 2OH^- \qquad [4\text{-}13]$$
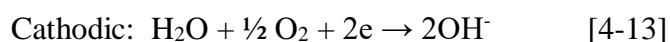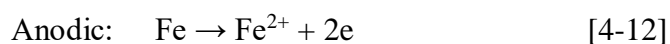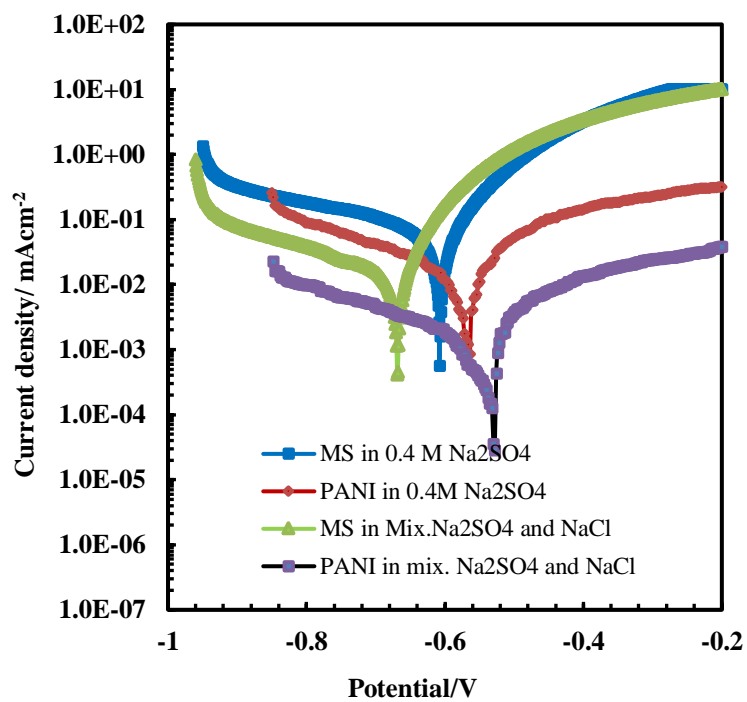
Figure 4.4.9: Potentiodynamic polarization showing corrosion protection in various media
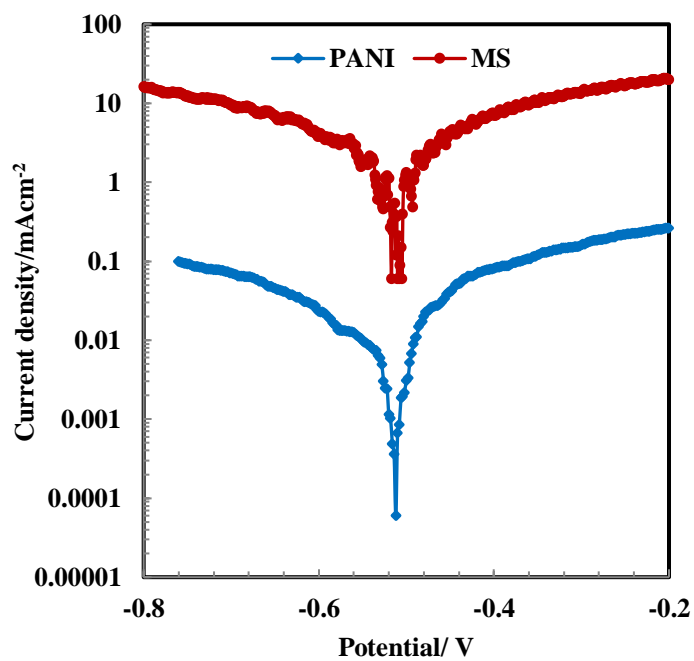
Figure 4.4.10: Potentiodynamic polarization showing corrosion protection in 0.1 M H_2SO_4

Table 4.7: Electrochemical polarization parameters for PANI prepared from BAW on MS in different media

Media	Sample	β_a (V/decade)	β_c (V/decade)	i_{corr} (mA/cm^2)	E_{corr} (V vs SCE)	Corrosion Rate (mm/year) CR= (I_CxM/dxn)x3270	Inhibition Efficiency (%)
0.1M H$_2$SO$_4$	MS	0.239	-0.26	2.69	-0.517	31.21	
	PANI Coated MS	0.12	-0.104	0.086	-0.55	0.997	99.0
0.4M Na$_2$SO$_4$	MS	0.082	-0.219	0.0596	-0.608	0.691	
	PANI Coated MS	0.054	-0.096	0.00476	-0.564	0.0552	92.01
Mixture	MS	0.088	-0.2	0.0154	-0.67	0.178	
	PANI Coated MS	0.078	-0.198	0.00085	-0.528	0.0098	94.48

4.4.6 Corrosion protection of galvanostatically prepared PANI from BAW in 0.4 M Na$_2$SO$_3$

The corrosion behavior of PANI coated MS in 0.4 M sodium sulphite has been investigated. **Fig. 4.4.11** shows potentiodynamic polarization curves. Corrosion current density (i_{corr}), corrosion potential (E_{corr}), and corrosion protection efficiency values are the electrochemical parameters that were obtained and shown in Table 4.8.

i_{corr} of the bare MS is much higher than the PANI coated MS. A lower i_{corr} value reflects better corrosion protection. The i_{corr} of PANI coated MS decreased by approximately 96 times, and a corrosion IE of 96.23% is obtained for the PANI deposited at the current density of 100 μA cm^{-2}. Similarly, the corrosion IE is found to be 85.27%, and 75.46% for PANI deposited at current density of 200 μA cm^{-2} and 300 μA cm^{-2}, respectively.

The anodic and cathodic polarization curves do not show a typical Tafel slope for iron dissolution (60 mV/decade) and hydrogen evolution (120 mV/ecade) (Mahato & Cho, 2016). This is due to participation of PANI in the reaction due it its redox properties. It

can be seen that the both anodic and cathodic curve is influenced by the presence of PANI. The anodic Tafel slope of PANI coated MS decreased with decrease in current density. This is in agreement with the finding that at lower current densities the PANI coating thickness was increased which slowed down the anodic reaction.

A clear shift in the OCP of PANI coated MS is not seen though it shifted slightly in negative direction. The shift of OCP value of PANI coating compared to the MS is less than 85 mV, reflecting that PANI coating acts as a mixed type inhibitor (Gupta et al., 2021b).
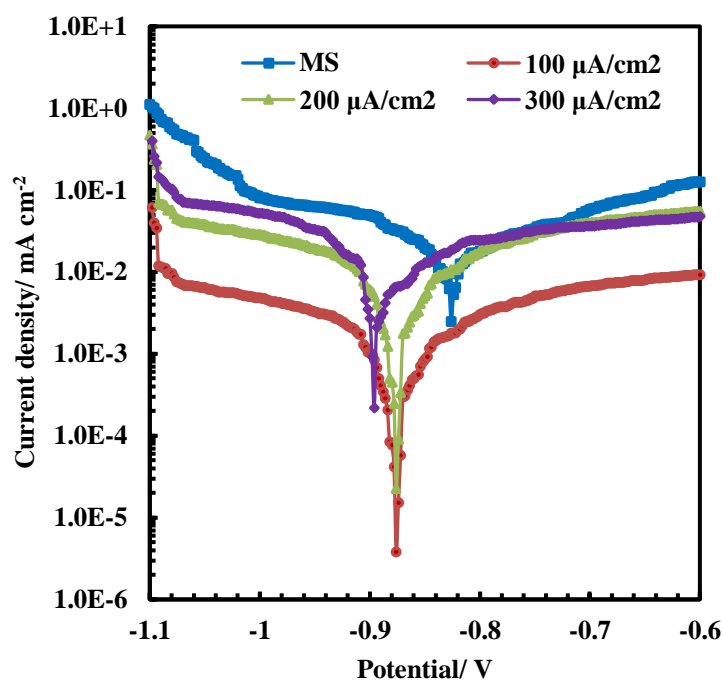
Figure 4.4.11: Potentiodynamic polarisation behaviour of MS and PANI coated MS in 0.4 M Na_2SO_3

Table4. 8: Corrosion behaviour of PANI coated MS at different current densities in 0.4 M Na_2SO_3 by potentiodynamic polarization

Current density ($\mu A/cm^2$)	β_a (V/decade)	β_c (V/decade)	i_{corr} (mA/cm^2)	E_{corr}/V	Inhibition Efficiency (%)
MS	0.102	-0.116	0.0163	-0.826	
300	0.082	-0.058	0.004	-0.896	75.46%
200	0.074	-0.056	0.0024	-0.876	85.27 %
100	0.052	-0.56	0.0005	-0.876	96.23 %

The change in surface morphology after polarization in 0.4 M Na$_2$SO$_3$ solution is shown in **Fig. 4.4.12.** It shows not much change in the morphology of the PANI coating obtained at 100 and 200 µA cm^{-2}. On the other hand, at higher current density, 300 µA cm^{-2} , the surface developed a much different morphology due to dissolution of the PANI coating and hence enhanced dissolution of substrate MS. The results clearly show that both the morphology of the PANI coating and its corrosion protection ability greatly depends on the current density employed for electropolymerization of aniline onto MS surface which can be helpful in obtaining an optimized condition for electrodeposition of PANI on MS in BAW electrolyte.

100 µA/cm^2 in Na$_2$SO$_3$ 200 µA/cm^2 in Na$_2$SO$_3$ 300 µA/cm^2 in Na$_2$SO$_3$
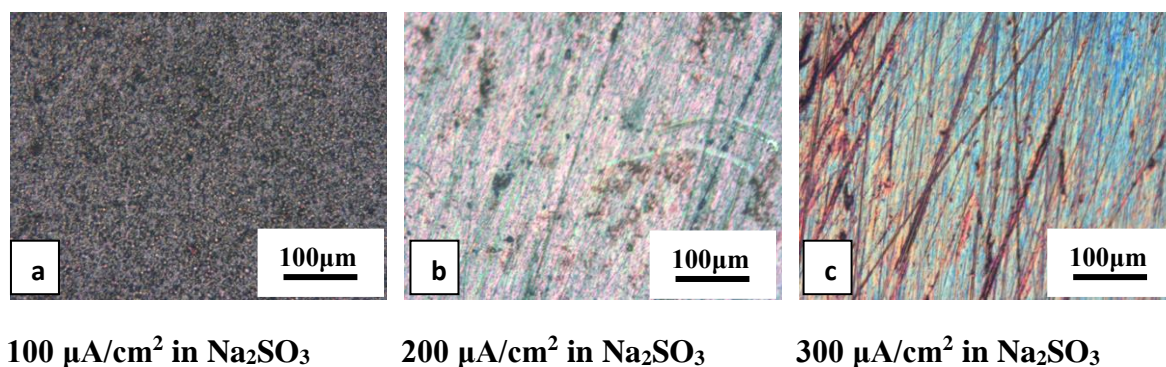
Figure 4.4.12: Optical images of PANI prepared from BAW deposited on MS by galvanostatically at various current densities after polarization in 0.4 M Na$_2$SO$_3$ solution

In order to further check the stability of the PANI coating at higher oxidation potential, the polarization was carried out at the anodic limit of -0.3 V. **Fig. 4.4.13** shows such potentiodynamic polarization curve till the anodic potential limit of -0.3 V. It shows a steady increase in current. This behaviour is attributed to stable PANI film at higher positive potential. This is further confirmed by optical image of the surface as shown in **Fig. 4.3.14** which shows no change in morphology.
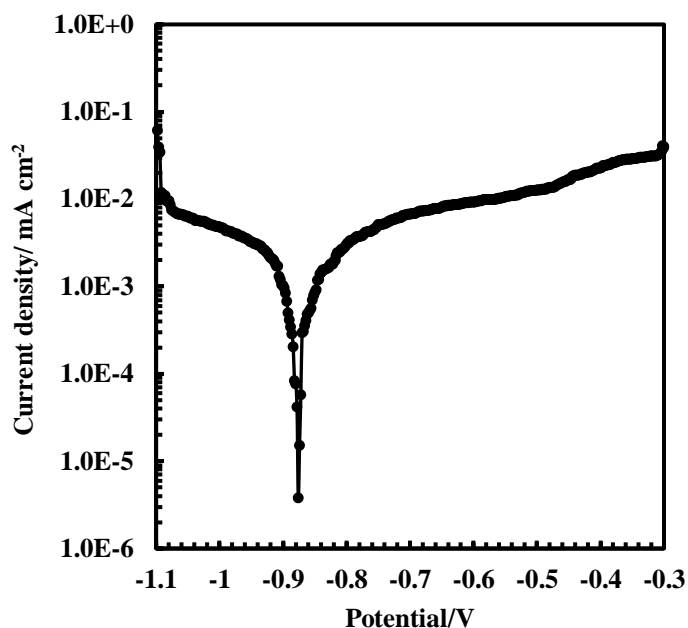
Figure 4.4. 13: Potentiodynamic polarisation behaviour of PANI prepared at 100 µA/cm^2 in 0.4 M Na$_2$SO$_3$ showing no breakdown of PANI film and passive layer
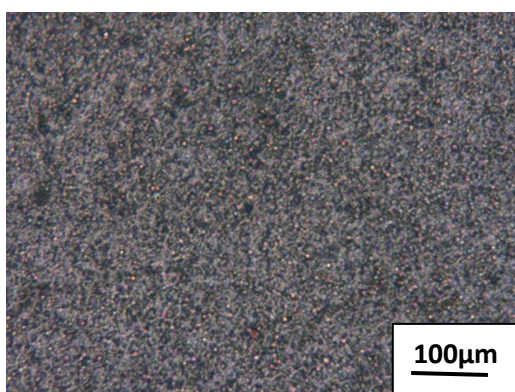
Figure 4.4.14: Optical images of a PANI on MS potentiodynamically polarized in 0.4 M Na$_2$SO$_3$ solution up to -0.3V.

4.4.7 Corrosion study by electrochemical impedance spectroscopy (EIS)

Electrochemical Impedance spectroscopy (EIS) was also used to study the corrosion behavior of PANI coating on MS obtained in both the electrolytes. **Fig. 4.4.15a-d** to **Fig. 4.4.20a-d** shows the EIS response of PANI coating in three different corrosion media. In all the cases, two distinct semicircles are obvious representing the two time constants. The experimental EIS response was fitted using an equivalent circuit shown in **Fig. 4.4.15b**. In the circuit, two parallel RC circuits are connected in series with solution

resistance. The element Cp and Rp represent the capacitance of PANI coating and coating resistance. Similarly, Cdl represents the double layer capacitance of the metal solution interface and Rct represents the charge transfer resistance at the metal solution interface.
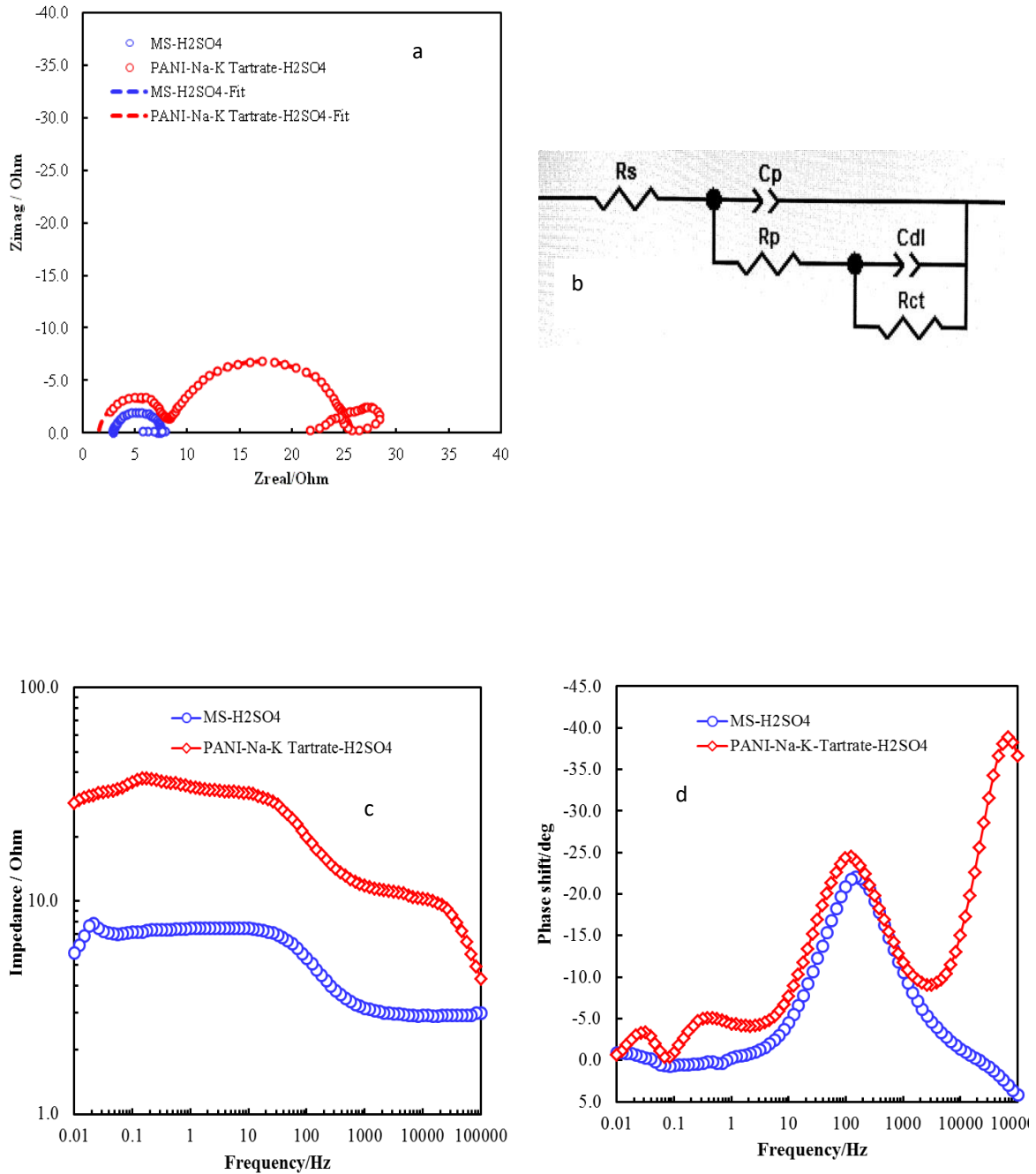
Figure 4.4. 15: Electrochemical impedance response of MS coated with PANI in Na-K Tartrate immersed in 0.1 M H_2SO_4 solution (a) Nyquist plot, (b) an equivalent circuit model to represent the experimental data, (c) Bode plot and (d) Phase shift
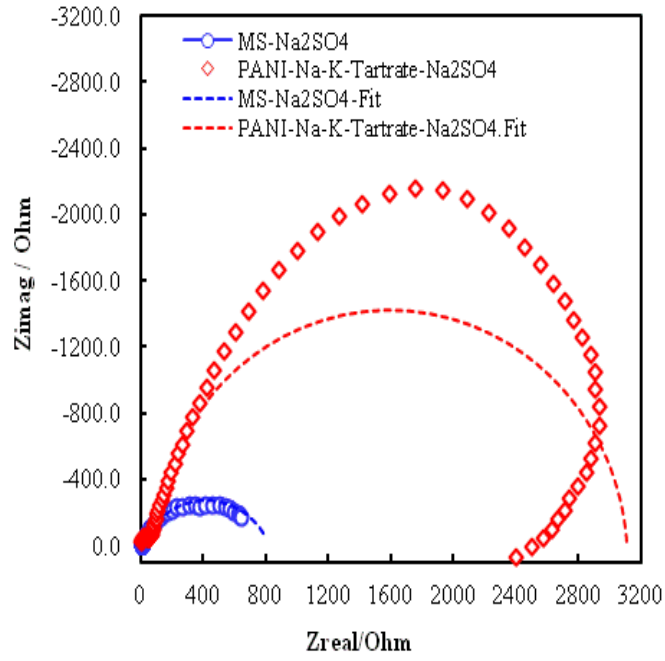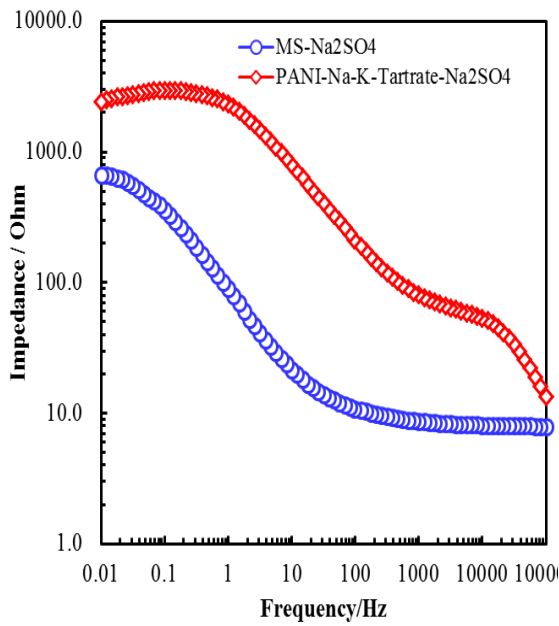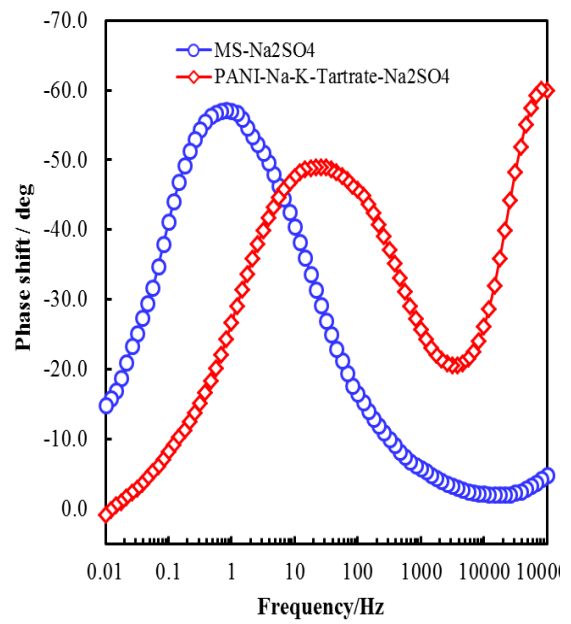
Figure 4.4. 16: Electrochemical impedance response of MS coated with PANI in Na-K Tartrate immersed in 0.4 M Na_2SO_4 solution (a) Nyquist plot, (b) Bode plot and (c) Phase shift
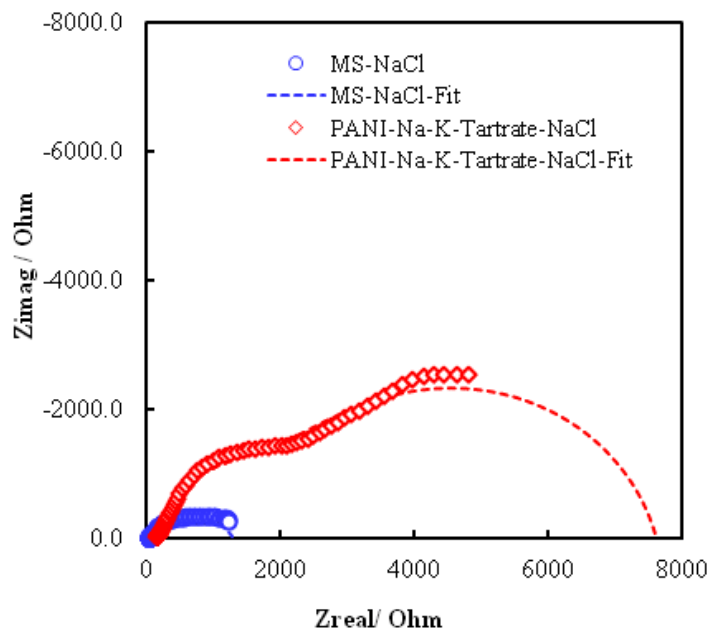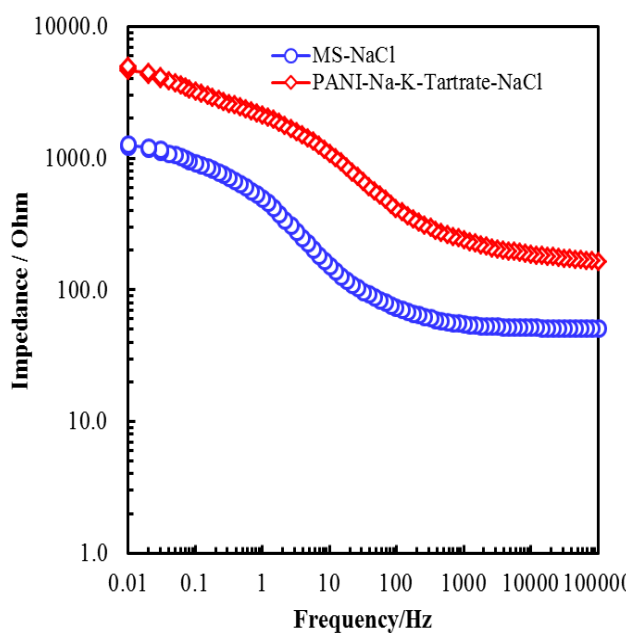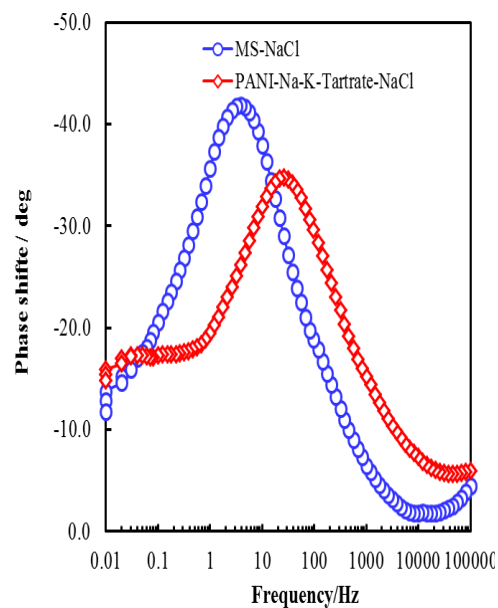
Figure 4.4. 17: Electrochemical impedance response of MS coated with PANI in Na-K Tartrate immersed in 0.1 M NaCl solution (a) Nyquist plot, (b) Bode plot and (c) Phase shift
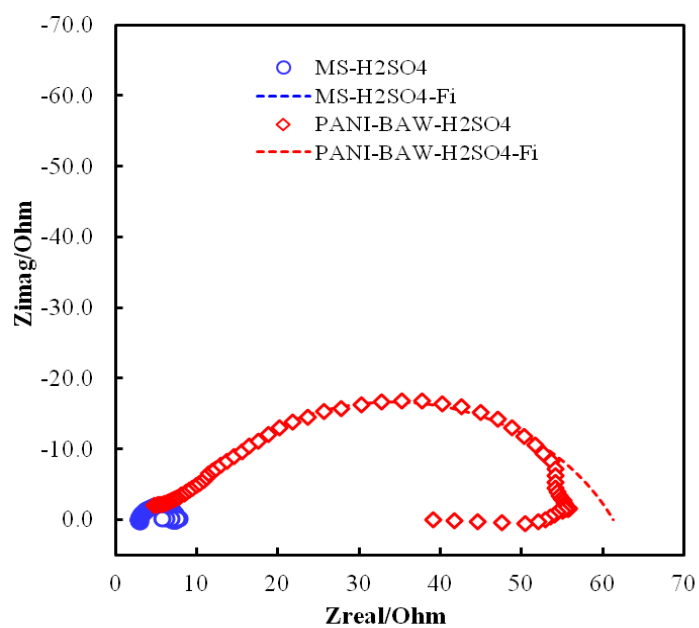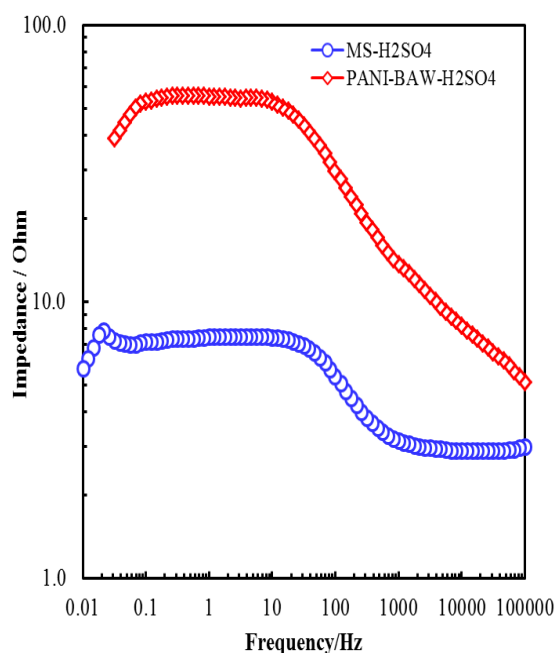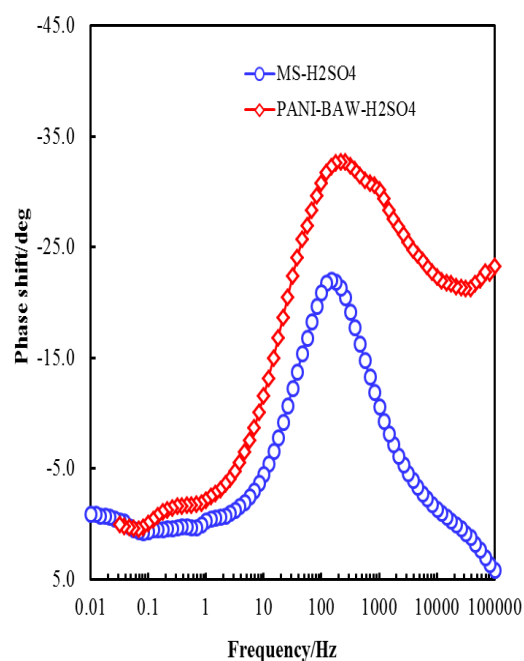
Figure 4.4. 18: Electrochemical impedance response of MS coated with PANI in BAW immersed in 0.1 M H_2SO_4 solution (a) Nyquist plot, (b) Bode plot and (c) Phase shift
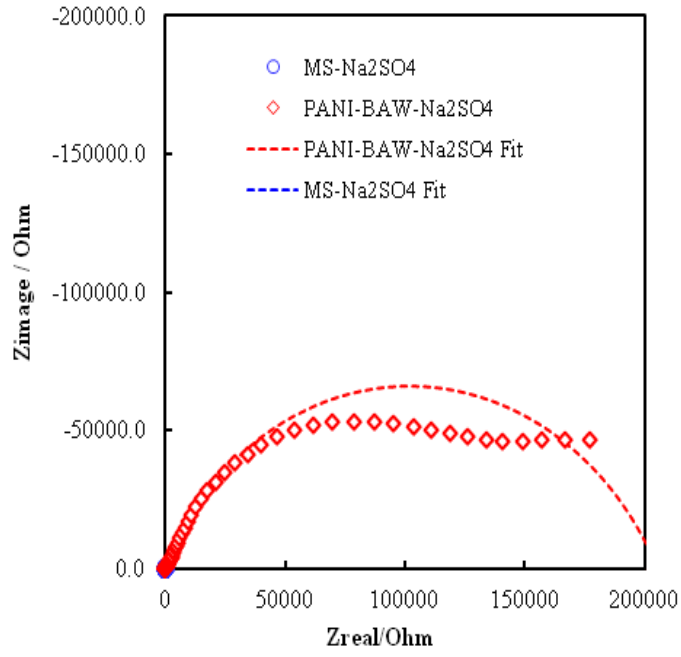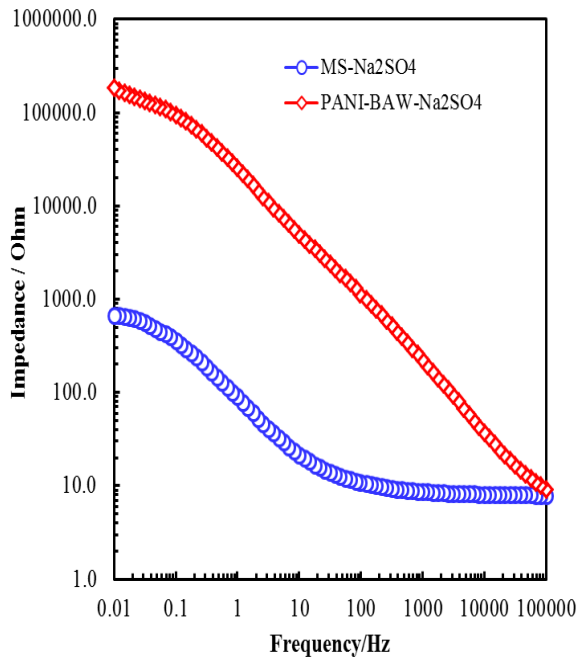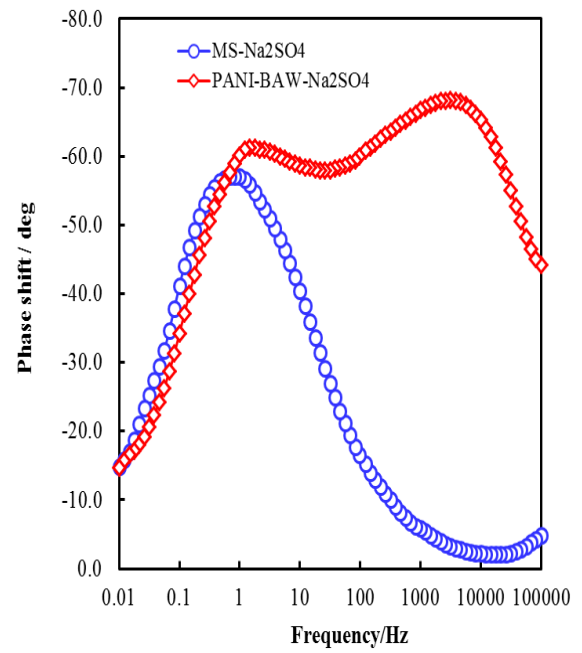
Figure 4.4. 19: Electrochemical impedance response of MS coated with PANI in BAW immersed in 0.4 M Na_2SO_4 solution (a) Nyquist plot, (b) Bode plot and (c) Phase shift
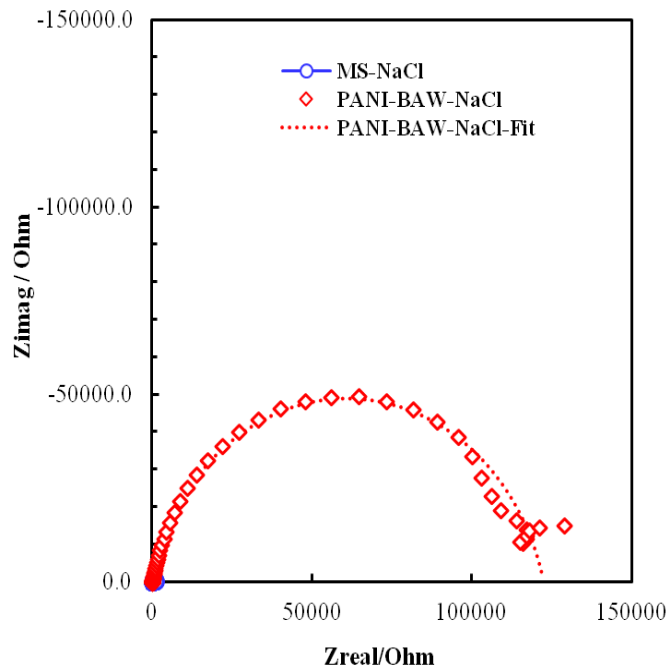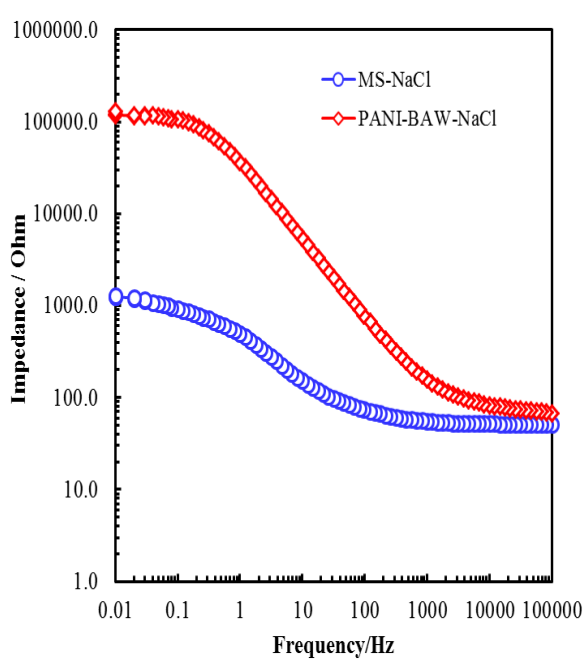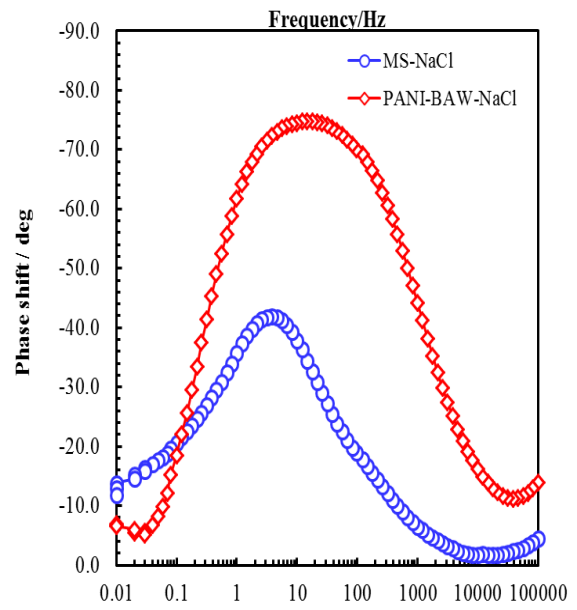
Figure 4.4. 20: Electrochemical impedance response of MS coated with PANI in BAW immersed in 0.1 M NaCl solution (a) Nyquist plot, (b) Bode plot and (c) Phase shift

In all the test solutions, the overall impedance of the MS coated with PANI increased significantly. In the case of H_2SO_4, the overall impedance of the PANI coated was found to be much less compared to Na_2SO_4 and NaCl solutions. This seems be due to conversion of PANI in conductive state due to protonation in acidic solution. In the case of Na_2SO_4 and NaCl solution, due to higher pH values of the solution, the PANI coating undergoes deprotonating and hence conductivity decreased significantly. This led to the drastic increase of impedance values as can be seen from Fig. 4.4.16, Fig.4.4.17, Fig. 4.4.19 and Fig. 4.4.20. The corrosion IE by PANI coating in three different media was calculated from the impedance values and tabulated in Table 4.9. The table shows that the PANI coating obtained in AB electrolytes shows superior IE in all the electrolytes. In Na_2SO_4 and NaCl electrolytes, PANI coating obtained in AB showed IE up to 99% which is among the best protection obtained for organic coating. Therefore, the new electrolyte reported in this study provides superior PANI coating by employing AB as an electrolyte. The corrosion IE obtained by EIS was comparable to those obtained from potentiodynamic polarization method in both cases.

Table 4.9: Corrosion inhibition efficiency of PANI coating in different electrolyes estimated form impedance data in Fig.4.4.16 to Fig.4.4.20

Electrolyte	IE (H_2SO_4) %	IE (Na_2SO_4) %	IE (NaCl) %
Na-K Tartrate	86.5	77.6	75.3
BAW	91.5	99.5	99.0

CHAPTER 5

5. CONCLUSION AND RECOMMENDATIONS

5.1 Conclusion

In this study, polyaniline (PANI) was electrochemically synthesized onto MS using Na-K Tartrate and BAW as two new supporting electrolytes. The PANI coating on MS was greatly affected by the concentration of both aniline and electrolytes. From the results, the concentration of 0.3 M aniline in 0.2 M Na-K Tartrate and 0.3 M aniline in 0.04 M BAW was chosen as the best composition due to better passivation and polymerization behaviors. In the case of BAW, benzoic acid in 3:1 alcohol-water was the optimized new system as a supporting electrolyte for the electropolymerization of aniline. BAW solution suppressed the dissolution of iron and the contamination-free PANI coating was obtained at a lower potential (less positive) than Na-K Tartrate. The PANI coating was characterized by FTIR, UV-Vis, and XRD which confirmed the formation of PANI. The surface morphology was studied by SEM-EDX, TEM, and AFM. The SEM micrograms showed the morphology of the PANI coating was much improved. In the case of Na-k Tartrate, the dissolution of Fe occurred, but the coating showed a smooth, compact, and pore-free structure. The cyclic voltammetry showed no anodic dissolution of iron during cathodic scans, unlike in oxalic acid solution. Thus, the results showed that both Na-K Tartrate and BAW offer better alternatives for polymerization of aniline onto MS surface with improved surface morphologies and cyclic stabilities. The TEM showed the formation of spherical PANI in the nanometer range but the size of PANI was smaller in BAW than in Na-K Tartrate. The AFM result revealed that PANI coating by CV was homogeneous and smooth with minimized roughness.

The effect of La(III) and Ce(IV) on the polymerization of aniline was also studied. The polymerization behaviors were similar in both electrolytes with La(III) and Ce(IV). The result showed there was a decrease in the passive region in Na-K Tartrate but an increase in current with polymerization of aniline in both electrolytes due to an increase in conductivity. The surface morphology showed the tailoring of PANI film with La(III). The size of PANI doped with La(III) was found to be smaller as compared to PANI in both electrolytes, confirmed by TEM micrograms.

Similarly, PANI coating on MS was also synthesized potentiostatically from the optimized concentration composition of both Na-K Tartrate and BAW electrolytes. The

chronoamperogram revealed that polymerization of aniline took place from the beginning in both cases. The PANI coating on MS was fine, uniform, and pore-free at 1.4 V. In the presence of La (III), the drop in current was significantly slower in BAW than Na-K Tartrate electrolyte because of the formation of stable Fe- benzoate passive layer. The presence of La(III) tailored the PANI film.

In galvanostatic polymerization of aniline, the thickening, uniformity, and adherence of PANI coating were influenced by employed current density. A higher current density resulted in the formation of a thin PANI coating which was not uniform and pores free. On the other hand, lower current density resulted in the formation of compact, uniform, and pores-free PANI coating.

Corrosion behavior of PANI coatings on MS in different media showed excellent corrosion protection of MS resulting as high as 90% inhibition efficiency by PANI obtained in both Na-K Tartrate and BAW solutions. Potentiodynamic polarization results revealed that PANI obtained in Na-K Tartrate and BAW solutions have 82.50% and 99.99% inhibition efficiency in 0.1 M NaCl solution respectively. The PANI prepared from Na-K Tartrate and BAW solutions showed 97.53% and 99.0% inhibition efficiency in 0.1 M H_2SO_4 respectively. In the case of 0.4 M Na_2SO_4, the inhibition efficiency of PANI obtained in Na-K Tartrate and BAW was 87.17% and 92.0% respectively. Similarly, in the mixture of 0.4 M Na_2SO_4 and 0.1 M NaCl, the inhibition efficiency of PANI obtained in BAW was 94.48% on the other hand PANI obtained in Na-K Tartrate showed 89.58% inhibition efficiency. Thus, corrosion protection by PANI obtained in BAW was more effective than PANI obtained in Na-K Tartrate. The electrochemical parameters obtained in both cases showed slower down the anodic and cathodic reactions. It also reflected that PANI coating acted as a mixed type of inhibitor in both cases.

PANI coating on MS obtained by galvanostatic polymerization showed above 90% corrosion inhibition efficiency in 0.4 M Na_2SO_3 solution in both cases. However, PANI coating obtained in BAW showed fairly stable in more positive potential than -0.6 V as compared to PANI obtained in Na-K Tartrate which showed breakdown of PANI film at higher potential. This study helped in obtaining an optimized condition for efficient PANI coating on MS in Na-K Tartrate and BAW solutions. Thus, the result showed that PANI coating obtained in BAW is the most effective and better corrosion protection than PANI coating obtained in Na-K Tartrate.

5.2 Recommendations

From the study of electroplymerization of aniline and subsequent coating on MS, the following recommendations are suggested for further research.

1. Potentiostatically prepared PANI can be further studied for corrosion protection because it gives fine and uniforms PANI coating.

2. The effect of La(III) and Ce(IV) doping in PANI coating as corrosion inhibitors can be studied.

3. The stability and degradation of PANI in atmospheric corrosion can also be studied and its biodegradability can also be investigated.

4. Corrosion protection by PANI in soil and concrete environment can also be examined for the sustainability of the material.

CHAPTER 6

6. SUMMARY

PANI is electrochemically synthesized on MS by various electrochemical methods. As the electrolytes play a vital role in the polymerization of aniline onto MS, Na-K Tartrate and BAW are selected as the new electrolytes due to the better passivation and polymerization of aniline on MS. Benzoic acid in 3:1 alcohol-water (BAW) is the optimized new system as a supporting electrolyte for the electropolymerization of aniline. The electrosynthesis of PANI in Na-K Tartrate and BAW is discussed in chapter 3 and chapter 4 discusses the results obtained. In Na-K Tartrate, the dissolution of Fe occurs but BAW prevents the dissolution of Fe and avoids contamination. The concentration of 0.3 M aniline in 0.2 M Na-K Tartrate and 0.3 M aniline in 0.04 M BAW is chosen as the best composition due to better passivation and polymerization behaviors. The BAW system is the most important from an economic point of view. In the BAW solution, PANI coating is obtained at a lower potential (less positive) than Na-K Tartrate as contaminations free.

The PANI is also prepared by the potentiostatic method. In both cases, polymerization of aniline occurs from the beginning. However, the current density falls abruptly to 1 mA/ cm^2 in BAW and attains a limiting current. This results in a fine, smooth, and compact coating.

The PANI coating by the galvanostatic method does not show an induction period in both cases. In the case of BAW, merely a charge of 0.1 mC cm^{-2} is needed for the oxidation of aniline which is 5 times lesser than the charge required for Na-K tartrate and hundreds of times lesser than for oxalic acid. This results in minimization of energy used for polymerization and deposition of PANI on MS in addition to preventing the loss of iron. Thus, the PANI coating obtained in BAW saves a huge amount of energy and forms a better coating at a lower current density than Na-K Tartrate solution.

The PANI coating is characterized by FTIR, UV-Vis, and XRD which confirmed the formation of PANI. The FTIR reveals the same spectra in both cases. The UV-Vis spectra show a shoulder at 430 nm in the case of BAW which is features of polyaniline oxidized to an oxidation state slightly lower than emeraldine. The XRD diffraction pattern reveals that the crystallite size of PANI prepared in BAW is smaller than that of Na-K tartrate.

The surface morphology is studied by optical microscopy, SEM-EDX, TEM, and AFM. The SEM micrograms show the morphology of the PANI coating is much improved in both cases. In the case of Na-k Tartrate, the dissolution of Fe occurs, but the coating shows a smooth, compact, and pore-free structure. But in BAW, the formation of PANI is compact and fine grains in the range of 10 nm. The TEM images also show that PANI formed in BAW is smaller in size than PANI formed in Na-K Tartrate. The AFM reveals that PANI obtained in BAW has little roughness as compared to PANI obtained in Na-K Tartrate.

The corrosion study shows the better corrosion protection of PANI obtained in BAW than Na-K Tartrate in all studied media as discussed in chapter 4. PANI obtained in BAW is stable at the more positive potential in Na_2SO_3 solution and no pores are developed unlike PANI obtained in Na-K Tartrate. Thus, PANI obtained in BAW is the best coating and corrosion protection inhibitor compared to PANI obtained in Na-K Tartrate.

REFERENCES

Abdel-Gaber, A. M., Abd-El-Nabey, B. A., Khamis, E., Salman, R. M., Rahal, H. T., & El Morr, Z. (2020). Electrochemical synthesis and corrosion behaviour of polyaniline on stainless steel in sodium hydroxide solutions. *Chemical Engineering Communications*, 1–10. https://doi.org/10.1080/00986445.2019.1710493

Abdiryim, T., Xiao-Gang, Z., & Jamal, R. (2005). Comparative studies of solid-state synthesized polyaniline doped with inorganic acids. *Materials Chemistry and Physics*, *90*(2–3), 367–372. https://doi.org/10.1016/j.matchemphys.2004.10.036

Ahmad, N., & MacDiarmid, A. G. (1996). Inhibition of corrosion of steels with the exploitation of conducting polymers. *Synthetic Metals*, *78*(2), 103–110. https://doi.org/10.1016/0379-6779(96)80109-3

Ahmad, Z. (2006). *Principles of corrosion engineering and corrosion control* (1st ed). Elsevier/BH.

Akbarinezhad, E. (2014). Evaluating protection performance of zinc rich epoxy paints modified with polyaniline and polyaniline-clay nanocomposite. *Progress in Organic Coatings*, 10.

Al-Owais, A. A., & El-Hallag, I. S. (2019). Voltammetric and chronoamperometric studies of aniline electropolymerization in different aqueous sulfuric acid solutions. *Polymer Bulletin*, *76*(9), 4571–4584. https://doi.org/10.1007/s00289-018-2610-9

Amaechi, I. C., Nwanya, A. C., Ekwealor, A. B. C., Asogwa, P. U., Osuji, R. U., Maaza, M., & Ezema, F. I. (2015). Electronic thermal conductivity, thermoelectric properties and supercapacitive behaviour of conjugated polymer nanocomposite (polyaniline-WO $_3$) thin film. *The European Physical Journal Applied Physics*, *69*(3), 30901. https://doi.org/10.1051/epjap/2015140441

Ananda Kumar, S., Shree Meenakshi, K., Sankaranarayanan, T. S. N., & Srikanth, S. (2008). Corrosion resistant behaviour of PANI–metal bilayer coatings. *Progress in Organic Coatings*, *62*(3), 285–292. https://doi.org/10.1016/j.porgcoat.2008.01.005

Araujo, W. S., Margarit, I. C. P., Ferreira, M., Mattos, O. R., & Neto, P. L. (2001). Undoped polyaniline anticorrosive properties. *Electrochimica Acta*, 6.

Armelin, E., Oliver, R., Liesa, F., Iribarren, J. I., Estrany, F., & Alemán, C. (2007). Marine paint fomulations: Conducting polymers as anticorrosive additives. *Progress in Organic Coatings*, *59*(1), 46–52. https://doi.org/10.1016/j.porgcoat.2007.01.013

Ashraf, P. M., & Shibli, S. M. A. (2007). Reinforcing aluminium with cerium oxide: A new and effective technique to prevent corrosion in marine environments. *Electrochemistry Communications*, *9*(3), 443–448. https://doi.org/10.1016/j.elecom.2006.09.010

Bandgar, D. K., Khuspe, G. D., Pawar, R. C., Lee, C. S., & Patil, V. B. (2014). Facile and novel route for preparation of nanostructured polyaniline (PANi) thin films. *Applied Nanoscience*, *4*(1), 27–36. https://doi.org/10.1007/s13204-012-0175-8

Bazzaoui, M., Martins, J. I., Bazzaoui, E. A., Reis, T. C., & Martins, L. (2004). Pyrrole Electropolymerization on Copper and Brass in a Single-Step Process from Aqueous Solution. *Journal of Applied Electrochemistry*, *34*(8), 815–822. https://doi.org/10.1023/B:JACH.0000035610.10869.43

Beck, F., Mi, R., Schu, F., Zrr, B., & Duisburg, U. (1994). *PYRROLE ON IRON IN AQUEOUS OXALIC ACID* (No. 2). *39*(2), 229–234.

Bera, A., Deb, K., Kathirvel, V., Bera, T., Thapa, R., & Saha, B. (2017). Flexible diode of polyaniline/ITO heterojunction on PET substrate. *Applied Surface Science*, *418*, 264–269. https://doi.org/10.1016/j.apsusc.2016.12.003

Bernard M. C. , A. Hugot-LeGoff, S. Joiret. (1999). *Polyaniline layer for Iron Protection in sulfate medium. 102*, 1383–1384.

Bhadra, J., Popelka, A., Abdulkareem, A., Ahmad, Z., Touati, F., & Al-Thani, N. (2019). Fabrication of polyaniline–graphene/polystyrene nanocomposites for flexible gas sensors. *RSC Advances*, *9*(22), 12496–12506. https://doi.org/10.1039/C9RA00936A

Boshkova, N., Tabakova, N., Atanassova, G., & Boshkov, N. (2019). Electrochemical Obtaining and Corrosion Behavior of Zinc-Polyaniline (Zn-PANI) Hybrid Coatings. *Coatings*, *9*(8), 487. https://doi.org/10.3390/coatings9080487

Buron, C. C., Lakard, B., Monnin, A. F., Moutarlier, V., & Lakard, S. (2011). Elaboration and characterization of polyaniline films electrodeposited on tin oxides. *Synthetic Metals*, *161*(19–20), 2162–2169. https://doi.org/10.1016/j.synthmet.2011.08.021

C. K. Chiang, A. Druy, S. C. Gau, S, A. J. Heeger, E. J. Louis, A. G . MacDiarmid, Y. W. Park, H. S h i r a k a ~, & A. J. Heeger, E. J. Louis, A. G . MacDiarmid.

(1978). Synthesis of Highly Conducting Films of Derivatives of Polyacetylene, (CH),. *American Chemical Society*.

Camalet, J. L., Lacroix, J. C., Aeiyach, S., Chane-Ching, K., & Lacaze, P. C. (1996). Electrodeposition of protective polyaniline films on mild steel. *Journal of Electroanalytical Chemistry*, *416*(1–2), 179–182. https://doi.org/10.1016/S0022-0728(96)01012-1

Camalet, J. L., Lacroix, J. C., Aeiyach, S., & Lacaze, P. C. (1998). Characterization of polyaniline films electrodeposited on mild steel in aqueous p-toluenesulfonic acid solution. *Journal of Electroanalytical Chemistry*, *445*(1), 117–124. https://doi.org/10.1016/S0022-0728(97)00526-3

Camalet, J.-L., Lacroix, J.-C., Nguyen, T. D., Aeiyach, S., Pham, M. C., Petitjean, J., & Lacaze, P.-C. (2000). Aniline electropolymerization on platinum and mild steel from neutral aqueous media. *Journal of Electroanalytical Chemistry*, *485*(1), 13–20. https://doi.org/10.1016/S0022-0728(00)00080-2

Can, M., Pekmez, K., Pekmez, N., & Yildiz, A. (2000). *Electropreparation and electrochemical stability of polythiophenes in acetonitrile containing anhydrous HBF4*. *77*, 412–322.

Canales, M., Torras, J., Fabregat, G., Meneguzzi, A., & Alemán, C. (2014). Polyaniline Emeraldine Salt in the Amorphous Solid State: Polaron versus Bipolaron. *The Journal of Physical Chemistry B*, *118*(39), 11552–11562. https://doi.org/10.1021/jp5067583

D. W. Deberry, A. Viehbeck. (1984). *Fundamental Aspects of Corrosion Protection by Surface Modification* (E. McCafferty, CR Clayton, J. Oudar, Eds). Pennington.

Dariva, C. G., & Galio, A. F. (2014). Corrosion Inhibitors – Principles, Mechanisms and Applications. In M. Aliofkhazraei (Ed.), *Developments in Corrosion Protection*. InTech. https://doi.org/10.5772/57255

Davis, J. R. (2000). *Corrosion: Understanding the basics*. A.S.M. International.

de Souza, S. (2007). Smart coating based on polyaniline acrylic blend for corrosion protection of different metals. *Surface and Coatings Technology*, *201*(16–17), 7574–7581. https://doi.org/10.1016/j.surfcoat.2007.02.027

DeBerry, D. W. (1985). Modification of the Electrochemical and Corrosion Behavior of Stainless Steels with an Electroactive Coating. *Journal of The Electrochemical Society*, *132*(5), 1022. https://doi.org/10.1149/1.2114008

Desai, P. S., & Indorwala, N. S. (2015). Triazoles used as a Corrosion inhibitor for mild steel in Hydrochloric Acid. *International Journal of Current Microbiology and Applied Sciences*, 928–938.

Dhawan, S. K., & Trivedi, D. C. (1991). Electrochemical behaviour of polyaniline in aromatic sulphonic acids. *Polymer International*, *25*(1), 55–60. https://doi.org/10.1002/pi.4990250110

Diaz, A. F., & Logan, J. A. (1980). Electroactive polyaniline films. *Journal of Electroanalytical Chemistry and Interfacial Electrochemistry*, *111*(1), 111–114. https://doi.org/10.1016/S0022-0728(80)80081-7

Dimitriev, O. P., Smertenko, P. S., Stiller, B., & Brehmer, L. (2005). Polyaniline–transition metal salt complexes: Insight into formation mechanisms. *Synthetic Metals*, *149*(2–3), 187–192. https://doi.org/10.1016/j.synthmet.2004.12.007

Ding, K., Jia, Z., Ma, W., Tong, R., & Wang, X. (2002). Polyaniline and polyaniline–thiokol rubber composite coatings for the corrosion protection of mild steel. *Materials Chemistry and Physics*, *76*(2), 137–142. https://doi.org/10.1016/S0254-0584(01)00518-1

E. Bardal. (2004). *Corrosion and Protection*. Springer-Verlag, London.

Eftekhari, A. (2002). Aluminum as a suitable substrate for the deposition of conducting polymers: Application to polyaniline and enzyme-modi®ed electrode. *Synthetic Metals*, 6.

Eftekhari, A. (2004). Electropolymerization of aniline onto passivated substrate and its application for preparation of enzyme-modified electrode. *Synthetic Metals*, *145*(2–3), 211–216. https://doi.org/10.1016/j.synthmet.2004.05.016

El-Etre, A. Y. (2007). Inhibition of acid corrosion of carbon steel using aqueous extract of olive leaves. *Journal of Colloid and Interface Science*, *314*(2), 578–583. https://doi.org/10.1016/j.jcis.2007.05.077

El-Shazly, A. H., & Al-Turaif, H. A. (2012). Improving the Corrosion Resistance of Buried Steel by Using Polyaniline Coating. *Int. J. Electrochem. Sci.*, *7*, 11.

Evans, U. R. (1972). *An introduction to metallic corrosion* (2nd Ed.). Edward Arnold Ltd.

F. Deflorian. (2012). *Understanding the role of conducting polymers*.

Fang, Z., Wang, G., Xiong, Y., Li, J., Yang, Y., Huang, L., Wang, P., Liao, J., & Wang, A. (2021). Anti-Corrosion Performance of Polyaniline Coated Basalt Rockwool Wastes/Epoxy Resin Coatings. *Coatings*, *11*(4), 463. https://doi.org/10.3390/coatings11040463

Finšgar, M., & Jackson, J. (2014). Application of corrosion inhibitors for steels in acidic media for the oil and gas industry: A review. *Corrosion Science*, *86*, 17–41. https://doi.org/10.1016/j.corsci.2014.04.044

Fusalba, F., & Bélanger, D. (1999). Electropolymerization of Polypyrrole and Polyaniline−Polypyrrole from Organic Acidic Medium. *The Journal of Physical Chemistry B*, *103*(42), 9044–9054. https://doi.org/10.1021/jp9916790

G. Fomo, T. T. Waryo, P. Baker and E. I. Iwuoh. (2016). Electrochemical Deposition and Properties of Polyaniline Films on Carbon and Precious Metal Surfaces in Perchloric Acid/Acetonitrile. *Int. J. Electrochem. Sci*, *11*, 10347–10361.

Ganash, A. A., Al-Nowaiser, F. M., Al-Thabaiti, S. A., & Hermas, A. A. (2011). Comparison study for passivation of stainless steel by coating with polyaniline from two different acids. *Progress in Organic Coatings*, *72*(3), 480–485. https://doi.org/10.1016/j.porgcoat.2011.06.006

Genies, E. M., & Tsintavis, C. (1985). *REDOX MECHANISM AND ELECTROCHEMICAL BEHAYIOUR OF POLYANILINE DEPOSITS*. *195*, 109–128.

Ghali, E., Sastri, V. S., & Elboujdaini, M. (2007). *Corrosion Prevention and Protection: Practical Solution*. John Wiley & Sons, Inc., England.

Gordon G. Wallace, Peter R. Teasdale, Geoffrey M. Spinks, & Leon A. P. Kane-Maguire. (2008). *Conductive Electroactive Polymers Intelligent Polymer Systems* (3rd Edition). CRC Press.

Green and wdoodhead, Arthugreorgegreen. (1910). *CXV1I.-Aniline-black and Allied Compounds. Part 11*. 7.

Gupta, D. K., Neupane, S., Singh, S., Karki, N., & Yadav, A. P. (2021). The effect of electrolytes on the coating of polyaniline on mild steel by electrochemical methods and its corrosion behavior. *Progress in Organic Coatings*, *152*, 106127. https://doi.org/10.1016/j.porgcoat.2020.106127

Gupta, D. K., Neupane, S., Singh, S., Karki, N., & Yadav, A. P. (2021). Dataset for the selection of electrolytes for Electropolymerization of aniline. *Data in Brief*, *35*, 106875. https://doi.org/10.1016/j.dib.2021.106875

Gvozdenovi, M., Jugovi, B., Jambrec, D., Stevanovi, J., & Grgur, B. (2012a). APPLICATION OF POLYANILINE IN CORROSION PROTECTION …. *ZAŠTITA MATERIJALA*, 8.

Gvozdenovi, M., Jugovi, B., Jambrec, D., Stevanovi, J., & Grgur, B. (2012b). APPLICATION OF POLYANILINE IN CORROSION PROTECTION …. *ZAŠTITA MATERIJALA*, 8.

Halambek, J., Berković, K., & Vorkapić-Furač, J. (2010). The influence of Lavandula angustifolia L. oil on corrosion of Al-3Mg alloy. *Corrosion Science*, *52*(12), 3978–3983. https://doi.org/10.1016/j.corsci.2010.08.012

HALL N. (2003). Twenty-five years of conducting polymers. *Chemical Communications*, *1*(1), 1–5.

Heeger, A. J. (2001). Nobel Lecture: Semiconducting and metallic polymers: The fourth generation of polymeric materials. *Reviews of Modern Physics*, *73*(3), 681–700. https://doi.org/10.1103/RevModPhys.73.681

Herrasti, P. (2003). *Electroactive polymer films for stainless steel corrosion protection*. *44*, 533–540.

Heusler, K. E., Landolt, D., & Trasatti, S. (1989). Electrochemical Corrosion Nomenclature. *Pure and Applied Chemistry*, *61*, 19–22.

Hu, J., Zhao, X. H., Tang, S. W., & Sun, M. R. (2006). Corrosion protection of aluminum borate whisker reinforced AA6061 composite by cerium oxide-based conversion coating. *Surface and Coatings Technology*, *201*(6), 3814–3818. https://doi.org/10.1016/j.surfcoat.2006.09.006

Huang, N., Liang, C., & Yi, B. (2008). Corrosion resistance of PANi-coated steel in simulated PEMFC anodic environment. *Materials and Corrosion*, *59*(1), 21–24. https://doi.org/10.1002/maco.200704062

Huang, W. S., & MacDiarmid, A. G. (1993). Optical properties of polyaniline. *Polymer*, *34*(9), 1833–1845. https://doi.org/10.1016/0032-3861(93)90424-9

Huh, J. H., Oh, E. J., & Cho, J. H. (2003). Investigation of corrosion protection of iron by polyaniline blend coatings. *Synthetic Metals*, *137*(1–3), 965–966. https://doi.org/10.1016/S0379-6779(02)00953-0

Hulser, P., & Beck, F. (1990). Electrodeposition of polypyrrole layers on aluminium from aqueous electrolytes. *Journal of Applied Electrochemistry*, *20*(4), 596–605. https://doi.org/10.1007/BF01008869

Inzelt, G. (2000). Simultaneous chronoamperometric and quartz crystal microbalance studies of redox transformations of polyaniline films. *Electrochimica Acta*, *45*(22–23), 3865–3876. https://doi.org/10.1016/S0013-4686(00)00455-2

Inzelt, György. (2008). *Conducting Polymers   A New Era in Electrochemistry*. Springer-Verlag,.

Izumi, C. M. S., Rodrigues, D. C., & Temperini, M. L. A. (2010). The role of solvent on the doping of polyaniline with Fe(III) ions. *Synthetic Metals*, *160*(23–24), 2552–2558. https://doi.org/10.1016/j.synthmet.2010.10.004

Jafari, Y., Ghoreishi, S. M., & Shabani-Nooshabadi, M. (2016). Electrochemical deposition and characterization of polyaniline-graphene nanocomposite films and its corrosion protection properties. *Journal of Polymer Research*, *23*(5), 91. https://doi.org/10.1007/s10965-016-0983-8

J.B. (1895). The use of molasses and vegetable oils to inhibit corrosion of pickling sheet steel in acids. *England*.

Jeyaprabha, C., Sathiyanarayanan, S., & Venkatachari, G. (2006). Polyaniline as corrosion inhibitor for iron in acid solutions. *Journal of Applied Polymer Science*, *101*(4), 2144–2153. https://doi.org/10.1002/app.22579

Kamaraj, K., Sathiyanarayanan, S., Muthukrishnan, S., & Venkatachari, G. (2009). Corrosion protection of iron by benzoate doped polyaniline containing coatings. *Progress   in   Organic   Coatings*, *64*(4), 460–465. https://doi.org/10.1016/j.porgcoat.2008.08.008

Kartsonakis, I. A., Koumoulos, E. P., Balaskas, A. C., Pappas, G. S., Charitidis, C. A., & Kordas, G. C. (2012). Hybrid organic–inorganic multilayer coatings including nanocontainers for corrosion protection of metal alloys. *Corrosion Science*, *57*, 56–66. https://doi.org/10.1016/j.corsci.2011.12.034

Kawashima, H., & Goto, H. (2011). Preparation and Properties of Polyaniline in the Presence of Trehalose. *Soft Nanoscience Letters*, *01*(03), 71–75. https://doi.org/10.4236/snl.2011.13013

Kazum, O., & Kannan, M. B. (2016). Optimising parameters for galvanostatic polyaniline coating on nanostructured bainitic steel. *Surface Engineering*, *32*(8), 607–614. https://doi.org/10.1080/02670844.2015.1108071

Kellenberger, A., Ambros, D., & Plesu, N. (2014). Scan Rate Dependent Morphology of Polyaniline Films Electrochemically Deposited on Nickel. *Int. J. Electrochem. Sci.*, *9*, 13.

Khodaei, P., Shabani-Nooshabadi, M., & Behpour, M. (2019). Epoxy-Based nanocomposite coating reinforced by a zeolite complex: Its anticorrosion

properties on mild steel in 3.5 wt% NaCl media. *Progress in Organic Coatings*, *136*, 105254. https://doi.org/10.1016/j.porgcoat.2019.105254

Kinlen, P. J., Menon, V., & Ding, Y. (1999). A Mechanistic Investigation of Polyaniline Corrosion Protection Using the Scanning Reference Electrode Technique. *Journal of The Electrochemical Society*, *146*(10), 3690–3695. https://doi.org/10.1149/1.1392535

Krzysztof Bieńkowski. (2006). *Polyaniline and its Derivatives Doped With Lewis Acids - Synthesis And Spectroscopic Properties* [Ph D Thesis]. Warsaw University of Technology Joseph Fourier University – Grenoble I.

L. L. Shreir, & R. A. Jarman and G. T. Burstein. (1994). *"Corrosion* (3rd Edition, Vol. 1). Oxford: Butterworth-Heinemann.

Laco, J. I. I., Villota, F. C., & Mestres, F. L. (2005). Corrosion protection of carbon steel with thermoplastic coatings and alkyd resins containing polyaniline as conductive polymer. *Progress in Organic Coatings*, *52*(2), 151–160. https://doi.org/10.1016/j.porgcoat.2004.10.005

Lacroix, J.-C., Camalet, J.-L., Aeiyach, S., Chane-Ching, K. I., Petitjean, J., Chauveau, E., & Lacaze, P.-C. (2000). Aniline electropolymerization on mild steel and zinc in a two-step process. *Journal of Electroanalytical Chemistry*, *481*(1), 76–81. https://doi.org/10.1016/S0022-0728(99)00490-8

Letheby, H. (1862). XXIX.—On the production of a blue substance by the electrolysis of sulphate of aniline. *J. Chem. Soc.*, *15*(0), 161–163. https://doi.org/10.1039/JS8621500161

Li, W. (2018). Electrodeposition of PANI/MWCNT Coatings on Stainless Steel and Their Corrosion Protection Performances. *Int. J. Electrochem. Sci.*, *13*, 1367–1375.

Li, Y., Zhao, P., Liang, Q., & Hou, B. (2005). Berberine as a natural source inhibitor for mild steel in 1M H2SO4. *Applied Surface Science*, *252*(5), 1245–1253. https://doi.org/10.1016/j.apsusc.2005.02.094

M. Fontana, N. Greene. (1986). *Corrosion Engineering*. Mcgraw-Hill Education.

MacDiarmid, A. G., & Epstein, A. J. (1989). Polyanilines: A novel class of conducting polymers. *Faraday Discussions of the Chemical Society*, *88*, 317. https://doi.org/10.1039/dc9898800317

MacDiarmid, Alan G. (2001). *Synthetic metals: A novel role for organic polymers—Nobel Prize 2000 Lecture*. *1*, 269–279.

Machnikova, E., Pazderova, M., Bazzaoui, M., & Hackerman, N. (2008). Corrosion study of PVD coatings and conductive polymer deposited on mild steel. *Surface and Coatings Technology*, *202*(8), 1543–1550. https://doi.org/10.1016/j.surfcoat.2007.07.006

Mahato, N., & Cho, M. H. (2016). Graphene integrated polyaniline nanostructured composite coating for protecting steels from corrosion: Synthesis, characterization, and protection mechanism of the coating material in acidic environment. *Construction and Building Materials*, *115*, 618–633. https://doi.org/10.1016/j.conbuildmat.2016.04.073

Martyak, N. M., McAndrew, P., McCaskie, J. E., & Dijon, J. (2002). Electrochemical polymerization of aniline from an oxalic acid medium. *Progress in Organic Coatings*, *45*(1), 23–32. https://doi.org/10.1016/S0300-9440(02)00070-X

Masdarolomoor, F., Hajizadeh, S., Arab Chamjangali, M., & Innis, P. C. (2019). Novel approach to the synthesis of polyaniline possessing electroactivity at neutral pH. *Synthetic Metals*, *250*, 121–130. https://doi.org/10.1016/j.synthmet.2019.03.011

Mathai, C. J., Saravanan, S., Jayalekshmi, S., Venkitachalam, S., & Anantharaman, M. R. (2003). Conduction mechanism in plasma polymerized aniline thin films. *Materials Letters*, *57*(15), 2253–2257. https://doi.org/10.1016/S0167-577X(02)01205-3

Mazumder, M. A. J. (2020). *Global Impact of Corrosion: Occurrence, Cost and Mitigation*. *5*(4), 5. https://doi.org/doi.org/10.33552/GJES.2020.05.000618

McCafferty, E. (2005). Validation of corrosion rates measured by the Tafel extrapolation method. *Corrosion Science*, *47*(12), 3202–3215. https://doi.org/10.1016/j.corsci.2005.05.046

Medhat Ibrahima and Eckhard Koglin. (2005). *Spectroscopic Study of Polyaniline Emeraldine Base: Modelling Approach*. *52*, 159–162.

Mohd, N., & Ishak, A. S. (2015). Thermodynamic Study of Corrosion Inhibition of Mild Steel in Corrosive Medium by Piper nigrum Extract. *Indian Journal of Science and Technology*, *8*(17), Article 17. https://doi.org/10.17485/ijst/2015/v8i17/63478

Mohd, Y., Ibrahim, R., & Zainal, M. F. (2012). Electrodeposition and characterization of Polyaniline films. *2012 IEEE Symposium on Humanities, Science and Engineering Research*, 1301–1306. https://doi.org/10.1109/SHUSER.2012.6268811

Molapo, K. M., Ndangili, P. M., Ajayi, R. F., Mbambisa, G., Mailu, S. M., Njomo, N., Masikini, M., Baker, P., & Iwuoha, E. I. (2012). Electronics of Conjugated Polymers (I): Polyaniline. *Int. J. Electrochem. Sci.*, *7*, 17.

Moraes, S. R., Huerta-Vilca, D., & Motheo, A. J. (2003). Corrosion protection of stainless steel by polyaniline electrosynthesized from phosphate buffer solutions. *Progress in Organic Coatings*, *48*(1), 28–33. https://doi.org/10.1016/S0300-9440(03)00075-4

Moreno, J. D., Marcos, M. L., Agulló-Rueda, F., Guerrero-Lemus, R., Martín-Palma, R. J., Martínez-Duart, J. M., & González-Velasco, J. (1999). A galvanostatic study of the electrodeposition of polypyrrole into porous silicon. *Thin Solid Films*, *348*(1–2), 152–156. https://doi.org/10.1016/S0040-6090(99)00056-5

Mostafaei, A., & Zolriasatein, A. (2012). Synthesis and characterization of conducting polyaniline nanocomposites containing ZnO nanorods. *Progress in Natural Science: Materials International*, *22*(4), 273–280. https://doi.org/10.1016/j.pnsc.2012.07.002

Mu, S., & Kan, J. (1998). The effect of salts on the electrochemical polymerization of aniline. *Synthetic Metals*, *92*(2), 149–155. https://doi.org/10.1016/S0379-6779(98)80104-5

Muto, I., Saito, E., & Ito, S. (1994). *Application of accelerated corrosion tests to service life prediction of materials*. ASTM STP.

N. B. Devkota, S. Singh, S. Neupane, D. K. Gupta and A. P. Yadav. (2016). Electro-Polymerization of Aniline onto Mild Steel Surface Using Sodium Benzoate. *Journal of Nepal Chemical Society*, *35*, 94–103.

Nabin Karki. (2018). *Development of Green Corrosion Inhibitor from Natural Products of Nepal* [Ph D Thesis].

NACE International Institute IMPACT PLUS. (2020). https://www.nace-impact.org

Narayanasamy, B., & Rajendran, S. (2010). Electropolymerized bilayer coatings of polyaniline and poly(N-methylaniline) on mild steel and their corrosion protection performance. *Progress in Organic Coatings*, *67*(3), 246–254. https://doi.org/10.1016/j.porgcoat.2009.12.001

Nautiyal, A., & Parida, S. (2016). Comparison of polyaniline electrodeposition on carbon steel from oxalic acid and salicylate medium. *Progress in Organic Coatings*, *94*, 28–33. https://doi.org/10.1016/j.porgcoat.2016.01.014

Ngouné, B., Pengou, M., Nouteza, A. M., Nanseu-Njiki, C. P., & Ngameni, E. (2019). Performances of Alkaloid Extract from *Rauvolfia macrophylla* Stapf toward Corrosion Inhibition of C38 Steel in Acidic Media. *ACS Omega*, *4*(5), 9081–9091. https://doi.org/10.1021/acsomega.9b01076

Nguyen, T. D., Nguyen, T. A., Pham, M. C., Piro, B., Normand, B., & Takenouti, H. (2004). Mechanism for protection of iron corrosion by an intrinsically electronic conducting polymer. *Journal of Electroanalytical Chemistry*, *572*(2), 225–234. https://doi.org/10.1016/j.jelechem.2003.09.028

Nguyen Thi Le, H., Garcia, B., Deslouis, C., & Le Xuan, Q. (2001). Corrosion protection and conducting polymers: Polypyrrole films on iron. *Electrochimica Acta*, *46*(26–27), 4259–4272. https://doi.org/10.1016/S0013-4686(01)00699-5

Obot, I. B., Obi-Egbedi, N. O., & Umoren, S. A. (2009). Antifungal drugs as corrosion inhibitors for aluminium in 0.1M HCl. *Corrosion Science*, *51*(8), 1868–1875. https://doi.org/10.1016/j.corsci.2009.05.017

Olad, A., & Naseri, B. (2010). Preparation, characterization and anticorrosive properties of a novel polyaniline/clinoptilolite nanocomposite. *Progress in Organic Coatings*, *67*(3), 233–238. https://doi.org/10.1016/j.porgcoat.2009.12.003

Özyılmaz, A. T., Tüken, T., Yazıcı, B., & Erbil, M. (2005). The electrochemical synthesis and corrosion performance of polyaniline on copper. *Progress in Organic Coatings*, *52*(2), 92–97. https://doi.org/10.1016/j.porgcoat.2004.09.003

Pawar, P., Gaikawad, A. B., & Patil, P. P. (2006). Electrochemical synthesis of corrosion protective polyaniline coatings on mild steel from aqueous salicylate medium. *Science and Technology of Advanced Materials*, *7*(7), 732–744. https://doi.org/10.1016/j.stam.2006.09.014

Pierre, R. R. (2008). *Corrosion Engineering: Principles and Practice* (1st ed.). McGraw-Hill Inc.

Popović, M. M., & Grgur, B. N. (2004). Electrochemical synthesis and corrosion behavior of thin polyaniline-benzoate film on mild steel. *Synthetic Metals*, *143*(2), 191–195. https://doi.org/10.1016/j.synthmet.2003.12.022

Prasutiyo, Y. J., Manaf, A., & Hafizah, M. A. E. (2020). Synthesis of polyaniline by chemical oxidative polymerization and characteristic of conductivity and reflection for various strong acid dopants. *Journal of Physics: Conference Series*, *1442*, 012003. https://doi.org/10.1088/1742-6596/1442/1/012003

Pron, A., & Rannou, P. (2002). Processible conjugated polymers: From organic semiconductors to organic metals and superconductors. *Progress in Polymer Science*, *27*(1), 135–190. https://doi.org/10.1016/S0079-6700(01)00043-0

Qiang, Y., Zhang, S., Tan, B., & Chen, S. (2018). Evaluation of Ginkgo leaf extract as an eco-friendly corrosion inhibitor of X70 steel in HCl solution. *Corrosion Science*, *133*, 6–16. https://doi.org/10.1016/j.corsci.2018.01.008

Rahman, Md., Kumar, P., Park, D.-S., & Shim, Y.-B. (2008). Electrochemical Sensors Based on Organic Conjugated Polymers. *Sensors*, *8*(1), 118–141. https://doi.org/10.3390/s8010118

Rajyalakshmi, T., Pasha, A., Khasim, S., Lakshmi, M., Murugendrappa, M. V., & Badi, N. (2020). Enhanced Charge Transport and Corrosion Protection Properties of Polyaniline–Carbon Nanotube Composite Coatings on Mild Steel. *Journal of Electronic Materials*, *49*(1), 341–352. https://doi.org/10.1007/s11664-019-07783-6

Rangel-Olivares, F. R., Arce-Estrada, E. M., & Cabrera-Sierra, R. (2021). Synthesis and Characterization of Polyaniline-Based Polymer Nanocomposites as Anti-Corrosion Coatings. *Coatings*, *11*(6), 653. https://doi.org/10.3390/coatings11060653

Rao, C. R. K., Muthukannan, R., & Vijayan, M. (2012). Studies on biphenyl disulphonic acid doped polyanilines: Synthesis, characterization and electrochemistry. *Bulletin of Materials Science*, *35*(3), 405–414. https://doi.org/10.1007/s12034-012-0315-5

Rayati, M., & Arefinia, R. (2020). Anticorrosion behavior of DBSA doped polyaniline nanoparticles/epoxy ester coating on carbon steel in saline-alkaline solution. *Progress in Organic Coatings*, 105451. https://doi.org/10.1016/j.porgcoat.2019.105451

Rimbu, G. A., Stamatin, I., Jackson, C. L., & Scott, K. (2006). *The morphology control of polyaniline as conducting polymer in fuel cell technology*. *8*(2), 670–674.

Roberge, P. R. (2012). *Handbook of Corrosion Engineering*. McGraw-Hill Inc.

Rohwerder, M., & Michalik, A. (2007). Conducting polymers for corrosion protection: What makes the difference between failure and success? *Electrochimica Acta*, *53*(3), 1300–1313. https://doi.org/10.1016/j.electacta.2007.05.026

S. Neupane. (2013). *Development of a Windows Based Program to Control the Analogue Potentiostat in Combination with an ADA Convertor* [M.Sc. Disertation]. Tri-Chandra Multiple Campus, Tribhuvan University, Nepal.

S. Roth. (1995). *One Dimensional Metals*. VCH Press, Weinheim.

Sakhri, A., Perrin, F. X., Aragon, E., Lamouric, S., & Benaboura, A. (2010). Chlorinated rubber paints for corrosion prevention of mild steel: A comparison between zinc phosphate and polyaniline pigments. *Corrosion Science*, *52*(3), 901–909. https://doi.org/10.1016/j.corsci.2009.11.010

Samui, A. B., & Phadnis, S. M. (2005). Polyaniline–dioctyl phosphate salt for corrosion protection of iron. *Progress in Organic Coatings*, *54*(3), 263–267. https://doi.org/10.1016/j.porgcoat.2005.07.002

Sastri, V. S. (2011). *Green Corrosion Inhibitors: Theory and Practice* (1st Ed.). John, Wiley & Sons, Inc. England.

Sathiyanarayanan, S., Jeyaprabha, C., & Venkatachari, G. (2008). Influence of metal cations on the inhibitive effect of polyaniline for iron in 0.5M H2SO4. *Materials Chemistry and Physics*, *107*(2–3), 350–355. https://doi.org/10.1016/j.matchemphys.2007.07.024

Sathiyanarayanan, S., Muthkrishnan, S., & Venkatachari, G. (2006). Corrosion protection of steel by polyaniline blended coating. *Electrochimica Acta*, *51*(28), 6313–6319. https://doi.org/10.1016/j.electacta.2006.04.015

Sathiyanarayanan, S., Muthukrishnan, S., Venkatachari, G., & Trivedi, D. C. (2005). Corrosion protection of steel by polyaniline (PANI) pigmented paint coating. *Progress in Organic Coatings*, *53*(4), 297–301. https://doi.org/10.1016/j.porgcoat.2005.03.007

Saxena, A., Prasad, D., Haldhar, R., Singh, G., & Kumar, A. (2018). Use of Saraca ashoka extract as green corrosion inhibitor for mild steel in 0.5 M H2SO4. *Journal of Molecular Liquids*, *258*, 89–97. https://doi.org/10.1016/j.molliq.2018.02.104

Sazou, D., & Georgolios, C. (1997). Formation of conducting polyaniline coatings on iron surfaces by electropolymerization of aniline in aqueous solutions. *Journal of Electroanalytical Chemistry*, *429*(1), 81–93. https://doi.org/10.1016/S0022-0728(96)05019-X

Sazou, D., Kourouzidou, M., & Pavlidou, E. (2007). Potentiodynamic and potentiostatic deposition of polyaniline on stainless steel: Electrochemical and structural studies for a potential application to corrosion control. *Electrochimica Acta*, *52*(13), 4385–4397. https://doi.org/10.1016/j.electacta.2006.12.020

Scott J. C. (2010). *Nano-structured Conductive Polymers*. John Wiley & Sons, Ltd.

Shabani-Nooshabadi, M. (2015). Electrosynthesis of a polyaniline/zeolite nanocomposite coating on copper in a three-step process and the effect of current density on its corrosion protection performance. *RSC Advances*, *5*, 96601–96610.

Shabani-Nooshabadi, M., Allahyary, E., & Jafari, Y. (2018). Electrosynthesis of Poly(ortho-phenetidine) Coatings on Steel and Investigation of Their Corrosion Protection Properties. *Protection of Metals and Physical Chemistry of Surfaces*, *54*(1), 104–112. https://doi.org/10.1134/S2070205118010276

Shabani-Nooshabadi, M., Ghoreishi, S. M., Jafari, Y., & Kashanizadeh, N. (2014). Electrodeposition of polyaniline-montmorrilonite nanocomposite coatings on 316L stainless steel for corrosion prevention. *Journal of Polymer Research*, *21*(4), 416. https://doi.org/10.1007/s10965-014-0416-5

Shabani-Nooshabadi, M., & Karimian-Taheri, F. (2015). Electrosynthesis of a polyaniline/zeolite nanocomposite coating on copper in a three-step process and the effect of current density on its corrosion protection performance. *RSC Advances*, *5*(117), 96601–96610. https://doi.org/10.1039/C5RA14333K

Shabani-Nooshabadi, M., Mollahoseiny, M., & Jafari, Y. (2014). Electropolymerized coatings of polyaniline on copper by using the galvanostatic method and their corrosion protection performance in HCl medium: Electropolymerized coatings of polyaniline on copper. *Surface and Interface Analysis*, *46*(7), 472–479. https://doi.org/10.1002/sia.5539

Shah A. A. (2007). *Electrochemical Synthesis and Spectroelectrochemical Characterization of Conducting Copolymers of Aniline and o-Aminophenol* [Ph D Thesis]. A thesis submitted to Institute of Chemistry, Chemnitz University of Technology,.

Shirakawa, H., Louis, E. J., MacDiarmid, A. G., Chiang, C. K., & Heeger, A. J. (1977). Synthesis of electrically conducting organic polymers: Halogen derivatives of polyacetylene, (CH) x. *Journal of the Chemical Society, Chemical Communications*, *16*, 578. https://doi.org/10.1039/c39770000578

Smertenko, P. S., Dimitriev, O. P., Schrader, S., & Brehmer, L. (2004). Doping of polyaniline by transition metal salts: Current–voltage characteristics of the ITO/polymer film/metal heterostructures. *Synthetic Metals*, 10.

Stejskal, J., Sapurina, I., & Trchová, M. (2010). Polyaniline nanostructures and the role of aniline oligomers in their formation. *Progress in Polymer Science*, *35*(12), 1420–1481. https://doi.org/10.1016/j.progpolymsci.2010.07.006

Stiadi, Y., Rahmayeni, Rahmawati, L., Efdi, M., Aziz, H., & Emriadi. (2020). Mangifera odorata GRIFF SEED EXTRACT AS CORROSION INHIBITOR OF MILD STEEL IN HYDROCHLORIC ACID MEDIUM. *Rasayan Journal of Chemistry*, *13*(01), 230–239. https://doi.org/10.31788/RJC.2020.1315325

Subathira, A., & Meyyappan, R. M. (2011). *ANTICORROSION BEHAVIOR OF POLYANILINE/ POLYPYRROLE COMPOSITE COATINGS ON STAINLESS STEEL*. 10.

Sydulu Singu, B., Srinivasan, P., & Pabba, S. (2011). Benzoyl Peroxide Oxidation Route to Nano Form Polyaniline Salt Containing Dual Dopants for Pseudocapacitor. *Journal of The Electrochemical Society*, *159*(1), A6–A13. https://doi.org/10.1149/2.036201jes

Talo, A., Passiniemi, P., Forsén, O., & Yläsaari, S. (1997). Polyaniline/epoxy coatings with good anti-corrosion properties. *Synthetic Metals*, *85*(1–3), 1333–1334. https://doi.org/10.1016/S0379-6779(97)80258-5

Tanaka, K., Wang, S., & Yamabe, T. (1990). Will bipolarons be formed in heavily oxidized polyaniline? *Synthetic Metals*, *36*(1), 129–135. https://doi.org/10.1016/0379-6779(90)90241-C

Tüken, T., Özyılmaz, A. T., Yazıcı, B., & Erbil, M. (2004). Electrochemical synthesis of polyaniline on mild steel in acetonitrile–LiClO4 and corrosion performance. *Applied Surface Science*, *236*(1–4), 292–305. https://doi.org/10.1016/j.apsusc.2004.05.001

Uhlig, H. H., & Revie, R. W. (2008). *Corrosion and Corrosion Control: An Introduction to Corrosion Science and Engineering* (4th ed.). Wiley and Sons, Inc. Publication.

Umoren, S. A., Obot, I. B., & Obi-Egbedi, N. O. (2009). Raphia hookeri gum as a potential eco-friendly inhibitor for mild steel in sulfuric acid. *Journal of Materials Science*, *44*(1), 274–279. https://doi.org/10.1007/s10853-008-3045-8

Verma, C., Quraishi, M. A., Ebenso, E. E., & Bahadur, I. (2018). A Green and Sustainable Approach for Mild Steel Acidic Corrosion Inhibition Using Leaves Extract: Experimental and DFT Studies. *Journal of Bio- and Tribo-Corrosion*, *4*(33), 1–12. https://doi.org/10.1007/s40735-018-0150-3

Vivekanandan, J., Ponnusamy, V., Mahudeswaran, A., & Vijayanand, P. S. (2011). *Synthesis, characterization and conductivity study of polyaniline prepared by chemical oxidative and electrochemical methods*. 7.

Wan, M., & Li, J. (1998). Synthesis and electrical–magnetic properties of polyaniline composites. *Journal of Polymer Science Part A: Polymer Chemistry*, *36*(15), 2799–2805. https://doi.org/10.1002/(SICI)1099-0518(19981115)36:15<2799::AID-POLA17>3.0.CO;2-1

Wan, M., Li, M., Li, J., & Liu, Z. (1994). Structure and electrical properties of the oriented polyaniline films. *Journal of Applied Polymer Science*, *53*(2), 131–139. https://doi.org/10.1002/app.1994.070530201

Wang, M., Yun, H., Tan, K., Guo, A., Ling, J., Jiang, F., Shen, X., & Xu, Q. (2020). One-step electrochemical synthesis of poly(vinyl pyrrolidone) modified polyaniline coating on stainless steel for high corrosion protection performance. *Progress in Organic Coatings*, *149*, 105908. https://doi.org/10.1016/j.porgcoat.2020.105908

Wessling, B. (1994). Passivation of metals by coating with polyaniline: Corrosion potential shift and morphological changes. *Advanced Materials*, *6*(3), 226–228. https://doi.org/10.1002/adma.19940060309

Wessling, B., & Posdorfer, J. (1999). Corrosion prevention with an organic metal (polyaniline): Corrosion test results. *Electrochimica Acta*, *44*, 9.

Xu, X., Singh, A., Sun, Z., Ansari, K. R., & Lin, Y. (2017). Theoretical, thermodynamic and electrochemical analysis of biotin drug as an impending corrosion inhibitor for mild steel in 15% hydrochloric acid. *Royal Society Open Science*, *4*(12), 170933. https://doi.org/10.1098/rsos.170933

Xue, S., Ma, Y., Miao, Y., & Li, W. (2020). Anti-Corrosion Performance of Conductive Copolymers of Polyaniline/Polythiophene on a Stainless Steel Surface in Acidic Media. *International Journal of Nanoscience*, 1950023. https://doi.org/10.1142/S0219581X19500236

Yang, C. J., & Jenekhe, S. A. (1991). Conjugated aromatic poly(azomethines). 1. Characterization of structure, electronic spectra, and processing of thin films from soluble complexes. *Chemistry of Materials*, *3*(5), 878–887. https://doi.org/10.1021/cm00017a025

Yıldırım, A., & Çetin, M. (2008). Synthesis and evaluation of new long alkyl side chain acetamide, isoxazolidine and isoxazoline derivatives as corrosion inhibitors. *Corrosion Science*, *50*(1), 155–165. https://doi.org/10.1016/j.corsci.2007.06.015

Zhang, S. H., & Lyon, S. B. (1994). Anodic processes on iron covered by thin, dilute electrolyte layers (I)—Anodic polarisation. *Corrosion Science*, *36*(8), 1289–1307. https://doi.org/10.1016/0010-938X(94)90182-1

Zhu, A., Wang, H., Sun, S., & Zhang, C. (2018). The synthesis and antistatic, anticorrosive properties of polyaniline composite coating. *Progress in Organic Coatings*, *122*, 270–279. https://doi.org/10.1016/j.porgcoat.2018.06.004

Zor, S., & Yakar, E. (2007). Corrosion behavior of PANI coated aluminum in oxalic acid containing different anions. *Bulletin of Electrochemistry*, 5.

APPENDIX
List of Articles

1. **DK Gupta**, S Neupane, S Singh, N Karki, AP Yadav, <u>Dataset for the selection of electrolytes for Electropolymerization of aniline</u>, Data in Brief 35, 106875, **2021**. https://doi.org/10.1016/j.dib.2021.106875

   Data in brief is Q4 Journal which is indexed and abstracted in PubMed Central, PubMed/Medline, Scopus, Emerging Sources Citation Index (ESCI), Directory of Open Access Journals (DOAJ).

2. **DK Gupta**, S Neupane, S Singh, N Karki, AP Yadav, <u>The effect of electrolytes on the coating of polyaniline on mild steel by electrochemical methods and its corrosion behavior</u>, Progress in Organic Coatings 152, 106127, **2021**. **DOI:** 10.1016/j.porgcoat.2020.106127

   Progress in organic coating is Q1 journal which is indexed and abstracted in Science Citation Index, Cambridge Scientific Abstracts, Chemical Abstracts, Current Contents, Engineering Index, Metals Abstracts, Pascal Francis, Physikalische Berichte, World Surface Coatings Abstracts, Research Alert, Applied Polymers Literature, Scopus, INSPEC.

3. **DK Gupta**, S Neupane, S Singh, A P Yadav, <u>Galvanostatic Optimization of Polyaniline Coating on Mild Steel in Tartrate Medium for Corrosion Protection</u>, **Submitted to Indian Journal of Chemical Technology (Accepted) SJR Q3.**
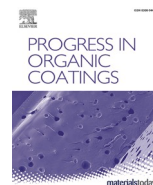
The effect of electrolytes on the coating of polyaniline on mild steel by electrochemical methods and its corrosion behavior

Dipak Kumar Gupta [a,b], Shova Neupane [a,1,**], Sanjay Singh [a], Nabin Karki [c], Amar Prasad Yadav [a,2,*]

[a] *Central Department of Chemistry, Tribhuvan University, Kirtipur, Kathmandu, Nepal*
[b] *Tri-Chandra Multiple Campus, Tribhuvan University, Ghantaghar, Kathmandu, Nepal*
[c] *Bhaktapur Multiple Campus, Tribhuvan University, Bhaktpur, Nepal*

ARTICLE INFO

ABSTRACT

Polyaniline (PANI) is extensively researched as a corrosion protection coating for mild steel (MS) against acidic and neutral media. Corrosion inhibition performance of PANI coating on MS depends on the electrolytic solution employed for polymerization. In this study, the electropolymerization of aniline onto MS using sodium potassium tartrate (Na-K tartrate) and benzoic acid in the alcohol-water (BAW) medium is reported. The composition of BAW system was optimized and used for electropolymerization of aniline for the first time. The results showed the formation of a passive yet electro-conductive layer before the polymerization initiated. A compact layer with a fine structured PANI coating in both media was obtained. Cyclic voltammetry (CV) produced a stable PANI coating without showing anodic current in the cathodic scan. The concentration of aniline and electrolytes were optimized for better coating conditions. The prepared PANI coating was characterized by Fourier-transform infrared (FTIR) spectroscopy, Ultraviolet-visible (UV–vis) spectroscopy, Scanning electron microscope (SEM) in combination with energy dispersion spectrometer (EDX) and X-ray diffractometer (XRD). The results of PANI coating in Na-K tartrate and BAW medium are compared with a standard PANI coating prepared in oxalic acid medium. The inhibition efficiencies of PANI coating obtained in Na-K tartrate and BAW were estimated to be 82.5 % and 99.99 %, respectively in 0.1 M NaCl solution.

1. Introduction

Electropolymerization is a powerful technique for thin-film formulation and surface modifications for desired applications. Conducting polymers have been extensively studied for corrosion protection purposes due to its superior barrier effect and inhibiting properties of polar groups [1–4]. A conducting polymer coating lowers the kinetics of corrosion of the underlying metal by shifting the open circuit potential (OCP) to a noble value. With this advantage, together with environmental regulations, recent trends have been to abandon phosphatization and chromatation conversion coating for conducting polymer coating [2,3]. However, this demands the optimization of electrochemical polymerization conditions to obtain a pore-free and adhesive coating with similar or even superior properties. Electropolymerization should be adopted in an aqueous medium as organic solvents are environmental hazards.

Polyaniline (PANI), a well-known conducting polymer, has been electrochemically synthesized in aqueous acidic and neutral media onto active metals (Fe, Zn, Cu, Al, Ni) [1,5–10]. In general, a good PANI coating is achieved in an acidic media with low pH [2]. However, if the substrate is an active metal, the electropolymerization of aniline becomes a challenge as the dissolution of metal precedes oxidation of aniline [2,3]. These issues can be overcome by finding electrochemical conditions that can lower the metal dissolution rate by forming a partial passivation layer at a potential lower than the potential of aniline monomer. Under such conditions, the role of electrolytes on

---

electropolymerization has prime importance. It should only partially passivate the metal surface and allow the passage of charge so that oxidation and subsequent polymerization of aniline can be achieved on the passivated metal surface. The polymerization of aniline initiates by the formation of a radical cation by the oxidation of aniline. Then, the oxidized aniline followed the formation of a di-cationic dimer due to the head-to-tail coupling of the radical cation [11–14]. Further, chain propagation results in polymerization, and doping of polymer by anions takes place [13]. Therefore, polymerization of aniline and PANI coating quality is influenced by the anionic nature of the electrolyte (dopant) [15].

The weak adhesion of PANI coating on active metal substrates is, however, the major obscurity. A PANI coating using mineral acid electrolytes has been reported to produce a weak adhesion onto the MS surface, hence low corrosion inhibition [16]. However, PANI formation using oxalic acid as an electrolyte produced an adhesive and functional anti-corrosion coating [2,17]. It is reported that the electropolymerization of aniline on MS surface can be achieved by various electrochemical methods employing different electrolytic solutions such as oxalic acid ($C_2H_2O_4.2H_2O$) [2], sodium benzoate (C_6H_5COONa) [18], sodium salicylate ($C_7H_5NaO_3$) [19], perchloric acid ($HClO_4$) [20], phosphoric acid (H_3PO_4) [21], sodium oxalate ($Na_2C_2O_4$) [7], benzene sulphonic acid ($C_6H_6O_3S$) [22], p-toluene sulfonic acid ($C_7H_8O_3S$) [22], acetonitrile (C_2H_3N)–lithium perchlorate ($LiClO_4$) [23], etc. with suitable mechanical and anti-corrosion properties.

Galvanostatic polymerizations of aniline on MS in oxalic acid, tosylic acid ($C_7H_8O_3S$), and neutral solution of lithium perchloric acid ($LiClO_4$) have been successfully achieved by Camlet et al. [2,24,25]. Also, Fenelon and Breslin et al. found that PANI coating obtained from aqueous oxalic acid solution showed a significant corrosion protection to MS in acidic solution but inadequate corrosion protection in acidic solutions containing acetate and borate anions in acidic solutions [26]. However, in an alkaline borate solution, these coatings showed an apparent beneficial effect on the local breakdown of the iron by chloride anions [18]. Recently, sodium benzoate (C_6H_5COONa) has been reported to produce optimized PANI coatings on MS with a small dissolution of iron for the formation of passive layer, unlike in oxalic acid solution [18,27]. It showed a remarkable corrosion protection behavior in 0.1 M H_2SO_4 and 0.5 M NaCl solutions studied by spectrophotometric, EIS, and polarization methods [18].

In this paper, we focus on continuing attempts to improve the PANI coatings on the MS surface for better anti-corrosion and mechanical properties. The attempts have been to obtain a compact and adhesive PANI coating by using electrolytes that limit the Fe-dissolution. The sodium-potassium tartrate ($NaKC_4H_4O_6.4H_2O$), and benzoic acid (C_6H_5COOH) in alcohol-water were used as electrolytes for electropolymerization of aniline onto MS surface. The electrolytes named Na-K tartrate and BAW for the sodium-potassium tartrate ($KNaC_4H_4O_6.4H_2O$) and benzoic acid (C_6H_5COOH) in alcohol-water, respectively in this paper. An optimized composition of BAW system for the electropolymerization of aniline is reported for the first time. The PANI formation parameters, such as concentration of aniline, the concentration of electrolyte, and potential range, were investigated. Fourier-transform infrared spectroscopy (FTIR), Ultraviolet-visible spectroscopy (UV–vis), Scanning electron microscope (SEM) in combination with energy dispersion spectrometer (EDX), and X-ray diffractometer (XRD) were used to characterize the PANI coatings. Corrosion protection behaviors of the coatings were studied in 0.1 M NaCl by polarization method.

2. Experimental

2.1. Materials

Commercial grade MS, purchased from Nepal's local market, was cut into the pieces of 3 cm × 3 cm x 0.15 cm. The sample was then abraded by silicon carbide (SiC) paper of different grades from #100 to #2000

until the working surface turned smooth. Finally, the sample was ultrasonicated in ethanol for 10 min, and dried with compressed air before each measurement.

Aniline ($C_6H_5NH_2$) and ethanol (C_2H_5OH) were acquired from Fisher Scientific, India, sodium orthophosphate ($Na_3PO_4.12H_2O$), succinic acid ($C_4H_6O_4$), sulphanilic acid ($C_6H_7NO_3S$), sodium potassium tartrate ($KNaC_4H_4O_6.4H_2O$), Acetone (C_3H_6O), Dimethyl sulphoxide (DMSO) and benzoic acid (C_6H_5COOH) were procured from Merck, India. Aniline was double distilled in the presence of nitrogen gas before use. Other chemicals mentioned in this work were used without further purification. Solutions of the required concentrations were prepared in double-distilled water.

2.2. Electropolymerization of aniline

Abraded MS samples were subjected to electrochemical polarization using a Hokuto Denko HA-151 potentiostat controlled by a self-made LabVIEW software interfaced with an IBM computer [28]. Polarization was done in a 3-electrode system using MS sample as a working electrode, a saturated calomel electrode (SCE) as a reference electrode, and a graphite rod as a counter electrode. Open circuit potential (OCP) was recorded for 30 min before each anodic polarization to get a steady-state condition. Then, anodic polarization was carried out in sodium orthophosphate, succinic acid, sulphanilic acid, Na-K Tartrate, BAW, and oxalic acid solutions. The concentration of aniline as monomer was varied from 0.1 M to 0.4 M. Similarly, cyclic voltammetry (CV) was also carried out for electropolymerization of aniline on MS sample to check the cathodic stability of the coating. The results were compared with PANI coating obtained on MS in oxalic acid medium.

2.3. Characterization of PANI coating

A Perkin Elmer Spectrum GX FTIR was used to obtain infrared emission spectra with wavenumber ranges from 500 to 4000 cm^{-1}. The PANI coating on the MS sample was dissolved by adding a few drops of pure acetone on it. The dissolved PANI coating was further dispersed in pure acetone by ultrasonication for 10 min, and FTIR characterization was performed.

Shimazdu UV/VIS 2600 Spectrophotometer was used to record UV–vis spectra of the PANI coatings. The scanning range for the measurement was 200−800 nm at a medium scanning rate and resolution of 1.0 nm. The baseline correction of the spectrophotometer was carried out using pure acetone as a blank. All the samples were loaded into a 2.0 mL quartz cuvette with a 1.0 cm path length for sampling. PANI was taken out in pure acetone by following the procedure adopted for FTIR measurement. Here, the dispersed PANI was diluted 10 times with pure acetone to obey Lambert-Beer's law.

The crystalline structure of PANI was studied by using an EMPYREAN diffractometer. A few drops of DMSO were added to the PANI coating to detach it from the MS surface. Then, the solution of PANI in DMSO was spread over a glass plate grid, dried at room temperature (RT), and XRD was performed on it. The data was recorded using a monochromatic Cu Kα of wavelength 1.5406 Å at an accelerating voltage of 40 kV with a current of 30 mA. The working conditions were 2θ scanning between 5° to 60° at a step size of 0.013°. Surface morphology and elemental composition of the PANI coating film were ascertained by SEM and EDX analysis using a JEM-1200EX electron microscope (JEOL, Tokyo, Japan).

2.4. Corrosion test by potentiodynamic polarization

A corrosion test was performed in 0.1 M NaCl solution at room temperature by potentiodynamic polarization. Open circuit potential (OCP) was allowed to stabilize for 30 min before each potentiodynamic polarization. The polarization curves were obtained by scanning potential ±300 mV from the OCP at the 1 mV/sec scan rate. From the
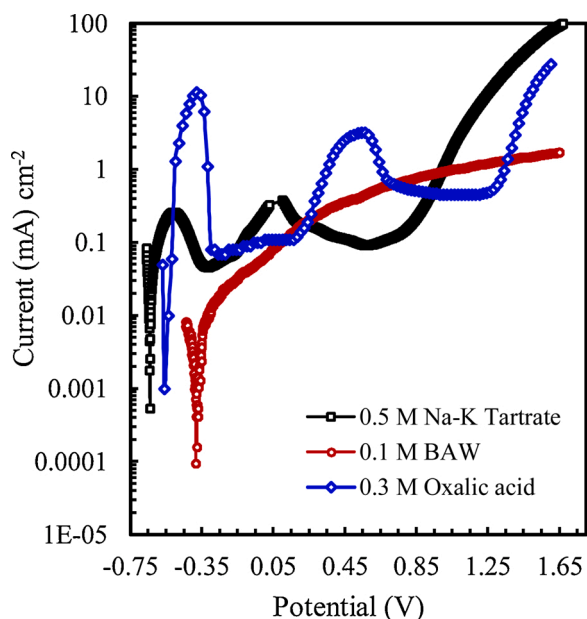
Fig. 1. Anodic Polarization of MS surface in 0.5 M Na-K Tartrate, 0.1 M BAW, and 0.3 M oxalic acid solution.

polarization curves, the corrosion current (I_{corr}), and corrosion potential (E_{corr}) were determined from the Tafel extrapolation method, and corrosion inhibition efficiency (*IE*) was calculated by the following relation [29]:

$$IE\% = \frac{\text{Icorr(Bare MS)} - \text{Icorr(PANI coated MS)}}{\text{Icorr(Bare MS)}} \times 100 \qquad (1)$$

3. Results and discussions

3.1. Effect of electrolytes on the polarization behavior of MS sample

For electropolymerization of aniline onto the MS surface, the surface should be passivated with an electro-conductive composition. In this work, the polarization of MS was performed using electrolytes such as succinic acid, sulphanilic acid, sodium orthophosphate, Na-K Tartrate, and BAW solutions. In the case of sulphanilic acid, succinic acid, and sodium orthophosphate solutions, a stable passive film was achieved until 2.0 V. Therefore, these films could only be helpful for corrosion inhibition but not for aniline oxidation; hence, no further investigation performed. The obtained polarization curves are presented in a supplementary material **S1**.

The passivation of the MS surface is necessary but not a sufficient condition for polymerization. The effects of Na-K tartrate and BAW on passivation, together with the curve obtained in oxalic acid on the MS sample, are depicted in Fig. 1. The polarization curve in Na-K Tartrate shows a similar polarization behavior to the oxalic acid medium. The OCP in 0.5 M Na-K Tartrate solution is -0.640 V, and the active dissolution of MS occurs up to the potential of -0.52 V, indicated by the rise of current. At the potentials positive than -0.52 V, passivation of the MS surface takes place due to the formation of the Fe-tartrate passive layer. The rise of the current between -0.36 V and +0.013 V is due to the thickening of the passive layer. This leakage of the charge represents the electrical activation of the Fe-tartrate layer. Therefore, electropolymerization of aniline could take place under such conditions. The dissolution of the passive layer occurred at the potential more positive than +0.013 V. The visual observation of the surface showed the formation of a white layer on the MS surface. Finally, a breakdown potential appears at +0.7 V. However; this potential is lower as compared to +1.2 V in oxalic acid [21].

In the case of polarization using benzoic acid, it is to be mentioned that benzoic acid is insoluble in water but soluble in alcohol. However, the benzoic acid-alcohol solution is not conducting. For having sufficient conductivity, alcohol-water in the 3:1 ratio was chosen after examining
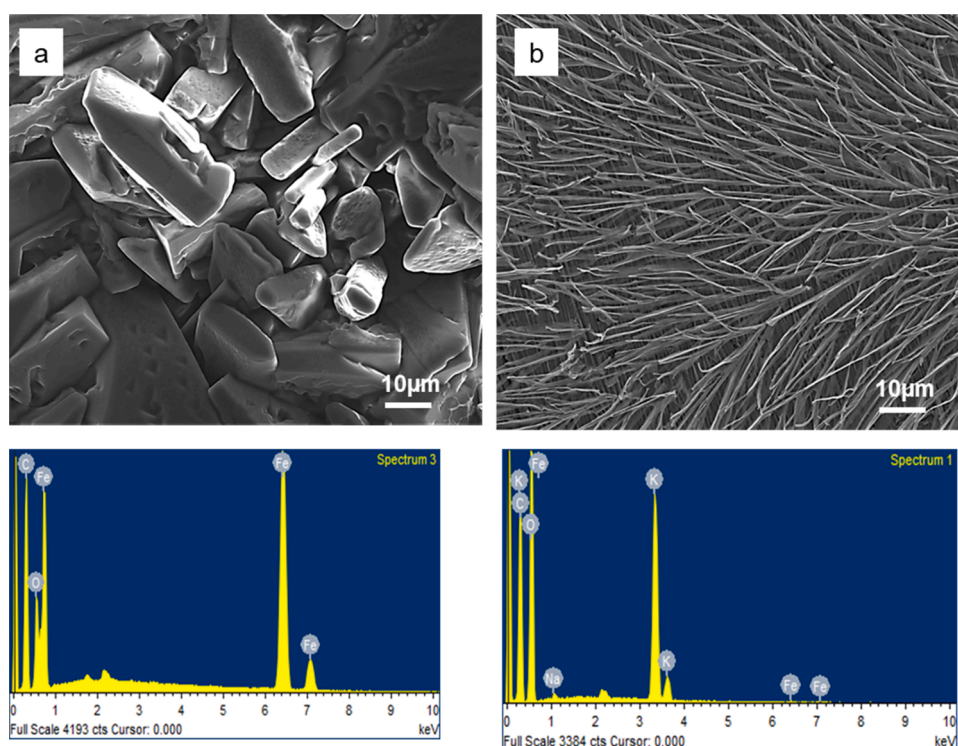

Fig. 2. SEM images of MS sample anodically polarized in (a) 0.5 M Na-K Tartrate (b) 0.1 M BAW with their corresponding EDX elemental analysis.
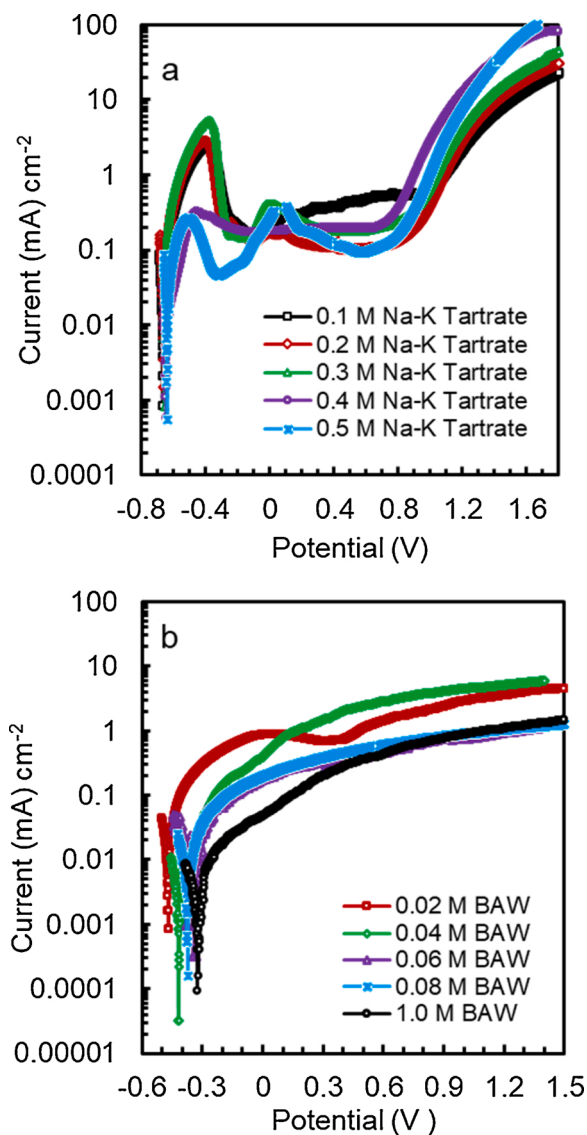
Fig. 3. Anodic polarization of MS in various concentrations of (a) Na-K Tartrate solutions, and (b) BAW at a scan rate of 1 mV/s.
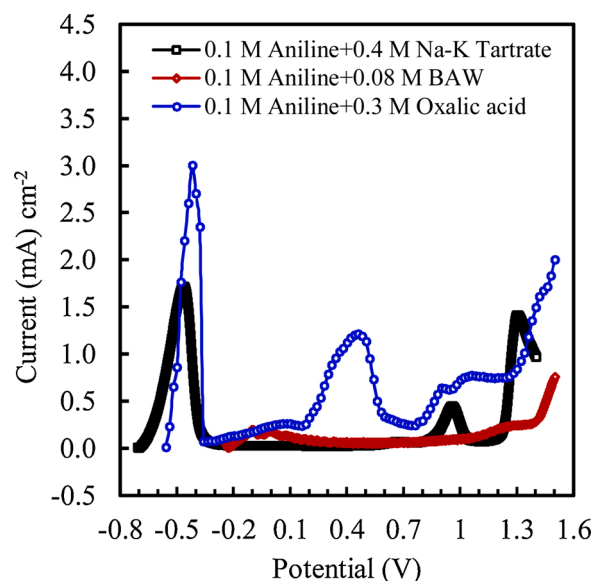

Fig. 4. Anodic Polarization of MS in 0.4 M Na-K Tartrate, 0.08 M BAW, and 0.3 M oxalic acid solutions containing 0.1 M aniline in each at a scan rate of 1.0 mV/s.

several combinations. In a 3:1 alcohol-water solution, 0.1 M benzoic acid solution was prepared after deliberation so that on further dilution, no precipitation of benzoic acid took place. An increase in water amount or benzoic acid or a decrease in alcohol amount led to the precipitation of benzoic acid. The polarization curve of the MS in 0.1 M benzoic acid in the 3:1 alcohol-water (BAW) system is presented in Fig. 1. It does not show a distinct active-passive region like in the case of Na-K Tartrate and oxalic acid solutions but the current increases steadily with potential.

The OCP is significantly shifted to the noble value at -0.38 V as compared to Na-K tartrate and oxalic acid solutions. The noble shift of OCP is attributed to the formation of the Fe-benzoate layer. This layer was probably formed during 30 min immersion at OCP. Indeed, the Fe-benzoate layer limits the dissolution of MS by its barrier effect [18]. As the potential shifts in a positive direction, the current increased gradually. The rise of the current between -0.3 V and -0.15 V represents the thickening of the passive layer. It indicates that the passive layer is electrically active, and there is leakage of charge from the Fe-benzoate layer, which can be used in the aniline oxidation. The shoulder between the potential of -0.15 V and +0.09 V is attributed to the dissolution of the passive layer. Oxygen evolution is observed after +1.1 V.

The supplementary S2 compares the OCP variation of MS in all the electrolytes used for passivation of MS in this study.

The SEM image of the MS surface anodically polarized in a 0.5 M aqueous Na-K tartrate solution is shown in Fig. 2a and a corresponding EDX spectrum. C, N, O, Na, K, and Fe are distinct in EDX, which confirmed the formation of the Fe-tartrate layer on the MS surface. The passive layer was composed of a thick and polygons shape granular particles of Fe-tartrate covering the MS surface.

Similarly, SEM image of the MS sample anodically polarized in 0.1 M BAW is shown in Fig. 2b. A thin dendritic layer due to the formation of Fe-benzoate (supported by the EDX result) indicates C, O, and Fe elements. The SEM image of the MS sample polarized in 0.3 M oxalic acid solution is shown in supplementary **S3** for comparison. Next, the effect of a passive layer on the oxidation and polymerization of aniline is studied at the optimized composition of monomer and electrolytes.

3.2. Optimization of the concentration of electrolyte

The electrolyte concentration also affects the nature of surface passivation; therefore, its concentration has to be optimized. Also, the optimization of concentration is essential from an economic point of view as it saves excess use of chemicals. Fig. 3a–b shows the anodic polarization of MS in 0.1 M to 0.5 M Na-K-Tartrate and 0.1 M to 0.02 M BAW solutions. The general features of the polarization curves in both electrolytes are similar to Fig. 1. There is a marginal shift of OCP towards positive values with increased concentration in both the solutions. In the case of Na-K Tartrate, the peak current for dissolution of Fe decreases, and passivation accomplishes swiftly with an increase in concentration. Similarly, in the case of BAW in Fig. 3(b), a positive shift of OCP and lowering of passivation current with the concentration is observed.

From the polarization curves, 0.4 M Na-K tartrate and 0.08 M BAW were chosen as the optimum concentrations for polymerization of aniline.

3.3. Electropolymerization of aniline

After optimizing the concentration of both electrolytes, electropolymerization of aniline onto MS sample was carried out using a 0.1 M aqueous solution of aniline in 0.4 M Na-K tartrate and 0.08 M BAW
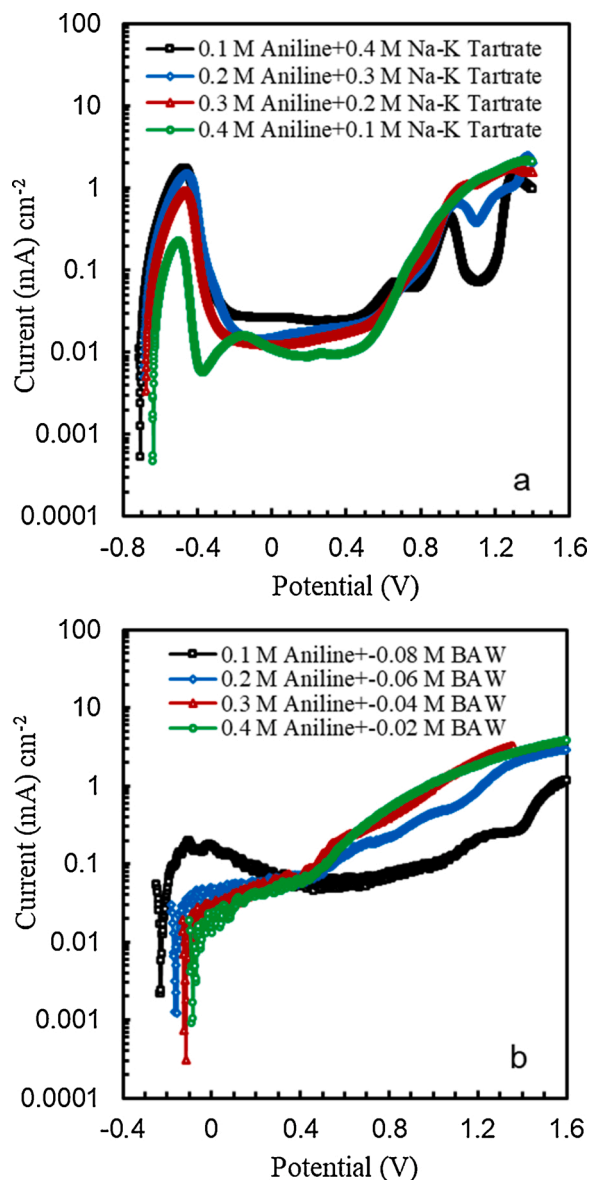
Fig. 5. Anodic polarization of MS in different concentration of aniline in **(a)** varying concentrations of Na-K Tartrate, and **5(b)** varying concentrations of BAW solutions. The scan rate was 1 mV/s, and polarization was started after remained at OCP for 30 min.

solutions. Fig. 4 shows the polymerization curves of aniline in 0.4 M Na-K tartrate, 0.08 M BAW, and 0.3 M oxalic acid. Na-K Tartrate and oxalic acid show similar polarization behaviors. The dissolution of Fe takes place near the OCP, followed by passivation at -0.47 V, as indicated by declining current in Na-K Tartrate. The current suddenly dropped off, causing passivation due to the formation of Fe-tartrate. On further increasing the potential, oxidation and subsequent polymerization of aniline takes place in a wide potential range of +0.40 V to +1.4 V. The current hump, shoulder, and plateau regions in between the above potential range are indicative of the formation of various forms of PANI. The oxidation of aniline starts at +0.40 V indicated by a sharp rise in the current. At potential +0.66 V, the current begins to decline. This peak corresponds to the conversion of leucoemeraldine to emeraldine [11, 12]. The current again rises at +0.8 V due to the conversion of emeraldine to pernigraniline with a pronounced peak at +0.97 V and, oxygen evolution is observed after +1.1 V. The conversion of leucoemeraldine to emeraldine, emeraldine to pernigraniline, green-colored PANI, and blue-green emeraldine salt are observed at +0.43 V, +0.506 V, +1.4 V, and +1.6 V, respectively [9,11,24,30,31].

In the case of BAW, the Fe-dissolution current is low, probably due to the formation of Fe- benzoate layer at OCP. After the initial decline of current from -0.14 V till +0.37 V, the current rises steadily with humps and shoulder formation till +1.37 V. As mentioned above, the formation of different forms of PANI also takes place in this potential range. The visual observations showed the formation of a brown colored coating on the MS surface in both cases. The features of polarization curves displaying oxidation and polymerization of aniline are not present in Figs. 1 and 3 due to the absence of aniline. The compositions of aniline with Na-K Tartrate and BAW are optimized after confirming the polymerization of aniline in these solutions.

3.4. Optimizing the concentration for polymerization of aniline

Anodic polarization was carried out in various concentrations of Na-K tartrate and BAW solutions containing different amounts of aniline to optimize the concentrations of electrolyte and aniline. Fig. 5(a) shows the polarization curves of MS in Na-K Tartrate and aniline concentrations. The concentrations of both varied from 0.1 M to 0.4 M. Polarization behavior is similar to that in Fig. 4 where dissolution, passivation, and polymerization takes place with potential. As the concentration of aniline increases, the OCP shifts slightly to a positive direction, and passivation occurs rapidly. From the results, a concentration of 0.3 M aniline in 0.2 M Na-K Tartrate is chosen as the best composition due to better passivation and polymerization behaviors. The visual observation showed a non-adhesive PANI layer formation at 0.4 M aniline concentration, also confirmed by the scotch-tape method. SEM image of the obtained PANI coating in 0.3 M aniline and 0.2 M Na-K Tartrate is shown in Fig. 6(a). It indicates a compact worm-like layer in the nanometer dimension, which was visible only at high magnification. The EDX result showing the presence of N and C supports the formation of PANI.

The effect of aniline concentration and BAW on polymerization is presented in Fig. 5(b). The concentration of aniline is varied from 0.1 M to 0.4 M, while the concentration of benzoic acid varied from 0.08 M to 0.02 M in 3:1 ethanol-water system. In 0.1 M aniline and 0.08 M benzoic acid, slight dissolution of iron is observed, and an increase in the concentration of aniline suppresses the dissolution of Fe. This phenomenon is also observed in the Na-K Tartrate solution (Fig. 5a). This indicates the effect of monomer concentration on dissolution and passivation of MS at OCP, which needs to be investigated further. The OCP shifts to a positive value with an increase in the concentration of aniline, and a better PANI coating was obtained at a lower potential (less positive) compared to Na-K tartrate solution. This is possibly due to the formation of Fe-benzoate layer [18], which limits the Fe-dissolution, and the available charge is used for aniline oxidation. From Fig. 5(b), 0.3 M aniline in 0.04 M BAW is chosen as the best composition because the higher concentration of both resulted in the non-adhesive coating as confirmed by visual
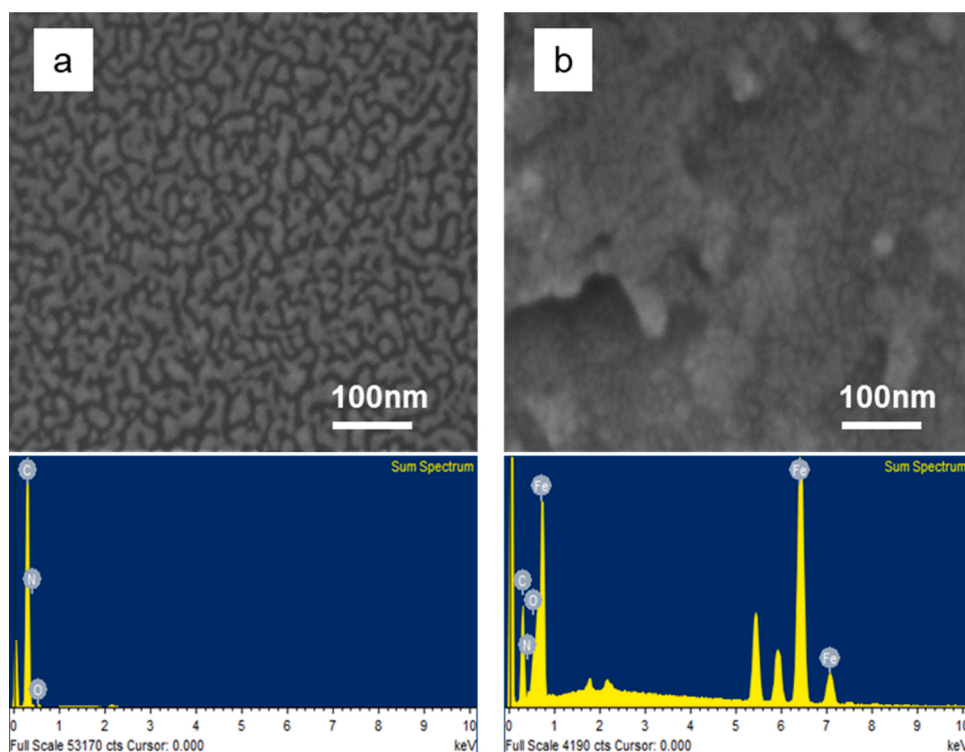
Fig. 6. (a) SEM image of PANI coating from 0.3 M aniline in 0.2 M Na-K Tartrate in anodic polarization and its EDX, **(b)** SEM image of PANI coating from 0.3 M aniline in 0.04 M BAW in anodic polarization and its EDX.

observation scotch-tape adhesion test. Fig. 6b shows a high magnification SEM image of PANI coating obtained in 0.3 M aniline and 0.04 M benzoic acid. The formation of compact and fine grains in the range of 10 nm is observed on the surface, further confirmed by the EDX mapping.

SEM micrograph of PANI deposited on MS sample from aqueous oxalic acid solution shows a more massive grain structure having a diameter of 100−200 nm (shown in supplementary **S4**).
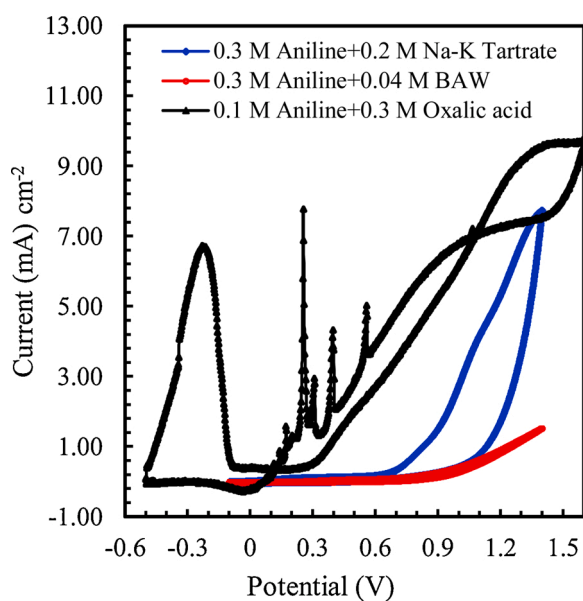

Fig. 7. PANI coating on MS obtained by cyclic voltammetry in 0.3 M aniline+0.2 M Na-K Tartrate, 0.3 M aniline+0.04 M W BA, and 0.1 M aniline+0.3 M Oxalic acid solutions.

In summary, the PANI formed in Na-K Tartrate and BAW electrolyte is a pore-free, compact, and fine-grained. BAW solution limited the dissolution of Fe near the OCP. Therefore, it will be subjected to corrosion protection testing of MS samples in various media, which is a part of the ongoing study.

3.5. Deposition of PANI by CV

PANI formation and its stability in the acidic medium have been the subject of many researches [9,20,21,32]. The PANI coating formed during CV showed an anodic dissolution peak at +0.3 V vs SCE in the cathodic scan, Fig. 7. Anodic dissolution peak in cathodic scan resulted from the breakdown of the PANI coating and iron-oxalate layer formed in the previous anodic scan. Therefore, the dissolution of Fe took place from the MS surface during the cathodic scan. Such behavior has been found to disappear after several cycles of CV. However, such behavior points to stability issues of PANI coating in oxalic acid medium [2]. Fig. 7 shows the cyclic volatmmograms of MS in solutions containing 0.3 M aniline in 0.2 M Na-K Tartrate and 0.04 M BAW solutions. Unlike in oxalic acid solution, a stable voltammogram with no anodic peak during cathodic scan is obtained in both cases. The polymerization occurs in various steps, as discussed in section 3.4, Fig. 5, and lower current values in Na-K Tartrate and BAW solutions reflect the better coating compared to oxalic acid. The results reveal that both Na-K Tartrate and BAW offer better alternatives for polymerization of aniline onto MS surface with improved surface morphologies and cyclic stabilities.

3.6. Characterization of PANI coating

3.6.1. FTIR- spectra

ATR-FTIR measurements were performed on both the PANI coatings after taking out the coating with acetone. Fig. 8 shows the FTIR spectra of PANI obtained from Na-K tartrate and BAW solutions. The band at
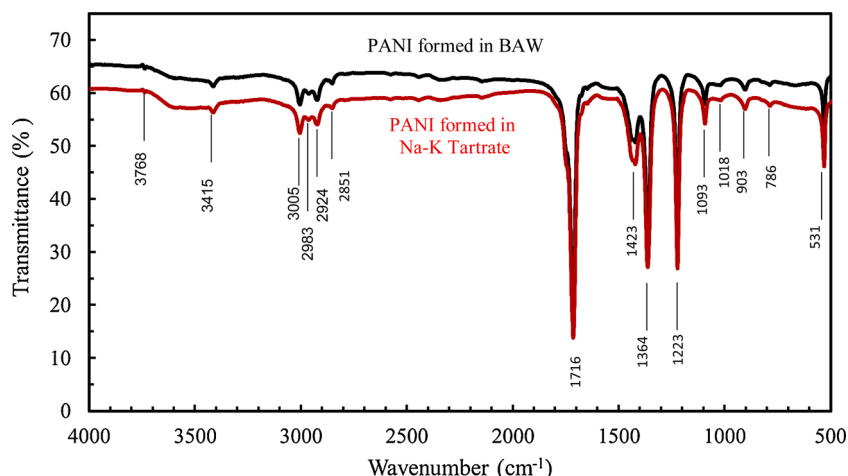
Fig. 8. FTIR spectra of PANI prepared from aniline in Na-K Tartrate and BAW solutions.

3415 cm^{-1} is assigned to the N—H stretching vibrations of amine groups. The band near 3005 cm^{-1}is attributed to the NH— bond between amine and imine sites, and 2924 cm^{-1} is due to the aliphatic C–H stretching of acetone. The obtained signals are distinguished between benzenoid rings and quinoid rings from the bands in the range of $1350–1960$ cm^{-1} region of the spectrum. Intensive bands close to 1716 cm^{-1} corresponds to CO= of acetone, and the one near 1423 cm^{-1} and 1364 cm^{-1} corresponds to the semi quinoid - N -ring mode of oxidized polyaniline. The 1223 cm^{-1} band corresponds to C—N vibration [17, 33–35]. The band intensity at 1423 cm^{-1} is stronger (benzenoid form) than that at 1560 cm-1(quinoid form) since PANI contains semiquinoid –N- ring and more potent benzenoid form, makes emeraldine salt. The band at 1093 cm^{-1} was related to N = Q=N, and 531 cm^{-1} is related to the C-N-C bonding mode of the aromatic ring [34,36].

3.6.2. UV–vis spectra

A sharp peak and a shoulder of PANI are observed in a UV–vis spectrum presented in Fig. 9. The PANI prepared in BAW shows a sharp peak at 325 nm due to the $\pi\to \pi$ * transition in the aromatic (benzoid)

ring [37]. A shoulder at 430 nm is characteristic of polyaniline oxidized to an oxidation state slightly lower than emeraldine, and another shoulder at 560 nm is due to the transition of benzenoid rings into quinoid rings (π–polaron transition) [38]. Similarly, PANI prepared in Na-K tartrate also shows an energetic broadband at 354 nm, which corresponds to the $\pi\to \pi$ * transition in the benzoid ring, and a weak band (shoulder) at 520 nm is due to the transition of benzenoid rings into quinoid rings (π–polaron transition) [38,39].

3.6.3. X-ray diffraction

X-ray diffraction was used to study the effect of electrolytes on the crystallinity of the PANI coating. XRD patterns of PANI in Na-K Tartrate and BAW solutions are shown in Fig. 10. A broad diffraction peak in the range of 10–30, 2θ values reflects diffraction from the parallel and perpendicular periodicity of the PANI chain [36]. The diffractions at $2\theta = 22.82°$ (PANI from Na-K Tartrate) and $2\theta = 29.7°$ (PANI from BAW) show the Bragg's reflection occurring from (020) and (200) Millar planes, respectively [40–42]. Bare MS shows an iron peak at 44° 2θ. As compared to the peak at 22.82° (Na-K Tartrate), the peak at 29.7° (BAW)
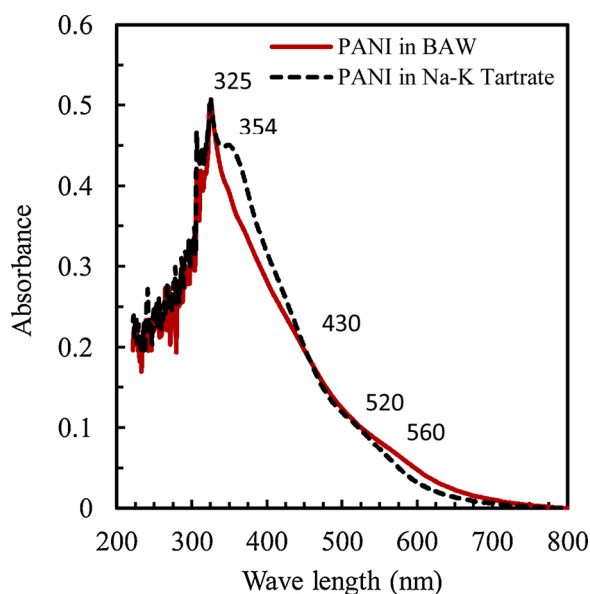

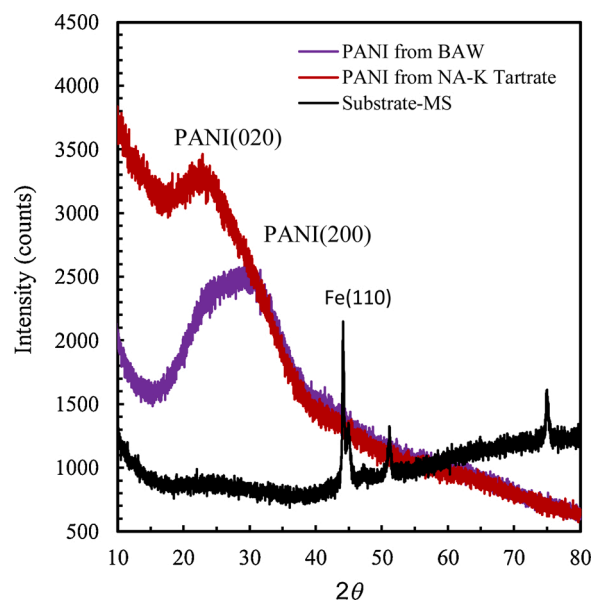**Fig. 9.** UV–vis spectra of PANI prepared from aniline in Na-K Tartrate and BAW.

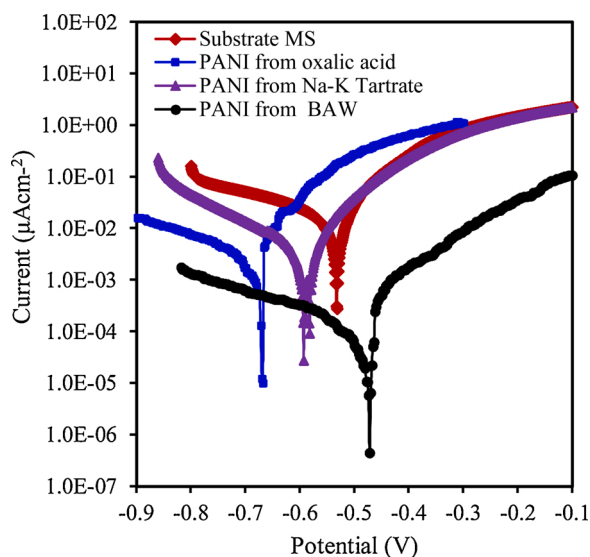**Fig. 10.** XRD spectra of PANI prepared from aniline in Na-K Tartrate, BAW, and bare mild steel.

Fig. 11. Tafel plot showing corrosion protection in 0.1 M NaCl.

this change in OCP value is less than 85 mV, PANI coating obtained in Na-K Tartrate acts as a mixed type inhibitor of corrosion [50].

The anodic Tafel slope (βa) and cathodic Tafel slope (β_c) are typical of such coatings on MS in aqueous saline media and in acidic media [19, 51,52]. The corrosion protection by PANI coating has been reported to be due to inhibitory action of the functional group C꞊N which can be adsorbed on the metal surface [53]. Soluble PANI can absorb on the metal surface and suppress the anodic and cathodic reaction [53]. The anodic reaction is the dissolution of iron, while the cathodic reaction is the reduction of oxygen on PANI coating in the above medium [54]:

Anodic: $Fe \rightarrow Fe^{2+} + 2e$

Cathodic: $H_2O + \frac{1}{2} O_2 + 2e \rightarrow 2OH^-$

4. Conclusions

In this study, electropolymerization of aniline onto MS sample using Na-K Tartrate and BAW as two new supporting electrolytes is reported. The coating of PANI on MS is greatly affected by the concentration of

Table 1
Electrochemical polarization parameters for PANI coated MS in 0.1 M NaCl.

Sample	βa (V/decade)	β c (V/decade)	I corr (µA/cm2)	E corr (V vs SCE)	Corrosion Rate (mm/year)	Inhibition Efficiency (%)
Bare MS	0.108	−0.254	20.04	−0.537	0.0294	
PANI/oxalic acid	0.086	−0.196	2.760	−0.674	0.0057	86.72
PANI/Na-K Tartrate	0.083	−0.164	3.500	−0.594	0.0017	82.50
PANI/ BAW	0.078	−0.246	0.012	−0.492	0.00043	99.99

is broader. The crystallite size of PANI prepared in BAW is smaller than that of Na-K tartrate. A similar observation is made from SEM images (Fig. 6(a) and (b)). Moreover, the peaks diffracted at an angle of 22.82 and 29.7 with d-spacing 3.89 Å and 2.89 Å, respectively, show low crystallinity of the PANI due to the repetition of benzoid and quinoid rings in the PANI chains [16,36,43–46].

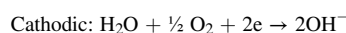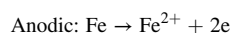### 3.7. Corrosion inhibition efficiency

Fig. 11 shows the potentiodynamic polarization curves of both the coating in 0.1 M NaCl solution. For comparison, polarization curves of bare MS and PANI coating in the presence of oxalic acid as electrolyte are also shown together. Corrosion current density (I_{corr}), corrosion potential (E_{corr}), anodic slopes, cathodic slopes, and corrosion inhibition efficiency were obtained from the polarization curves and presented in Table 1.

The coating of MS by PANI has lowered Icorr by one to two orders of magnitude, reflecting better corrosion protection. I_{corr} is much lowered in PANI coating obtained in BAW, while PANI coating obtained in Na-K Tartrate shows almost similar I_{corr} to that obtained in oxalic acid. The polarization curves show a significant reduction in cathodic current density in both cases. However, in PANI coating obtained in BAW, the anodic current density is also suppressed appreciably and the corrosion inhibition efficiency is estimated at 99.99 % compared to 82.50 % inhibition efficiency showed by PANI coating obtained in Na-K Tartrate. Such a high inhibition efficiency has been reported in epoxy-based multi-layer coatings [47].

The OCP of PANI coating obtained in BAW shifted significantly to a positive (anodic) direction suggesting the formation of an efficient barrier for the aggressive medium [48] and thus revealing the improved corrosion protection of the coated MS [49]. In PANI obtained in Na-K Tartrate, the OCP shifted to 57 mV negative compared to MS. Since

aniline and electrolytes. In the case of BAW, benzoic acid in 3:1 alcohol-water is the optimized new system as a supporting electrolyte for the electropolymerization of aniline. The dissolution of Fe is suppressed in the presence of BAW, and a contamination-free coating is achieved. Also, the morphology of the PANI coating is much improved. In the case of Na-k Tartrate, the dissolution of Fe occurs, but coating shows a smooth, compact, and pore-free structure. The cyclic voltammetry shows no anodic dissolution of iron during cathodic scans, unlike in oxalic acid solution. FTIR, UV–vis, and XRD confirm the formation of PANI. Thus, these two new-electrolytes facilitate improving PANI coating onto MS, and their effects on corrosion protection are a new study. Corrosion behavior of PANI coatings on MS in 0.1 M NaCl shows excellent corrosion protection of MS resulting in 82.50 % and 99.99 % inhibition efficiency by PANI obtained in Na-K Tartrate and BAW solutions, respectively.

Tribhuvan University and Tri- Chandra Multiple Campus, Ghantaghar, Kathmandu for providing laboratory facilities and Central Salt and Marine Chemical Research Institute (CSIR), Bhavnagar, Gujarat, India for providing SEM-EDX, XRD, FTIR, and UV–vis facilities. D.K. Gupta would also like to acknowledge center for Co-operation in Science and Technology among Developing Societies (CCSTDS), DST, India for providing India Science and Research Fellowship (ISRF) and Nepal Academy of Science and Technology (NAST) for the partial Ph.D. financial support to carry out this study.

Appendix A. Supplementary data

Supplementary material related to this article can be found, in the online version, at doi:https://doi.org/10.1016/j.porgcoat.2020.1061 27.

References

[1] S. Ananda Kumar, K. Shree Meenakshi, T.S.N. Sankaranarayanan, S. Srikanth, Corrosion resistant behaviour of PANI–metal bilayer coatings, Prog. Org. Coat. 62 (2008) 285–292, https://doi.org/10.1016/j.porgcoat.2008.01.005.

[2] J.L. Camalet, J.C. Lacroix, S. Aeiyach, et al., Electrodeposition of protective polyaniline films on mild steel, J. Electroanal. Chem. 416 (1996) 179–182, https://doi.org/10.1016/S0022-0728(96)01012-1.

[3] D.W. Deberry, A. Viehbeck, in: E. McCafferty, C.R. Clayton, J. Oudar (Eds.), Fundamental Aspects of Corrosion Protection by Surface Modification, 1984. Pennington.

[4] P. Khodaei, M. Shabani-Nooshabadi, M. Behpour, Epoxy-based nanocomposite coating reinforced by a zeolite complex: its anticorrosion properties on mild steel in 3.5 wt% NaCl media, Prog. Org. Coat. 136 (2019) 105254, https://doi.org/10.1016/j.porgcoat.2019.105254.

[5] D. Sazou, C. Georgolios, Formation of conducting polyaniline coatings on iron surfaces by electropolymerization of aniline in aqueous solutions, J. Electroanal. Chem. 429 (1997) 81–93, https://doi.org/10.1016/S0022-0728(96)05019-X.

[6] J.-C. Lacroix, J.-L. Camalet, S. Aeiyach, et al., Aniline electropolymerization on mild steel and zinc in a two-step process, J. Electroanal. Chem. 481 (2000) 76–81, https://doi.org/10.1016/S0022-0728(99)00490-8.

[7] A.T. Özyılmaz, T. Tüken, B. Yazıcı, M. Erbil, The electrochemical synthesis and corrosion performance of polyaniline on copper, Prog. Org. Coat. 52 (2005) 92–97, https://doi.org/10.1016/j.porgcoat.2004.09.003.

[8] I.A. Kartsonakis, E.P. Koumoulos, A.C. Balaskas, et al., Hybrid organic–inorganic multilayer coatings including nanocontainers for corrosion protection of metal alloys, Corros. Sci. 57 (2012) 56–66, https://doi.org/10.1016/j.corsci.2011.12.034.

[9] S. Zor, E. Yakar, Corrosion behavior of PANI coated aluminum in oxalic acid containing different anions, Bull. Electrochem. 5 (2007).

[10] M. Rayati, R. Arefinia, Anticorrosion behavior of DBSA doped polyaniline nanoparticles/epoxy ester coating on carbon steel in saline-alkaline solution, Prog. Org. Coat. (2020) 105451, https://doi.org/10.1016/j.porgcoat.2019.105451.

[11] E.M. Genies, C. Tsintavis, Redox mechanism and electrochemical behaviour or polyaniline deposits, J. Electroanal. Chem. Interfacial Electrochem. 195 (1985) 109–128, https://doi.org/10.1016/0022-0728(85)80009-7.

[12] A.F. Diaz, J.A. Logan, Electroactive polyaniline films, J. Electroanal. Chem. Interfacial Electrochem. 111 (1980) 111–114, https://doi.org/10.1016/S0022-0728(80)80081-7.

[13] B. Wang, J. Tang, F. Wang, Electrochemical polymerization of aniline, Synth. Met. 18 (1987) 323–328, https://doi.org/10.1016/0379-6779(87)90899-X.

[14] G. Ćirić-Marjanović, Recent advances in polyaniline research: polymerization mechanisms, structural aspects, properties and applications, Synth. Met. 177 (2013) 1–47, https://doi.org/10.1016/j.synthmet.2013.06.004.

[15] C.M.S. Izumi, D.C. Rodrigues, M.L.A. Temperini, The role of solvent on the doping of polyaniline with Fe(III) ions, Synth. Met. 160 (2010) 2552–2558, https://doi.org/10.1016/j.synthmet.2010.10.004.

[16] T. Abdiryim, Z. Xiao-Gang, R. Jamal, Comparative studies of solid-state synthesized polyaniline doped with inorganic acids, Mater. Chem. Phys. 90 (2005) 367–372, https://doi.org/10.1016/j.matchemphys.2004.10.036.

[17] F. Fusalba, D. Bélanger, Electropolymerization of polypyrrole and polyaniline−polypyrrole from organic acidic medium, J. Phys. Chem. B 103 (1999) 9044–9054, https://doi.org/10.1021/jp9916790.

[18] M.M. Popović, B.N. Grgur, Electrochemical synthesis and corrosion behavior of thin polyaniline-benzoate film on mild steel, Synth. Met. 143 (2004) 191–195, https://doi.org/10.1016/j.synthmet.2003.12.022.

[19] P. Pawar, A.B. Gaikawad, P.P. Patil, Electrochemical synthesis of corrosion protective polyaniline coatings on mild steel from aqueous salicylate medium, Sci. Technol. Adv. Mater. 7 (2006) 732–744, https://doi.org/10.1016/j.stam.2006.09.014.

[20] G. Fomo, T.T. Waryo, P. Baker, E.I. Iwuoh, Electrochemical deposition and properties of polyaniline films on carbon and precious metal surfaces in perchloric acid/acetonitrile, Int. J. Electrochem. Sci. 11 (2016) 10347–10361.

[21] A.A. Ganash, F.M. Al-Nowaiser, S.A. Al-Thabaiti, A.A. Hermas, Comparison study for passivation of stainless steel by coating with polyaniline from two different

[22] S.K. Dhawan, D.C. Trivedi, Electrochemical behaviour of polyaniline in aromatic sulphonic acids, Polym. Int. 25 (1991) 55–60, https://doi.org/10.1002/pi.4990250110.

[23] T. Tüken, A.T. Özyılmaz, B. Yazıcı, M. Erbil, Electrochemical synthesis of polyaniline on mild steel in acetonitrile–LiClO4 and corrosion performance, Appl. Surf. Sci. 236 (2004) 292–305, https://doi.org/10.1016/j.apsusc.2004.05.001.

[24] J.L. Camalet, J.C. Lacroix, S. Aeiyach, P.C. Lacaze, Characterization of polyaniline films electrodeposited on mild steel in aqueous p-toluenesulfonic acid solution, J. Electroanal. Chem. 445 (1998) 117–124, https://doi.org/10.1016/S0022-0728(97)00526-3.

[25] J.-L. Camalet, J.-C. Lacroix, T.D. Nguyen, et al., Aniline electropolymerization on platinum and mild steel from neutral aqueous media, J. Electroanal. Chem. 485 (2000) 13–20, https://doi.org/10.1016/S0022-0728(00)00080-2.

[26] A.M. Fenelon, C.B. Breslin, Polyaniline-coated iron: studies on the dissolution and electrochemical activity as a function of pH, Surf. Coat. Technol. 190 (2005) 264–270, https://doi.org/10.1016/j.surfcoat.2004.04.083.

[27] N.B. Devkota, S. Singh, S. Neupane, D.K. Gupta, A.P. Yadav, Electro-polymerization of aniline onto mild steel surface using sodium benzoate, J. Nepal Chem. Soc. 35 (2016) 94–103.

[28] S. Neupane, Development of a Windows Based Program to Control the Analogue Potentiostat in Combination With an ADA Convertor, M.Sc. Disertation, Tri-Chandra Multiple Campus, Tribhuvan University, Nepal, 2013.

[29] M. Shabani-Nooshabadi, E. Allahyary, Y. Jafari, Enhanced anti-corrosive properties of electrosynthesized Polyaniline/zeolite nanocomposite coatings on steel, J. Nanostruct. 8 (2018), https://doi.org/10.22052/JNS.2018.02.003.

[30] N.M. Martyak, P. McAndrew, J.E. McCaskie, J. Dijon, Electropolymerization polymerization of aniline from an oxalic acid medium, Prog. Org. Coat. 45 (2002) 23–32, https://doi.org/10.1016/S0300-9440(02)00070-X.

[31] J. Stejskal, I. Sapurina, M. Trchová, Polyaniline nanostructures and the role of aniline oligomers in their formation, Prog. Polym. Sci. 35 (2010) 1420–1481, https://doi.org/10.1016/j.progpolymsci.2010.07.006.

[32] Y. Mohd, R. Ibrahim, M.F. Zainal, Electrodeposition and characterization of polyaniline films, in: 2012 IEEE Symposium on Humanities, Science and Engineering Research, IEEE, Kuala Lumpur, 2012, pp. 1301–1306.

[33] Medhat Ibrahima, Eckhard Koglin, Spectroscopic Study of Polyaniline Emeraldine Base: Modelling Approach, 52, 2005, pp. 159–162.

[34] H. Kawashima, H. Goto, Preparation and properties of polyaniline in the presence of trehalose, Soft Nanosci. Lett. 01 (2011) 71–75, https://doi.org/10.4236/snl.2011.13013.

[35] C.R.K. Rao, R. Muthukannan, M. Vijayan, Studies on biphenyl disulphonic acid doped polyanilines: synthesis, characterization and electrochemistry, Bull. Mater. Sci. 35 (2012) 405–414, https://doi.org/10.1007/s12034-012-0315-5.

[36] A. Mostafaei, A. Zolriasatein, Synthesis and characterization of conducting polyaniline nanocomposites containing ZnO nanorods, Prog. Nat. Sci. Mater. Int. 22 (2012) 273–280, https://doi.org/10.1016/j.pnsc.2012.07.002.

[37] M. Shabani-Nooshabadi, S.M. Ghoreishi, Y. Jafari, Electrodeposition of polyaniline-montmorillonite nanocomposite coatings on 316L stainless steel for corrosion prevention, J. Polym. Res. 21 (2014) 416, https://doi.org/10.1007/s10965-014-0416-5.

[38] W.S. Huang, A.G. MacDiarmid, Optical properties of polyaniline, Polymer 34 (1993) 1833–1845, https://doi.org/10.1016/0032-3861(93)90424-9.

[39] M. Canales, J. Torras, G. Fabregat, et al., Polyaniline emeraldine salt in the amorphous solid state: polaron versus bipolaron, J. Phys. Chem. B 118 (2014) 11552–11562, https://doi.org/10.1021/jp5067583.

[40] B. Sydulu Singu, P. Srinivasan, S. Pabba, Benzoyl peroxide oxidation route to nano form polyaniline salt containing dual dopants for pseudocapacitor, J. Electrochem. Soc. 159 (2011) A6–A13, https://doi.org/10.1149/2.036201jes.

[41] A. Bera, K. Deb, V. Kathirvel, et al., Flexible diode of polyaniline/ITO heterojunction on PET substrate, Appl. Surf. Sci. 418 (2017) 264–269, https://doi.org/10.1016/j.apsusc.2016.12.003.

[42] I.C. Amaechi, A.C. Nwanya, A.B.C. Ekwealor, et al., Electronic thermal conductivity, thermoelectric properties and supercapacitive behaviour of conjugated polymer nanocomposite (polyaniline-WO$_3$) thin film, Eur. Phys. J. Appl. Phys. 69 (2015) 30901, https://doi.org/10.1051/epjap/2015140441.

[43] S. Sathiyanarayanan, S. Muthukrishnan, G. Venkatachari, D.C. Trivedi, Corrosion protection of steel by polyaniline (PANI) pigmented paint coating, Prog. Org. Coat. 53 (2005) 297–301, https://doi.org/10.1016/j.porgcoat.2005.03.007.

[44] M. Wan, J. Li, Synthesis and electrical–magnetic properties of polyaniline composites, J. Polym. Sci. Part Polym. Chem. 36 (1998) 2799–2805, https://doi.org/10.1002/(SICI)1099-0518(19981115)36:15<2799::AID-POLA17>3.0.CO;2-1.

[45] M. Wan, M. Li, J. Li, Z. Liu, Structure and electrical properties of the oriented polyaniline films, J. Appl. Polym. Sci. 53 (1994) 131–139, https://doi.org/10.1002/app.1994.070530201.

[46] D.K. Bandgar, G.D. Khuspe, R.C. Pawar, et al., Facile and novel route for preparation of nanostructured polyaniline (PANi) thin films, Appl. Nanosci. 4 (2014) 27–36, https://doi.org/10.1007/s13204-012-0175-8.

[47] M. Shabani-Nooshabadi, M. Mollahoseiny, Y. Jafari, Electropolymerized coatings of polyaniline on copper by using the galvanostatic method and their corrosion protection performance in HCl medium: electropolymerized coatings of polyaniline on copper, Surf. Interface Anal. 46 (2014) 472–479, https://doi.org/10.1002/sia.5539.

[48] M. Shabani-Nooshabadi, E. Allahyary, Y. Jafari, Electrosynthesis of poly(ortho-phenetidine) coatings on steel and investigation of their corrosion protection

properties, Prot. Met. Phys. Chem. Surf. 54 (2018) 104–112, https://doi.org/10.1134/S2070205118010276.

[49] Y. Jafari, S.M. Ghoreishi, M. Shabani-Nooshabadi, Polyaniline/graphene nanocomposite coatings on copper: electropolymerization, characterization, and evaluation of corrosion protection performance, Synth. Met. 217 (2016) 220–230, https://doi.org/10.1016/j.synthmet.2016.04.001.

[50] M. Gvozdenovi, B. Jugovi, D. Jambrec, et al., Application of polyaniline in corrosion protection …, Zašt Mater. 8 (2012).

[51] N. Mahato, M.H. Cho, Graphene integrated polyaniline nanostructured composite coating for protecting steels from corrosion: synthesis, characterization, and protection mechanism of the coating material in acidic environment, Constr. Build. Mater. 115 (2016) 618–633, https://doi.org/10.1016/j.conbuildmat.2016.04.073.

[52] M. Shabani-Nooshabadi, F. Karimian-Taheri, Electrosynthesis of a polyaniline/zeolite nanocomposite coating on copper in a three-step process and the effect of current density on its corrosion protection performance, RSC Adv. 5 (2015) 96601–96610, https://doi.org/10.1039/C5RA14333K.

[53] Y. Jafari, S.M. Ghoreishi, M. Shabani-Nooshabadi, Electrochemical deposition and characterization of polyaniline-graphene nanocomposite films and its corrosion protection properties, J. Polym. Res. 23 (2016) 91, https://doi.org/10.1007/s10965-016-0983-8.

[54] T. Rajyalakshmi, A. Pasha, S. Khasim, et al., Enhanced charge transport and corrosion protection properties of polyaniline–carbon nanotube composite coatings on mild steel, J. Electron Mater. 49 (2020) 341–352, https://doi.org/10.1007/s11664-019-07783-6.

Data Article

Dataset for the selection of electrolytes for Electropolymerization of aniline

Dipak Kumar Gupta [a,b], Shova Neupane [a,#], Sanjay Singh [a],
Nabin Karki [c], Amar Prasad Yadav [a,§,*]

[a] Central Department of Chemistry, Tribhuvan University, Kirtipur, Kathmandu, Nepal
[b] Tri-Chandra Multiple Campus, Tribhuvan University, Ghantaghar, Kathmandu, Nepal
[c] Bhaktapur Multiple Campus, Tribhuvan University, Bhaktpur, Nepal

ABSTRACT

The most investigated conducting polymer (CP) is polyaniline (PANI)), a promising polymer due to its excellent environmental stability, simplicity of synthesis, and high electrical conductivity [1–4]. In corrosion protection applications, the PANI film has shown promising potential in protecting active metals such as iron by acting as physical barrier coatings, as a primer layer and as component in a multi-layer coating system [5]. The PANI has an excellent potential to replace the toxic metal, such as chromates, in corrosion protection and is considered a green anti-corrosion candidate [5–7]. The electrochemical synthesis of PANI coatings on active metals is accomplished by the dissolution of the metal at a potential lower than the monomer oxidation potential [8,9]. Therefore, electrochemical synthesis of PANI coatings on active metal requires a proper choice of the electrolyte and solvent that should strongly passivate the metal without hindering the electropolymerization process [10,11]. The data reported here are obtained while the anodic polarization of mild steel (MS) is carried out in succinic acid, sulphanilic acid, sodium orthophosphate, sodium potassium tartrate (Na-K tartrate), and

benzoic acid in 3:1 alcohol-water (BAW) solutions [11]. However, the results of electrolytes sodium-potassium tartrate (Na-K tartrate) and benzoic acid in alcohol-water (BAW) are reported for the polymerization of aniline onto MS [11]. The SEM image of MS sample polarized in 0.3 M oxalic acid solution and 0.1 M aniline in 0.3 M oxalic acid is reported as a dataset or a supplementary material of the main manuscript 'The Effect of Electrolytes on the Coating of Polyaniline on Mild Steel by Electrochemical Methods and Its Corrosion Behaviour [11].'

Specifications Table

Subject	Electrochemistry
Specific subject area	Conducting polymer
Type of data	Graphs and Images
How data were acquired	Polarization curve using a Hokuto Denko HA-151 potentiostat controlled by a self-made LabVIEW software interfaced with an IBM computer [12] and SEM image by a JEM-1200EX electron microscope.
Data format	Raw Analyzed
Parameters for data collection	Open circuit potential (OCP) was recorded for 30 min at an interval of 2 min using a 3-electrode setup. Anodic polarization was then carried out in electrolytes from OCP to 2 V with a 1 mV/*sec* scan rate, and SEM image of MS surface after polarization was acquired at 10 kV at a working distance of 10.3 mm.
Description of data collection	Polarization was done in a 3-electrode system using MS specimen as a working electrode, a saturated calomel electrode (SCE) as a reference electrode, and a graphite rod as a counter electrode. OCP was recorded for 30 min before each anodic polarization to get a steady-state condition. Prior to electrochemical measurements, the MS surface was abraded with SiC paper till #1200 grits and ultrasonicated in ethanol, rinsed with distilled water and dried with air stream. SEM image was taken after PANI formation on the MS surface.
Data source location	Central Department of Chemistry, Tribhuvan University, Kirtipur, Nepal and CSIR- Central Salt and Marine Chemical Research Institute (CSMCRI), Bhavnagar, Gujarat, India
Data accessibility	With Article
Related research article	Dipak Kumar Gupta, Shova Neupane, Sanjay Singh, Nabin Karki, Amar Prasad Yadav, The effect of electrolytes on the coating of polyaniline on mild steel by electrochemical methods and its corrosion behavior, Progress in organic coating, 152 (2021) 106,127. https://doi.org/10.1016/j.porgcoat.2020.106127

Value of the Data

- The polyaniline coating is extensively used to protect metals and alloys as a single layer coating, multi-layer coating, or primer. Therefore, the presented data provide valuable input for industries working on corrosion protection coating of PANI on active metals used in various environments.
- The acquired data reveals that succinic acid, sulphanilic acid, and sodium orthophosphate only passivate the MS surface without electropolymerization of aniline. On the other hand, Na-K tartrate and BAW both passivated the MS surface and help in the electropolymerization of aniline to polyaniline onto the MS surface and act as a corrosion inhibitor.

• Electropolymerization of aniline in BAW results in suppressing iron dissolution so that low contamination of electrolyte occurs.

1. Data Description

The shared data were recorded to select proper electrolytes that cause passivation of mild steel (MS) and subsequently electropolymerization of aniline using a Hokuto Denko HA-151 potentiostat controlled by a self-made LabVIEW software interfaced with an IBM computer [12]. Open circuit potential (OCP) of MS was recorded as a function of time in various electrolytes, and anodic polarization was recorded as a function of the electrolyte composition. The MS passivated surface morphology in oxalic acid and PANI film formed on MS was ascertained by SEM using a JEM-1200EX electron microscope (JEOL, Tokyo, Japan).

Fig. 1 depicts the variation of OCP of MS in different electrolytes. A shift of OCP to positive value indicates faster passivation of MS surface by forming compound with iron, e.g., sodium orthophosphate. In the case of a negative shift of OCP, the dissolution of iron occurs, followed by passivation of MS due to the formation of iron-salt, e.g., sodium-potassium tartrate. In succinic acid, sulphanilic acid, and sodium orthophosphate, OCP remains constant throughout the immersion period, indicating rapid passive layer formation on MS. The raw data in the attached zip archive present the complete acquired data range.

Fig. 2 shows the anodic polarization of MS in succinic acid, sulphanilic acid, and sodium orthophosphate solutions. After OCP remained constant for 30 min, anodic polarization was then carried out in 0.5 M succinic acid, 0.05 M sulphanilic acid and 0.5 M sodium orthophosphate from OCP to 2 V a scan rate of 1 mV/sec. In the whole anodic potential range, there is no change of current due to dissolution of iron and breakdown of the passivation layer, which are prerequisites for polymerization of aniline to polyaniline. Therefore, these three electrolytes cannot be used for electropolymerization of aniline on MS, unlike sodium-potassium tartrate and BAW [11]

Fig. 3 shows the SEM micrograph of MS specimen anodically polarized in 0.3 M aqueous oxalic acid up to 0.1 V vs. SCE so that only passive layer is formed, and Fig. 4 shows the SEM micrograph of PANI deposited on MS sample in 0.3 M aqueous oxalic acid solution containing
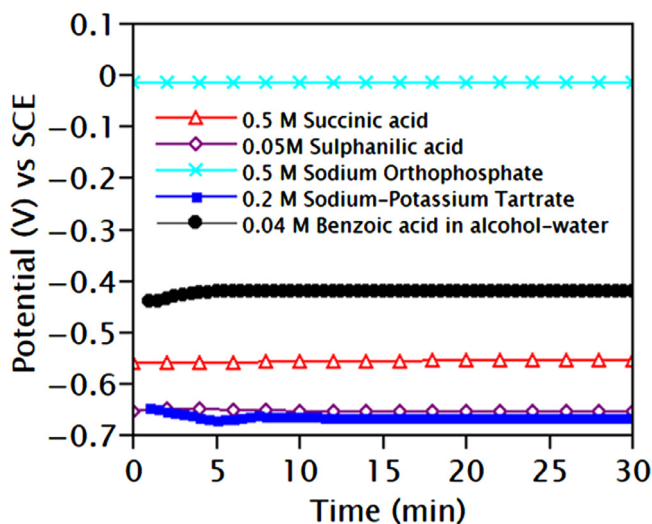

Fig. 1. Variation of open circuit potential (OCP) of MS specimen immersed in 0.5 M succinic acid, 0.05 M sulphanilic acid, 0.5 M sodium orthophosphate, 0.2 M Na-K Tartrate, and 0.04 M BAW solutions. The OCP was recorded in the interval of every 2 min for 30 min.
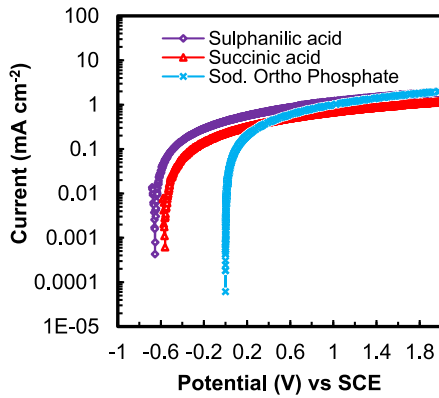
Fig. 2. Anodic polarization of MS specimen in 0.5 M succinic acid, 0.05 M sulphanilic acid, and 0.5 M sodium orthophosphate solutions after 30 min immersion in respective solution.
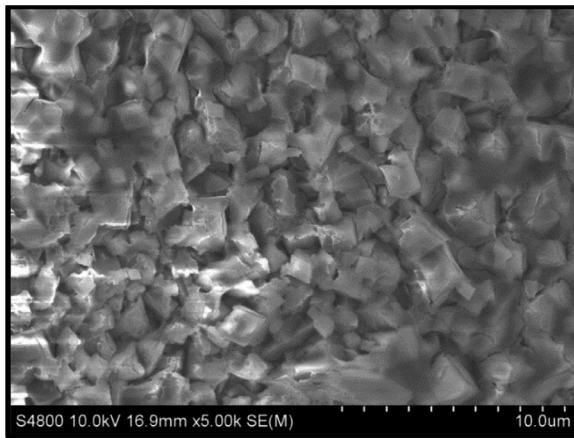

Fig. 3. The SEM image of MS sample polarized in 0.3 M oxalic acid solution.
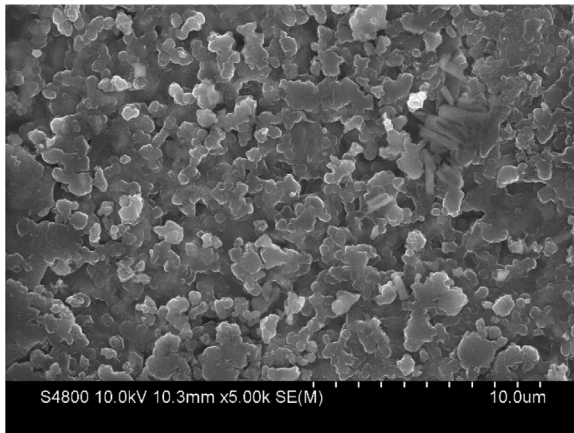

Fig. 4. SEM image of MS sample polarized in 0.1 M aniline in 0.3 M oxalic acid solution showing the formation of granular PANI coating.

0.1 M aniline by anodic polarization up to 1.6 V. In Fig. 3, the formation of Fe-oxalate takes place, giving a granular structure. The formation of granular and some niddle shaped PANI is obvious in Fig. 4 when the polarization is carried out till 1.6 V in the presence of aniline solution.In the case of Na-K tartrate and BAW, the formation of very fine morphology took place [11].

2. Experimental Design, Materials and Methods

The electrochemical measurements were performed by using a Hokuto Denko HA-151 potentiostat controlled by self-made LabVIEW software interfaced with an IBM computer. First of all, a mild steel (MS) sample with dimensions 3 cm x 3 cm x 0.15 cm was taken as working electrode, abraded on SiC paper till 1200 grits. It was ultrasonicated in ethanol, rinsed with distilled water and dipped into electrolytic solution (0.3 M oxalic acid containing 0.1 M aniline monomer) and graphite electrode as a counter electrode in a cell coupled with saturated calomel electrode as reference electrode. Aqueous solution of aniline was prepared after distillation of as purchased aniline. Oxalic acid was reagent grade and used without any treatments. Before the potentiodynamic polarization, OCP was recorded for 30 min at the interval of 2 min. Anodic polarization was then carried out in electrolytes from OCP to 2 V with a 1 mV/*sec* scan rate. The analysis of data was performed using the Microsoft Excel program. SEM images were recorded using a JEM-1200EX electron microscope after the anodic polarization in the potential limit specific for passive layer formation and PANI formation.

Ethics Statement

The experiments were performed in the Central Department of Chemistry laboratory, Tribhuvan University, Nepal, and all the relevant references have been cited. Data reproducibility was confirmed by repeating several measurements.

CRediT Author Statement

Dipak Kumar Gupta: Data collection, Analysis, and Original draft preparation; **Shova Neupane:** Reviewing the obtained data and manuscript editing; **Sanjay Singh:** Helped in experimental setup; Nabin Karki: Draft review; **Amar Prasad Yadav:** Conceptualization and Supervision.

Declaration of Competing Interest

The authors declare that they have no known competing financial interests or personal relationships which have or could be perceived to have influenced the work reported in this article.

Acknowledgments

Supplementary Materials

Supplementary material associated with this article can be found in the online version at doi:10.1016/j.dib.2021.106875.

References

[1] D. Sazou, M. Kourouzidou, E. Pavlidou, Potentiodynamic and potentiostatic deposition of polyaniline on stainless steel: electrochemical and structural studies for a potential application to corrosion control, Electrochim. Acta 52 (2007) 4385–4397, doi:10.1016/j.electacta.2006.12.020.

[2] M.M. Popović, B.N. Grgur, Electrochemical synthesis and corrosion behavior of thin polyaniline-benzoate film on mild steel, Synth. Met. 143 (2004) 191–195, doi:10.1016/j.synthmet.2003.12.022.

[3] F. Masdarolomoor, S. Hajizadeh, M. Arab Chamjangali, P.C. Innis, Novel approach to the synthesis of polyaniline possessing electroactivity at neutral pH, Synth. Met. 250 (2019) 121–130, doi:10.1016/j.synthmet.2019.03.011.

[4] A.M. Abdel-Gaber, B.A. Abd-El-Nabey, E. Khamis, R.M. Salman, H.T. Rahal, Z. El Morr, Electrochemical synthesis and corrosion behaviour of polyaniline on stainless steel in sodium hydroxide solutions, Chem Eng. Commun. (2020) 1–10, doi:10.1080/00986445.2019.1710493.

[5] A. Zhu, H. Wang, S. Sun, C. Zhang, The synthesis and antistatic, anticorrosive properties of polyaniline composite coating, Progr. Org. Coat. 122 (2018) 270–279, doi:10.1016/j.porgcoat.2018.06.004.

[6] M. Wang, H. Yun, K. Tan, A. Guo, J. Ling, F. Jiang, X. Shen, Q. Xu, One-step electrochemical synthesis of poly(vinyl pyrrolidone) modified polyaniline coating on stainless steel for high corrosion protection performance, Progr. Organic Coat. 149 (2020) 105908, doi:10.1016/j.porgcoat.2020.105908.

[7] N. Boshkova, N. Tabakova, G. Atanassova, N. Boshkov, Electrochemical obtaining and corrosion behavior of Zinc-Polyaniline (Zn-PANI) hybrid coatings, Coatings 9 (2019) 487, doi:10.3390/coatings9080487.

[8] P. Pawar, A.B. Gaikawad, P.P. Patil, Electrochemical synthesis of corrosion protective polyaniline coatings on mild steel from aqueous salicylate medium, Sci. Technol. Adv. Mater. 7 (2006) 732–744, doi:10.1016/j.stam.2006.09.014.

[9] N.A. Ogurtsov, A.A. Pud, P. Kamarchik, G.S. Shapoval, Corrosion inhibition of aluminum alloy in chloride mediums by undoped and doped forms of polyaniline, Synth. Met (2004) 5.

[10] S. Chaudhari, P.P. Patil, Inhibition of nickel coated mild steel corrosion by electrosynthesized polyaniline coatings, Electrochim. Acta 56 (2011) 3049–3059, doi:10.1016/j.electacta.2010.12.096.

[11] Dipak Kumar Gupta, Shova Neupane, Sanjay Singh, Nabin Karki, Amar Prasad Yadav, The effect of electrolytes on the coating of polyaniline on mild steel by electrochemical methods and its corrosion behaviour, Progr. Org. Coat. 152 (2021) 106127, doi:10.1016/j.porgcoat.2020.106127.

[12] S. Neupane, Development of a Windows Based Program to Control the Analogue Potentiostat in Combination with an ADA Convertor, M.*Sc.* Disertation, Tri-Chandra Multiple Campus, Tribhuvan University, Nepal, 2013.

APCCC18 Asian Pacific Corrosion Control Conference

5th – 9th November, 2018, Pattaya, Thailand

CERTIFICATE OF PRESENTATION

We hereby certify that

Dipak K. Gupta

has presented an oral presentation entitled

Effects of Electrolytes on the Polymerization
of Aniline and Its Deposition onto Mild Steel

Gobboon Lothongkum

Assoc. Prof. Dr.-Ing. Gobboon Lothongkum
APCCC18 Chairman
President of Thai Corrosion of Metals and Materials Association
Head of Metallurgical Engineering Department,
Faculty of Engineering, Chulalongkorn University
Thailand

Dr. Julathep Kajornchaiyakul
APCCC18 Chairman
Executive Director
National Metal and Materials Technology Center
Thailand

OG-157

DST & ACS
WORKSHOP

Department of Science & Technology
Government of India

ACS
Chemistry for Life

Certificate of Participation

VERIFYING THAT

Dipak Kumar Gupta

ATTENDED THE FULL AGENDA OF THE DST & ACS WORKSHOP:
CSIR CSMCRI BHAVNAGAR
NOVEMBER 15, 2019

DR. JAMES MILNE
Acting President, Publications Division
American Chemical Society

APA-STERMI
2019 | GOA

Organised by

Asian Polymer Association

stermi

Society For Tissue Engineering and
Regenerative Medicine India

International Conference on
Advances in Polymeric Materials & Human Healthcare

16-18 October, 2019 | Goa, India

Certificate of Participation

This is to certify that

Dipak Kumar Gupta

Participated as Delegate & Presented Invited Talk

Titled

Preparation of Polyaniline Coating on Mild Steel Surface and
Study of its Corrosion Inhibition

Bhuvanesh Gupta
Conference Chair

Anup K Ghosh
Organising Chair

Manohar V Badigar
Organising Chair

National Chemical Congress

Organized by
Nepal Chemical Society
In co-operation with
Amrit Campus
Lainchaur, Kathmandu, Nepal

Best Oral Award

This is to certify that

Mr. Dipak Kumar Gupta

is awared Best Oral presentation in the

National Chemical Congress

held on August 29, 2017, Amrit Campus, Lainchaur,
Kathmandu, Nepal

Prof. Dr. Amar Prasad Yadav
President
Nepal Chemical Society

Prof. Dr. Jiba Raj Pokharel
Vice Chancellor
Nepal Academy of Science & Technology
Chief Guest

Dr. Surya Kant Kalauni
General Secretary
Nepal Chemical Society

23RD INTERNATIONAL CONFERENCE OF INTERNATIONAL ACADEMY OF PHYSICAL SCIENCES

(CONIAPS XXIII)

On

Advances in Physical Sciences to Achieve Sustainable Development Goals
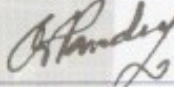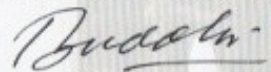
November 18, 2018

Organized by

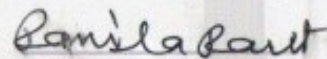## NEPAL ACADEMY OF SCIENCE AND TECHNOLOGY, KATHMANDU, NEPAL

Certificate

This is to certify that Prof. /Dr./ Mr./Ms. ...Dipak Kumar Gupta..., ...Central...
Department of ...Chemistry..., T.U., Nepal... has participated in the
23rd International Conference of International Academy of Physical Sciences on **Advances in Physical Sciences to Achieve Sustainable Development Goals** held at **Nepal Academy of Science and Technology** during November 16-18, 2018 and delivered Invited Lecture/Chaired a Session/ Presented a paper /Presented a paper in Young Scientist Award Category.

Title of the Invited Lecture/Paper ...Effects of electrolytes on the polymerization of aniline and its deposition on to mild steel...

Prof. P. N. Pandey
General Secretary
IAPS

Dr. Buddhi Ratna Khadge
Convenor
CONIAPS XXIII

Ms. Ramila Raut
Organizing Secretary
CONIAPS XXIII

International Conference on Advances in Polymer Science & Technology

November 1-3, 2018 | Kathmandu, Nepal

APA 2018

CERTIFICATE OF PARTICIPATION

This is to certify that

Dipak Kumar Gupta

Participated as a Delegate & Presented Oral Talk

Titled

Electropolymerization of Aniline onto Mild Steel Using
Benzoic Acid as Electrolytes and Its Morphological Study

Bhuvanesh Gupta
Chairman (India)

Amar Yadav
Chairman (Nepal)

Regional Chimcal Congress-2017

Organized by

Nepal Chemical Society

In co-operation with

Prithivi Narayan Campus, Pokhara, Tribhuvan University

Certificate of Participation

This is to certify that

Mr. Dipak Kumar Gupta

participated as Keynote/Invited/Oral Lecture/Poster/Delegate in the Regional Chemical Congress hel on October 14, 2017 Pokhara, Nepal

Prof. Dr. Amar Prasad Yadav
President
Nepal Chemical Society

Prof. Dr. Chandra Bahadur Thapa
Chief Guest
Campus Chief, P.N. Campus, Pokhara